## SUPERCONDUCTIVITY, INCLUDING HIGH-TEMPERATURE SUPERCONDUCTIVITY

# Surface impedance of a thin superconducting film in a parallel magnetic field

D. A. Luzhbin,* A. L. Kasatkin, and V. M. Pan

*Institute of Metal Physics, National Academy of Sciences of Ukraine, bul'v. Akad. Vernadskogo 36, 03680 Kiev-142, Ukraine*

(Submitted August 22, 2000; revised November 13, 2000)
Fiz. Nizk. Temp. **27**, 455–462 (May 2001)

The problem of the surface microwave impedance of a superconducting film in a static magnetic field **H** parallel to the surface is considered. In films of thickness $d<\lambda$ ($\lambda$ is the London penetration depth) the mixed state for a parallel orientation of the external field is a set of vortex rows, the number of which varies in a discrete manner at certain characteristic values $H_{c1}^{(N)}(d)$ of the magnetic field ($H_{c1}^{(N)}(d)$ is the insertion field for the $N$th vortex row). The surface impedance of the film in the field of a normally incident microwave field is calculated with allowance for the contribution of oscillating vortex rows. The results obtained in the known theoretical models (Coffey–Clem and Brandt) for the surface impedance of superconductors in the mixed state are generalized to the case of thin films, for which size effects play an important role in the structure and dynamics of the vortex lattice. © *2001 American Institute of Physics.* [DOI: 10.1063/1.1374716]

### INTRODUCTION

Research on the surface impedance of superconductors in the mixed state is an effective method of studying the properties of the ensemble of Abrikosov vortices in superconductors, permitting investigation of their dynamical characteristics, pinning mechanisms, and possible phase states in the vortex ensemble.[1–8] For the case of a normally incident electromagnetic plane wave $(h_{rf}(z,t),e_{rf}(z,t)\sim\exp(ikz-i\omega t))$ the surface impedance $Z_S$ of a bulk superconductor in the mixed state is determined by the complex penetration depth $\lambda_{AC}(\omega,T,B)$:[9–12]

$$Z_S=\frac{E_{AC}(0)}{H_{AC}(0)}=-\frac{i\omega\lambda_{AC}}{c} \tag{1}$$

where $E_{AC}(0)$ and $H_{AC}(0)$ are the total complex amplitudes of the alternating components of the field at the surface of the superconductor, and $c$ is the speed of light. The value of $\lambda_{AC}$ is determined by the response of the vortices to the alternating electromagnetic field and depends in an important way on the temperature $T$, the magnitude of the magnetic induction $B$ in the sample (i.e., on the vortex concentration), and the frequency $\omega$.

According to the results of the well-known theoretical models of Coffey and Clem[9,10] and of Brandt,[11,12] the value of $\lambda_{AC}$ at temperatures low enough that one can neglect the contribution of normal quasiparticles is given by the expression

$$\lambda_{AC}^2=\lambda^2+\lambda_C^2(\omega), \tag{2}$$

where $\lambda$ is the London penetration depth and $\lambda_C(\omega)$ is the generalized Campbell depth, which characterizes the reaction of the vortices to the alternating field. In the general case $\lambda_{AC}$ depends on the frequency $\omega$, the coefficient of viscosity $\eta$ of the vortices, and the force constant $\alpha$ (the Labusch parameter), which characterizes the pinning in the sample, and on the elastic modulus $\overline{C}$ of the vortex lattice ($\overline{C}=C_{11}(B)$ for the case when the vortices are parallel to the surface, and $\overline{C}=C_{44}(B)$ for the perpendicular orientation of the vortices):[10,11]

$$\lambda_C^2(\omega)=\frac{\overline{C}}{\alpha(\omega)}=\frac{B\Phi_0}{4\pi(\alpha-i\omega\eta)}, \tag{3}$$

where $\Phi_0$ is the flux quantum.

In calculations of the surface impedance, the transition from bulk material of thickness $d\gg\lambda$ to the thin-film geometry ($d\leqslant\lambda$) is usually taken into account by means of the matching formula:

$$Z_S(d)=Z_S f(d),$$

$$f(d)=\frac{\dfrac{Z_d}{Z_S}-\tanh(ik_2d)}{1-\dfrac{Z_d}{Z_S}\tanh(ik_2d)}, \tag{4}$$

where $k_2=i\lambda_{AC}^{-1}$ is the complex wave vector characterizing the film material, $Z_S$ is the surface impedance of the bulk superconductor ($d\gg\lambda$), and $Z_d$ is the wave impedance of the dielectric substrate. For films of high-$T_c$ superconductors (HTSCs) the quantity $Z_S(d)$ defined by expression (4) has been investigated in a number of experimental studies (see, e.g., Refs. 13–16). For superconducting films of thickness $d\leqslant\lambda$ the use of expression (4) is justified for superconductors found in the Meissner state, i.e., in the absence of vortices. At the same time, the possibility of using expression (4) for the impedance of a superconducting film ($d\leqslant\lambda$) in the mixed state by starting from Eqs. (1)–(3) for the surface impedance $Z_S$ of a bulk superconductor in the vortex phase is unjustified, since the film geometry can lead to certain size

 

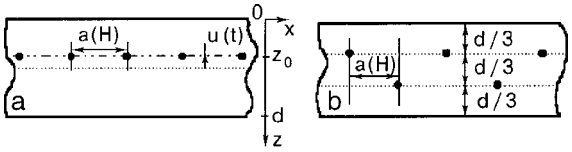


FIG. 1. Structure of the vortex lattice in a thin film in a magnetic field **H** parallel to the surface. a: $H_{c1}^{(1)}(d)<H<H_{c1}^{(2)}(d)$, the vortices are arranged in a single row, with a distance $a$ between vortices in the row; the arrow indicates the displacement $u(t)$ of the vortices under the influence of the incident wave. b: $H_{c1}^{(2)}(d)<H<H_{c1}^{(3)}(d)$; the vortices are arranged in two rows; their equilibrium positions are indicated.

effects in the structure and elastic characteristics of the vortex lattice, altering the electrodynamic characteristics of the conducting medium in the film in comparison with the bulk superconductor.

In this paper we investigate these size effects in the structure and high-frequency dynamics of the vortex lattice for the case of a parallel orientation of the static magnetic field **H**, in which case the Abrikosov vortices generated by this field lie in the plane of the film. It is known[17,18] that in the case of a parallel orientation of the external field **H** the insertion of the first row of vortices into the film begins at a field $H_{c1}^{(1)}(d)$, which for thin films can be substantially higher than the lower critical field $H_{c1}^{\rm bulk}$ of the bulk material: $H_{c1}^{(1)}(d)\sim(\lambda/d)^2 H_{c1}^{\rm bulk}$.

As the external field **H** is increased further, the concentration of vortices, which are arranged in a row at the center of the film, increases until the external field reaches the value $H_{c1}^{(2)}(d)$. At the field $H_{c1}^{(2)}(d)$ a structural transition occurs in the vortex lattice, and two vortex rows are formed, as is shown schematically in Fig. 1. At this transition the distance $a(H)$ between neighboring vortices increases with a jump. As the field is increased further, the number of vortex rows changes in a discrete manner at certain field values $H_{c1}^{(N)}(d)$ at which the transition from $N-1$ to $N$ vortex rows occurs. The value of $H_{c1}^{(N)}(d)$ was calculated numerically in Refs. 19–24; such a rearrangement of the vortex lattice has been observed experimentally in the form of oscillations of the magnetic moment of the film as the external field $H$ is raised.[24–27]

In this paper we calculate the surface impedance $Z_S(d,H)$ of a film in which there is a substantial contribution from discrete vortex rows oscillating in the incident microwave field. We show that $Z_S(d,H)$ should change in a stepwise manner at field values $H=H_{c1}^{(N)}(d)$. The field dependence of $Z_S(d,H)$ is found in the cases of high and low frequencies (in comparison with the ''depinning frequency'' $\omega_p$).

## MIXED STATE OF A FILM IN A PARALLEL MAGNETIC FIELD

For superconductors with a Ginzburg–Landau parameter $\chi\gg 1$ the magnetic field $H_V$ produced by vortices lying parallel to the surface of the film can be found from the London equation[28]

$$H_V+\lambda^2\,\mathrm{curl}\;\mathrm{curl}\,H_V=\Phi_0\sum_{m,n}\delta(r-R_{m,n}) \tag{5}$$

with the boundary conditions

$$H_V|_{z=0}=H_V|_{z=d}=0, \tag{6}$$

where $R_{m,n}$ are the coordinates of the centers of the vortices inside the film, $\Phi_0$ is the flux quantum, and the $z$ axis is normal to the surface. In the case of an isolated vortex row ($x=ma$, $m=0,\pm1,\pm2,\ldots$) lying in the plane $z=z_0$ ($0\leqslant z_0\leqslant d$), the solution of equations (5), (6) can be expressed, following Refs. 17 and 29, in the form

$$H_V(x,z)=\frac{\Phi_0}{2a\lambda}\sum_m\cos\left(\frac{2\pi m x}{a}\right)\times\frac{\cosh\left(u_m\dfrac{d-|z-z_0|}{\lambda}\right)-\cosh\left(u_m\dfrac{d-z-z_0}{\lambda}\right)}{u_m\sinh\left(u_m\dfrac{d}{\lambda}\right)}, \tag{7a}$$

which is valid in the region $0\leqslant z,\ z_0\leqslant d,\ -\infty<x<\infty$, or, following Ref. 28, in the equivalent form

$$H_V(x,z)=\frac{\Phi_0}{2d\lambda}\times\sum_{n=1}^{\infty}\frac{\cos\dfrac{n\pi}{d}(z-z_0)-\cos\dfrac{n\pi}{d}(z+z_0)}{v_n}\times\frac{\cosh\left(v_n\dfrac{a-2x}{2\lambda}\right)}{\sinh\left(v_n\dfrac{a}{2\lambda}\right)}, \tag{7b}$$

which is valid in the region $0\leqslant z,\ z_0\leqslant d$, $0\leqslant x\leqslant a$, where, in Eqs. (7a) and (7b), $u_m=[1+(2\pi\lambda m/a)^2]^{1/2}$, $m=0,\pm1,\pm2,\ldots$, $v_n=[1+(n\pi\lambda/d)^2]^{1/2}$, and $a=a(H)$ is the distance between adjacent vortices.

In calculating the surface impedance we will be interested in the average (over the coordinate $x$ field (7a), which has the form

$$H_V(z)=\frac{\Phi_0}{2a\lambda}\,\frac{\cosh\left(\dfrac{d-|z-z_0|}{\lambda}\right)-\cosh\left(\dfrac{d-z-z_0}{\lambda}\right)}{\sinh\left(\dfrac{d}{\lambda}\right)}. \tag{8}$$

The Gibbs free energy per unit length of the film in the case of a single vortex row can be written[28]

$$G=\frac{1}{8\pi}\int d^3r[H_V^2+\lambda^2(\mathrm{curl}\;H_V)^2]-\frac{1}{4\pi}H\int H_V d^3r=\frac{1}{a}\left[\frac{H_V(0)\Phi_0}{8\pi}-\frac{H\Phi_0}{4\pi}\left(1-\frac{\cosh\left(\dfrac{d-2z_0}{2\lambda}\right)}{\cosh\left(\dfrac{d}{2\lambda}\right)}\right)\right], \tag{9}$$

where $H_V(0)$ is the field produced at the center of a vortex (for $r\to R_{m,n}$) by the vortex system alone, which follows from Eq. (7b):

$$H_V(0)=\frac{\Phi}{2d\lambda}\sum_{n=1}^{\infty}\frac{1-\cos\left(\frac{2\pi n z_0}{d}\right)\cosh\left(v_n\frac{a-2\xi}{2\lambda}\right)}{\sinh\left(v_n\frac{a}{2\lambda}\right)}. \tag{10}$$

To avoid the divergence that arises here we use the standard cutoff $\min|r-R_{m,n}|=\xi$.

Starting from the expression for the free energy, we can find the thermodynamic equilibrium value of the intervortex distance $a(H)$, which is determined by the condition $\partial G/\partial a=0$, and the elastic constant $\alpha_p$ characterizing the elastic force that arises upon small displacements of the vortex rows from the center of the film (per vortex):

$$\alpha_p=\left.\frac{\partial^2 G}{\partial z_0^2}\right|_{z_0=d/2}=\frac{\Phi_0 H}{4\pi\lambda^2}\frac{1}{\cosh(d/2\lambda)}+\frac{\Phi_0^2\pi}{4\lambda d^3}\sum_{n=1}^{\infty}\frac{(-1)^n n^2}{v_n}\frac{\cosh\left(v_n\frac{a-2\xi}{2\lambda}\right)}{\sinh\left(v_n\frac{a}{2\lambda}\right)}, \tag{11}$$

which in this case is due to the interaction of the vortex row with the surface of the film.

In the case of two vortex rows, expressions (9)–(11) are modified as follows: Eq. (9) becomes

$$G=\frac{1}{2a}\left[\frac{\Phi_0[H_V^{(1)}(0)+H_V^{(2)}(0)]}{8\pi}-\frac{H\Phi_0}{4\pi}\times\left(2-\frac{\cosh\left(\frac{d-2z_0^{(1)}}{2\lambda}\right)+\cosh\left(\frac{d-2z_0^{(2)}}{2\lambda}\right)}{\cosh(d/2\lambda)}\right)\right], \tag{12}$$

where $a$ is the distance between adjacent vortices (here the distance between nearest vortices of the same row is $2a$; Fig. 1); $z_0^{(1)}$ and $z_0^{(2)}$ are the coordinates of the first and second vortex rows, $H_V^{(i)}(0)$ is now the field produced by both vortex rows at the center of any vortex of the $i$th row ($i=1,2$). To find the dependence of $a(H)$ we use the equation $\partial G/\partial a=0$ under the condition that $z_0^{(1)}=d/3$, $z_0^{(2)}=2d/3$. Here it is taken into account that, according to Ref. 24, the structural transition from one to two rows of vortices occurs in a small field interval $\Delta H$, i.e., $\Delta H\ll H_{c1}^{(N+1)}(d)-H_{c1}^{(N)}(d)$. Outside the transition region $\Delta H$ the only quantity that depends on the field is the intervortex distance $a(H)$; the distance between rows is independent of $H$ and equal to $d/3$.[24] This transition is accompanied by a jump in $a(H)$ (Ref. 24) and in $\alpha_p(H)$ (Ref. 21) due to the structural transition in the vortex system.

For finding the function $\alpha_p(H)$ we note the following: analysis shows that under the influence of the Lorentz force exerted by the incident microwave field, the two vortex rows move mainly as a rigid structure. The corrections due to the relative motion of the rows are of order $d/\lambda$ and will not be taken into account in the present discussion. Then, introducing $z_0^{(1)}=d/3+u$, $z_0^{(2)}=2d/3+u$, we find that $\partial^2/\partial z_0^2$ in Eq. (11) goes over to $\partial^2/\partial u^2$, and

$$\alpha_p=\frac{\Phi_0 H}{4\pi\lambda^2}\frac{\cosh(d/6\lambda)}{\cosh(d/2\lambda)}+\frac{\Phi_0^2\pi}{4\lambda d^3}\times\sum_{n=1}^{\infty}\frac{n^2}{v_n}\frac{\cos\left(\frac{2n\pi}{3}\right)\cosh\left(v_n\frac{a-2\xi}{2\lambda}\right)+(-1)^n}{\sinh\left(v_n\frac{a}{2\lambda}\right)}. \tag{13}$$

The field dependence of $a(H)$ and $\alpha_p(H)$ for $d/\lambda=0.5$ is shown in Figs. 2 and 3 for $\chi=100$, $\lambda=10^{-5}$ cm. We see that the $a(H)$ and $\alpha_p(H)$ curves undergo a jump at a field $H_{c1}^{(2)}(d)$. Analogous jumps on the $a(H)$ and $\alpha_p(H)$ curves should appear at external field values $H=H_{c1}^{(N)}(d)$ corresponding to unit changes in the number of vortex rows.

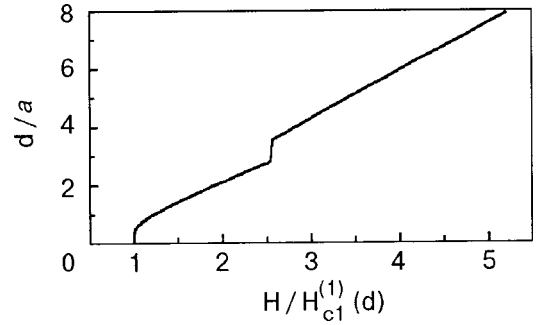


FIG. 2. Intervortex distance $a$ as a function of the external field $H$ for the geometry of Fig. 1 with $d/\lambda=0.5$, where $d$ is the thickness of the film.

## CONTRIBUTION OF THE VORTEX ROWS TO THE SURFACE IMPEDANCE OF A FILM

Under the influence of an incident electromagnetic wave, alternating Meissner currents are induced in the film, which cause oscillations of the vortex rows about their equilibrium positions. In the case of a single vortex row the equation of the oscillations has the form

$$\frac{j_{rf}(z_0)\Phi_0}{c}=\eta\frac{du}{dt}+\alpha_\Sigma u; \tag{14}$$

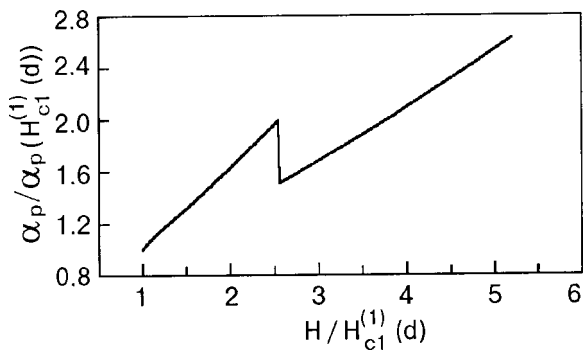


FIG. 3. Dependence of the elastic constant $\alpha_p$ on the external field $H$. The jump at a field $H\approx 2.5H_{c1}^{(1)}(d)$ is due to a change of the structure of the vortex lattice in the film.

here $u(t)=u_0\exp(-i\omega t)$ is the displacement of the vortex row along the $z$ axis relative to the equilibrium position in the plane $z_0=d/2$, $\eta$ is the viscosity coefficient, and $\alpha_\Sigma=\alpha+\alpha_p$, where $\alpha_p$ the elastic constant (11) and $\alpha$ is the Labusch parameter (per vortex), which is due to defects in the film material. The quantity $j_{rf}$ in (14) is determined solely by the field of the incident electromagnetic wave:

$$j_{rf}=\frac{c}{4\pi}\operatorname{curl} h_{rf}(z)$$

$$=-\frac{ick_2h_{rf}(0)}{2\pi D_0}[\exp(ik_2z)]+D_1\exp(-ik_2z), \quad (15)$$

where $D_1=(Z_d-Z_{S,M}/Z_d+Z_{S,M})\exp(2ik_2d)$, $k_2=i\lambda^{-1}$, $D_0=1+Z_{S,M}+D_1(Z_{S,M}-1)$, $Z_d$ is the wave impedance of the substrate (in the case of a dielectric, $Z_d=\sqrt{\mu/\varepsilon}$), and $Z_{S,M}$ is the impedance of the bulk superconductor in the Meissner state (expression (1) with $\lambda_{AC}$ replaced by $\lambda$). It should be stressed once again that in this paper we are considering the case of an ideal superconductor at low temperatures, i.e., $\operatorname{Re} Z_{S,M}=0$. The solution of equations (14), (15) has the form

$$u_0=\frac{\Phi_0h_{rf}(0)(1-D_1)[f(d)-d/2\lambda]}{2\pi\lambda D_0(\alpha_\Sigma-i\omega\eta)}, \quad (16)$$

where $f(d)$ is determined by expression (4) with $\lambda_{AC}$ replaced by $\lambda$. Here, according to the boundary conditions (6), the displacement (16) of the vortex row does not cause an additional alternating magnetic field to appear at the surface of the film: $H_V(z=0,t)=H_V(z=d,t)=0$. The alternating electric field produced at the surface by the oscillations of the vortex row is found from the Maxwell equation

$$\operatorname{curl}\ E_V=-\frac{dH_V}{cdt}=-\frac{\partial H_V}{c\partial z_0}\frac{du}{dt}=\frac{i\omega}{c}\frac{\partial H_V}{\partial z_0}u(t). \quad (17)$$

From Eqs. (8) and (17) we obtain the following expression for $E_V(z,t)$:

$$E_V(z,t)=-\frac{i\Phi_0u(t)\omega}{2ca\lambda}$$

$$\times\frac{\cosh\left(\frac{d-|z-z_0|}{\lambda}\right)+\cosh\left(\frac{d-z-z_0}{\lambda}\right)}{\sinh\left(\frac{d}{2\lambda}\right)}. \quad (18)$$

Here the surface impedance

$$Z_S(d,H)=\frac{E_{AC}(z=0)}{H_{AC}(z=0)}$$

$$=\frac{e_{rf}(z=0)+E_V(z=0)}{h_{rf}(z=0)}$$

$$=Z_{S,M}(d)+Z_V(d,H), \quad (19)$$

where $Z_{S,M}(d)$ is the impedance of the film in the Meissner state (i.e., in the absence of vortices), which is given by expression (4) with $k_2=i\lambda^{-1}$, and $Z_V(d,H)$ is an additive term giving the vortex contribution to the surface impedance:

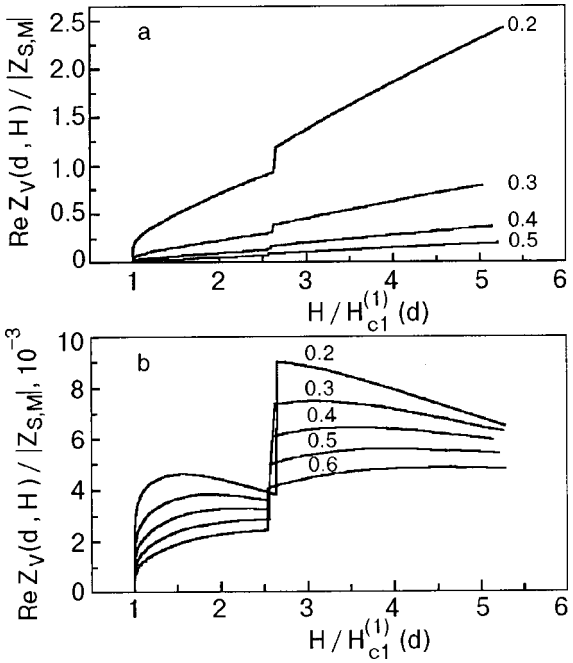


FIG. 4. Field dependence of the surface resistance of a film, normalized to the absolute value of the impedance of a bulk sample in the Meissner state for different film thicknesses ($d/\lambda=0.2$, 0.3, 0.4, 0.5, 0.6) at frequencies of 800 GHz (higher than the ''depinning frequency'') (a) and 100 MHz (lower than the ''depinning frequency'') (b). The jump in $R_V$ occurs at a field $H=H_{c1}^{(2)}(d)\approx 2.5H_{c1}^{(1)}(d)$ and is due to the insertion of a second vortex row in the film. Changing the frequency (within the region $\omega\ll\omega_p$ or $\omega\gg\omega_p$) leads only to a change of the scale on the vertical axis, while the character of the field dependence is unaffected.

$$Z_V(d,H)=\frac{E_V(z=0)}{h_{rf}(z=0)}$$

$$=-\frac{i\Phi_0^2\omega}{4\pi ca(H)d\lambda}\frac{f(d)-d/2\lambda}{\alpha_\Sigma(H)-i\omega\eta}. \quad (20)$$

For the case when two vortex rows are present in the film the expression for $Z_V(d,H)$ is still given formally by Eq. (20), but with allowance for the fact that in the two-row case $\alpha_p$ is given by Eq. (13).

The field curves of the surface resistance $R_V(d,H)=\operatorname{Re} Z_V(d,H)$ due to oscillations of the vortices are shown in Fig. 4 for the cases of high and low frequencies (in comparison the ''depinning frequency'' $\omega_p=\alpha_\Sigma/\eta$). The values of the material parameters used in the calculations were typical of HTSC materials: $\chi=100$, $\lambda=10^{-5}$ cm, the values $\alpha=2\times10^5$ N/m$^2$ and $\eta=2\times10^{-6}$ N·s/m$^2$ taken from Ref. 1, and $\varepsilon=20$.

It should be noted that the results obtained in the present paper differ from the results of the ''continuum'' model[9–12] generalized to the thin-film geometry by means of the transformation (4). Indeed, it follows from (2)–(4) that the expressions for the surface resistance $R_S$ in the ''continuum'' model have the following forms for the bulk and thin-film geometries. In the case of a bulk superconductor ($d\gg\lambda$)

$$R_S=\frac{\omega}{c}\operatorname{Im}\lambda_{AC}\cong\begin{cases}\dfrac{1}{2c}\dfrac{\omega^2}{\omega_0}\dfrac{\lambda_C^2(0)}{\lambda_{AC}(0)}, & \omega\ll\omega_0\\ \dfrac{\lambda_C(0)}{c}\left(\dfrac{\omega\omega_0}{2}\right), & \omega\gg\omega_0,\end{cases} \quad (21)$$

where $\lambda_{AC}(0)$ and $\lambda_C(0)$ are given by expressions (2) and (3) with $\omega=0$. Expression (21) describes a monotonic dependence of the surface resistance of a bulk superconductor on the frequency and on the static magnetic field $H$: $R_S \sim \omega^2 H^{1/2}$ for $\omega \ll \omega_0$ and $R_S \sim \omega^{1/2} H^{1/2}$ for $\omega \gg \omega_0$ (in the Coffey–Clem model $\omega_0 = \alpha/\eta$ and lies in the range $10^{10}$–$10^{12}\,\mathrm{s}^{-1}$; Ref. 1). In the case of the film geometry ($d < \lambda_C < \lambda_{AC}$) the ''continuum'' model with the transformation formula (4) used in the approximate form $f(d) \approx i/k_2 d$, which is ordinarily permissible in the microwave range,[30] gives the following expression for $R_S(d)$:

$$R_S(d) \cong \mathrm{Re}\left( -i \frac{\omega}{cd} \lambda_{AC}^2 \right) = \frac{\lambda_C^2(0)}{cd} \frac{\omega^2}{\omega_0 [1 + (\omega/\omega_0)^2]}. \tag{22}$$

According to Eq. (22), $R_S \sim \omega^2 H$ for $\omega \ll \omega_0$ and $R_S \sim (1 - \omega_0^2/\omega^2) H$ for $\omega \gg \omega_0$. It should be emphasized that expressions (21) and (22) describe the frequency dependence of the surface resistance due to the oscillations of vortices only.

The field dependence and frequency dependence of the impedance obtained in experiments on the high-frequency dynamics of the vortices have been compared with the Coffey–Clem theoretical model for the case when the static magnetic field **H** is perpendicular to the surface of the superconductor (see, e.g., Refs. 1–8).

Taking into account the ''size'' effects in the structure and dynamics of the vortex lattice for a parallel orientation of the external static magnetic field, as we have done in this paper, leads to certain features on the curves of the field dependence of the surface resistance, which are shown in Fig. 4 for various values of the frequency and film thickness. The most important feature is the appearance of a stepped structure on the $R_V(H)$ curves, which is due to the discrete changes in the number of vortex rows at the fields $H_{c1}^{(N)}(d)$ (in this paper $N=1,2$).

In addition, we should mention the different character of the $R_V(H)$ curves at a fixed number of vortex rows (i.e., in the intervals $H_{c1}^{(N)} < H < H_{c1}^{(N+1)}$, $N=1,2$) for the cases of high and low frequencies (compared with $\omega_p$): for $\omega \gg \omega_p$ the $R_V(H)$ curve increases monotonically in these field intervals for the films of various thicknesses [Fig. 4(a)]; for $\omega \ll \omega_p$ an unusual descending segment can appear on the $R_V(H)$ curves in the same field intervals [Fig. 4(b)]. For analysis of this different behavior of the field dependence of the surface resistance at high and low frequencies, let us consider the expression for $R_V(d,H)$ that follows from Eq. (20):

$$R_V(d,H) = \mathrm{Re}\, Z_V \cong \frac{\Phi_0^2 \omega^2 \eta}{4\pi d^2 c\, a(H) [\alpha_\Sigma^2(H) + (\omega\eta)^2]}, \tag{23}$$

where we have used the approximation $f(d) \approx i/k_2 d \gg d/2\lambda$. As we see from Eq. (23), for a fixed number of vortex rows

$$R_V(d,H) \cong \frac{\Phi_0^2}{4\pi c d^2 \eta} \times \begin{cases} \dfrac{\omega^2 \eta^2}{a(H)\alpha_\Sigma^2(H)}, & \omega \ll \omega_p \\ \dfrac{1 - \omega_p^2/\omega^2}{a(H)}, & \omega \gg \omega_p \end{cases}. \tag{24}$$

Thus, as follows from (24), the field dependence of $R_V(d,H)$ at high frequencies is governed by the field dependence of $a^{-1}(H)$, while that at low frequencies is governed by the field dependence of $[a(H)(\alpha + \alpha_p(H))^2]^{-1}$. At fields $H > H_{c1}^{(1)}(d)$ (i.e., $\xi \ll a(H) \ll d$, $d < \lambda$) the asymptotic expressions for $a(H)$ and $\alpha_p(H)$, as can be shown by proceeding from expressions (9) and (11), have the form

$$a(H) = \frac{\Phi_0 d}{4\lambda^2 H} \frac{1}{1 - \cosh^{-1}(d/2\lambda)}, \tag{25}$$

$$\alpha_p(H) = \frac{H\Phi_0}{4\pi\lambda^2 \cosh(d/2\lambda)} - \frac{\Phi_0^2}{4\pi d \lambda^2 a(H)}. \tag{26}$$

Thus for $\omega \gg \omega_p$, when the viscous reaction of the vortices is the governing factor, one has $R_V(d,H) \sim H$ according to (24), while at low frequencies, when the reaction of the vortices is governed by the pinning constant $\alpha_\Sigma(H)$, descending segments can appear on the $R_V(H)$ curve. Physically this means that the stiffness of the vortex system increases with increasing field faster than the number of vortices, and this can decrease the dissipation caused by vortex oscillations in the microwave field.

It can also be shown that at very large values of $H$ (and, hence, $N \gg 1$) the curve of $R_{S,M}(d) + R_V(d,H)$ asymptotically approaches the corresponding $R_S(d)$ curve that follows from the models of Refs. 9–12.

At a fixed value of $H$ the frequency dependence of the surface resistance in the model considered here agrees with that in the ''continuum'' model[9–12] for a thin film, as follows from a comparison of Eqs. (22) and (24).

## CONCLUSION

In this paper we have shown that for thin ($d < \lambda$) superconducting films placed in a magnetic field parallel to the surface, the dynamic response of the vortices to an external alternating field exhibits features due to size effects in the pinning and dynamics of the vortices. In particular, such effects should appear as steps on the curves of the surface impedance of the film as a function of the external static magnetic field because of the discrete changes in the number of vortex rows at characteristic field values $H_{c1}^{(N)}(d)$ and the corresponding changes in the vortex concentration and the elastic constants characterizing small oscillations of the vortex system about its equilibrium position. Here the frequency dependence of the surface resistance at a fixed value of the field $H$ corresponds to the analogous frequency dependence in the Coffey–Clem model.[9–12]

This study was supported in part by the Ministry for Education and Research of Germany (BMBF) through the grant TRANSFORM by way of the University of Leipzig (Grant 13 No. 7218/7), by the Ukrainian Center for Science and Technology (Project No. 1455), and by the international association INTAS (Grant No. 99-00585).

*E-mail: luzhbin@d24.imp.kiev.ua

[1] M. Golosovsky, M. Tsindlekht, and D. Davidov, Supercond. Sci. Technol. **9**, 1 (1996).
[2] N. Belk, D. E. Oates, D. A. Feld, G. Dresselhaus, and M. S. Dresselhaus, Phys. Rev. B **56**, 11951 (1997).
[3] E. Silva, M. Giura, R. Marcon, R. Fastampa, G. Balestrino, M. Marinelli, and E. Milani, Phys. Rev. B **45**, 12566 (1992).
[4] M. Giura, R. Marcon, R. Fastampa, and E. Silva, Phys. Rev. B **45**, 7387 (1992).
[5] J. Owliaei, S. Sridhar, and J. Talvacchio, Phys. Rev. Lett. **69**, 3366 (1992).
[6] A. Dulcic and M. Pozek, Physica C **218**, 449 (1993).
[7] E. K. Moser, W. J. Tomasch, M. J. McClorey, J. K. Furdyna, M. W. Coffey, C. L. Pettiete-Hall, and S. M. Schwarzbek, Phys. Rev. B **49**, 4199 (1994).
[8] V. A. Berezin, E. V. Il'ichev, V. A. Tulin, E. B. Sonin, A. K. Tagantsev, and K. B. Traito, Phys. Rev. B **49**, 4331 (1994).
[9] M. W. Coffey and J. R. Clem, Phys. Rev. Lett. **67**, 386 (1991).
[10] M. W. Coffey and J. R. Clem, IEEE Trans. Magn. **MAG-27**, 2136 (1991).
[11] E. H. Brandt, Physica C **195**, 1 (1992).
[12] E. H. Brandt, Phys. Rev. Lett. **67**, 2219 (1991).
[13] N. Klein, H. Chaloupka, G. Müller, S. Orbach, H. Piel, B. Roas, L. Schultz, U. Klein, and H. Peiniger, J. Appl. Phys. **67**, 6940 (1990).
[14] N. Klein, U. Dähne, U. Poppe, N. Tellmann, K. Urban, S. Orbach, S. Heusen, G. Müller, and H. Piel, J. Supercond. **5**, 195 (1992).
[15] P. Hartemann, IEEE Trans. Appl. Supercond. **AS-2**, 228 (1992).
[16] O. G. Vendik, M. M. Gaĭdukov, A. B. Kozyrev, S. G. Kolesov, A. Yu. Popov, and T. B. Samoĭlova, *Reviews of High-Temperature Superconductivity* [in Russian], issue 4(8), MTsNTI, Moscow (1992).
[17] A. A. Abrikosov, Zh. Éksp. Teor. Fiz. **46**, 1464 (1964) [Sov. Phys. JETP **19**, 988 (1964)].
[18] A. A. Abrikosov, *Fundamentals of the Theory of Metals* [in Russian], Nauka, Moscow (1987).
[19] S. Takács, Czech. J. Phys., Sect. B **33**, 1248 (1983).
[20] S. Takács, Czech. J. Phys., Sect. B **28**, 1260 (1978).
[21] S. Takács, Czech. J. Phys., Sect. B **38**, 1050 (1988).
[22] C. Carter, Can. J. Phys. **47**, 1447 (1969).
[23] G. Garneiro, Phys. Rev. B **57**, 6077 (1998).
[24] S. H. Brongersma, PhD Dissertation, Vrije Universiteit, Amsterdam (1996).
[25] S. H. Brongersma, E. Verweij, N. J. Koeman, D. G. de Groot, and R. Griessen, Phys. Rev. Lett. **71**, 2319 (1993).
[26] M. Ziese, P. Esquinazi, P. Wagner, H. Adrian, S. H. Brongersma, and R. Griessen, Phys. Rev. B **53**, 8658 (1996).
[27] A. Pan, M. Ziese, R. Höhne, P. Esquinazi, and S. Knappe, Physica C **301**, 72 (1998).
[28] V. V. Shmidt and G. S. Mkrtchyan, Usp. Fiz. Nauk, **112**, 353 (1974) [Sov. Phys. Usp. **17**, 459 (1974)].
[29] V. V. Shmidt, Zh. Éksp. Teor. Fiz. **57**, 2095 (1969) [Sov. Phys. JETP **30**, 1137 (1970)].
[30] O. G. Vendik, L. Kovalevich, A. P. Mitrofanov, O. V. Pakhomov, A. Yu. Popov, and T. B. Samoilova, Sverkhprovod. KIAE, **3**, 2133 (1990) [Superconductivity **3**, 1573 (1990)].

Translated by Steve Torstveit

# Anisotropy of the flux creep in the motion of vortices along twin-boundary planes in $YBa_2Cu_3O_{7-x}$ single crystals

A. V. Bondarenko,[a] A. A. Prodan, M. A. Obolenskiĭ, and R. V. Vovk

*V. N. Karazin Kharkov National University, pl. Svobody 4, 61077 Kharkov, Ukraine*

T. R. Arouri

*Physics Department of Bir-Zeit University, P.O. Box 15, Bir-Zeit, West Bank, Israel*

(Submitted September 19, 2000)
Fiz. Nizk. Temp. **27**, 463–470 (May 2001)

The anisotropy of the magnetic flux creep in vortex motion parallel to the planes of twin boundaries is investigated experimentally. It is shown that at relatively low magnetic fields the creep velocity is independent of the magnetic field and of the angle $\alpha \equiv \angle \mathbf{H}, ab$. It is found that the differential resistivity $\rho_d \equiv dE/dJ$ tends to saturation at large transport currents, where its value is approximately equal to the viscous drag on vortices in the Bardeen–Stephen model. In low magnetic fields oriented near the $ab$ plane of the crystal the trapping of flux lines between CuO superconducting planes is observed. © *2001 American Institute of Physics.* [DOI: 10.1063/1.1374717]

In spite of the many intensive experimental studies of the dynamics of the magnetic flux in the high-$T_c$ superconductor $YBa_2Cu_3O_{7-x}$ over the last ten years, a number of questions pertaining to the phase state, pinning, and dynamics of Abrikosov vortices remain open. One such question is the anisotropy of the magnetic flux pinning and creep. This situation is due to the fact that the results of magnetic experiments are subject to various interpretations. Indeed, for an orientation of the magnetic field noncollinear with the **c** axis the induced currents in single-crystal samples flow both along the $ab$ plane and along the **c** axis. In the flow of current along the **c** axis the Lorentz force is parallel to the $ab$ plane, while for current flow along the $ab$ plane it is directed off the $ab$ plane. Since the relative values of the currents flowing in the $ab$ plane and along the **c** axis vary with the angle $\alpha \equiv \angle \mathbf{H}, ab$, the relative values of the Lorentz force also vary. Therefore the results of magnetic measurements are difficult to interpret, since one does not know whether the predominant direction of the magnetic flux creep is along or off the $ab$ plane.

The most correct way to study the anisotropy of the pinning and dynamics of the magnetic flux is to make resistive measurements in which the direction of flow of the transport current is determined. However, the results of measurements in YBaCuO single crystals are hard to interpret, since they exhibit an additional anisotropy due to the presence of twin boundaries, which are two-dimensional defects. Visualization of the motion of the magnetic flux shows that the pinning on twins is minimum for motion of the magnetic flux along the planes of the twin boundaries (TBs) and is large for flux motion perpendicular to these planes; this difference is due to the different mechanisms by which the pinning force is generated at the twins. In the case of parallel motion the pinning by an ideal TB plane is zero; the pinning is mainly determined by the density of point defects, which can be higher at the twin boundary than in the bulk of the crystal. For motion of vortices perpendicular to a TB plane, on the other hand, the pinning is due to suppression of the order parameter at the twins and can be large.[1] A comparison of the current–voltage (I–V) characteristics measured in the motion of the magnetic flux parallel to and perpendicular to the TB plane shows that in the second case the pinning is approximately ten times as high as in the first.[2]

Pinning on twins is also manifested in a rotation of the field vector **H** out of the TB plane. This is due to the fact that in tilted fields at angles $\theta \equiv \angle \mathbf{H}$,TB less than a certain critical value $\theta_{cr}$, a portion of the vortex line is trapped by the TB plane.[3] Experimental studies show that the critical angle can reach a value of 50° (Ref. 4) or even 70° (Ref. 5).

Previous resistive studies of the anisotropy of flux creep in YBaCuO single crystals have been done in a geometry in which the Lorentz force is noncollinear with the plane of the twin boundary.[5,6] In this case the magnetic flux will move along the direction of the Lorentz force, provided that the motive force is large enough to break the trapped vortex segments away from the TB plane. Otherwise there will either be no creep or else the magnetic flux will move parallel to the component of the Lorentz force directed along the TB plane. Such motion has actually been observed for a field orientation $\mathbf{H} \| \mathbf{c}$ (Ref. 7) and in magnetic fields tilted with respect to the TB plane.[5] The foregoing arguments and the experimental data mentioned show that for angles $\theta \leqslant \theta_{cr}$ the measured values can differ, depending on the orientation of the Lorentz force relative to the TB plane; this is confirmed by a comparison of the results in Refs. 5 and 6.

The goal of the present study was to investigate the anisotropy of the magnetic flux creep in the motion of vortices along the planes of the twin boundaries, i.e., in the direction of easiest vortex motion, when the influence of the TB on the dynamics of the magnetic flux is apparently minimal. Measurements of the current–voltage (I–V) characteristics were made on a bridge cut from a $YBa_2Cu_3O_{7-x}$ single crystal. The boundaries of the twins in the measured part of the bridge were oriented in the same direction. The critical tem-

 

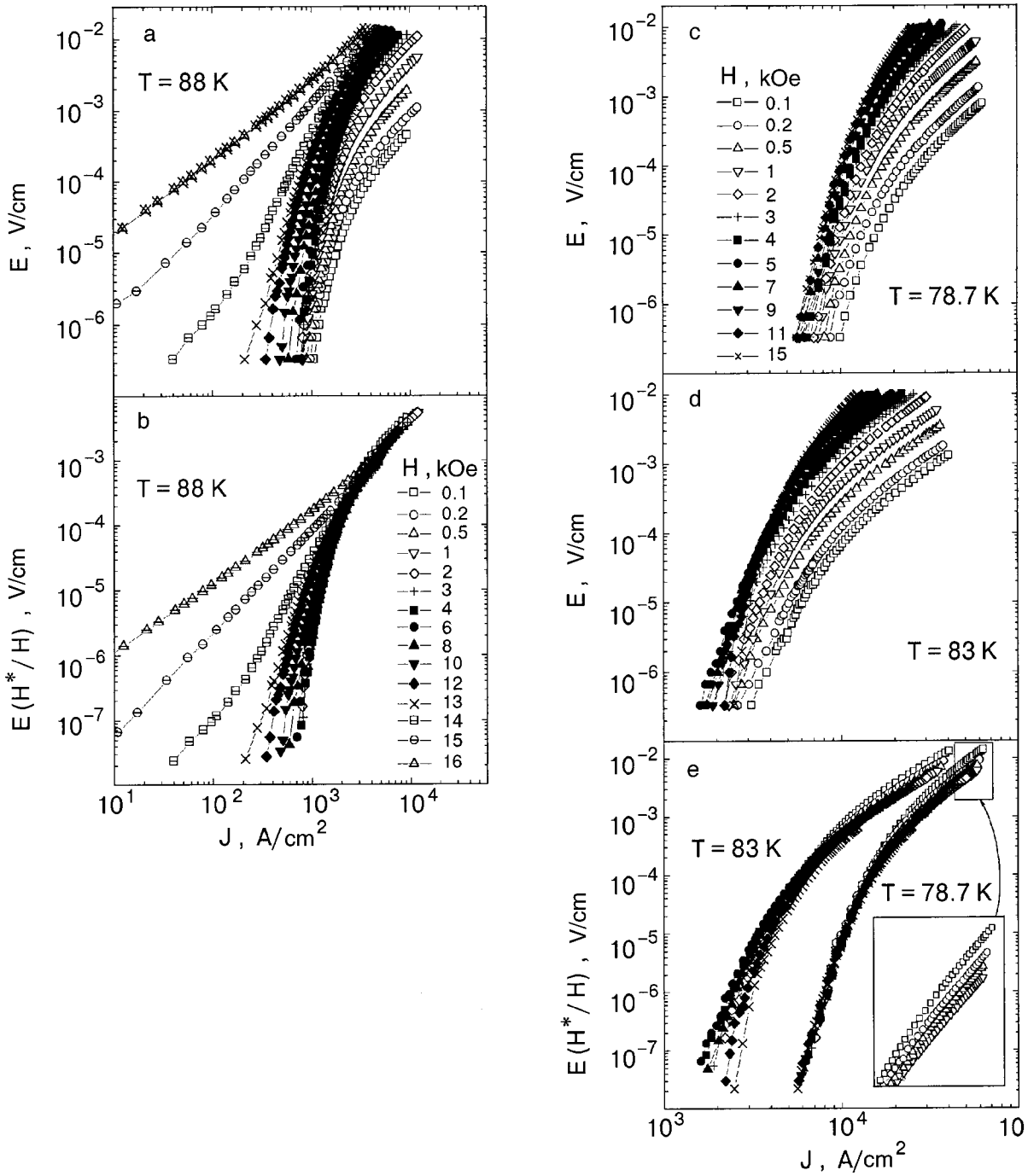


FIG. 1. Current–voltage (I–V) characteristics obtained in a field $\mathbf{H}\|\mathbf{c}$ at various $H$ for $T=88$ K (a), 83 K (d), and 78.7 K (c); the corresponding I–V characteristics normalized to the magnitude of the magnetic field, $E(H^*/H)$, where $H^*=1$ kOe (b,e).

perature of the sample was 93 K, and the width of the superconducting transition was 0.3 K. The transport current vector **J** was parallel to the $ab$ plane of the crystal and was oriented perpendicular to the plane of the TBs. The magnetic field vector **H** was rotated away from the **c** axis toward the $ab$ plane in such a way that it was always oriented parallel to the TB plane; this parallelism was maintained to an accuracy of 0.3° by making use of the minimum observed on the angle dependence of the resistivity at temperatures slightly above the melting temperature of the vortex lattice. The angle $\alpha \equiv \angle \mathbf{H},ab$ was adjusted to within 0.1°. The stability of the temperature during the measurements was $\approx 0.03$ K, and that of the magnetic field was 0.05% or better. Measurements of the sample in the normal state showed that its overheating at the highest level of energy dissipation, $10^{-4}$ W, was not more than 0.05 K.

Figure 1 shows the I–V characteristics measured at $T=88$, 83, and 78.7 K in various magnetic fields for the orientation of the field vector $\mathbf{H}\|\mathbf{c}$. It is seen that at 88 K and 78.7 K the $E(J)$ curves are continuously shifted to lower transport currents as the magnetic field is increased. Similarly, at $T=83$ K and in magnetic fields up to 7 kOe the $E(J)$ curves are also shifted to lower transport currents with increasing magnetic field. As the magnetic field is increased further, a substantial increase in the slope of the I–V characteristics is observed, so that the upper parts of the $E(J)$

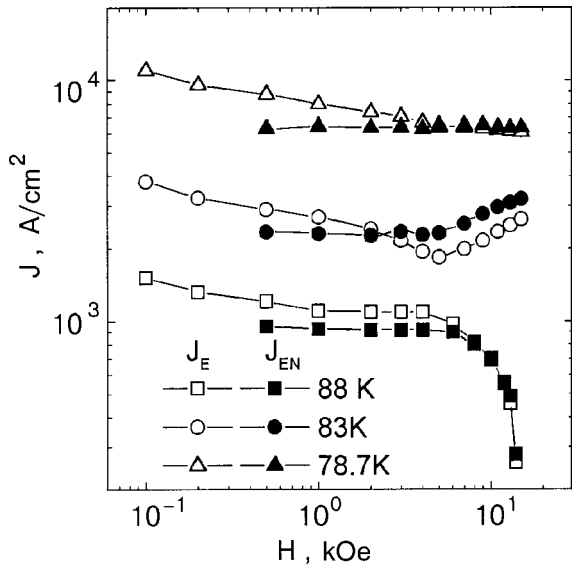


FIG. 2. Field dependence of the ''critical'' current $J_E$ determined according to the electric field levels $E=10^{-6}$ V/cm and $E_N \equiv E(H^*/H)=10^{-5}$ V/cm and normalized to the value of the magnetic field.

curves as before are shifted to lower transport currents, while the lower parts, corresponding to small transport currents, are now shifted to higher currents. Thus, if the critical current $J_E$ is determined from the level of the measured electric field $E=\text{const}$ at a low level of energy dissipation, e.g., at $E=10^{-6}$ V/cm, then at temperatures of 88 K and 78.7 K the current $J_E$ will decrease continuously with increasing magnetic field, while at $T=83$ K the $J_E(H)$ curve will be nonmonotonic, as is seen in Fig. 2.

Figure 1b and 1d shows the I–V characteristics normalized to the value of the magnetic field, $E(H^*/H)(J)$, where $H^*=1$ kOe. We see that at $T=88$ K in magnetic fields $H \leqslant 5$ kOe the curve of $E(H^*/H)$ versus $J$ lies along a universal curve. When the temperature is lowered, the interval of magnetic fields in which field scaling of the I–V characteristics is observed increases: at $T=83$ K scaling is observed in the field range $H \leqslant 9$ kOe, while at 78.7 K it is observed over the entire range of magnetic fields investigated, $H \leqslant 15$ kOe. For the magnetic field orientation $\mathbf{H} \| \mathbf{c}$ the electric field is given by the relation $E=vB$, where $v$ is the velocity of the magnetic flux and $B$ is the magnetic induction. Therefore, the observed field scaling of the I–V characteristic is evidence that the velocity of the vortices in low magnetic fields is independent of the magnitude of the magnetic field.

Figure 3a shows the I–V characteristics measured at different angles $\alpha$ in a magnetic field of 15 kOe at 78.7 K, and Fig. 3b shows those measured in a magnetic field of 0.1 kOe at 83 K. We see that the electric field increases continuously with increasing angle $\alpha$. This means that $J_E$ decreases with increasing angle $\alpha$. Figure 3c and 3d show the same I–V characteristics normalized to an anisotropy parameter that depends on the angle $\alpha$, $\varepsilon_\alpha \equiv (\varepsilon^2 \cos^2\alpha + \sin^2\alpha)^{1/2}$, which for the superconductor YBaCuO is approximately equal to 1/6. We see that for $\alpha \geqslant 15°$ the curves of $E/\varepsilon_\alpha(J)$ lie on a universal curve. According to the Bardeen–Stephen model,[8] the energy dissipation occurs on account of ordinary resistive processes in the cores of the vortices, the size of which is approximately equal to the coherence length $\xi$. In a layered superconductor the coherence length along the $ab$ plane is independent of $\alpha$, while in the perpendicular direction it decreases as $\xi\varepsilon_\alpha$. Consequently, the transverse cross-sectional area of the vortices and, accordingly, the total volume of the cores, decrease with angle $\alpha$ as $\varepsilon_\alpha$. Therefore, in a layered superconductor the electric field during the motion of vortices with a velocity $v$ is given by the relation $E=Bv\varepsilon_\alpha$, in which the cofactor $\varepsilon_\alpha$ determines the anisotropy of the viscous drag of the vortex lines. The observed angular scaling of the I–V characteristics, on the other hand, attests to the fact that at angles $\alpha > 15°$ the velocity of the vortices is independent of $\alpha$.

For $\alpha < 15°$, as can be seen in Fig. 3c and 3d, the electric field decreases with angle $\alpha$ faster than is given by the relation $E=Bv\varepsilon_\alpha$ under the assumption that $v=\text{const}$. The most probable reason for this behavior is self-pinning. This type of pinning occurs in layered superconductors and is due to modulation of the order parameter along the **c** axis. It is assumed that when the vector **H** is oriented parallel to the $ab$ plane the vortex lines lie between CuO superconducting layers to minimize the core energy.[9] Therefore, they are found in the field of a periodic potential whose maxima correspond to the cores of the vortex lines being situated in the CuO planes. It is assumed that in a magnetic field tilted at angles $\alpha \leqslant \varepsilon$ a stepped structure of the vortex lines is realized. A part of the vortex line as before lies between the CuO planes, and part of it is oriented parallel to the **c** axis, as is shown in the inset in Fig. 3e. If the pinning of the vortex segments $L_{ab}$ oriented along the $ab$ plane is very large, then energy dissipation can arise as a result of the motion of the vortex segments $L_c$. In fact, since the segments $L_{ab}$ and $L_c$ are mutually orthogonal, they will not interact with each other and thus will move independently of each other.[10] In the motion of the vortex segments $L_c$ the electric field can be written as $E=B_c v$, where $B_c = B\sin\alpha$ is the magnetic induction along the **c** axis. Figure 3e and 3f shows the I–V characteristics measured at $\alpha = 90°$ and at angles $\alpha \leqslant \varepsilon (\alpha \leqslant 15°)$ and normalized to $\sin\alpha$. It is seen that at a magnetic field 15 kOe and in the angle interval $1° \leqslant \alpha \leqslant 15°$ the normalized I–V characteristics lie on a universal curve corresponding to $E(J)$ measured at $\alpha = 90°$. This means that the velocity of the vortex segments $L_c$ $(v = E/B\sin\alpha)$ is independent of the angle $\alpha$ and is equal to the velocity of the vortices for a field orientation $\mathbf{H} \| \mathbf{c}$. Analogous behavior is also observed at a magnetic field $H=0.1$ kOe in the angle interval $4° \leqslant \alpha \leqslant 15°$. At angles $\alpha \leqslant 2°$ [see Fig. 3b] the electric field is independent of the angle $\alpha$. This behavior of the I–V characteristics in very weak magnetic fields can be explained by the trapping of the vortex lines between CuO superconducting planes. It is assumed that at angles $\alpha$ less than the trapping angle $\alpha_L$ the vortex lines are localized between CuO superconducting planes to minimize the core energy. Therefore, the pinning of the magnetic flux at angles in the range $\alpha < \alpha_L$ is independent of the orientation of the field vector **H**. The value of the trapping angle is given by the relation $\alpha_L \cong 2\nu H_{c1}/H$,[11] where $\nu \cong l_c/l_{ab}$ is the demagnetizing factor, $H_{c1}$ is the lower critical field, and $l_c$ and $l_{ab}$ are the dimensions of the sample along the **c** axis and along the $ab$ plane, respectively. The demagnetizing factor of our sample was approximately 0.05, and the field $H_{c1}^c \approx 100$ Oe at $T=82$ K;

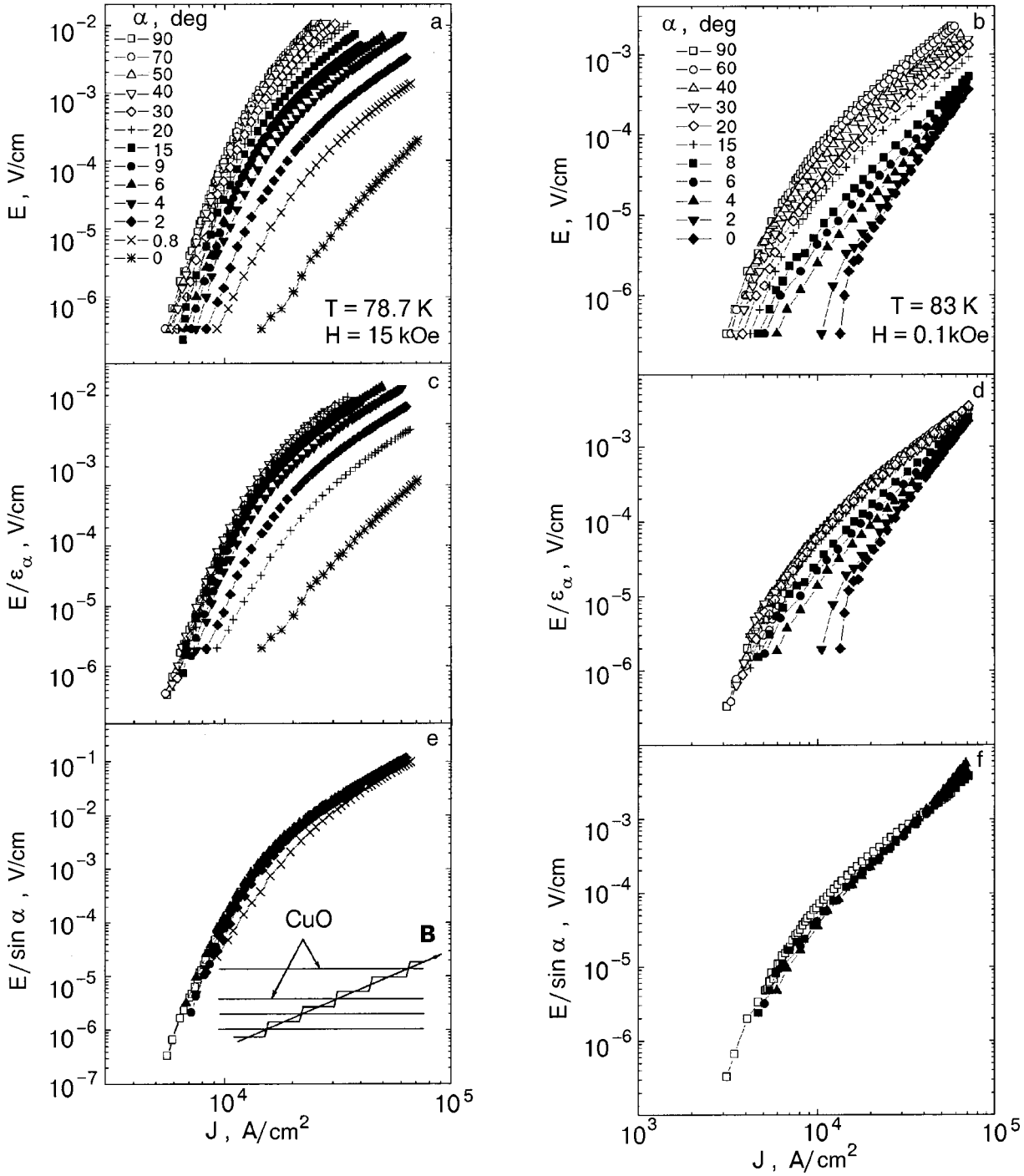


FIG. 3. I–V characteristics measured at $T=78.7$ K in a field of 15 kOe (a) and at $T=83$ K and $H=0.1$ kOe (b) for different angles $\alpha\equiv\angle\mathbf{H},ab$; the corresponding I–V characteristics normalized to the anisotropy parameter $\varepsilon_\alpha$ (c,d); the I–V characteristics measured at $\alpha=90°$ and at $1°\leqslant\alpha\leqslant15°$, normalized to $\sin\alpha$ (e,f). The inset in Fig. 3e shows the stepped structure taken on by the vortex line at angles $\alpha\leqslant15°$.

consequently, in a magnetic field of 100 Oe the value of the trapping angles is estimated as $\alpha_L\cong0.1(\alpha_L\cong3°)$. The value obtained from the experiment, $\alpha_L(100\text{ Oe})\cong2°$, is in satisfactory agreement with the theoretical estimates. In a magnetic field of 15 kOe, in contrast, the trapping angle is very small, $\alpha_L\cong0.1°$, and therefore trapping of the vortex lines is not observed within experimental accuracy.

Let us turn to a discussion of the results. As has been shown, in low magnetic fields and at angles $\alpha>\varepsilon$ the velocity of the magnetic flux is independent of the magnitude of the magnetic field and of the angle $\alpha$. From the standpoint of the collective pinning theory[1] this attests to the realization of single-vortex creep. Indeed, according to the collective pinning theory, at angles $\alpha<\varepsilon$ the Lorentz force and pinning force are given by the relations $F_L=J\Phi_0L(\alpha)/c$ and $F_p=U_0/r_p$, in which the correlation length $L(\alpha)=L_0/\varepsilon_\alpha$, the pinning radius $r_p\approx\xi\varepsilon_\alpha$ in the given experimental geometry, and the correlation length $L_0$ and pinning potential $U_0$ corresponding to the field orientation $\mathbf{H}\|\mathbf{c}$ are independent of the magnitude of the magnetic field. Therefore, by equating the Lorentz force to the pinning force, we obtain for the critical current the relation $J_c=U_0c/\Phi_0L_0$, which depends on nei-

ther the magnitude of the magnetic field nor on the angle $\alpha$.

As we have said, at angles $\alpha < \varepsilon$ the I–V characteristics constructed in the coordinates $E/\sin\alpha$–$J$ lie on a universal curve, corresponding to $E(J)$ measured for a field orientation $\mathbf{H}\|\mathbf{c}$. The angle scaling found is experimental confirmation of the realization of a stepped structure of the vortex lines for a magnetic field orientation in the vicinity of the $ab$ plane. Here it is assumed that the pinning of the vortex segments trapped between CuO superconducting planes is strong enough that the magnetic flux creep is determined by the motion of the vortex segments $L_c$ oriented along the **c** axis. According to the collective pinning theory, the angle dependence of the critical current and pinning potential of the $L_c$ segments is determined by the relations $J_c(\alpha) = J_c\varepsilon/|\alpha|$ and $U(\alpha) = U_0|\alpha|/\varepsilon$, in which the critical current $J_c^c$ and pinning potential $U_0$ correspond to the field orientation $\mathbf{H}\|\mathbf{c}$. We note that in low magnetic fields the measured I–V characteristics are described well by the equation

$$E = E_0 \exp[-U/k_B T(J_c/J)^{\mu}] \tag{1}$$

with a value of the exponent $\mu = 1$. When the functions $U(\alpha)$ and $J_c(\alpha)$ are substituted into this equation, it turns out that the product $U(\alpha)J_c(\alpha)$ in the argument of the exponential function for $\mu = 1$ is independent of the angle $\alpha$ and has the same value as for the field orientation $\mathbf{H}\|\mathbf{c}$. Thus the angular scaling of the $E(J)$ curves over the entire interval of angles $\pi/2 \leqslant \alpha \leqslant 0$ can be explained using the concepts of collective pinning theory.

We note that this angular scaling of the I–V characteristic was not observed in the previous resistive studies of the anisotropy of the magnetic flux creep.[5,6] The most probable reason for this difference is the influence of twins. In our experimental geometry the vortices move parallel to the TB plane, and their pinning is governed solely by the interaction with point defects. In the previous experiments, in contrast, the Lorentz force was oriented at an angle of 45° (Ref. 6) or perpendicular (Ref. 5) to the TB plane. For such a mutual orientation of the Lorentz force and the TB plane, the pinning force along the vortex lines in tilted magnetic fields is substantially nonuniform, and the pinning of the vortex segments trapped by the planes of the twin boundaries is due to the suppression of the order parameter at the twins. In the motion of vortex lines perpendicular to the TB plane this pinning is very large, and the influence of the TBs is already felt at angles $\alpha \geqslant 20°$ (Ref. 5). Therefore the difference between our experimental data and the previously published results is entirely reasonable.

As we have said, the field scaling of the I–V characteristics is realized in a restricted interval of magnetic fields. Let us consider the possible factors that can disrupt the scaling of the I–V characteristics measured at different temperatures. It is seen in Fig. 1e that at $T = 78.7$ K the $E(J)$ curves normalized to the magnitude of the external field conform to the universal curve at transport currents that are not very large. At large transport currents the field scaling is realized in magnetic fields $H \geqslant 1$ kOe, while in low fields ($H \leqslant 0.5$ kOe) a slight growth of the normalized electric field is observed as the magnetic field is decreased. This behavior is probably due to the influence of twins. In a magnetic field of 0.1 kOe the intervortex distance $a_0 \cong (\Phi_0/B)^{1/2} \cong 450$ nm is

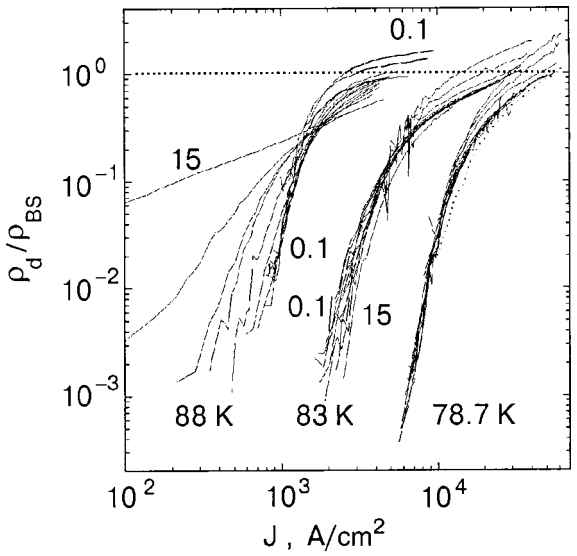


FIG. 4. Current dependence of the normalized differential resistivity, obtained for the I–V characteristics presented in Fig. 1.

comparable to the distance between twins. Since the order parameter in the TB plane is suppressed,[12] one expects that in low magnetic fields a significant part of the vortex lines will be trapped by the TB planes, and the cores of the trapped vortex lines are deformed:[13] the size of the core in the direction parallel to the plane of the defect increases, while in the perpendicular direction it remains equal to the coherence length $\xi$. Since the volume of the core of the trapped vortices increases, so does the viscous drag force on these vortices. Therefore, at an equal velocity the electric field induced by a vortex line trapped by a planar defect will be larger than the electric field induced by a vortex localized outside the planar defect. This situation corresponds to growth of the differential resistivity $\rho_d \equiv dE/dJ$ in low magnetic fields (see Fig. 4). Figure 4 shows the $\rho_d(J)$ curves normalized to the viscous drag of the magnetic flux flow in the Bardeen–Stephen model, $\rho_{BS} = \rho_N B/B_{c2}$ (Ref. 8), where $\rho_N$ is the resistivity of the sample in the normal state and $B_{c2}$ is the magnetic induction corresponding to the second critical field. We determined the value of $\rho_N$ by extrapolating the linear part of the $\rho(T)$ curve, and $B_{c2} = -(dB_{c2}/dT)(T_c - T)$ was estimated using the value $dB_{c2}/dT = -1.8$ T/K.[14] As we see in Fig. 4, at a temperature of 78.7 K in magnetic fields $H \geqslant 1$ kOe the ratio $\rho_d/\rho_{BS}$ as a function of current is independent of the current density, and $\rho_d \to \rho_{BS}$ at large currents. This indicates that the current density is close to critical. In magnetic fields $H \leqslant 0.5$ kOe, on the other hand, at large values of the transport current the differential resistivity exceeds $\rho_{BS}$, and the ratio $\rho_d/\rho_{BS}$ increases with decreasing field. In addition, $\rho_d$ increases continuously with increasing current in the investigated current range. This last fact probably means that the critical current for vortices trapped by the TB planes is higher than for vortices immersed in the bulk of the crystal; this agrees with previous experimental studies. The growth of the differential resistivity with decreasing magnetic field at constant current density is due to an increase in the fraction of vortex lines trapped by TB planes.

Similar behavior of the I–V characteristic and the differ-

ential resistivity at large transport currents is also observed at $T=83$ K. The difference between the I–V characteristics measured at 78.7 and 83 K is that at 83 K in fields $H \geqslant 8$ kOe at a low transport current density the $E(J)$ curves are shifted to higher transport currents. This corresponds to a nonmonotonic field dependence of the measured ''critical'' current $J_E$ and $J_{EN}$. At present there are two widely discussed mechanisms that predict an increase of the measured current with increasing magnetic field. One of them is based on the collective pinning theory and assumes that the critical current for depinning is independent of the magnetic field, and that the observed increase in the measured current $J_E$ is due to a transition from single-vortex creep at high transport currents to flux-bundle creep at low currents. This crossover takes place at currents $J<J_b \approx J_0(L_c/\varepsilon a_0)^{7/5} \propto B^{0.7}$. Since for $J<J_b$ the activation energy of flux bundles decreases rapidly with decreasing transport current, $U(J) \propto J^{5/2}$, the creep velocity of the vortices and the electric field decrease rapidly, and the measured current $J_E$ increases. The experimental data presented in Fig. 1 agree with the predictions of the collective pinning theory: the crossover current and the current $J_E$ indeed increase with increasing magnetic field. The second mechanism[15] assumes a transition from a quasi-ordered vortex lattice in low magnetic fields to a highly disordered vortex system, characterized by braiding of the vortex lines, in high fields. Up till now the dynamic properties and pinning of such a disordered vortex system have not been investigated theoretically, and it is therefore impossible to draw any conclusions about whether the experimental data can be interpreted in the framework of that model.

The I–V characteristics measured at 88 K differ from those measured at lower temperatures in that at magnetic fields $H>8$ kOe the $E(H^*/H)(J)$ curves deviate from the universal curve. At low current densities the electric field increases continuously with increasing magnetic field. This corresponds to a decrease of the current $J_{EN}$. Also, as we see in Fig. 1a and 1b, the negative curvature of the I–V characteristics observed in the entire investigated current range at magnetic fields below 8 kOe gives way at $H>8$ kOe to a positive curvature at low currents. This circumstance indicates that when Eq. (1) is used to describe the I–V characteristics, the exponent $\mu$ changes sign: $\mu>0$ in low fields, and $\mu<0$ in high fields. The transition from positive values of the exponent $\mu$ to negative values is indicative of a change in the current dependence of the activation energy for creep and, hence, of a change of creep mechanisms. This transition is in agreement with previous resistive studies,[16] which showed that as the magnetic field is increased at high temperatures, elastic creep, for which the exponent $\mu>0$, gives way to plastic creep, which is due to the motion of dislocations of the vortex lattice and is characterized by an exponent $\mu=-1/2$. Since the activation energy for plastic creep decreases with increasing magnetic field,[16,17] the vortex velocity and the electric field increase with increasing magnetic field, while the current $J_E$ decreases.

Let us conclude with a summary of the main conclusions. We have shown that in relatively low magnetic fields the velocity of the vortices is independent of the magnitude and orientation of the magnetic field. The results indicate that when the magnetic field is oriented near the $ab$ plane of the crystal, the vortex lines have a stepped structure. Dissipative processes arise here because of the creep of vortex segments oriented along the **c** axis of the crystal, and the velocity of these segments is equal to the velocity of vortices in the case of a field orientation $\mathbf{H} \| \mathbf{c}$. These features of the magnetic flux creep can be explained in the framework of the collective pinning theory. We have also shown that at high transport currents and not very low magnetic fields the differential resistivity goes to saturation and is approximately equal to the viscous drag of the magnetic flux in the Bardeen–Stephen model. In low magnetic fields a deviation from the Bardeen–Stephen model is observed which can be explained by the deformation of the cores of the vortex lines trapped by the planes of twin boundaries. We have discussed the details of the behavior of the field dependence of the ''critical'' current measured at different temperatures.

[a)]E-mail: Aleksandr.V.Bondarenko@univer.kharkov.ua

[1] G. Blatter, M. V. Feigel'man, V. B. Geshkenbein, A. I. Larkin, and V. M. Vinokur, Rev. Mod. Phys. **66**, 1125 (1994).
[2] M. A. Obolenskiĭ, A. V. Bondarenko, V. I. Beletskiĭ, R. V. Vovk, A. A. Prodan, M. Él'-Siidavi, D. Niarkhos, M. Pissas, G. Kallias, and A. G. Sivakov, Funktsional'nye Materialy **2**, 403 (1995).
[3] G. Blatter, J. Rhyner, and V. M. Vinokur, Phys. Rev. B **43**, 7826 (1991); E. B. Sonin, *ibid.* **48**, 10287 (1993); W. K. Kwok, J. A. Frendrich, V. M. Vinokur, A. E. Koshelev, and G. W. Grabtree, Phys. Rev. Lett. **76**, 4596 (1996).
[4] R. Hiergeist and R. Hergt, Phys. Rev. B **55**, 3258 (1997).
[5] A. V. Bondarenko, Physica B **284–288**, 833 (2000).
[6] V. F. Solovjov, V. M. Pan, and H. C. Freyhardt, Phys. Rev. B **50**, 13724 (1994); V. M. Pan, V. F. Solovjov, and H. C. Freyhardt, Physica C **279**, 18 (1997).
[7] C. Duran, P. L. Gammel, R. Wolfe, V. J. Fratello, D. J. Bishop, J. P. Rice, and D. M. Ginsberg, Nature (London) **357**, 474 (1992); A. I. Belyaeva, S. V. Vojtsenya, V. P. Yurijev, M. A. Obolenskii, and A. V. Bondarenko, Solid State Commun. **85**, 427 (1993).
[8] J. Bardeen and M. J. Stephen, Phys. Rev. A **140**, 1179 (1965).
[9] M. Tachiki and S. Takahashi, Solid State Commun. **70**, 291 (1989).
[10] P. H. Kes, J. Aarts, V. M. Vinokur, and C. J. van der Beek, Phys. Rev. Lett. **64**, 1063 (1990); S. Theodorakis, Phys. Rev. B **42**, 10172 (1990); L. N. Bulaevskii, L. N. Ledvij, and V. G. Kogan, *ibid.* **46**, 366 (1992).
[11] B. I. Ivlev, Yu. N. Ovchinnikov, and V. L. Pokrovsky, Mod. Phys. Lett. B **5**, 73 (1991); S. S. Maslov and V. L. Pokrovsky, Europhys. Lett. **14**, 591 (1991).
[12] L. Ya. Vinnikov, I. V. Grigor'eva, A. Gurevich, and A. E. Koshelev, Superconductivity **3**, 1121 (1990).
[13] A. Gurevich, Phys. Rev. B **46**, 3187 (1992); *ibid.*, **48**, 12857 (1993).
[14] U. Welp, S. Flesher, W. K. Kwok, J. Downey, G. W. Crabtree, H. Claus, A. Erb, and G. Muller-Vogt, Phys. Rev. B **47**, 12369 (1993).
[15] D. Etras and D. R. Nelson, Physica C **272**, 79 (1996).
[16] M. A. Obolenskii, A. V. Bondarenko, V. A. Shklovskii, R. V. Vovk, and A. A. Prodan, Low Temp. Phys. **24**, 53 (1998); A. V. Bondarenko, V. A. Shklovskij, M. A. Obolenskii, R. V. Vovk, A. A. Prodan, M. Pissas, D. Niarchos, and G. Kallias, Phys. Rev. B **58**, 2445 (1998).
[17] Y. Abulafia, A. Shaulov, Y. Wolfus, R. Prozorov, L. Burlachkov, Y. Yeshurun, D. Majer, E. Zeldov, H. Wuhl, V. B. Geshkenbein, and V. M. Vinokur, Phys. Rev. Lett. **77**, 1596 (1996).

Translated by Steve Torstveit

# Change of the superconducting, transport, and microscopic properties of transition metals upon introduction of interstitial impurities and deformation-induced defects

V. I. Sokolenko[a] and Ya. D. Starodubov

*National Science Center, ''Kharkov Institute of Physics and Technology,'' ul. Akademicheskaya 1, 61108 Kharkov, Ukraine*

B. A. Merisov[b] and G. Ya. Khadzhay

*V. N. Karazin Kharkov National University, pl. Svobody 4, 61007 Kharkov, Ukraine*

(Submitted November 16, 2000)
Fiz. Nizk. Temp. **27**, 471–481 (May 2001)

For group-V transition metals (Nb, Ta) containing different concentrations of interstitial impurities (O, C, N, H) and deformation-induced defects, a numerical calculation of various effective microscopic characteristics averaged over the Fermi surface and of the band parameters in the framework of the Friedel model is carried out using the experimentally determined values of the superconducting transition temperature $T_c$ and the temperature dependence of the resistivity in the interval $T_c < T \lesssim 300$ K. The causes of the polar character discerned in the influence of interstitial impurities and dislocations on the investigated physical characteristics are discussed.  [DOI: 10.1063/1.1374718]

## INTRODUCTION

Group-V transition metals are *d*-band superconductors, the superconducting transition temperature $T_c$ of which is the highest among the monatomic substances. Quantitative calculations have been carried out for their electronic and phonon spectra, microscopic parameters, quasiparticle interaction characteristics, and superconducting and transport properties.[1–9] The results agree with the experimentally measured values of $T_c$ and of the superconducting gap and with the temperature dependence of the resistivity $\rho$ and other properties in the temperature interval $T_c < T \lesssim \Theta$ ($\Theta$ is the Debye temperature).[9,10]

There are data on how various physical characteristics of group-V transition metals are affected by hydrostatic compression,[11–15] amorphization and plastic deformation,[16] and interstitial impurities.[17–23] It is of considerable fundamental and practical interest to investigate further how the properties of these metals depend on the form of the distortions and the type of defects of the crystal lattice.

Simplified calculations of the effective changes in a number of microscopic characteristics of nonideal transition metals can be done using the approach proposed in Ref. 24. This approach is based on the results of Refs. 25 and 26, which takes into account the influence of the lifetime of the electrons on some of the basic physical parameters of A-15 compounds and bcc transition metals. In this model one uses the band parameters of the perfect crystal and an experimentally determined quantity — the resistivity — characterizing the real object. In Ref. 25 certain assumptions about the relation of the parameters of the superconductivity to the corresponding quantities characterizing the band structure were incorporated into the general scheme. The theoretical development of this approach has been elaborated in a number of papers (see, e.g., Ref. 25 and references cited therein). The present paper is a development of the research reported in Ref. 24 and is devoted to investigation of how a complex of superconducting, transport, and microscopic characteristics are altered for group-V transition metals containing interstitial impurities and deformation-induced defects.

## SAMPLES AND PROCEDURES

We investigated samples of Nb and Ta with various concentrations of interstitial impurities (O, C, N, H) in the initial state. The samples are labeled with the rounded-off value of the resistivity ratio $\rho_{294\,\mathrm{K}}/\rho_n$. The sample Nb-13 was obtained by rolling sample Nb-17 to a deformation of 57% at 20 K. The average density of dislocations $N_{\mathrm{dis}}$ for Nb-13 was $\sim 10^{11}$ cm$^{-2}$, which is approximately $10^3$ times larger than for Nb-17.[24] The values of $\rho_{294\,\mathrm{K}}$ were determined at $T = 294$ K, while those of $\rho_n$ were determined in the normal state at 10 K for Nb and at 5 K for Ta. The characteristics of the samples studied are presented in Table I, from which it is seen that the value of $\rho_{294\,\mathrm{K}}/\rho_n$ for Nb decreases with increasing concentration of interstitial impurities. The quantitative concentration of interstitial impurities in the Ta samples was not determined, but from a comparison of the data for the Ta and Nb samples in Table I it follows that the concentration of interstitial impurities is higher in Ta-16 than in Ta-420. This is probably because of the relatively low vacuum in which sample Ta-16 was annealed.

The resistivity of the samples was measured in a medium of gaseous helium in the temperature interval $T_c < T \lesssim 300$ K. The measurements of $T_c$ were done by a resistive method (accurate to $\pm 0.01$ K).

The experimental temperature dependence of the resistivity of the Nb and Ta samples was processed using the formula

$$\rho(T) = \rho_0 + b(T/\Theta)^3 J_3(\Theta/T) + c(T/\Theta)^5 J_5(\Theta/T), \quad (1)$$

where $\rho_0$ is the residual resistivity, $b$ and $c$ are the intensities of interband and intraband scattering, $\Theta$ is the Debye temperature, and $J_n(\Theta/T)$ are the Debye integrals. The value of

 

TABLE I. Characteristics of the niobium and tantalum samples.

| Sample | State | Preparation conditions | Total interstitial impurity concentration $C_i$, $10^{-2}$ at. % | $\rho_{294\,K}/\rho_n$ |
|---|---|---|---|---|
| Nb-80 | Large-grained polycrystalline | Electron-beam melting in oil-free vacuum | ≅20 | 80.1 |
| Nb-17 | Single-crystal | Electron-beam melting + annealing in a vacuum of $10^{-4}$ Pa, $T=1623$ K, $t=8$ h | ≅32 | 16.7 |
| Nb-13 | Single-crystal deformed 57% by rolling at 20 K | Electron-beam melting + annealing in a vacuum of $10^{-4}$ Pa, $T=1623$ K, $t=8$ h | ≅32 | 13.4 |
| Ta-420 | Single-crystal | Electric-arc melting + annealing in a vacuum of $1.3\times10^{-5}$ Pa, $T=2300$ K, $t=6$ h | ··· | 420.2 |
| Ta-16 | Single-crystal | Electric-arc melting + annealing in a vacuum of $1.3\times10^{-3}$ Pa, $T=1000$ K, $t=6$ h | ··· | 15.7 |

$\Theta$ in this case is determined to an accuracy of $\pm0.5$ K. Formula (1) describes to good accuracy ($\sim$0.2–1.0%) the experimental values of $\rho(T)$ for the transition metals.[17,24,27]

Table II gives the values of the parameters $\rho_0$, $b$, $c$, and $\Theta$ calculated according to formula (1) with minimization of the rms error $\sigma$; also shown are the measured values of $T_c$ and the values of $d\rho/dT|_{T\cong1.11\Theta}$ determined graphically. The values of $\rho_0$, $b$, $c$, and $\Theta$ for Ta-16 and Ta-420 and the values of $\rho_0$, $b$, $c$, $\Theta$, and $d\rho/dT|_{T\cong1.11\Theta}$ for Nb-17 and Nb-13 were determined previously.[17,24] The possibility of using formula (1) to describe the electrophysical properties of transition metals containing defects in the normal state makes it possible to pose the question of the effective influence of defects on the parameters of the theory of the superconducting state of these metals; this corresponds to the basic ideas of Refs. 25 and 26 (see Introduction). Naturally, here it is assumed that the presence of defects does not affect the basic qualitative ideas of the two-band theory of transition metals[5,28] or of the ''scenario'' for the onset of superconductivity described in Refs. 1 and 10.

For calculating a number of effective microscopic parameters averaged over the Fermi surface for Nb and Ta (taking into account effects due to the lifetime of the electrons in their scattering on defects and thermal phonons) we used a system of equations constructed from the following:

$$\lambda_{tr}=\frac{\hbar\Omega_p^2}{8\pi^2k_B}\left.\frac{d\rho}{dT}\right|_{T>\Theta} \tag{2}$$

is the transport electron–phonon coupling constant,[29]

$$T_c=\frac{\omega_{\log}f_1f_2}{1.2}\exp\left\{\frac{1.04(1+\lambda)}{\lambda-\mu^*(1+0.62\lambda)}\right\} \tag{3}$$

is the expression for $T_c$ from Ref. 30 and is a modification of the McMillan formula,[31]

$$\frac{\Omega_p^2\overline{\tau}}{4\pi\hbar^2}=\rho^{-1} \tag{4}$$

is the expression relating the mean lifetime $\overline{\tau}$ with the plasma frequency and the resistivity,[29]

$$\Omega_p=\left(\frac{4}{3}\pi e^2\hbar^2v_F^2N(0)\right)^{1/2} \tag{5}$$

is the plasma frequency,[32]

$$Z=\frac{0.88\xi_0^*(0)}{l_{tr}}=\frac{0.158\rho_n\Omega_p^2}{4\pi(1+\lambda)k_BT_c} \tag{6}$$

is the reduced collision frequency,[26]

$$\lambda_L^*(0)=\frac{c\hbar(1+\lambda)^{1/2}}{\Omega_p} \tag{7}$$

is the London penetration depth,[26]

$$\xi_0^*(0)=\frac{0.18\hbar v_F}{k_BT_c(1+\lambda)} \tag{8}$$

is the BCS coherence length at zero temperature,[26]

TABLE II. Parameters of the temperature dependence of $\rho$ and the values of $T_c$ for Nb and Ta in different structural states.

| Sample | $\rho_0\cdot10^3$ | $b$ | $c$ | $\Theta$, | $dp/dT\|_{T\cong1.11\Theta}$, | $\sigma$, | $T_c$, |
|---|---|---|---|---|---|---|---|
| | μΩ·m | | | K | $10^{-4}$ μΩ·m·K$^{-1}$ | % | K |
| Nb-80 | 1.91 | 0.210 | 0.175 | 271 | 5.34 | 0.48 | 9.31 |
| Nb-17 | 9.36 | 0.223 | 0.143 | 276 | 4.80 | 0.89 | 9.15 |
| Nb-13 | 14.99 | 0.201 | 0.276 | 260 | 6.20 | 1.60 | 9.28 |
| Ta-420 | 0.032 | 0.055 | 0.325 | 230 | 5.00 | 0.35 | 4.48 |
| Ta-16 | 8.58 | 0.121 | 0.184 | 229 | 4.80 | 0.20 | 4.33 |

$$\kappa^* = \frac{5.33c(1+\lambda)^{3/2}T_c\eta_{H_{c2}}}{\chi(z)v_F\Omega_p} \tag{9}$$

is the Ginzburg–Landau parameter near $T_c$,[26] and

$$\alpha = 0.5\left[1-\left(\mu^* \ln\frac{\omega_{\log}f_1f_2}{1.2T_c}\right)^2\frac{1+0.62\lambda}{1+\lambda}\right] \tag{10}$$

is the expression for the isotope effect,[31] modified in accordance with formula (3).

In these expressions $\eta_{H_{c2}}=1.25$ is the correlation for the strong-coupling case, $\chi(z)=(1+z/1.173)^{-1}$ is the correlation for the ''dirty'' limit, $c$ is the speed of light, $v_F$ is the Fermi velocity, $e$ is the charge of the electron, $\hbar$ is Planck's constant, $k_B$ is Boltzmann's constant, $\lambda$ is the electron–phonon coupling constant ($\lambda\cong\lambda_{\rm tr}$ for Nb and Ta; Ref. 8), $\mu^*$ is the Coulomb pseudopotential, $N(0)$ is the density of states at the Fermi level, $l_{\rm tr}$ is the electron mean free path, and $\omega_{\log}$ is the logarithmic mean frequency. In accordance with Ref. 30, the empirically chosen functions $f_1$ and $f_2$ have the form

$$f_1=[1+(1+\lambda/\Lambda_1)^{3/2}]^{1/3};$$

$$f_2=1+(\overline{\omega_2}/\omega_{\log}-1)\lambda^2/(\lambda^2+\Lambda_2^2),$$

with $\overline{\omega_2}/\omega_{\log}\approx 1.1$. Here $\Lambda_1=2.46(1+3.8\mu^*)$, and $\Lambda_2=1.82(1+6.3\mu^*)(\overline{\omega_2}/\omega_{\log})$.

The system of equations (2)–(10) differs from the system used in Ref. 24 by the introduction of an equation relating the magnitude of the isotope effect with the parameters of Eq. (3), making it possible to estimate the effective change of $\mu^*$ upon a change in the structural state of the superconductor.

## RESULTS

After a logarithmic averaging of Eq. (3) and the substitution of expressions for $f_1$ and $f_2$, we obtain a transcendental equation with respect to $\lambda$. This equation was solved by the method of successive approximations with the use of the values of $\mu^*$ and $\omega_{\log}$ given in Ref. 9 for Nb and Ta. As the values $T_{c0}$ corresponding to the ''ideal'' substances we took the maximum values of $T_c$ characteristic for the highly pure elements: $T_{c0}=9.46$ K for Nb,[33] and $T_{c0}=4.49$ K for Ta.[34] For Nb the value given may be an overestimate, but the data of Ref. 35, which are illustrated in Fig. 1, attest that it is realistic. It follows from Fig. 1 that at the minimum total concentration $C_i$ of interstitial impurities the curve of $T_c(C_i)$ goes to saturation near $T_{c0}=9.46$ K. The effective values obtained for the electron–phonon coupling constant $\lambda$ were used to determine the effective value of the isotope effect (there are no published data on the isotope effect for Nb and Ta) and the values of $f_1$ and $f_2$. From the character of the dependence of $f_1$ and $f_2$ on $\lambda$ it is seen that they vary extremely weakly upon small variations in $\lambda$. We therefore used in the calculations the values $f_1=\text{const}=1.142$ and $f_2=\text{const}=1.006$ for Nb and $f_1=\text{const}=1.029$ and $f_2=\text{const}=1.004$ for Ta.

From Eqs. (2) and (8) it is easy to obtain a quadratic equation with respect to $\lambda$ as a function of $\omega_{\log}$ and $T_c$ at $\alpha=\text{const}$, which makes it possible to estimate the change of $\lambda$ of a superconductor in different structural states. Unlike

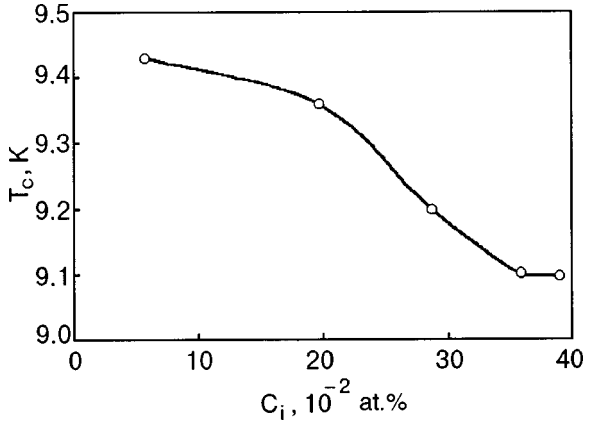


FIG. 1. Dependence of the superconducting transition temperature of Nb on the total concentration of interstitial impurities (C, O, N, H).[35]

$T_c$, the value of $\omega_{\log}$ has not been determined directly in experiment, but it can be obtained in an indirect way. It follows from Fig. 2, in which the experimental values of $\Theta$ for a number of metals (Pb, Ta, Nb, V, and Mo) are compared with the values of $\omega_{\log}$ calculated in Ref. 9, that $\omega_{\log}\cong 0.67\Theta$. We note that this dependence correlates with the known relation for transition metals $\langle\omega^2\rangle^{1/2}\cong 0.69\Theta$ (Ref. 2).

The values of $\lambda$, $\mu^*$, $\Omega_p$, $v_F$, $N(0)$, $z$, $\chi(z)$, $\kappa^*$, $\xi_0^*(0)$, and $\lambda_L^*(0)$ calculated according to Eqs. (1)–(8) for Nb and Ta in different structural states are presented in Table III. In the calculations we used the relations $\langle\rho_0 l_{\rm tr}\rangle=3.75\times10^{-12}\ \Omega\cdot\text{cm}^2$ for Nb (Ref. 36) and $\langle\rho_0 l_{\rm tr}\rangle=4.55\times10^{-12}\ \Omega\cdot\text{cm}^2$ for Ta. The latter value was obtained using the values of $v_F$ and $N(0)$ given in Refs. 8 and 9. It follows from Table III that for Nb and Ta with a minimal interstitial impurity content the values of $N(0)$, $v_F$, $\lambda$, $\mu^*$, $\Omega_p$, $\xi_0^*(0)$, and $\lambda_L^*(0)$ agree to within 10% with the previously published data.[9,15,36–38]

The properties of transition metals are substantially determined by the $d$ electrons, which are highly localized in space.[5,39] In calculations of the characteristics of a transition metal by the method of MT orbitals the set of parameters describing the energy spectrum of the transition metal reduces to two: $W_d$, the width of the $d$ band, and $E_d$, its position relative to the minimum of the $s$ band; these parameters are related to the radius $r_d$ of the $d$ state, the electron

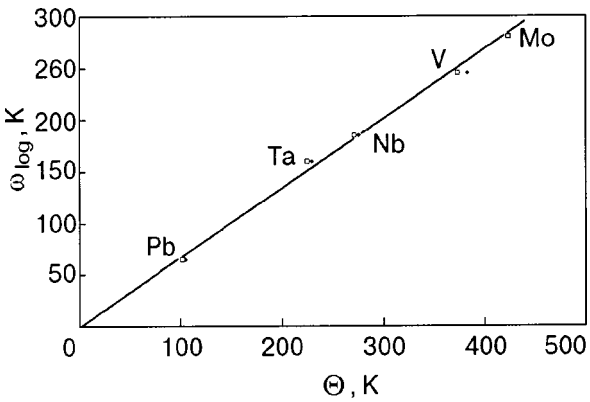


FIG. 2. Dependence of $\omega_{\log}$ on $\Theta$ for Pb, Ta, Nb, V, and Mo. The values of $\omega_{\log}$ were calculated in Ref. 9. The values of $\Theta$ correspond to the experimental data for Pb,[10,39] Ta,[7,17] Nb,[24,39] V,[17,39] and Mo.[10]

TABLE III. Effective microscopic parameters averaged over the Fermi surface for Nb and Ta in different structural states.

| Sample Образец | $\lambda$ | $\mu^*$ | $\Omega_p$, eV | $v_F$, $10^8$ cm/s | $N(0)$, states / eV per atom | $z$ | $\chi(z)$ | $\kappa^*$ | $\xi_0^*(0)$, $10^{-8}$ cm | $\lambda_L^*(0)$, $10^{-8}$ cm |
|---|---|---|---|---|---|---|---|---|---|---|
| Nb-80 | 1.148 | 0.210 | 9.32 | 0.663 | 1.357 | 0.204 | 0.852 | 0.953 | 456 | 334 |
| Nb-17 | 1.133 | 0.209 | 9.83 | 0.728 | 1.237 | 1.127 | 0.510 | 1.137 | 513 | 299 |
| Nb-13 | 1.181 | 0.214 | 8.65 | 0.588 | 1.533 | 1.404 | 0.455 | 2.139 | 399 | 391 |
| Ta-420 | 0.817 | 0.172 | 8.12 | 0.611 | 1.216 | 0.064 | 0.948 | 0.438 | 1032 | 328 |
| Ta-16 | 0.804 | 0.171 | 8.16 | 0.627 | 1.191 | 1.183 | 0.316 | 1.104 | 1103 | 323 |

wave vector $k_d$, and the radius $r_0$ of the atomic sphere. These quantities are characteristics of the ''ideal'' material and are listed in the periodic table in Ref. 5. In this approach the formation of the electronic structure of a transition metal is due to multiple scattering of electrons on nonoverlapping MT spheres. External influences (hydrostatic pressure, the introduction of impurities, deformation-induced defects, etc.) disrupt the ideal crystalline symmetry, alter the characteristics of the scattering centers, create new scattering centers due to lattice defects, and, hence, alter the characteristics of the energy spectrum. For example, under hydrostatic compression group-V elements typically suffer an increase of $W_d$, $v_F$, $\Omega_p$, $E_F$, and $z_d$ (the number of $d$ electrons per atom) and a decrease of $N(0)$, $\lambda$, and $\mu^*$ (Refs. 1,7,12, and 15).

In the approximate Friedel model of a two-band transition metal[5,28] one can do a simplified calculation of the effective parameters of the band structure of a transition metal and estimate the character of the changes of these parameters upon a change in the structural state. In this model the $s$ electrons form a band of free electrons with an effective mass $m_s^*$, and the density of states for the $d$ electrons in the energy interval $E_d-0.5W_d<E<E_d+0.5W_d$ is represented in the form $N_d(E)=10/W_d$. In this case $W_d$, $E_d$, $E_F$, and $z_d$ will be connected by the relation $0.5W_d-(E_d-E_F)=0.1z_dW_d$, which for Nb and Ta ($z_s+z_d=5$) leads to the expression

$$E_d=E_F+0.1z_sW_d. \tag{11}$$

Using the relation $W_d=6.83\hbar^2r_d^3/(m_0r_0^5)$, $m_s^*=m_0/(1+5r_d^3/\pi r_0^3)$, $E_F=\hbar^2k_s^2/2m_s^*$ (Ref. 5) and taking into account that the wave vector of the $s$ electrons has the form $k_s^2=(3\pi^2n_0z_s)^{2/3}$, we obtain the following equation for $z_s$:

$$\frac{6.83\hbar^2r_d^3z_s}{10m_0r_0^5}+\frac{\hbar^2(3\pi^2n_0)^{2/3}(1+5r_d^3/\pi r_0^3)z_s^{2/3}}{2m_0}-E_d=0. \tag{12}$$

Here $m_0$ is the mass of a free electron, and $n_0$ is the atomic density. Equation (12) can be solved using as parameters the tabulated values of $n_0$ (Ref. 40), $E_d$ (Ref. 5), $r_0$ (Ref. 5), and $r_d$ (Ref. 5) for Nb and Ta. As a result, we obtain the effective values of the number of $s$ electrons per atom: $z_{s0}=0.941$ for Nb and 0.796 for Ta. These values are close to the experimentally determined value $z_s=0.809$ for Nb.[41]

To calculate the radius of a $d$ state of Nb and Ta at minimal impurity content we use the relation $N_d(E)+N_s(0)=N(0)$. We thus obtain an equation for $r_{d0}$ in the form

$$\frac{10m_0r_0^5}{6.83\hbar^2r_{d0}^3}+\frac{3m_0n_0^{1/3}z_s^{1/3}}{\hbar^2(3\pi^2)^{2/3}(1+5r_{d0}^3/\pi r_0^3)}-N(0)=0. \tag{13}$$

Using the values of $N(0)$ as parameters (see Table III) and also the tabulated values of $n_0$ (Ref. 40), $r_0$ (Ref. 5), and $z_s=z_{s0}$, we get $r_{d0}=1.216\times10^{-8}$ cm for Nb and $1.263\times10^{-8}$ cm for Ta. The calculated values agree to within $\sim5\%$ with the values of $r_d$ given for these elements in the periodic table in Ref. 5.

It is instructive to compare the values obtained for $r_{s0}$ and $r_{d0}$ to the values of these parameters for Nb and Ta in other structural states. In the framework of the Friedel model the calculations needed for doing this can be carried out on the assumption that $E_F=\text{const}$. This condition is realistic in our case for the following reasons. It is known that the Fermi energy is determined by the number of carriers in the unit cell and can change appreciably under certain conditions, e.g., for alloys in which the valence of the dopant element differs strongly from the valence of the host. In the samples studied here the impurity content is small, and the difference of the impurity content in the alloy pairs being compared, Nb-80 with Nb-17 and Ta-420 with Ta-16, is not over $10^{-2}$ at. %, a level which is reflected extremely weakly in the value of $E_F$. For Nb-13 the mean density of dislocations is $N_{\text{dis}}\sim10^{11}$ cm$^{-2}$ (Ref. 24). At such a value of $N_{\text{dis}}$ the lowering of the chemical potential of the electrons will not exceed $10^{-3}$ (Ref. 42). The condition $E_F=\text{const}$ implies the expression $z_s=z_{s0}\{[1+5r_{d0}^3/(\pi r_0^3)]/[1+5r_d^3/(\pi r_0^3)]\}^{3/2}$. Substituting this expression into formula (13), we obtain an equation for $r_d$:

$$\frac{10m_0r_0^5}{6.83\hbar^2r_d^3}+\frac{3m_0n_0^{1/3}z_{s0}^{1/3}}{\hbar^2(3\pi^2)^{2/3}}\times\left(1+\frac{5r_{d0}^3}{\pi r_0^3}\right)^{1/2}\left(1+\frac{5r_d^3}{\pi r_0^3}\right)^{-3/2}-N(0)=0. \tag{14}$$

Table IV presents the values of $r_d$ calculated from Eq. (14), the values obtained for $z_s$, and the values determined

TABLE IV. Effective parameters of the band structure of Nb and Ta in different structural.

| Sample | $N_s(0)$ | $N_d(0)$ | $E_F$ | $E_d$ | $W_d$ | $m_s^*$ | $m_d^*$ | $m_d^*/m_s^*$ | $v_s$ | $v_d$ | $v_s/v_d$ | $r_d$, | $z_s$ | $z_d$ |
|---|---|---|---|---|---|---|---|---|---|---|---|---|---|---|
| | states / eV per atom | | eV | | | $10^{-28}$ g | | | $10^8$ cm/s | | | $10^{-8}$ cm | | |
| Nb-80 | 0.165 | 1.192 | 8.54 | 9.33 | 8.39 | 5.45 | 39.39 | 7.34 | 2.591 | 0.324 | 8.01 | 1.216 | 0.941 | 4.059 |
| Nb-17 | 0.156 | 1.081 | 8.54 | 9.36 | 9.25 | 5.23 | 35.72 | 6.83 | 2.592 | 0.350 | 7.41 | 1.256 | 0.886 | 4.114 |
| Nb-13 | 0.178 | 1.355 | 8.54 | 9.29 | 7.38 | 5.72 | 44.75 | 7.83 | 2.592 | 0.291 | 8.81 | 1.165 | 1.013 | 3.987 |
| Ta-420 | 0.149 | 1.067 | 8.00 | 8.75 | 9.39 | 5.20 | 35.18 | 6.77 | 2.427 | 0.343 | 7.08 | 1.263 | 0.796 | 4.204 |
| Ta-16 | 0.136 | 1.050 | 8.00 | 8.75 | 9.54 | 5.16 | 34.61 | 6.71 | 2.429 | 0.362 | 6.71 | 1.269 | 0.788 | 4.212 |

from them for the Friedel model parameters and the other microscopic characteristics of Nb and Ta in different structural states.

## DISCUSSION

Tables II, III, and IV indicate a polar character of the changes in $T_c$, $\rho(T)$, and the effective microscopic and band characteristics of Nb and Ta upon the introduction of interstitial impurities and deformation-induced defects in the lattice. In view of the lack of consistent theoretical models describing the electrophysical properties of nonideal transition metals, it is sensible to compare the results obtained here with the experimental and theoretical results of other authors and to make a qualitative judgment as to the nature of certain effects.

*Interstitial impurities.* The impurity-induced changes of the characteristics mentioned are less pronounced for Ta than for Nb, since the difference of the values of $\rho_{294\,K}/\rho_n$ for our Ta samples is larger. The values of $E_d$ and $\Theta$ for Ta remain practically unchanged. The fact that the sensitivity of Ta to interstitial impurities is weaker than that of Nb should be attributed to the greater stiffness of the interatomic coupling and the higher stability of the crystal lattice.[43,44]

The interstitial atoms in $\alpha$-solid solutions of group-V metals occupy octahedral (O, C, N)[45,46] and tetrahedral (H, D)[47,48] positions in the bcc lattice and lead to an effective increase in the interatomic distances, which causes an effective change of the microscopic characteristics. According to x-ray photoemission results,[18] with increasing nitrogen concentration in Nb the electrons of the Nb4$d$ and Nb5$s$ bands move into higher-binding-energy Nb4$d$–N2$p$ bonding states, and this decreases the density of states at the Fermi level. The remaining Nb5$s$ electrons are lost, and the Nb4$d$ electrons acquire the binding energy; this corresponds to an effective widening of the bands of the host crystal. The data of Ref. 18 are close to the results of band calculations for solid solutions of N and C in Nb (Ref. 46) and to the results of positron annihilation studies in $VD_{0.68}$ and $TaH_{0.15}$ single crystals.[19] The widening of the energy bands presupposes a weakening of the electron–electron interaction, which is characterized by the quantity $\mu^*$ (Ref. 49). For Nb-17 and Ta-16, which have a $\sim$0.1 at. % higher impurity concentration as compared to Nb-80 and Ta-420, the value of $\mu^*$ is lowered by $\sim$0.5% (see Table III). This change in $\mu^*$ attests to a comparatively weak decrease of the electron–electron interaction. The transfer of a fraction of the 5$s$ electrons to bound states lying below the Fermi level corresponds, in the framework of the two-band model under consideration, to an effective decrease in the number of $s$ electrons and, hence, to an increase in $z_d$, $r_d$, and $W_d$ and a decrease of the effective mass of the charge carriers in each of the bands (see Table IV). There is also a decrease in $m_d^*$, $m_s^*$, and $v_s/v_d$. For the real Fermi surface such a transformation of the energy spectrum means an effective increase in its mean curvature and a lowering of the degree of anisotropy. The latter corresponds to the known theoretical idea of Markovitz and Kadanoff[50] that the energy spectrum of the metal becomes more isotropic when impurities are added. Thus the data obtained in the present study on the effective changes of the characteristics of the energy spectrum are consistent with the independent experimental results and the existing model concepts.

Let us consider how the lattice dynamics of the metal is affected by the introduction of an impurity. Increasing the number of valence electrons having a higher value of the binding energy enhances the stiffness of the lattice.[18] Direct information about the enhancement of the high-frequency contribution to the vibrational spectrum of transition metals containing interstitial impurities has been obtained in low-energy neutron scattering experiments[20,21] and measurements of the low-temperature heat capacity.[22] It follows from Ref. 21 that for all group-V metals the introduction of oxygen and nitrogen within the solid solution region is accompanied by a qualitatively similar change in the lattice dynamics: the peaks of the distribution function are broadened and shifted to higher energies. There are also two peaks of high-frequency localized vibrations split off from the main spectrum; their position depends on the species of interstitial atom. The average increase of $\langle\omega^2\rangle$ in vanadium containing O and N impurities is $\sim$3% per at. % impurity. This value is in practical agreement with the estimate of the change in $\langle\omega^2\rangle$ for Nb-80 and Nb-17. Such a transformation of the phonon spectrum upon a relatively small change in impurity concentration may be a consequence of the interaction of harmonic vibrations of the unperturbed lattice with waves scattered on point defects.

*Deformation-induced defects.* For Nb-13, which was obtained from Nb-17 by deformation at 20 K with a subsequent warming to 300 K, the main type of defects are dislocations

TABLE V. Values of $N(0)$, $\langle\omega^2\rangle^{1/2}$, $\langle J^2\rangle$, $\eta$, $\lambda$, and $\lambda_c$ for niobium in different structural states.

| Sample | $N(0)$, states / eV per atom | $\langle\omega^2\rangle^{1/2}$, $10^{13}\,s^{-1}$ | $\langle J^2\rangle$, $eV^2/Å^2$ | $\eta$, $eV/Å^2$ | $\lambda_c=\frac{\eta}{M\langle\omega^2\rangle}$ | $\lambda$ | $\frac{\lambda_c-\lambda}{\lambda}$, % |
|---|---|---|---|---|---|---|---|
| Nb-80 | 1.357 | 2.448 | 4,889 | 6.634 | 1.148 | 1.148 | 0 |
| Nb-17 | 1.237 | 2.493 | 5,388 | 6.665 | 1.111 | 1.133 | ~2 |
| Nb-13 | 1.533 | 2.349 | 4,336 | 6.647 | 1.249 | 1.181 | ~6 |

with predominantly screw components and an average density of $\sim 10^{11}$ cm$^{-2}$ in the middle of the sample. Estimates show that the bulk concentration of defects of the vacancy type in Nb-13 is comparatively low, and the change of $T_c$, $\rho(T)$, and the microscopic and band parameters should be attributed mainly to dislocation effects. At the indicated values of $N_{\rm dis}$ one expects the appearance of quasi-one-dimensional electronic states bound to the dislocations and quasi-one-dimensional superconductivity due to them. It follows from Ref. 51 that for Nb in the framework of the theory of localized superconductivity[52] the calculated growth of $T_c$ due to dislocation pileups of maximum strength is $\sim 5\times 10^{-4}$ K. This value is substantially lower than the value determined experimentally for the increase of $T_c$ (see Table II). According to Ref. 51, for Nb with a density of uniformly distributed dislocations in the interval $(0.9–1.3)\times 10^{11}$ cm$^{-2}$ the values of the increase of $T_c$ are in good agreement with the results of a calculation in the framework of the theory of bulk superconductivity enhanced by the interaction of electrons with the zero-point oscillations of the dislocations.[53] In addition, the anomalies in $\rho(T)$ — in particular, the decrease of $\rho_0$ — which should precede the onset of quasi-one-dimensional superconductivity,[54] have not been detected experimentally. These arguments indicate that the quasi-one-dimensional electronic states and the quasi-one-dimensional superconductivity due to them do not play a major role. Consequently, in view of the results of Refs. 25 and 26, one can assume that the properties of a transition metal containing dislocations, as in the case of impurities, admits an analysis in terms of effective microscopic and band characteristics.

It follows from Tables III and IV that for Nb-13 there is a characteristic increase of $\lambda$ and $N(0)$ and a lowering of the Debye temperature and $\langle\omega^2\rangle$ in comparison with Nb-17, in agreement with the results of measurements of the electronic heat capacity of deformed V, Nb, and Ta.[55] In the framework of the Friedel model with the adopted condition $E_F=$const the growth of $N(0)$ is mainly due to an increase of $N_d(E)$, corresponding to an effective decrease of the width of the $d$ band, which is inversely proportional to $m_d^*$ (Ref. 5). The increase of the effective mass of the charge carriers in a metal containing dislocations is caused by a change in the character of the electron–phonon coupling.[56] Direct data on the change of the electron–phonon coupling of Nb containing dislocations are presented in Ref. 57. The transformation of the electron–phonon interaction spectrum obtained by tunneling spectroscopy is expressed in a broadening of the peaks, an increase in the density of the low-frequency modes, and a decrease in $\langle\omega^2\rangle$, which leads to growth of $\lambda$. It can be assumed that another factor that increases $\lambda$, besides the less tightly packed lattice near the dislocation cores,[57] is the presence of low-frequency modes localized at the dislocations.

The lattice distortions due to dislocation cores lead to changes in the characteristics of the energy spectrum of a transition metal. Possible causes of this are as follows. Because of the strong atomic displacements, comparable to the interatomic distances, near the axis of a dislocation, the characteristic directional bonds formed by the wave functions of the $d$ electrons (the states $t_{2g}$ and $e_g$) in the undistorted bcc lattice of the transition metal[1] will be broken or altered in character. In the crystal matrix this leads to an effective lowering of the density of states $N(E)$ in the region of the low-energy peaks. Since the total number of states in the energy range $E<E_F$ per unit volume of the crystal changes insignificantly ($\delta V/V_0\approx N_{\rm dis}b_B^2\sim 10^{-4}$, where $b_B$ is the Burgers vector), under the condition $E_F=$const the lowering of the height and the smearing of the low-energy peaks cause an effective increase of the density of states at the Fermi level, which intersects the sloping part of the ''A'' peak at the boundary of the filled part of the spectrum (see, e.g., Ref. 1).

*Electron–phonon interaction.* In the approach of Ref. 31 the electron–phonon coupling constant has the form $\lambda=N(0)\langle J^2\rangle/M\langle\omega^2\rangle$. The numerator of this expression is the electronic Hopfield parameter $\eta=N(0)\langle J^2\rangle$. The change in $\lambda$ upon a change in the structural state depends on the behavior of each of the three cofactors. The characteristics of the phonon ($\Theta$) and electronic [$N(0)$] spectra are presented in Tables II and III. For an estimate of the changes of the square matrix element of the electron–ion interaction averaged over the Fermi surface, we use the relation $\langle J^2\rangle\approx a_d\langle v_F^2\rangle$ (Ref. 3), where $a_d$ is a measure of the ordering of the bonds of the $d$ electrons. We shall assume that $a_d=$const and that the change of the matrix element is due mainly to the behavior of $v_F$. For Nb with a minimal impurity content the value of $a_d$ was determined using the corresponding values of $N(0)$, $\Theta$, and $\lambda$ and in turn was used to calculate $\langle J^2\rangle$. For Nb in different structural states the parameters characterizing the electron–phonon interaction are listed in Table V. It follows from the tables that the total effect of the change of the three cofactors determining $\lambda_c$ is in good agreement with the independently calculated value of $\lambda$. It is also seen that the value of $\eta$ is practically the same for all the structural states. Consequently, the weakening of the electron–phonon coupling with increasing impurity concentration and the enhancement of the electron–phonon cou-

pling when dislocations are introduced in the material are mainly due to the increase and decrease, respectively, of the average phonon frequencies. This conclusion agrees with the existing idea that the electronic Hopfield parameter is constant for transition metals.[31]

## CONCLUSIONS

1. We have obtained experimental data on the temperature dependence of the resistivity $\rho$ in the interval $T_c < T \lesssim 300$ K and on the values of $T_c$ for group-V transition metals (Nb, Ta) containing interstitial impurities with various concentrations (within the solid solution region) and defects induced by deformation. For the investigated structural states of Nb and Ta the temperature dependence $\rho(T)$ is described to good accuracy in the framework of the Mott–Wilson model of transition metals; this has allowed us to determine the residual resistivity $\rho_0$, the intensity of the interband $(s-d)$ and intraband $(s-s)$ scattering of charge carriers, and the Debye temperature.

2. We have calculated the effective microscopic characteristics averaged over the Fermi surface (the electron–phonon interaction constant, Coulomb pseudopotential, Fermi velocity, density of states, plasma frequency, effective mass, Ginzburg–Landau parameter, and London penetration depth) for Nb and Ta in various structural states. In the calculations we used a closed system of equations that took into account the effects due to the lifetime of the electrons in their scattering on defects and thermal phonons. The parameters of this system were $\rho_0$, $d\rho/dT$, $T_c$, and $\Theta$, the values of which were determined experimentally for each of the structural states.

3. For all the structural states of Nb and Ta we have determined the effective band parameters corresponding to the Friedel model of a two-band transition metal and the relations describing the electronic structure of the *d* states in resonant scattering: the width and mean energy of the *d* band, the Fermi energy, the effective masses and the velocities in each of the bands, the relative numbers of *s* and *d* electrons, and the radius of the *d* state.

4. We have determined the trends in respect to the influence of interstitial impurities and dislocations on the effective characteristics of the electronic and phonon spectra and the electron–phonon interaction of transition metals. Increasing the impurity concentration tends to increase $\Theta$, to weaken the intraband and enhance the intraband scattering, to decrease $T_c$, $\lambda$, $\mu^*$, $N(0)$, and $\lambda_L^*(0)$, and to increase $\rho_0$, $v_F$, $\xi_0^*(0)$, and $\kappa^*$. In the two-band Friedel model impurities cause the energy spectrum to become more isotropic, widen the *d* band and raise its mean energy increase the velocity and decrease the effective mass of the carriers in the *d* band, increase $z_d$ and $r_d$, and decrease $z_s$, $N_s(0)$, and $N_d(E)$. Dislocations cause effects of the opposite sign (except for the changes in $\rho_0$ and $\kappa^*$).

5. The polar character of the influence of interstitial impurities and dislocations on the complex of superconducting, transport, and microscopic parameters of transition metals may be due to the following causes. In the first case states coupled to the impurity appear below the Fermi level, and a portion of the valence electrons of the metal go into these states. As a result, a broadening of the *d* band, a decrease of the density of states at the Fermi level, and an increase in the lattice stiffness occur. These changes are accompanied by a weakening of the electron–phonon coupling. In the deformed material a breaking of the characteristic interatomic bonds of the bcc lattice and a change in the character of the overlap of the wave functions of the *d*-type states of the atoms occur, causing an effective increase in the density of states at the Fermi level and a softening of the phonon spectrum. This leads to enhancement of the electron–phonon coupling.

6. For Nb containing different concentrations of interstitial impurities and a high density of dislocations the value of the electronic part of the electron–phonon coupling constant remains practically unchanged, indicating that $\lambda$ is correlated with the characteristics of the phonon spectrum.

The authors thank V. D. Natsik for a discussion of this study and for constructive criticism.

[a)]E-mail: vsokol@kipt.kharkov.ua
[b)]E-mail: Boris.A.Merisov@univer.kharkov.ua

[1] S. V. Vonsovskiĭ, Yu. A. Izyumov, and É. Z. Kurmaev, *Superconductivity of Transition Metals, Their Alloys and Compounds* [Springer-Verlag, Berlin (1982); Nauka, Moscow (1977)].
[2] W. H. Butler, Phys. Rev. B **15**, 5267 (1977).
[3] C. M. Varma, E. I. Blount, P. Vashishta, and W. Weber, Phys. Rev. B **19**, 6130 (1979).
[4] C. M. Varma and W. Weber, Phys. Rev. B **19**, 6142 (1979).
[5] W. A. Harrison, *Electronic Structure and the Properties of Solids: The Physics of the Chemical Bond*, Freeman, San Francisco (1980); Mir, Moscow (1983).
[6] I. I. Mazin, E. M. Savitskii, and Yu. A. Uspenskii, J. Phys. F: Met. Phys. **14**, 167 (1984).
[7] V. John, ''Electron–phonon interaction,'' in *Progress in the Electronic Theory of Metals* edited by P. Ziesche and G. Lehmann, Vol. 2 [in Russian], Mir, Moscow (1984).
[8] P. B. Allen, T. P. Beaulac, F. S. Khan, W. H. Butler, F. J. Pinski, and J. C. Swihart, Phys. Rev. B **34**, 4331 (1986).
[9] S. Y. Savrasov and D. Y. Savrasov, Phys. Rev. B **54**, 16 487 (1996).
[10] M. L. Cohen, in *Superconductivity*, edited by R. D. Parks, Dekker, New York (1969), Chap. 12, p. 615; G. Gladstone, M. A. Jensen, and J. R. Schrieffer, *ibid.*, Chap. 13, p. 665; Russian translation published as *Superconductivity of Semiconductors and Transition Metals*, Mir, Moscow (1972).
[11] J. R. Anderson, D. A. Papaconstantopoulos, J. W. McCaffrey, and J. E. Shirber, Phys. Rev. B **7**, 5115 (1973).
[12] D. G. Pettifor, J. Phys. F: Met. Phys. **7**, 613 (1977).
[13] Yu. F. Revenko, A. I. D'yachenko, V. N. Svistunov, and B. Shonaikh, Fiz. Nizk. Temp. **6**, 1304 (1980) [Sov. J. Low Temp. Phys. **6**, 634 (1980)].
[14] Ö. Rapp and B. Sundqvist, Phys. Rev. B **24**, 144 (1981).
[15] J. Neve, B. Sundqvist, and Ö. Rapp, Phys. Rev. B **28**, 629 (1983).
[16] V. I. Sokolenko and Ya. D. Starodubov, Fiz. Nizk. Temp. **19**, 951 (1993) [Low Temp. Phys. **19**, 675 (1993)].
[17] V. I. Khotkevich, B. A. Merisov, A. M. Ermolaev, and A. V. Krasnokutskii, Fiz. Nizk. Temp. **9**, 1056 (1983) [Sov. J. Low Temp. Phys. **9**, 546 (1983)].
[18] G. Aeppli, H. J. Stolz, and R. A. Pollak, Phys. Rev. B **24**, 4128 (1984).
[19] V. S. Mikhalenkov, ''Study of the electronic structure of metals and alloys by positron methods,'' in *Electronic Structure and Electronic Properties of Metals and Alloys* [in Russian], Naukova Dumka, Kiev (1988).
[20] S. A. Danilkin, N. G. Zemlyanov, V. P. Minaev, P. P. Parshin, and V. V. Sumin, Fiz. Tverd. Tela (Leningrad) **29**, 2112 (1987) [Sov. Phys. Solid State **29**, 1213 (1987)].
[21] S. A. Danilkin, N. G. Zemlyanov, V. P. Minaev, P. P. Parshin, and V. V. Sumin, Fiz. Tverd. Tela (Leningrad) **31**(5), 8 (1989) [Sov. Phys. Solid State **31**, 725 (1989)].
[22] C. C. Koch, J. O. Scarbrough, and D. V. Kroeger, Phys. Rev. B **9**, 888 (1974).
[23] H. G. Smith, N. Wakabayashi, and Mark Mostoller, in *Proceedings of the Second Rochester Conference on Superconductivity in d- and f-Band Met-*

*als*, edited by D. H. Douglass, Plenum, New York (1976), p. 223.
[24] V. I. Sokolenko, Ya. D. Starodubov, B. A. Merisov, and I. F. Borisova, Fiz. Nizk. Temp. **16**, 246 (1990) [Sov. J. Low Temp. Phys. **16**, 136 (1990)].
[25] L. R. Testardi and L. F. Mattheiss, Phys. Rev. Lett. **41**, 1612 (1978).
[26] L. F. Mattheiss and L. R. Testardi, Phys. Rev. B **20**, 2196 (1979).
[27] G. W. Webb, Phys. Rev. **181**, 1127 (1968).
[28] J. Friedel, ''Transition metals. Electron band structure. Its role in the crystalline and magnetic structures,'' in *The Physics of Metals*, Vol. 1 (Electrons), edited by J. M. Ziman, Cambridge University Press, Cambridge (1969); Mir, Moscow (1972), p. 375.
[29] B. Chakraborty, W. E. Pickett, and P. B. Allen, Phys. Rev. B **14**, 3227 (1976).
[30] P. B. Allen and R. C. Dynes, Phys. Rev. B **12**, 905 (1975).
[31] W. L. McMillan, Phys. Rev. **167**, 331 (1968).
[32] M. H. Cohen, Philos. Mag. **3**, 762 (1958).
[33] W. DeSorbo, Phys. Rev. **132**, 107 (1963).
[34] A. Inaba, Jpn. J. Appl. Phys. **19**, 1553 (1980).
[35] V. M. Azhazha, P. N. V'yugov, S. D. Lavrinenko, and V. S. Gumenyuk, Vopr. At. Nauki Tekh. Ser. Obshch. Yad. Fiz., No. 1(26), 66 (1984).
[36] R. A. French, Cryogenics **8**, 301 (1968).
[37] A. Ikishima and T. Mizusaki, J. Phys. Chem. Solids **30**, 873 (1969).
[38] J. Buchanan, G. K. Chang, and B. Serin, J. Phys. Chem. Solids **26**, 1183 (1965).
[39] G. Lehmann, ''Scattering theory and the band structure of transition metals,'' in *Progress in the Electronic Theory of Metals*, edited by P. Ziesche and G. Lehmann, Vol. 1, [in Russian], Mir, Moscow (1984).
[40] C. Kittel, *Introduction to Solid State Physics*, 4th ed. [Wiley, New York (1971); Nauka, Moscow, (1978)].
[41] A. I. Golovashkin and A. L. Shelekhov, Tr. Fiz. Inst. Akad. Nauk SSSR **151**, 137 (1984).
[42] V. D. Natsik, S. N. Smirnov, and N. É. Tikhonenkov, Fiz. Nizk. Temp. **19**, 931 (1993) [Low Temp. Phys. **19**, 662 (1993)].
[43] H. W. King, ''Structure of pure metals,'' in *Physical Metallurgy*, Vol. 1, edited by R. W. Cahn [Wiley, New York (1965); Mir, Moscow (1967), p. 11].
[44] V. I. Trefilov, F. V. Mil'man, and S. A. Firstov, *Physical Principles of the Strength of Refractory Metals* [in Russian], Naukova Dumka, Kiev (1975).
[45] P. P. Matyash, N. A. Skakun, and N. P. Dikiĭ, JETP Lett. **19**, 18 (1974).
[46] V. V. Domnich, A. N. Yaresko, V. N. Antonov, V. V. Nemoshkalenko, V. K. Soolshenko, and I. Smurov, Metallofizika Noveĭshie Tekhnol. **20**, 67 (1998).
[47] N. Behr, H. M. Keppler, G. Steyrer, H. Metzger, and J. Peisl, J. Phys. Chem. Solids **44**, 958 (1983).
[48] A. Klam and H. Teichler, Phys. Status Solidi B **134**, 103 (1986).
[49] J. W. Garland and K. H. Bennemann, in *Superconductivity in d- and f-Band Metals*, edited by D. H. Douglass, Plenum, New York (1972), p. 255.
[50] D. Markovitz and L. P. Kadanoff, Phys. Rev. **131**, 563 (1963).
[51] V. K. Aksenov, V. I. Sokolenko, and Ya. D. Starodubov, Fiz. Nizk. Temp. **19**, 1083 (1993) [Low Temp. Phys. **19**, 768 (1993)].
[52] V. M. Nabutovskiĭ and V. Ya. Shapiro, Zh. Éksp. Fiz. **75**, 948 (1978) [Sov. Phys. JETP **48**, 480 (1978)].
[53] R. O. Zaĭtsev, Zh. Éksp. Teor. Fiz. **54**, 1445 (1968) [Sov. Phys. JETP **27**, 775 (1968)].
[54] I. M. Dubrovskiĭ, *Theory of Electronic Phenomena in Deformed Crystals* [in Russian], RIO IMF, Kiev (1999).
[55] R. Küentzler, Phys. Lett. A **104**, 221 (1984).
[56] G. O. Zaĭtsev, Fiz. Tverd. Tela (Leningrad) **22**, 917 (1980) [Sov. Phys. Solid State **22**, 538 (1980)].
[57] V. A. Pervakov, *Thermophysical Properties of Metals Containing Lattice Defects at Low Temperatures* [in Russian], Osnova, Kharkov (1990).

Translated by Steve Torstveit

# Structure parameters and degradation of the critical current of the alloy NT-50 after cryogenic drawing in an ultrasonic field

O. I. Volchok, M. B. Lazareva, V. S. Okovit, Ya. D. Starodubov, O. V. Chernyi, and L. A. Chirkina

*Kharkov Physicotechnical Institute National Science Center, ul. Akademicheskaya 1, 61108 Kharkov, Ukraine**

(Submitted November 16, 2000)
Fiz. Nizk. Temp. **27**, 482–488 (May 2001)

The parameters of the defect and phase structure of the alloy NT-50 are investigated after low-temperature (77 K) deformation by drawing in an ultrasonic field, and the influence of these parameters on the amount of degradation of the critical current under tensile loading at 4.2 K is studied. It is found that cryogenic ultrasonic deformation leads to intensified decomposition of the $\beta$-solid solution with precipitation of Ti-rich phases according to the kinetics of the spontaneous martensitic transformation and results in a reduction of the internal stress level in the alloys. The structural features found promote stabilization of the $\beta$-solid solution during a subsequent deep cooling, as is manifested in a lowering of the degree of completion of the low-temperature deformation-induced martensitic transformation, which in turn raises the threshold for degradation of the critical current and reduces the degree of degradation in a wide range of external mechanical loads.  [DOI: 10.1063/1.1374719]

It has been shown previously[1] that deformation of a niobium–titanium alloy by drawing under cryogenic conditions (77 K) leads to intensification of the diffusive decomposition of the $\beta$-solid solution even in the initial stages of the subsequent heat treatment. This results in the formation of a structure with a high volume density of a finely dispersed $\alpha$-phase, which increases the value of the critical current of the superconducting alloy. It is known[2] that the use of ultrasonic mechanical vibrations during drawing (ultrasonic drawing) helps to reduce the contact friction at the site of the deformation and thus facilitates the drawing process. This is especially important for the cryogenic deformation of materials with a bcc lattice, for which, by virtue of the strong temperature dependence of the strength characteristics, the drawing forces and, hence, the length of the drawing path increase and the breaking strength of the wire increases.

An important characteristic of superconducting niobium–titanium alloys from the standpoint of applications is the degree to which the critical current is lowered (degraded) under tensile loading, which is largely determined by the low-temperature phase transformations taking place according to martensitic kinetics and by the internal stress level in the material.[3–6]

The present study was undertaken to investigate the features of the structure parameters of a niobium–titanium alloy during cryogenic ultrasonic drawing and their influence on the degree of degradation of the critical current.

## EXPERIMENTAL PROCEDURE

Samples of the niobium–titanium alloy NT-50 (48.5 wt. % Ti) were subjected to a preliminary multidirectional deformation[7] and drawing at 300 K to a diameter $d=1.5$ mm. The subsequent drawing and ultrasonic drawing to $d=0.6$ mm ($\varepsilon=84\%$) were done at 77 K on a special apparatus.[8] The amplitude of the displacement of the end of the ultrasonic vibration concentrator was 3 $\mu$m, and the vibrational frequency was 20.5 kHz. The efficacy of introducing longitudinal ultrasonic vibrations at the deformation site was monitored from the diagrams of the variation of the drawing force.

The amplitude dependence of the internal friction (ADIF) was investigated at 300 K in order to assess the defect structure of the material, and the temperature dependences of the internal friction $\delta(T)$ and dynamic shear modulus $G(T)$ were studied in the temperature range 4.2–150 K in order to establish the features of the change in phase structure of the alloy both after deformation and after a subsequent deep cooling. The measurements of the ADIF and temperature dependence of $\delta$ and $G$ were done on an apparatus of the inverted torsion pendulum type, which was described in detail in Ref. 9. The frequency of the torsional oscillations was 0.5 Hz. The ADIF was measured for strain amplitudes in the range $5\times10^{-6}-2\times10^{-3}$. The curves of $\delta(T)$ and $G(T)$ were obtained at a strain amplitude of $8\times10^{6}$, which lies in the region of amplitude-independent internal friction. The measurements of $\delta(T)$ and $G(T)$ were made in a heating regime, with the sample placed in a steady flow of helium produced by a microheater and a constant pumping off of the helium vapor. The temperature was monitored in the range 4.2–20 K by a carbon resistance thermometer and at temperatures above 20 K by a copper–Constantan thermocouple with an accuracy of 0.3–0.5 K. The rate of change of the temperature was 0.5 deg/min in the range 4.2–100 K and 1.5 deg/min above 100 K. The temperature was stabilized during the internal friction measurement. The error in the determination of the damping decre-

 

ment was not over 10%. The shear modulus was calculated by the formula

$$G = \frac{128\pi Jl}{d^4} f^2,$$

where $l$ and $d$ are the length and diameter of the sample, $J$ is a characteristic that determines the stiffness of the apparatus, and $f$ is the measured vibrational frequency of the sample. The error in the determination of the shear modulus was 0.1%.

The amount of degradation of the critical current of the superconductors under tension was measured at 4.2 K in a transverse magnetic field $H=5$ T on the apparatus described in Ref. 10. We determined the degradation threshold $\sigma_0$, i.e., the stress above which the degradation of the critical current begins to be manifested,[5] and the dependence of the reduced critical current $J_{ci}/J_{c0}$ on the tensile stress, where $J_{ci}$ is the value of the current at a fixed voltage and $J_{c0}$ is the current before the tensile stress is applied. The critical current was recorded to an error of 1% as the current at which a voltage of 10 $\mu$V appeared, and it was measured both under load and after the sample was unloaded.

The mechanical characteristics after various drawing regimes were obtained at 300 and 77 K under conditions of tensile straining at a rate of $10^{-3}\,s^{-1}$. For the measurements of the mechanical characteristics and the degradation of the critical current we used samples 80 mm long, and for the measurements of the internal friction parameters we used samples 30 mm long, with the copper sheath removed.

## RESULTS AND DISCUSSION

Table I gives the results of measurements of the ADIF at 300 K after various types of cryogenic drawing of the alloy NT-50. It is seen that ultrasonic drawing results in a reduced internal friction background and a higher critical amplitude for breakaway of the edge component of a dislocation from pinning points. This indicates that drawing in an ultrasonic field, when the material is subjected to simultaneous static and vibrational loading, increases the efficiency of the interaction of dislocations with point defects, since dislocations oscillating in an ultrasonic field have a larger cross section for trapping of point defects. As a result, the length of a dislocation segment decreases, and the starting stress for the motion of dislocations increases. The precipitation of point defects on dislocations clears them from the matrix, as is confirmed by the decrease in the level of the internal friction background after ultrasonic cryogenic drawing. This results in a reduced level of internal stresses in the alloy.

TABLE I. Parameters of the amplitude-dependent internal friction of the alloy NT-50 after various forms of treatment.

| Treatment | Background level $\delta$, $10^{-3}$ | Critical amplitude for the breakaway of dislocations from pinning points $\gamma_e$, $10^{-6}$ |
|---|---|---|
| Drawing at 77 K | 5.3 | 56 |
| Drawing at 77 K in an ultrasonic field | 2.3 | 186 |

TABLE II. Mechanical properties of the alloy NT-50 after various forms of treatment.

| Treatment | Yield stress $\sigma_{0.2}$, MPa | | Shear modulus $G$, GPa |
|---|---|---|---|
| | $T_{ex}=300$ K | $T_{ex}=77$ K | |
| Drawing at 77 K | 800 | 910 | 30.4 |
| Drawing at 77 K in an ultrasonic field | 640 | 760 | 30.9 |

The fact that relaxation processes occur during drawing in an ultrasonic field is also evidenced by the mechanical properties of the NT-50 alloy (Table II). Table II shows that drawing in an ultrasonic field lowers the yield stress (the softening effect amounts to 20% at a testing temperature of 300 K and to 16.5% at a testing temperature of 77 K) and increases the dynamic shear modulus by 1.6%.

It is important to note that the dynamic shear modulus for alloys undergoing phase transformations is determined mainly by the change in the chemical composition of the solid solution after one of the components has precipitated out of it in the form of separate phases.[11] Against the background of the change in shear modulus due to the change in the ratios of the different elements in the solid solution, the observed changes in the defect structure of the alloy have an insignificant effect on the shear modulus.[12] Since, according to Ref. 3, there is an inverse linear relation between the Ti content in the $\beta$-solid solution and the value of $G$, the increase of the dynamic shear modulus after drawing in an ultrasonic field is evidence of processes of precipitation of particles of titanium-rich phases.

Let us consider in more detail the dynamics of the processes of decomposition of the $\beta$-solid solution after the sample is subjected to different types of actions, basing the discussion on measurements of the temperature dependence of the internal friction and dynamic shear modulus of the NT-50 alloy. Figure 1 shows the temperature dependence of the damping decrement of the NT-50 alloy in the homogenized state (single-phase $\beta$-solid solution), after cryogenic

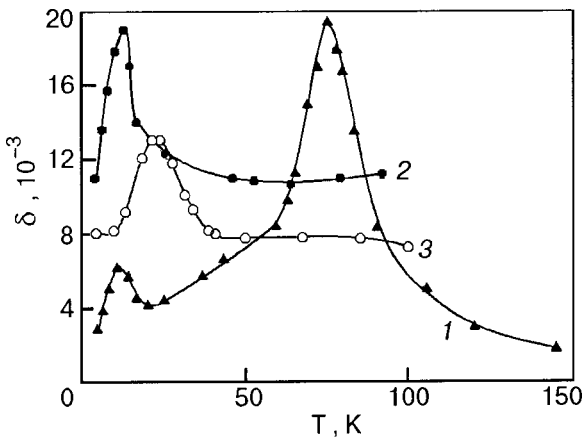


FIG. 1. Temperature dependence of the damping decrement of the alloy NT-50 in the homogenized state (*1*), after drawing at 77 K (*2*), and after drawing at 77 K in an ultrasonic field (*3*).

drawing, and after cryogenic ultrasonic drawing. We see that for the homogenized state the $\delta(T)$ curve is characterized by the presence of two pronounced peaks at 10 and 70 K (Fig. 1, curve *1*). A previous detailed investigation into the nature of these peaks showed us that the first is due to a deformation-induced martensitic transformation and the second to a spontaneous martensitic transformation.[13,14] Let us use these ideas to analyze the influence of the drawing regimes on the dynamics of these transformations and, hence, on the structural–phase state of the alloy. It is shown in Fig. 1 (curves *2* and *3*) that after drawing in either regime the second internal friction peak vanishes, and the low-temperature peak increases in height and shifts to higher temperatures, i.e., the spontaneous martensitic transformation is completely suppressed, and the deformation-induced transformation is enhanced. The ultrasonic cryogenic drawing led to a lower height of this peak and a larger upshift the peak in temperature. Consequently, after ultrasonic drawing the decomposition of the $\beta$-solid solution according to deformation-induced martensitic kinetics occurs less intensely and is shifted to higher temperatures in comparison with the sample that has undergone only cryogenic drawing. It is interesting to note that ultrasonic drawing promotes a lowering of the internal friction background. This is indicative of a lower level of internal stresses in the alloy and is confirmed by the above data on the change in the ADIF background and mechanical properties after deformation by drawing in various regimes.

Let us consider the dynamics of the martensitic transformation of the $\beta$-solid solution and estimate its degree of completion on the basis of the character of the change in the modulus defect $\Delta G$ ($\Delta G = G_{T0} - G_{T1}$, where $G_{T0}$ is the shear modulus at the start of the jump in $G$, and $G_{T1}$ is the modulus at the end of the jump).[11]

Curve *1* in Fig. 2 exhibits two modulus defects for the homogenized state; these correspond to the internal friction peaks in the regions 4.2–30 K and 45–100 K (Fig. 1, curve *1*), which characterize the deformation-induced and spontaneous martensitic transformations, respectively, of the NT-50 alloy. For the alloy that has been subjected to deformation by drawing, only one modulus defect can be discerned, and that is governed by the deformation-induced martensitic transformation (Fig. 2, curves *2* and *3*). This indicates that the spontaneous martensitic transformation is suppressed after both deformation regimes, in agreement with the results of the internal friction measurements. The observed deformation-induced martensitic transformation, as may be judged from the value of the modulus defect, is intensified to a greater degree on drawing in the absence of ultrasonic vibrations. The introduction of ultrasonic vibrations at the deformation site decreases the value of the modulus defect and decreases the width of the temperature interval in which it is manifested (Fig. 2, curve *3*). It follows that in ultrasonic drawing a structure is formed in which the intensity of the deformation-induced martensitic transformation upon subsequent deep cooling is suppressed, and the temperature region in which the $\beta$ phase is unstable is narrowed in comparison with the case of cryogenic drawing in the absence of ultrasound. One notices that the slopes of the $G(T)$ curves in the phase transformation region are close in value for all three of the structural states considered, indicating that the rates of the process are comparable and that it occurs by a common mechanism.

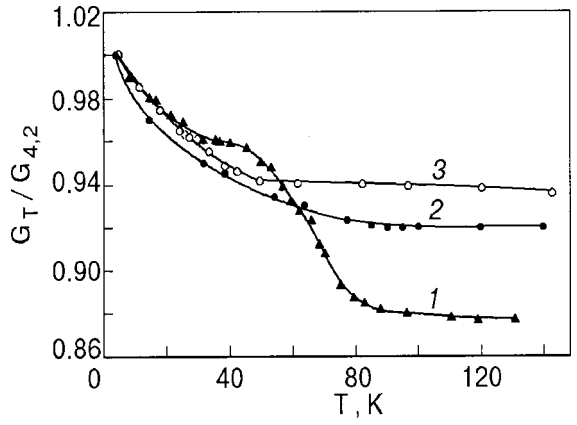


FIG. 2. Temperature dependence of the reduced dynamic shear modulus of the alloy NT-50 in the homogenized state (*1*), after drawing at 77 K (*2*), and after drawing at 77 K in an ultrasonic field (*3*).

As we see from Fig. 2, for the alloy that had been subjected to low-temperature drawing a stabilization of the shear modulus occurs at $T > 90$ K. Since the change in shear modulus in the region of the martensitic transformations is due to a change in the ratio of the titanium and niobium concentrations in the $\beta$-solid solution,[3] the observed constant trend of the shear modulus at low temperatures ($T < 90$ K) is evidence of a constant process of decomposition of the $\beta$-solid solution. It can be assumed that for $T < 90$ K the chemical composition of the $\beta$-solid solution does indeed change. Knowing the value of the shear modulus after the different drawing regimes and after the deformation-induced martensitic transformations on cooling to 4.2 K, one can determine both the amount of titanium in the $\beta$-solid solution and the amount of precipitated titanium-rich phases.

The measurements of $\delta(T)$ and $G(T)$ are done in a heating regime, and we therefore observe the development of the inverse martensitic transformation. The result of the direct martensitic transformation can be determined from the value of the shear modulus after the alloy is cooled to 4.2 K. Let us estimate the degree of completion of the decomposition of the $\beta$-solid solution according to the martensitic kinetics, i.e., the amounts of titanium-rich phases that are precipitated under different actions, assuming that $C_0$ is the titanium concentration in the $\beta$-solid solution of the alloy in the homogenized state ($C_0 = 48.5$ wt. % Ti), and $C_i$ is the titanium concentration in the $\beta$ phase after the various actions. Then $\Delta C = C + 0 - C_i$ characterizes the concentration of titanium-rich phases that have precipitated out of the solid solution. Using the dependence $G(C_i)$ from Ref. 3 for calibration, we estimate the value of $\Delta C$ from the known experimental values of the shear modulus after the different drawing regimes employed and establish the tendency of the resulting structure of the NT-50 alloy to undergo low-temperature martensitic transformation on subsequent cooling. The resulting estimates of the amounts of titanium-rich phases precipitating out of the $\beta$-solid solution of the alloy after all of the actions described above are presented in Table III.

TABLE III. Amount of titanium-rich phases precipitating out of the $\beta$-solid solution of the alloy NT-50 as a result of various regimes of cryogenic drawing followed by low-temperature martensitic transformations.

| State of the alloy | $\Delta C$, wt. % Ti | | |
|---|---|---|---|
| | After drawing | After cooling to 4.2 K | After heating to 100 K |
| Homogenized | — | 12.5 | 6.0 |
| Drawn at 77 K | 7.5 | 11.8 | 10.0 |
| Drawn at 77 K in an ultrasonic field | 8.5 | 9.7 | 9.0 |

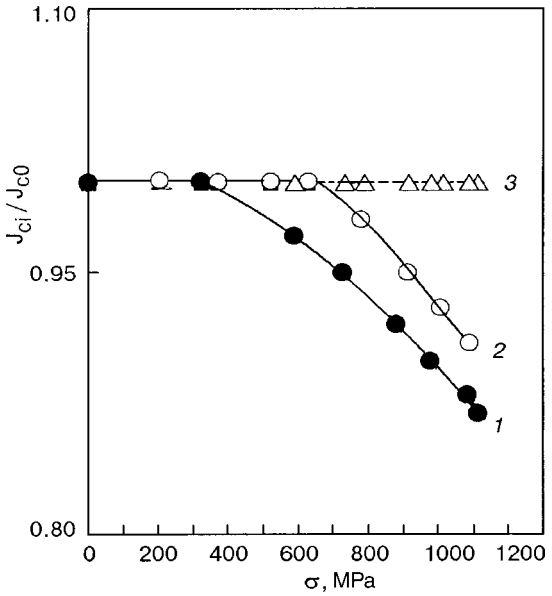


FIG. 3. Reduced critical current of samples of the alloy NT-50 versus the tensile stress at 4.2 K in a field of 5 T: after drawing at 77 K (*1*) and after drawing at 77 K in an ultrasonic field (*2*). Curve *3* corresponds to the value of the reduced critical current when the sample is relieved after each step of the loading.

In determining the degree of completion of the decomposition of the $\beta$-phase matrix at low temperatures it is necessary to take into account that the redistribution of the Ti atoms from the solid solution to the $\alpha''$ and $\omega$ phases occurs by local processes. Thus the decrease of the titanium content in the $\beta$ phase is localized in the regions of precipitation of the titanium-rich phases and in zones depleted or enriched with titanium as a result of the liquation of the Ti and Nb atoms in the $\beta$-solid solution. The intensity of the precipitation of titanium-rich phases according to the martensitic kinetics is quite high, since, despite the metastability of these phases, they can be detected (by electron microscopy[15] and by an x-ray method[16]) even after heating to 300 K. Since the method of measuring the internal friction and shear modulus is an integral one, the measured changes of the shear modulus after the various forms of drawing are averaged over the whole volume of the sample. Consequently, the local changes of the concentration ratio of Nb and Ti in the $\beta$-solid solution near the precipitating titanium-rich phases must be substantially larger.

It is seen in Table III that the use of ultrasonic vibrations in cryogenic drawing intensifies the development of the martensitic transformation in the drawing process (8.5 wt. % Ti as against 7.5 wt. %). Thus the depletion of the $\beta$ phase in titanium should lower the tendency of the $\beta$ phase to undergo low-temperature martensitic transformations,[4] i.e., it should lead to stabilization of the $\beta$ phase on subsequent cooling of the alloy to 4.2 K. Indeed, as a result of the development of the direct deformation-induced martensitic transformation in a sample obtained by ultrasonic drawing, the amount of precipitated titanium-rich phases was 2.1 wt. % less than in the sample obtained by drawing in the absence of ultrasonic vibrations (see Table III). The higher phase stability of the $\beta$ phase of the alloy after drawing in an ultrasonic field is also noted during the inverse martensitic transformation upon heating, where the amount of titanium-rich phases that were not dissolved in the solid solution was 10% for cryogenic drawing without ultrasound, and 9% for drawing in an ultrasonic field (see Table III), i.e., 1.8 wt. % Ti was dissolved in the solid solution as against 0.7 wt. %, respectively.

Thus ultrasonic cryogenic drawing promotes stabilization of the $\beta$ phase and a reduction of the internal stresses in the alloy in comparison with conventional drawing at 77 K.

Let us analyze how the observed structural–phase changes of the NT-50 alloy affect the degradation of the critical current under tensile loading. Figure 3 shows the dependence of the reduced critical current on the tensile stress at 4.2 K in a field of 5 T. We see that ultrasonic cryogenic drawing raises the degradation threshold $\sigma_0$ from 320 to 630 MPa and reduces the degree of degradation of the critical current. We note that when the sample is relieved after each stage of the loading, the value of the critical current returns to its initial value (Fig. 3, dashed line).

The mechanism of the degradation of the critical current under loading has been discussed quite widely in the literature.[3–6] A decisive role in the lowering of the critical current under tensile loading may be played by elastic martensitic transformations involving the formation of nonsuperconducting phases or phases with poorer superconducting characteristics. However, there is not a unified point of view as to the nature of the degradation. Since the degradation effect is reversible when the load is removed, probable mechanisms for the degradation are a reversible martensitic transformation, in particular, the onset of superelasticity, and reversible mechanical twinning. The ''twin'' mechanism of degradation is based on the fact that twin boundaries have a substantial effect on the pinning and dynamics of the magnetic flux, causing a plastic flow of vortices along channels formed by the twin boundaries. For example, in Ref. 6 a twofold decrease of the critical current was observed in a field parallel to the twins.

In this paper the degradation of the critical current is manifested more weakly for the superconductor obtained by ultrasonic cryogenic drawing, which results in a structure with less tendency to undergo low-temperature martensitic transformations and with a reduced level of internal stresses. This niobium–titanium superconductor therefore has a smaller amount of martensitic phases forming in it (see Table III) at temperatures close to the temperatures at which it will

be used (4.2 K). According to the mechanism based on a reversible martensitic transformation,[5] this should lead to partial suppression of the degradation. On the other hand, lowering the peak stresses, which can act as centers for the nucleation of twins, and the formation of a cellular structure on drawing,[1] especially in an ultrasonic field,[17] should make the twinning process more difficult. We therefore surmise that the predominant mechanism for the degradation of the critical current after cryogenic ultrasonic drawing is that of reversible martensitic transformations.

## CONCLUSION

A comparative analysis of the tendency of the alloy NT-50 to undergo low-temperature martensitic transformations and of the degree of degradation of the critical current after different forms of cryogenic drawing has yielded the following conclusions.

In the temperature range 4.2–90 K continual changes in the chemical composition of the $\beta$-solid solution occur. On cooling, they are due to precipitation of metastable titanium-rich phases from it according to martensitic kinetics, and on heating, to the partial return of these phases into the $\beta$-solid solution.

Low-temperature deformation by drawing in an ultrasonic field, leading, on the one hand, to maximal depletion of the $\beta$ phase in titanium on account of the intensification of the deformation-induced martensitic transformation and, on the other, to the development of relaxation of the internal stresses, promotes the stabilization of the $\beta$-solid solution upon subsequent cooling of the sample and raises the threshold and reduces the degree of degradation of the critical current under tensile loading.

This study was done with the support of the Science and Technology Center of Ukraine, Project No. 931.

*E-mail: marbor@rocket.kharkov.ua

[1] V. K. Aksenov, O. I. Volchok, V. M. Gorbatenko, V. A. Emlyaninov, M. B. Lazareva, A. V. Mats, V. S. Okovit, Ya. D. Starodubov, O. V. Chernyi, and L. A. Chirkina, Fiz. Nizk. Temp. **20**, 595 (1994) [Low Temp. Phys. **20**, 471 (1994)].
[2] V. G. Severdenko, V. V. Klubovich, and A. V. Stepanenko, *Pressure-Treatment of Metals* [in Russian], Nauka i Tekhnika, Minsk (1973).
[3] S. S. Koch and D. S. Easton, Cryogenics **17**, 391 (1977).
[4] D. K. Larbalest'er, *Metallurgy and Technology of Superconducting Materials* [in Russian], edited by S. I. Foner and B. Shvarts, Metallurgiya, Moscow (1987).
[5] V. S. Boiko, M. B. Lazareva, Ya. D. Starodubov, O. V. Chernyi, and V. M. Gorbatenko, Fiz. Nizk. Temp. **18**, 121 (1992) [Sov. J. Low Temp. Phys. **18**, 83 (1992)].
[6] A. V. Bondarenko, V. A. Shklovskij, R. V. Vovk, M. A. Obolenskii, and A. A. Prodan, Fiz. Nizk. Temp. **23**, 1281 (1997) [Low Temp. Phys. **23**, 962 (1997)].
[7] O. V. Chernyj, L. G. Udov, G. E. Starozhilov, M. B. Lazareva, N. F. Andrievskaya, L. A. Kornienko, V. V. Slezov, V. V. Sagalovich, Ya. D. Starodubov, and T. Yu. Rudycheva, Cryogenics **32**, ICMC Suppl. 597 (1992).
[8] O. I. Volchok, I. M. Nekludov, Ya. D. Starodubov, and B. P. Chernyi, Cryogenics **32**, ICMC Suppl. 114 (1992).
[9] I. A. Gindin, V. I. Kovalenko, V. S. Okovit, Ya. D. Starodubov, and L. A. Chirkina, Zavod. Lab. No. 11, 1397 (1970).
[10] I. A. Gindin, M. B. Lazareva, Ya. D. Starodubov, and M. P. Starolat, Vopr. At. Nauki Tekh. Ser. Fund. Prikl. Sverkhprovodimost', issue 1(4), 62 (1976).
[11] M. A. Krishtal, Yu. V. Piguzov, and S. A. Golovin, *Internal Friction in Metals and Alloys*, Metallurgiya, Moscow (1964).
[12] M. L. Bernshteĭn and V. A. Zaĭmovskiĭ, *Structure and Mechanical Properties of Metals* [in Russian], Metallurgiya, Moscow (1970).
[13] V. S. Okovit, L. A. Chirkina, O. V. Chernyi, V. K. Aksenov, A. V. Mats, Ya. D. Starodubov, and G. E. Storozhilov, Vopr. At. Nauki Tekh. Ser. Yad.-Fiz. Issled. (Teor. Éksp.), issue 9(17), 61 (1990).
[14] V. S. Okovit and L. A. Chirkina, Fiz. Met. Metalloved. **56**, 819 (1983).
[15] B. Obst, D. Pattanayak, and P. Hockstuhl, J. Low Temp. Phys. **401**, 595 (1980).
[16] V. A. Lototskaya, V. Ya. Il'ichev, A. I. Prokhvatilov, and A. P. Isakina, Metallofizika (Kiev) **12**, No. 2, 78 (1990).
[17] N. N. Noskova, N. F. Vil'danova, A. F. Kondrat'ev, A. F. Komissarov, Yu. I. Filippov, and V. A. Pavlov, Fiz. Met. Metalloved. **52**, 433 (1981).

Translated by Steve Torstveit

## LOW-TEMPERATURE MAGNETISM

# On the magnetoelastic nature of the anisotropic domains in easy-plane crystals of iron-group dihalides

V. M. Kalita and A. F. Lozenko

*Institute of Physics, National Academy of Sciences of Ukraine, pr. Nauki 46, 03028 Kiev-28, Ukraine**
(Submitted June 14, 2000; revised December 27, 2000)
Fiz. Nizk. Temp. **27**, 489–494 (May 2001)

A structure is proposed for the magnetoelastic antiferromagnetic domains in easy-plane antiferromagnets of the iron-group dihalides. The proposed structure is made up of a triad of regions with 120° rotation of the antiferromagnetic vector on passing between adjacent regions. This domain structure may be stabilized by defects which are isotropic in the easy plane and which preserve the orientational degeneracy of the directions of the antiferromagnetic vector in the easy plane. © *2001 American Institute of Physics.* [DOI: 10.1063/1.1374720]

120-degree antiferromagnetic (AFM) domains have been observed previously[1,2] in $CoCl_2$, $CoBr_2$, and $NiCl_2$. These crystals have a layered structure. The intralayer exchange interaction between metal ions is of the ferromagnetic type and is much stronger than the interlayer AFM exchange,[3] and the ''easy-plane'' anisotropy leads to an orientation of the AFM vector in the plane, which coincides with an ionic layer in the crystal. All directions of the AFM vector in that plane are nearly equivalent, although the symmetry admits the presence of anisotropy in it on account of the twofold crystallographic axes. The existence of domain structure is confirmed by neutron-scattering experiments[1] and studies of the magnetoelastic[4,5] and magnetic[6] properties. It has been shown[4,5] that these materials typically have a very large magnetostriction.

In dilatometric measurements of the induced magnetostriction in Refs. 4 and 5 it was shown that the multidomain crystal on the whole is initially undeformed in the case of ''nearly unstressed'' domains. The imposition of a magnetic field oriented in the easy plane destroys the domain structure, and a uniform striction corresponding to a single-domain state appears. The transition from the multidomain state to the single-domain state occurs in fields much lower than the spin-flip field.[4] In $CoCl_2$ at $T=4.2$ K this transition is complete at $H\approx 8$ kOe and is accompanied by a relative lengthening of the crystal by an amount of the order of $6\times 10^{-4}$. When the field is removed the crystals reversibly pass into a multidomain state that almost completely restores the initial form.

The existence of a domain structure that is nearly reversible in a cycle of imposition and removal of a magnetic field raises the question of the nature of its equilibrium or quasiequilibrium.[2] Magnetostatic fields, as in the case of a ferromagnet, do not exist in antiferromagnets.

The formation of AFM domains may result from entropy growth due to an additional entropy contribution resulting from the decrease of the order in the crystal.[7] Such a small energy benefit may be entirely sufficient if the domain walls are parallel to the easy plane and the energy cost of the rotation of the spins at such a domain wall is due to the small intersublattice exchange.[2] A multidomain equilibrium state arises, but as the temperature is lowered away from the phase transition temperature the entropic mechanism ceases to have an effect. In the crystals under discussion the reversible multidomain situation is observed at $T=4.2$ K, raising doubts that the entropic mechanism is responsible for it, whereas the $NiCl_2$ crystal has a Néel temperature $T_N=49.6$ K. The entropic mechanism for the crystals under study must be reconciled with the large magnetoelasticity observed in them, and the 120° domain structure should be accompanied by stress-relief regions; consequently, besides the energy cost of domain-wall formation, one must take into account the appreciable cost in elastic energy. Therefore, it is likely that a different mechanism is responsible for the equilibrium of the multidomain state.

The formation of AFM domains may be caused by imperfections of the crystal lattices.[2] For example, metallurgical inhomogeneities that locally lower the symmetry of the crystal may cause the AFM vector **L** to be oriented accordingly. This sort of lattice imperfections, which on average preserve the symmetry of the crystal, require a larger field than is observed experimentally for the crystal to be brought to a single-domain state and a greater broadening of the AFM resonance lines in the multidomain state.[8,9]

The formation of the AFM domain structure may be caused by screw dislocations.[10,11] In this case, as was shown in Ref. 10, the domain structure is stabilized by the in-plane crystalline anisotropy.

In Ref. 12 a mechanism in which the formation of domains in layered antiferromagnets is influenced by the surface was considered with allowance for the magnetoelastic interaction. The principal feature of such a mechanism is the existence of a limiting size of the sample such that for crystals with larger dimensions the formation of the multidomain state by this mechanism becomes unfavorable.

In Ref. 4 it was conjectured that the magnetoelasticity is decisive for the AFM multidomain state in $CoCl_2$, $CoBr_2$,

 

and $NiCl_2$, and the formation of domains preserves the degeneracy of directions in the layer.

In the present paper we propose a geometric structure of magnetoelastic AFM domains which satisfies the requirements of orientational degeneracy in the layer. We show that the realization of such a domain structure presupposes the presence of defects in the crystal, which expand or compress the lattice in the layer around the defect. We analyze the deformation of the domains in the proposed domain structure and give the possible types of domain walls.

Uniform strains are realized far from the defects in the interior of a free domain in neglect of its boundaries. The values of the uniform strain in the easy plane are determined from minimization of the free energy, including the magnetoelastic and elastic terms:

$$e=\gamma(L_x^2-L_y^2)(U_{xx}-U_{yy})+\delta L_x L_y U_{xy} + \frac{C_{11}}{2}(U_{xx}^2+U_{yy}^2)+C_{12}U_{xx}U_{yy}+(C_{11}-C_{12})U_{xy}^2, \tag{1}$$

where $\gamma$ and $\delta$ are parameters of the magnetoelastic interactions. At low temperatures the magnitude of the AFM vector is constant, $|\mathbf{L}|=L$. Equation (1) does not include the terms due to the isotropic expansion in the plane, which do not affect the domain structure. The energy (1) is isotropic in the easy plane.

An orientation of the vector **L** in the easy plane is brought about by the easy-plane type of anisotropy in the crystals under study, with a positive uniaxial (along the $z$ axis) contribution $DL_z^2$ to the anisotropy energy, with $D>0$. In $NiCl_2$ the value of $D$ amounts to only a few percent of the intrasublattice exchange, while in $CoCl_2$ it is of the order of 50%.[3] In spite of such differences, in the crystals under study $D$ is much greater than the in-plane anisotropy, which we write in the form

$$e_a=AL^6\cos(6\theta), \tag{2}$$

where $A$ is a constant, and $\theta$ is the direction angle of the vector **L** in the easy plane. The anisotropy (2) orients the vector **L** along one of the twofold axes. In all the crystals the constant $A$ is much less than $D$.

When **L** is parallel to the $x$ axis the uniform strain has the values

$$U_{xx}=-U_{yy}=-\frac{\gamma L^2}{C11-C_{12}}. \tag{3}$$

The strain (3) is equilibrium: the mechanical stresses are compensated by the magnetoelastic forces (the total stress is zero).

Analysis of the structure of a magnetoelastic antiferromagnet containing domains in the presence of several ''easy'' axes in the plane requires a mutual coordination of the domains, since because of the continuity of the crystal the spontaneous magnetostriction in one of the domains can cause stresses in the neighboring domains, thereby increasing the total energy. For two neighboring domains lying in the same layer and having different directions of **L** the domain boundary can be situated so that the strain components along the boundary will be equal in neighboring domains.

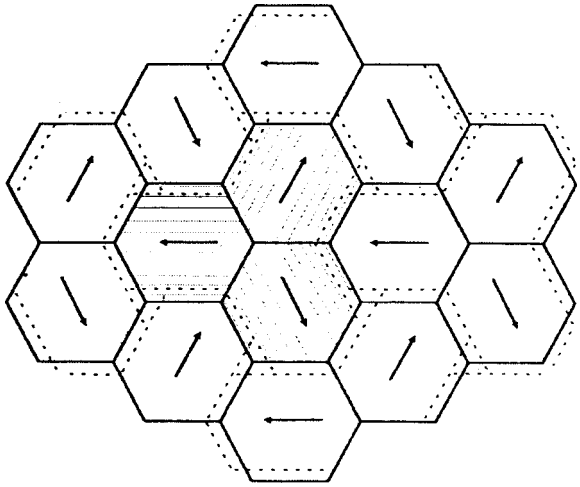

FIG. 1. Hexagons of an undeformed crystal (solid lines) and their deformation (dotted lines). The three shaded domains form a triad. The arrows indicate the direction of the AFM vector in each domain.

Considering the possibility that three domains in the same layer with different directions of **L** can come together in a certain region, we see that the condition that there be no mutual stresses cannot be satisfied. Such a region will be stressed. The basic idea of the present paper is that one can achieve elastic matching at places where three domains come together in a plane by placing on it defects having intrinsic strains of the same kind as those in the region where the domains come together.

*The structure of 120° domains* in the crystals under study is shown in Fig. 1. The solid lines depict regular hexagonal regions introduced in the the crystal in the absence of AFM ordering. The presence of nonzero **L** in each region will lead to spontaneous deformation of the hexagons, e.g., as in Fig. 1, to extension along the diagonal of the hexagon parallel to **L**, and to compression in the perpendicular direction. The deformed hexagons are depicted by the dotted lines parallel to the boundaries of the undeformed hexagons.

In all of the regions of the structure the stresses are basically compensated by magnetoelastic forces, except for local regions in which, as can be seen in the Fig. 1, the free existence of the domains presupposes the presence of uncompensated stresses (tensile in this illustration). These are the regions enclosed by the equilateral triangles at the sites where three domains belonging to different ''triads'' come together (one such triad is indicated by shading in Fig. 1). As a result of the deformation, a hexagon becomes biaxial, with $C_3$ symmetry of the local expansion at the sites.

The domain structure in the form of a set of deformed hexagons with vertex angles of 120°, as in Fig. 1, leaves the domains unstressed in the ideal crystal. The uniform strains (3) do not affect the volume, and for such a strain the 120° angles at the vertices of the deformed hexagons are not preserved. The formation of the triangular dilatation regions in Fig. 1 means that the illustrated domains are deformed without conserving area, and so Eq. (3) is not satisfied.

Let us determine the value of the energy cost due to the actual nonuniformity of the deformations of the hexagons in Fig. 1. The strain $U_{yy}$ of a hexagon in the direction perpendicular to **L** is uniform and remains the same as in (3), while

the strain $U_{xx}$ along **L** is nonuniform. Placing the origin of the coordinate system at the center of a hexagon, we obtain the following expressions for $U_{xx}$ and $U_{yy}$:

$$U_{xx}=-\frac{\gamma L^2}{C_{11}-C_{12}}\left(\frac{1}{2}+\frac{|y|}{\sqrt{3}a}\right);\quad U_{yy}=\frac{\gamma L^2}{C_{11}-C_{12}},\qquad (4)$$

where $a$ is the length of a side of the undeformed hexagon. For $y=a\sqrt{3}/2$ the strain $U_{xx}=-\gamma L^2/(C_{11}-C_{12})$, and for $y=0$ it is a factor of two smaller.

For the strain (4) the total energy of the elastic and magnetoelastic components of the nonuniformly deformed hexagon is

$$E=-\frac{3\sqrt{3}}{2}\frac{\gamma^2L^4}{C_{11}-C_{12}}a^2\left(1-\frac{7C_{11}}{3^2 2^4(C_{11}-C_{12})}\right)\qquad (5)$$

or

$$E=E_0\left(1-\frac{7C_{11}}{3^2 2^4(C_{11}-C_{12})}\right)$$
$$\approx E_0\left(1-0.0486\frac{C_{11}}{C_{11}-C_{12}}\right),\qquad (6)$$

where $E_0$ is the total energy of the uniformly deformed hexagon, $E_0=-a^2(3\sqrt{3}/2)[\gamma^2L^4/(C_{11}-C_{12})]$.

We write the magnetoelastic energy cost due to the nonuniform deformation of a hexagon as

$$\Delta E_d=0.0486\frac{3\sqrt{3}}{2}\frac{\gamma^2L^4C_{11}}{(C_{11}-C_{12})^2}a^2.\qquad (7)$$

For the actual values of the elastic constants of the crystals studied, the cost (7) amounts to several percent of $E_0$. The structure in Fig. 1 can be regarded as a rather good approximation of the magnetoelastic domains in these crystals.

Let us place dilatative point defects at the sites where three domains come together. The modulus of the strain vector of such a defect will decay at large distances in proportion to the inverse square of the distance from it.[13] The stresses created by the defect will be inversely proportional to the cube of the distance. Matching the strains of the defect and domains will limit the defect region to the magnetoelastically strained regions formed where the three domains come together. This decreases the volume of the region deformed by the defect and, hence, decreases the energy cost of the defect. Point defects arising during growth increase the elastic energy of the crystal; this contribution to the energy of the crystal is decreased when a site at which three domains come together is placed at the point of the defect described above, i.e., the multidomain state becomes preferable.

An analogous elastic matching can be obtained if a disclination perpendicular to the easy plane passes through the region where three domains come together.[13] Let us estimate the energy benefit of surrounding a disclination with domains. The strain created by a disclination in the paramagnetic phase is symmetric in the plane and depends only on the distance $r$ from the defect. The strain vector is[14]

$$U_r=br^{-1},\qquad (8)$$

where $b$ is a constant. The elastic strain (8) has an energy cost to the crystal.

When the defect is surrounded by domains in the AFM state, the elasticity created by the defect is limited to a volume determined from the condition that the strain of the defect be equal to the strain created by surrounding it with domains. The value of this distance $r_0$ can be determined by the formula

$$r_0=\left(\frac{b(C_{11}-C_{12})}{\gamma L^2}\right)^{1/2}.\qquad (9)$$

The limiting of the size of the elastic strain region of a defect is accompanied by a decrease of its elastic energy and, hence, lends an energy benefit to the crystal as a whole. The energy benefit $\Delta E$ is determined by integrating the elastic energy density with the strain (8) over the limits from $r_0$ to $\infty$. This gives

$$\Delta E=b\gamma L^2.\qquad (10)$$

The temperature dependence of the energy benefit (10) is similar to that of the square of $L$.

If a defect is located in a uniform region, then its strains must be matched with the dilatative strains along **L** and the compressive strains perpendicular to **L**. In relation to the case when the defect is located at the point where three domains come together, a defect in the uniform region makes for a larger volume of the strain created by the defect and for an angular dependence of the position of its boundaries. Even in the case when matching the elasticity of the defect with the uniform strains gives an energy benefit, i.e., when there is a decrease of the elastic energy at the defect, this benefit will be less than that given by (10) if the defect region is bounded by three domains, as in Fig. 1.

The geometric structure of the domains shown in Fig. 1 presupposes the presence of defects which isotropically dilate the crystal in the plane. Here the defect does not impose directions on the AFM vectors in the domains, and the orientational degeneracy in the easy plane is preserved.

For the structure shown in Fig. 1 it was assumed that the crystal expands along the diagonal of the hexagon, and dilatative defects are required for its stabilization. If the crystal instead expands along the direction perpendicular to the diagonals of the hexagon, then the places where three domains come together will be compression regions. The stabilization of such a structure would require defects of a different type, e.g., vacancies. The real picture of the domains in a crystal will be determined by the whether dilatative or compressive defects are in the majority in the crystal.

In Fig. 1 the AFM vectors in the domains around the defects have different rotations—clockwise and counterclockwise. Two directions are possible for **L**—parallel and antiparallel to the axis of the hexagon, i.e., in each of the domains in the proposed structure the vector **L** can be rotated by 180° independently of its neighbors. This arbitrariness is eliminated either by imposed symmetry restrictions or by the mechanism of domain formation itself, as in the case of AFM domains caused by screw dislocations.[10] The orientation of **L** in the triad of domains in Fig. 1, in each of which the easy-plane symmetry is spontaneously lowered, restores the initial symmetry of the crystal. Figure 2 shows the struc-

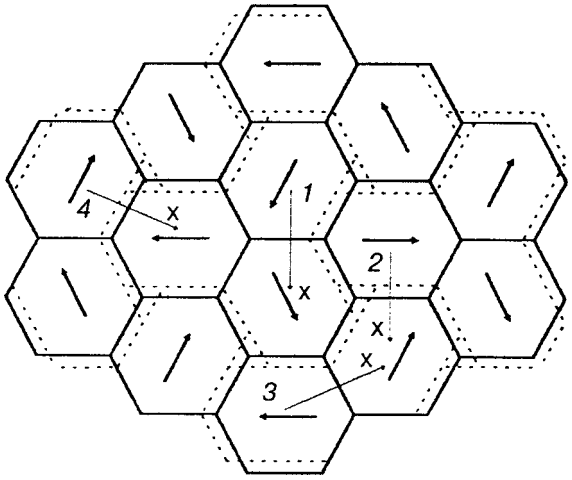


FIG. 2. The structure of domains with an uncompensated AFM vector of the triad. The *x* axes denote the direction of passage through the domain walls *1–4*.

ture of AFM domains obtained by a 180° rotation of the vector **L** in each of the domains of a triad. In this structure the resultant **L** of a triad is nonzero, while the average value of **L** for the whole crystal is zero. In this structure, however, the symmetry is broken at some of the sites. In passing around such a site the vectors **L** of the domains do not go over progressively from one domain to the next.

*The domain walls* in these structures, on passing from one domain to another, occur in the form of symmetric and asymmetric walls, with a rotation of the vector **L** by 60° and 120°. For each of the domains the direction of the *x* axis, perpendicular to the plane of the wall, is indicated in Fig. 2.

For a symmetric 60° wall (Fig. 2, case *1*) the boundary conditions are specified by the orientation of **L** in the uniform state in the form $\theta=-\pi/6$ if $x=-\infty$ and $\theta=\pi/6$ if $x=+\infty$. For the asymmetric 60° domain wall (case *2*) the boundary conditions at an infinite distance from the wall are specified by the angles $\theta=\pi/2$ and $\theta=\pi/2+\pi/3$.

The symmetric 120° wall (case *3*) is specified by boundary conditions at infinity in the form $\theta=\pi-\pi/6$ and $\theta=\pi/6$. The asymmetric 120° wall (case *4*) is specified by the boundary angles $\theta=\pi/2$ and $\theta=\pi+\pi/6$. The structures in Figs. 1 and 2 characterize the number of 60° and 120° walls.

The energy density $e_d$ of a 60° wall is estimated by assuming that it is determined by the competition of the exchange interaction and the in-plane anisotropy:[15]

$$e_d=\frac{2^3}{3}L^4\sqrt{\alpha|A|}, \tag{11}$$

where $\alpha$ is the inhomogeneity parameter of the exchange energy. The energy of a 120° wall is equal to twice the value given in (11). The temperature dependence of the energy cost of domain-wall formation (11) is governed by the fourth power of the temperature dependence of $L$.

For equilibrium realization of the domain structure (see Fig. 1) it is necessary that the energy benefit (10) be larger than the sum of the costs (7) and (11). The temperature dependence of the benefit goes like that of $L^2$, while the temperature dependence of the cost is like that of $L^4$. At high temperatures, when $L$ is small, an energy benefit is almost always realized. At low temperatures it can happen that the energy (10) is insufficient to bring about an equilibrium multidomain state, and it is therefore possible for the equilibrium multidomain state to vanish as the temperature is lowered. When the benefit (10) is small, this behavior of the multidomain state is similar to that for a multidomain state of entropic origin, which always vanishes at low temperature.

## CONCLUSION

We note that one of the possible mechanisms of formation of a magnetoelastic domain structure, consistent with the assumptions and remarks made above, is the elastic interaction of spontaneously deformed (with a uniform orientation of the AFM vector) regions—triads with local defects in the easy plane which create compressive or dilatative strains in it. Such defects ensure the stability of the domain structure and preserve the degeneracy of the orientation of the directions of the spontaneous striction of the domains in the easy plane. Here the domains will be practically unstressed, and in the crystal as a whole in a multidomain state in zero field there will be compensation of the anisotropic spontaneous striction.

The authors thank S. M. Ryabchenko and V. M. Loktev for fruitful discussions in the course of this study and for making some suggestions and comments.

*E-mail: ryabch@labmag.ip.kiev.ua

[1] M. K. Wilkinson, J. W. Cable, E. O. Wollan, and W. C. Koehler, Phys. Rev. **113**, 497 (1959).
[2] M. M. Farztdinov, Usp. Fiz. Nauk **84**, 611 (1964) [Sov. Phys. Usp. **7**, 855 (1965)].
[3] M. E. Lines, Phys. Rev. **131**, 546 (1963).
[4] V. M. Kalita, A. F. Lozenko, S. M. Ryabchenko, and P. A. Trotsenko, Ukr. Fiz. Zh. **43**, 1469 (1998).
[5] A. F. Lozenko, P. E. Parkhomchuk, S. M. Ryabchenko, and P. A. Trotsenko, Fiz. Nizk. Temp. **14**, 941 (1988) [Sov. J. Low Temp. Phys. **14**, 517 (1988)].
[6] D. Billerey, C. Terrier, A. J. Pointon, and J. P. Redoules, J. Magn. Magn. Mater. **21**, 187 (1980).
[7] Y. Y. Li, Phys. Rev. **101**, 1450 (1956).
[8] I. S. Jacobs, S. Roberts, and S. D. Silverstein, J. Appl. Phys. **39**, 816 (1968).
[9] A. F. Lozenko and S. M. Ryabchenko, Zh. Éksp. Teor. Fiz. **65**, 1085 (1973) [Sov. Phys. JETP **38**, 538 (1974)].
[10] A. S. Kovalev and A. M. Kosevich, Fiz. Nizk. Temp. **3**, 259 (1977) [Sov. J. Low Temp. Phys. **3**, 125 (1977)].
[11] I. E. Dzyaloshinskiĭ, JETP Lett. **25**, 414 (1977).
[12] E. V. Gomonaj and V. M. Loktev, Fiz. Nizk. Temp. **25**, 699 (1999) [Low Temp. Phys. **25**, 520 (1999)].
[13] A. M. Kosevich, *Theory of the Crystal Lattice* [in Russian], Vishcha Shkola, Kharkov (1988).
[14] L. D. Landau and E. M. Lifshitz, *Fluid Mechanics*, 2nd ed. [Pergamon Press, Oxford–New York (1987); Nauka, Moscow (1987)].
[15] L. D. Landau and E. M. Lifshitz, *Electrodynamics of Continuous Media*, 2nd ed., rev. and enl., by E. M. Lifshitz and L. P. Pitaevskii [Pergamon Press, Oxford (1986); Nauka, Moscow (1982)].

Translated by Steve Torstveit

# Effect of a negative biquadratic interaction on the phase states and spectra of coupled magnetoelastic waves of an easy-plane ferromagnet

Yu. A. Fridman, O. V. Kozhemyako, and B. L. Eingorn

*V. I. Vernadskii Tavricheskii National University, ul. Yarminskaya 4, 95007 Simferopol, Ukraine**

(Submitted November 7, 2000; revised December 25, 2000)
Fiz. Nizk. Temp. **27**, 495–499 (May 2001)

The spectra of the coupled magnetoelastic waves of an easy-plane ferromagnet with a negative biquadratic interaction are investigated. It is shown that in this case the existence region of the quadrupolar phase is narrowed substantially in comparison with the case of a positive biquadratic interaction. The phase diagram of the system is constructed. © *2001 American Institute of Physics.* [DOI: 10.1063/1.1374721]

## INTRODUCTION

A great deal of interest is now being devoted to the study of magnets in which the interaction between magnetic ions is more complex than the Heisenberg exchange.[1–4] It is of interest from a practical standpoint to study the characteristics of the excitation spectrum of such magnets as the external magnetic field is varied. Such studies are important because of the existence of a number of singlet magnets,[4–6] which can be found in a nonmagnetic state at $H=0$ (the so-called quadrupolar (QP) phases) and undergo a transition to a magnetic phase when a sufficiently strong external magnetic field is applied.

In Refs. 1–3 it was shown that the inclusion of a biquadratic interaction leads to a number of purely quantum effects, in particular, to the formation of phases with a tensor order parameter, i.e., QP phases. The mechanism of formation of these phases depends on the relationship between the constants of the Heisenberg and biquadratic exchange interactions.[2] Systems with a positive biquadratic interaction constant $K_0$ were studied in Refs. 1–3. Taking a negative biquadratic interaction ($K_0<0$) into account even in isotropic systems leads to qualitatively new results.[7,8]

In this connection it is of interest to investigate the dynamical properties and phase states of highly anisotropic non-Heisenberg ferromagnets with $K_0<0$. In studying such a system, we shall also take into account the magnetoelastic interaction. This generally weak interaction is taken into account because in the vicinity of orientational phase transitions the influence of the magnetoelastic coupling on the dynamical properties of the system becomes decisive (see, e.g., Ref. 9).

## DISPERSION RELATION OF COUPLED MAGNETOELASTIC WAVES

Let us investigate the well-studied model of a non-Heisenberg ferromagnet with one-ion anisotropy of the easy-plane type in an external magnetic field perpendicular to the basal plane ($X0Y$).[2] Unlike Ref. 2, however, here we consider the case in which the biquadratic exchange constant is negative. Such a situation is realized in $DyVO_4$, for example.[7,8] In addition, we take into account the magnetoelastic interaction, since, as we have said, this interaction becomes important in the neighborhood of an orientational phase transition.

The Hamiltonian of the system can be written in the form

$$\mathcal{H}=-H\sum_n S_n^z-\frac{1}{2}\sum_{n,n'}[J(n-n')\mathbf{S}_n\cdot\mathbf{S}_{n'}+K(n-n')\times(\mathbf{S}_n\cdot\mathbf{S}_{n'})^2]+\frac{\beta}{2}\sum_n (S_n^z)^2+\nu\sum_{n,i,j} S_n^i S_n^j u_{ij}(n)+\int dr\left[\frac{\lambda+\eta}{2}\sum_i u_{ii}^2+\eta\sum_{i,j} u_{ij}^2+\lambda\sum_{i\neq j} u_{ii}u_{jj}\right], \quad (1)$$

where $S_n^i$ is the spin operator at site $n$, $J(n-n')>0$ and $K(n-n')<0$ are the Heisenberg and biquadratic interaction constants, $\beta>0$ is the one-ion anisotropy constant, $\nu$ is the magnetoelastic coupling constant, $\lambda$ and $\eta$ are the elastic moduli, and $u_{ij}=1/2[\partial u_i/\partial x_j+\partial u_j/\partial x_i]$ is the symmetric part of the components of the elastic strain tensor.

The first three terms in Eq. (1) describe the magnetic subsystem, the fourth describes the magnetoelastic coupling, and the last term, which for simplicity we have written in continuum form, describes the elastic energy of the system. From now on, we shall assume that the magnetic ion has spin $S=1$.

Taking the one-ion anisotropy and the magnetoelastic interaction into account, as we have said, leads to a number of interesting effects of a purely quantum nature. An adequate mathematical formalism by which the effects of both the one-ion anisotropy and the magnetoelastic interaction can be taken into account exactly is the Hubbard operator technique.[10] The Hubbard operators are constructed in a basis of the eigenfunctions of the one-ion Hamiltonian and are related to the spin operators as follows:

$$S_n^+=\sqrt{2}[\sin\theta(X_n^{01}-X_n^{-10})+\cos\theta(X_n^{0-1}+X_n^{10})];$$

$$S_n^z=\cos 2\theta(X_n^{11}-X_n^{-1-1})-\sin 2\theta(X_n^{1-1}+X_n^{-11}),$$

$$S_n^-=(S_n^+)^+. \quad (2)$$

 

Here $X_n^{M'M}=|\Psi_n(M')\rangle\langle\Psi_n(M)|$ are the Hubbard operators describing the transition of a magnetic ion from the state $M'$ to the state $M$ (for $S=1$, $M$ can take the values $-1$, 0, 1); $\theta=\theta_1+\theta_2$;

$$\cos\theta_1=\left[\frac{\sqrt{\overline{H}^2+(B_2^2)^2}+\overline{H}}{2\sqrt{\overline{H}^2+(B_2^2)^2}}\right]^{1/2};\quad \cos\theta_2=\frac{\nu/2(u_{xx}^{(0)}-u_{yy}^{(0)})\cos 2\theta_1}{\sqrt{\chi(\chi/2-\overline{H}\cos 2\theta_1+B_2^2\sin 2\theta_1+\nu/2(u_{xx}^{(0)}-u_{yy}^{(0)})\sin 2\theta_1)}};$$

$$\overline{H}=H+\left(J_0+\frac{|K_0|}{2}\right)\langle S^z\rangle;\quad B_2^2=-\frac{|K_0|}{2}q_2^2;\quad B_2^0=-\frac{\beta+|K_0|q_2^0}{6};\quad q_2^0=3\langle(S^z)^2\rangle-2;\quad q_2^2=\frac{\langle(S^+)^2\rangle+\langle(S^-)^2\rangle}{2};$$

$$\chi^2=4\overline{H}^2+[2B_2^2-\nu(u_{xx}^{(0)}-u_{yy}^{(0)})]^2.$$

The quantities $q_2^p$ ($p=0,2$) relate to the additional (to the mean field) field due to the quadrupole moment, and $u_{ij}^{(0)}$ are the spontaneous strains, which are determined for the minimum of the free energy density in the case of low temperatures ($T\ll T_C$, where $T_C$ is the Curie temperature) and have the form

$$u_{xx}^{(0)}=\frac{\nu}{2\eta(\eta+3\lambda)}\left[\lambda-\eta+\frac{B_2^2}{\chi_0}(\eta+3\lambda)\right];$$

$$u_{yy}^{(0)}=\frac{\nu}{2\eta(\eta+3\lambda)}\left[\lambda-\eta-\frac{B_2^2}{\chi_0}(\eta+3\lambda)\right];\qquad(3)$$

$$u_{zz}^{(0)}=-\frac{\nu(\lambda+\eta)}{\eta(\eta+3\lambda)};\quad u_{ij}^{(0)}=0,\quad i\neq j,\quad \chi_0=\chi_{\nu=0}.$$

The energy levels of a magnetic ion in this case are

$$E_{1,-1}=-3B_2^0+\frac{\nu}{2}(u_{xx}^{(0)}+u_{yy}^{(0)}+2u_{zz}^{(0)})\mp\frac{\chi}{2},$$

$$E_0=\nu(u_{xx}^{(0)}+u_{yy}^{(0)}).\qquad(4)$$

Writing the components of the strain tensor in the form $u_{ij}=u_{ij}^{(0)}+u_{ij}^{(1)}$, where $u_{ij}^{(1)}$ is the dynamic part of the strain tensor, which describes vibrations of the crystal lattice, and quantizing it in the standard manner, we obtain the transformation Hamiltonian describing the processes of transformation of magnons into phonons and *vice versa*:

$$\mathcal{H}_{\rm tr}=\sum_n\left(\sum_M P_M X_n^{MM}+\sum_\alpha P_\alpha X_n^{\alpha(M'M)}\right),$$

where

$$P_{M(\alpha)}=\frac{1}{N^{1/2}}\sum_{k,\lambda}(b_{k,\lambda}+b_{-k,\lambda}^+)T_n^{M(\alpha)}(k,\lambda),$$

$b_{k,\lambda}$ and $b_{k,\lambda}^+$ are the annihilation and creation operators for $\lambda$-polarized phonons, $T_n^{M(\alpha)}(k,\lambda)$ are the transformation amplitudes, and $\alpha=\alpha(M',M)$ are the root vectors.

To obtain the equations for the Green's function, whose poles determine the spectra of the elementary excitations,

$$G^{\alpha\alpha'}(n,\tau;n',\tau')=-\langle T\tilde{X}_n^\alpha(\tau)\tilde{X}_{n'}^{-\alpha'}(\tau')\rangle,$$

we must write the exchange part of Hamiltonian (1) in terms of the Hubbard operators.

The following calculations will be done in the mean field approximation, and we shall therefore need only the ''transverse'' part of the exchange Hamiltonian, which has the form

$$\mathcal{H}_{\rm int}^\perp=-\frac{1}{2}\sum_{\substack{nn'\\ \alpha\beta}}[\mathbf{c}(\alpha),A_{nn'}\mathbf{c}(\beta)]X_n^\alpha X_{n'}^\beta.$$

Here $\mathbf{c}(\alpha)$ is an eight-dimensional vector having the components

$$\mathbf{c}(\alpha)=\{\gamma_1^\parallel(\alpha),\gamma_1^\perp(\alpha),\gamma_1^{*\perp}(-\alpha),\gamma_2^\parallel(\alpha),\gamma_2^\perp(\alpha),\gamma_2^{*\perp}(-\alpha),\gamma_3^\perp(\alpha),\gamma_3^{*\perp}(-\alpha)\}.$$

The functions $\gamma_i^{\parallel(\perp)}(\alpha)$ are determined from the relation (2) between the spin operators and the Hubbard operators, and the $8\times 8$ matrix $A_{nn'}$ decomposes into a direct sum of matrices:

$$A_{nn'}=A_{nn'}^{(3)}\oplus A_{nn'}^{(5)},$$

$$A_{nn'}^{(3)}=\left\{J(n-n')+\frac{1}{2}|K(n-n')|\right\}\begin{pmatrix}1&0&0\\0&0&\frac{1}{2}\\0&\frac{1}{2}&0\end{pmatrix},$$

$$A_{nn'}^{(5)}=-\frac{1}{2}|K(n-n')|\begin{pmatrix}1&0&0&0&0\\0&0&\frac{1}{2}&0&0\\0&\frac{1}{2}&0&0&0\\0&0&0&0&\frac{1}{2}\\0&0&0&\frac{1}{2}&0\end{pmatrix}.$$

The inclusion of the biquadratic interaction has formally reduced to an increase in the dimensionality of the vectors $\mathbf{c}(\alpha)$ and matrix $A_{nn'}$ in comparison with the case of the Heisenberg model.

The dispersion relation of the coupled magnetoelastic waves (in the mean field approximation) has the form

$$\det\| \delta_{ij} + G_0^{\alpha} b(\alpha) a_{ik}(\alpha) A_{kj} + \Phi(k,\lambda,\lambda') T^{-\alpha}(k,\lambda) G_0^{\alpha} b \times (\alpha) T^{\beta}(-k,\lambda') G_0^{\beta} b(\beta) a_{ik}(\alpha,\beta) A_{kj} \| = 0, \quad (5)$$

where $G_0^{\alpha}$ is the zeroth Green's function, $b(\alpha) = \langle \boldsymbol{\alpha} \mathbf{X} \rangle$ are the terminal factors, $\Phi(k,\lambda,\lambda') = D_{\lambda}(k,\omega)/1 - Q_{\lambda\lambda'} D_{\lambda'}(k,\omega)$, $D_{\lambda}(k,\omega)$ is the Green's function of a noninteracting phonon, and

$$Q_{\lambda\lambda'} = T^{\alpha}(-k,\lambda) G_0^{\alpha} b(\alpha) T^{-\alpha}(k,\lambda');$$

$$a_{ik}(\alpha,\beta) = c_{ir}(\alpha) c_{rk}(-\beta); \quad a_{ik}(\alpha) = a_{ik}(\alpha,\alpha).$$

Equation (5) describes the spectra of coupled magnetoelastic waves for arbitrary values of the one-ion anisotropy constants and arbitrary temperatures (up to the critical temperatures).

## PHASE STATES AND SPECTRA OF COUPLED MAGNETOELASTIC WAVES

Let us investigate the spectra of coupled magnetoelastic waves in the low-temperature range ($T \ll T_C$). We shall consider a highly anisotropic ferromagnet, i.e., $\beta \gg J_0, |K_0|$.

We analyze Eq. (5) in the case when the wave vector $\mathbf{k} \| 0Y$. In this geometry the nonzero components of the unit vector of the phonon polarization are $e_{\tau}^{x}$, $e_t^{z}$, $e_l^{y}$, and the dispersion relation (5) decomposes into two equations describing the spectra of ''longitudinal'' and ''transverse'' vibrations, respectively:

$$\begin{vmatrix} 1+x_{11} & x_{15} & x_{16} \\ x_{51} & 1+x_{55} & x_{56} \\ x_{61} & x_{65} & 1+x_{66} \end{vmatrix} = 0, \quad (6)$$

$$\begin{vmatrix} 1+x_{22} & x_{23} & x_{27} & x_{28} \\ x_{32} & 1+x_{33} & x_{37} & x_{38} \\ x_{72} & x_{73} & 1+x_{77} & x_{78} \\ x_{82} & x_{83} & x_{87} & 1+x_{88} \end{vmatrix} = 0, \quad (7)$$

where

$$x_{ij} = G_0^{\alpha} b(\alpha) a_{ik}(\alpha) A_{kj} + \Phi(k,\lambda,\lambda') T^{-\alpha} \times (k,\lambda) G_0^{\alpha} b(\alpha) T^{\beta}(-k,\lambda') G_0^{\beta} b(\beta) a_{ik}(\alpha,\beta) A_{kj}.$$

We assume that the field $H > H_{c1}$, where the system is in the ferromagnetic (FM) phase. The order parameters in this phase have the form

$$\langle S^z \rangle = 1, \quad q_2^0 = 1, \quad q_2^2 = 0 (\cos\theta = 1).$$

In this case the lowest energy level, corresponding to the ground state, is the level $E_1$.

Analysis of Eqs. (6) and (7) shows that the high-frequency magnon branch does not interact with the elastic subsystem. However, the low-frequency quasimagnons actively interact with $t$-polarized quasiphonons. The spectra of these excitations are determined by Eq. (7) and have the form

$$\varepsilon_{\perp}(k) = \alpha k^2 + H - \frac{\beta}{2} + a_0, \quad (8)$$

$$\omega^2(k) = \omega_t^2(k) \frac{\alpha k^2 + H - \beta/2}{\alpha k^2 + H - \beta/2 + a_0}.$$

Here $\alpha = J_0 R_0^2$, where $R_0$ is the radius of the Heisenberg interaction; $a_0 = \nu^2/2\eta$ is the magnetoelastic interaction parameter; $\omega_t(k) = c_t k$ is the spectrum of the $t$-polarized noninteracting phonon.

It follows from formula (8) that in the long-wavelength limit ($\alpha k^2 \ll a_0$) for $H = H_{c1} = \beta/2$ the $t$-polarized quasiphonon branch softens, and a magnetoelastic gap, $\varepsilon_{\perp}(0) = a_0$, appears in the quasimagnon spectrum.

At $H = H_{c1}$ the system undergoes a phase transition from the ferromagnetic to a quadrupolar–ferromagnetic (QFM) phase.[2,3] It is seen that this phase transition does not reflect the influence of the biquadratic interaction. The behavior of the system is largely determined by the one-ion anisotropy and the magnetic field.

In the field interval $0 \leqslant H \leqslant H_{c2}$ a quadrupolar (QP) phase is realized in the system. This is due to the influence of the large one-ion anisotropy, which leads to an inversion of the energy levels for $H < H_{c2}$. In this range of fields the lowest energy level is $E_0$, and the order parameters of the system in this phase are

$$\langle S^z \rangle = 0, \quad q_2^0 = -2, \quad q_2^2 = 0.$$

Equation (7) determines the spectrum of coupled magnetoelastic waves, which in the long-wavelength limit ($\mathbf{k} \to 0$) decomposes into the spectrum of quasimagnons and quasiphonons:

$$\varepsilon_{\perp}(k) = \left\{ (\beta - 2a_0) \left[ ak^2 + \frac{\beta}{4} - \left( |K_0| + J_0 + \frac{a_0}{2} \right) \right] \right\}^{1/2} - H, \quad (9)$$

$$\omega^2(k) = \omega_t^2(k) \left[ (\beta - 2|K_0| - 2J_0) \alpha k^2 + \left( \frac{\beta}{2} - |K_0| - J_0 \right)^2 - (|K_0| + J_0)^2 - 2a_0(\beta - 3|K_0| - 3J_0) \right] \times \left[ (\beta - 2|K_0| - 2J_0) \alpha k^2 + \left( \frac{\beta}{2} - |K_0| - J_0 \right)^2 - (|K_0| + J_0)^2 - 2a_0 \left( \frac{\beta}{2} - |K_0| - J_0 \right) \right]^{-1}. \quad (10)$$

It follows from Eq. (10) that

$$H_{c2} = \sqrt{\beta[\beta/4 - (|K_0| + J_0)] - 2a_0[\beta - 3(|K_0| + J_0)]}$$

is the field of the orientational phase transition from the QP phase to the QFM phase. At $H = H_{c2}$ in the long-wavelength limit the spectrum of $t$-polarized quasiphonons softens:

$$\omega^2(k) = \omega_t^2(k) \frac{\alpha k^2}{a_0[1 - 2(|K_0| + J_0)/\beta]}, \quad (11)$$

and a magnetoelastic gap appears in the quasimagnon spectrum:

$$\varepsilon_{\perp}(0) = a_0 \left( 1 - 4 \frac{|K_0| + J_0}{\beta} \right)^{1/2}. \quad (12)$$

It follows from the expression for $H_{c2}$ that the QP phase in the system under study can arise only at the following

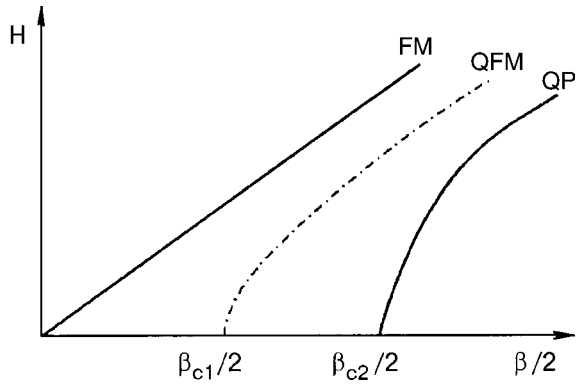


FIG. 1. Phase diagram of an easy-plane ferromagnet with a negative biquadratic interaction.

values of the one-ion anisotropy constants: $\beta_{c2}/2=\beta/2 \geqslant 2(|K_0|+J_0+a_0/2)$. The effect of the negative biquadratic interaction on the formation of the QP phase is shown on the phase diagram of the system studied here (Fig. 1). It follows from the expression for $H_{c2}$ that the existence region of the QP phase is narrowed substantially in comparison with the $K_0>0$ case considered in Ref. 2. There is also an increase (in comparison with the case $K_0>0$; Ref. 2) in the critical value of the one-ion anisotropy constant above which the QP phase can exist: $\beta_{c1}/2=\beta/2\geqslant 2(J_0-K_0-a_0)$. This fact is reflected in Fig. 1, where the dot-and-dash line corresponds to the case $K_0>0$.[2] The value of the magnetoelastic gap (12) in the case of a negative biquadratic interaction is smaller than in the case $K_0>0$, for which $\varepsilon_\perp(0)=a_0[1-4(J_0-K_0)/\beta]^{1/2}$, as was shown in Ref. 2. Our results are indifferent to which particular form of the exchange interaction is dominant. In contrast to the case studied in Ref. 2, our system is insensitive to the difference between $|K_0|>J_0$ and $|K_0|<J_0$.

This behavior of the system at the QP–QFM phase transition can be explained as follows. The positive exchange interaction gives rise to an AFM-like ordering of the magnetic moments. The spin direction of the magnetic ion is equiprobably in either direction.[1] Thus, in addition to the competition between the magnetic field and the quadrupole field of the large one-atom anisotropy, there is also a competition between the Heisenberg and biquadratic exchange interactions, which induce opposing mechanisms of ordering.

In the case considered here, the negative biquadratic exchange ''enhances'' the influence of the Heisenberg interaction, and this is manifested in a narrowing of the existence region of the quadrupolar phase and in the behavior of the other parameters of the system in comparison with the case $K_0>0$.[2]

*E-mail: MAN@expl.cris.crimea.ua

[1] É. L. Nagaev, *Magnets with Complicated Exchange Interactions* [in Russian], Nauka, Moscow (1988).
[2] Yu. N. Mitsaĭ, A. N. Maĭorova, and Yu. A. Fridman, Fiz. Tverd. Tela (Leningrad), **34**, 66 (1992) [Sov. Phys. Solid State **34**, 34 (1992)].
[3] V. V. Val'kov, G. N. Matsuleva, and S. G. Ovchinnikov, Fiz. Tverd. Tela (Leningrad), **31**(6), 60 (1989) [Sov. Phys. Solid State **31**, 948 (1989)].
[4] H. H. Chen, Phys. Rev. Lett. **27**, 1383 (1971).
[5] R. Aleonaro and P. Morin, Phys. Rev. B **19**, 3869 (1979).
[6] P. Morin, L. Rouchy, and D. Schmitt, Phys. Rev. B **17**, 3684 (1978).
[7] H. H. Chen and P. M. Levy, Phys. Rev. B **7**, 4267 (1973).
[8] S. T. Chiu-Tsao, P. M. Levy, and C. Paulson, Phys. Rev. B **12**, 1819 (1975).
[9] E. A. Turov and V. G. Shavrov, Usp. Fiz. Nauk, **140**, 429 (1983) [Sov. Phys. Usp. **26**, 593 (1983)].
[10] R. O. Zaĭtsev, Zh. Éksp. Teor. Fiz., **68**, 207 (1975) [Sov. Phys. JETP **41**, 100 (1975)].

Translated by Steve Torstveit

## ELECTRONIC PROPERTIES OF METALS AND ALLOYS

# Unusual substitutional properties of Cu in bulk polycrystalline samples of $La_{0.7}Ca_{0.3}Mn_{1-x}Cu_xO_{3-\delta}$

A. I. Tovstolytkin* and A. N. Pogorilyi

*Institute of Magnetism, 36-b, Vernadskii St., Kiev 03142, Ukraine*

A. G. Belous and O. Z. Yanchevski

*Institute of General and Inorganic Chemistry, 32/34, Palladina Pr., Kiev 03142, Ukraine*

(Submitted June 23, 2000; revised December 12, 2000)
Fiz. Nizk. Temp. **27**, 500–507 (May 2001)

The transport and magnetoresistive properties of bulk polycrystalline samples of the $La_{0.7}Ca_{0.3}Mn_{1-x}Cu_xO_{3-\delta}$ ($x \leqslant 0.15$) system are studied in the temperature range 77 K–300 K. All the samples investigated exhibit the giant magnetoresistance effect associated with the transition from the ferromagnetic metallic to the paramagnetic insulating state. As a function of copper concentration, the temperature $T_p$ of the resistivity peak first decreases from 193 K ($x=0$) to 108 K ($x=0.10$) and then gradually grows, reaching 120 K at $x=0.15$. Significant temperature broadening of the resistive transition as well as anomalous behavior of the peak value of the resistivity are observed near $x=0.10$. The unusual properties of the $La_{0.7}Ca_{0.3}Mn_{1-x}Cu_xO_{3-\delta}$ system are well explained in terms of a mixed valence of the Cu ions.
 [DOI: 10.1063/1.1374722]

### INTRODUCTION

An intense research effort has recently been devoted to studying the interplay between the structure, magnetism, and electronic transport in doped manganites $La_{1-x}M_xMnO_3$ (M=alkaline earth).[1,2] By tuning the size mismatch of the A- and B-site ions in these $ABO_3$-type perovskites one can control the competition between the double exchange, superexchange, and Coulomb interactions among the Mn ions and, thus, their magnetoresistive properties, which are of crucial importance for applications.[3] It has been shown that both the ferromagnetic ordering, $T_C$, and metal–insulator, $T_p$, temperatures are very sensitive to the structural distortions induced by changing the average A-site radius $\langle r_A \rangle$. A few percent substitution of La by smaller rare-earth cations could result in a significant drop in the Curie temperature $T_C$ and in a drastic enhancement of the magnetoresistance effect. On the basis of the double exchange model with the strong electron–phonon interaction taken into account, the complex lattice effects can be understood, at least qualitatively, in both the paramagnetic and ferromagnetic regions. The introduction of smaller A-site ions leads to a larger steric buckling of the corner-shared octahedra in the perovskites, to bending of the Mn–O–Mn bonds and, as a result, to weakening of the double exchange between $Mn^{3+}$ and $Mn^{4+}$ ions and enhancement of the antiferromagnetic superexchange interaction.[1]

An interesting way to modify the crucial $Mn^{3+}$–O–$Mn^{4+}$ network is to dope at the Mn site itself. Co and Ni substitutions for Mn in $La_{2/3}Ca_{1/3}MnO_3$ thin films have been shown to lower the magnetic transition temperature because of weakening of the double exchange between two unlike ions.[4] Recently, Sun *et al.*[5] reported the effects of Fe and Ge doping at the Mn site in bulk polycrystalline $La_{0.7}Ca_{0.3}MnO_3$. It was shown that Mn-site doping favored a reduced magnetic/resistive transitions and elevated resistivity. No metal-insulator transition occurred when the content of Fe exceeded $\sim 0.1$. Similar results were obtained by substitution of $Mn^{3+}$ by $Al^{3+}$, although both ferromagnetic and resistive transitions were reported still to occur in $La_{0.67}Ca_{0.33}Mn_{1-x}Al_xO_3$ at $x \approx 0.1$.[6]

Recently, several studies have been undertaken to clarify the effect of Cu doping at the Mn site of bulk polycrystalline $La_{1-x}M_xMnO_3$ (M=Ba, Sr).[7–10] The results of a detailed structural investigation of $La_{1-z}Sr_zMn_{1-x}Cu_xO_3$ ($z=0$; 0.1; 0.3; $0 \leqslant x \leqslant 0.5$) polycrystalline samples[9] show that Cu doping favors rhombohedral distortions of the perovskite structure and that copper ions can be found both in $2^+$ and $3^+$ valence states in these compounds. The electronic transport, magnetic, and infrared properties of $La_{1-z}Ba_zMn_{1-x}Cu_xO_{3-\delta}$ and $La_{0.8}Sr_{0.2}Mn_{1-x}Cu_xO_{3-\delta}$ ($x=0$; 0.1; ...) systems were reported in Refs. 7 and 8. It was found that 20% copper was sufficient to suppress ferromagnetism in the latter system and to lead to the cluster spin-glass state at $0.2 \leqslant x \leqslant 0.4$. A broadened ferromagnetic transition and a double-peaked character of the resistivity versus temperature curve were observed at $x=0.1$.

During the past few years, rather controversial results have been reported[11–13] concerning the influence of Cu doping on the transport properties of $La_{0.7}Ca_{0.3}MnO_3$. Sergeenkov *et al.*[12] examined a 4% Cu-doped $La_{2/3}Ca_{1/3}MnO_3$ compound and found both a sharp drop ($\sim$50%) in resistivity and a slight decrease ($\sim$ 15 K) in $T_p$ with respect to the original Cu-free sample. Similar effects were observed in

 

$La_{0.7}Ca_{0.3}Mn_{0.95}Cu_{0.05}O_3$ by Ghosh *et al.*[11] By contrast, unusual temperature and concentration behavior of the resistivity in $La_{0.7}Ca_{0.3}Mn_{1-x}Cu_xO_3$ was reported in Ref. 13. Introduction of a small amount of copper ($x \leqslant 0.05$) was found to result in a splitting of the resistivity maximum around the metal-insulator transition temperature into two peaks, evolving differently with copper concentration. Although the experimental data were well fitted assuming a nonthermal tunnel conductivity theory with randomly distributed hopping sites, it is not easy to correlate these data with those described in Refs. 11 and 12.

In view of such ambiguous results, there appears to be a need to explore in more detail the effect of Cu doping on the behavior of the $La_{0.7}Ca_{0.3}MnO_3$ compound. It seems that at least some of the controversies resulting from Refs. 11–13 would have been avoided if the authors had comprehensively characterized the chemical composition as well as the quality of the resulting samples by means of a set of various measurement techniques. The work reported here is intended to be a step in this direction. We present the results of a study of transport and magnetoresistive properties of a series of $La_{0.7}Ca_{0.3}Mn_{1-x}Cu_xO_{3-\delta}$ samples with $0 \leqslant x \leqslant 0.15$. In addition to conventional electrical and magnetic measurements, we have characterized the composition and quality of representative samples using x-ray fluorescence and electron paramagnetic resonance (EPR) techniques.

## EXPERIMENTAL PROCEDURE

Polycrystalline $La_{0.7}Ca_{0.3}Mn_{1-x}Cu_xO_{3-\delta}$ (LCMC) with $x=0$; 0.05; 0.075; 0.10; 0.125, and 0.15 were prepared through two-stage solid-state reaction in air.[14] The starting mixture of $La_2O_3$, $Mn_2O_3$, CuO, and $CaCO_3$ was first calcined for 2 h at a temperature of 1100 °C. After subsequent ball milling and uniaxial pressing into pellets, the resulting products were sintered for 2 h at $T_s = 1300$ °C and then furnace cooled down to room temperature. Lattice parameters of the samples were obtained from a least-squares fitting to the relevant diffraction lines in x-ray powder diffraction experiments carried out on a DRON diffractometer in Cu $K_\alpha$ radiation. DC resistance measurements were performed in the temperature range 77–300 K using the standard four-probe method. Samples for resistance measurements were cut into rectangular bars, with typical dimensions of $2 \times 3 \times 10$ mm. The magnetoresistance was measured in fields up to 1.5 T and is defined as $(\rho - \rho_H)/\rho$, where $\rho$ and $\rho_H$ are the resistivity in zero field and applied field, respectively. We note that the magnetoresistance ratio defined in such a way cannot exceed 100%. AC magnetic susceptibility ($\chi$) measurements were performed at a frequency of 1000 Hz by a mutual inductance bridge. DC magnetization was measured by means of a SQUID magnetometer (Quantum Design MPMS-5S). EPR measurements on powder samples were performed in the temperature range 77–300 K using a Radiopan spectrometer operating at 9.2 GHz.

## RESULTS AND DISCUSSION

To begin with, let us present the results of a set of measurements, which allow one to achieve rather complete characterization of the parent, i.e., $La_{0.7}Ca_{0.3}MnO_{3-\delta}$, sample.

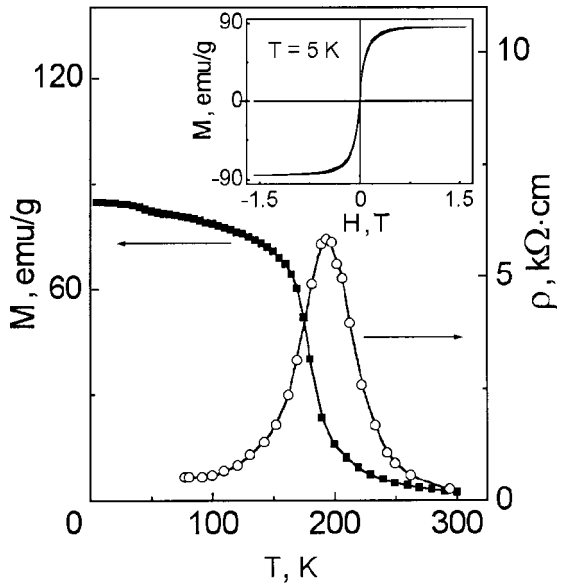


FIG. 1. Temperature dependence of the magnetization in a field $H=1$ T and of the electrical resistivity for a $La_{0.7}Ca_{0.3}MnO_{3-\delta}$ sample. The inset shows the hysteresis loop $M(H)$ at $T=5$ K.

Figure 1 shows the temperature dependence of the magnetization $M$ measured in a field of 1 T. At high temperatures, $M(T)$ obeys the Curie–Weiss law, and its behavior is characteristic of a paramagnetic state. As the temperature decreases, a sharp rise in magnetization occurs slightly below 200 K, after which $M$ grows more slowly and, finally, reaches a value of 84.7 emu/g at $T=5$ K. From the hysteresis loop $M(H)$ at this temperature (see Fig. 1, inset) one can estimate the saturation magnetization $M_s$ and coercive field $H_c$, which will be used in the detailed analysis below.

To observe the onset of magnetic ordering in more detail, we studied the temperature dependence of the EPR spectrum from 300 down to 77 K. A strong symmetric EPR signal with a line shape very close to Lorentzian is observed at room temperature. When the temperature is lowered, the linewidth decreases, passes through a minimum at $T_{\min} \cong 220$ K, and increases on further cooling. Around 200 K($T_C$) the spectrum splits into two lines, indicating the appearance of spontaneous magnetization coexisting with a remainder of the paramagnetic phase.[15] It is noteworthy that it is near this temperature that both the resistance peak and sharp change in magnetization are observed (see Fig. 1). As the temperature is reduced further, the intensity of the resonance line corresponding to the paramagnetic phase decreases drastically, and this line almost completely disappears below ~ 170 K.

In our opinion, both the sharp ferromagnetic transition and narrow hysteresis loop are evidence of rather good chemical and magnetic homogeneity of the sample. Both the value of $M_s$ ($\sim 85$ emu/g) and $H_c$ ($\leqslant 3$ mT) correlate well with other data reported in the literature.[5,16,17] Nevertheless, the Curie temperature $T_C$ is much lower than that observed in stoichiometric $La_{0.7}Ca_{0.3}MnO_3$ ($T_C \cong 260$–$270$ K).[16–18] To find out the reason for this discrepancy, we checked the chemical composition of the samples with $x=0$; 0.05; and 0.10, using the x-ray fluorescence technique. The results of the analysis have shown that, across the series of samples,

the atomic ratio between constituent metal atoms (La, Ca, Mn and Cu) keeps close to the nominal one (for each of the elements, deviation from the nominal value does not exceed 3%). Thus the most likely reason for the lowered $T_C$ in our case lies in a deviation of oxygen content from the stoichiometric value. Comparison of the data plotted in Fig. 1 with the results presented in Refs. 14, 17, 19, and 20 shows that the parent sample is oxygen-deficient, with $\delta \sim 0.06$ (different methods give different values of $\delta$ ranging from 0.04 to 0.08). Taking into account that all the samples of the $La_{0.7}Ca_{0.3}Mn_{1-x}Cu_xO_{3-\delta}$ family were synthesized under exactly the same conditions, we hold the opinion that $\delta$ remains nearly constant as $x$ varies from 0 to 0.15, although, at this stage, we are unable to determine its exact value.

The effect of oxygen nonstoichiometry on the electrical, magnetic, and resonance properties of perovskite manganite thin films was studied in detail by Rajeswari *et al.*[21] It was found that a decrease in oxygen content strongly affected the sharpness of both the resistive and magnetic transitions and led to a significant growth in EPR linewidth. As one of the important results to be mentioned, the authors showed that the increase of $\delta$ in epitaxial films of $Nd_{0.67}Ca_{0.33}MnO_{3-\delta}$ could change the minimal peak-to-peak linewidth $\Gamma_{min}$ from about 20 to 100 mT. Turning to our EPR data, $\Gamma_{min}$ is equal to 34 mT for the parent ($x=0$) sample and is around 35 mT for LCMC with $x=0.05$. These values are higher than those observed[21] in high-quality epitaxial films of $La_{0.67}Ca_{0.33}MnO_{3-\delta}$, but they are less than or comparable to $\Gamma_{min}$ in bulk polycrystalline samples synthesized by other researchers.[4,22,23] So, despite the considerable oxygen deficiency of our samples, this parameter is very close to the best values reported before, and it can serve as an additional conformation of the rather good quality of the materials synthesized in the present study.

As can be seen from Fig. 1, the resistivity $\rho$ of the $La_{0.7}Ca_{0.3}MnO_{3-\delta}$ sample is several orders of magnitude greater than typical values reported for epitaxial films of the same composition.[24] This is not surprising for polycrystalline (ceramic) materials consisting of low-resistivity grains and high-resistivity intergrain regions. When high- and low-resistive regions are connected in series, the DC response is strongly dependent on the high-resistivity region. Thus in such materials the amount and quality (chemical composition, structural and magnetic disorder, etc.) of the intergrain regions greatly affects both the electrical resistance and magnetoresistance but scarcely influences most of other properties, since the relative volume of the intergrain region is negligibly small. To shed further light upon the origin of high-resistivity behavior of $La_{0.7}Ca_{0.3}MnO_{3-\delta}$, a part of the sample was subjected to different kinds of heat treatment. After it was annealed in air at 800 °C for 1 h, its resistivity dropped by 3 orders of magnitude. Further annealing at this temperature gave rise to a further decrease in $\rho$, but neither the bulk magnetization nor the width of the insulator-to-metal transition was changed. This seems to indicate that this kind of heat treatment affects only the intergrain regions and that it apparently results in an improvement of their structure and/or a slight increase in oxygen content. However, these experiments have also led to a slight reduction in the low-temperature magnetoresistance, which is one of the crucial

TABLE I. Room-temperature crystallographic parameters for rhombohedral samples of $La_{0.7}Ca_{0.3}Mn_{1-x}Cu_xO_{3-\delta}$.

| $x$ | $a$, Å | $\alpha$, deg |
|---|---|---|
| 0.050 | 15.489 | 91.53 |
| 0.075 | 15.478 | 91.50 |
| 0.100 | 15.474 | 91.49 |
| 0.125 | 15.481 | 91.53 |
| 0.150 | 15.467 | 91.49 |

parameters for this class of materials. Therefore, in what follows we concentrate only on the properties of unannealed $La_{0.7}Ca_{0.3}Mn_{1-x}Cu_xO_{3-\delta}$ samples, keeping in mind that each one consists of perfectly crystallized grains divided by highly disordered and/or strongly oxygen-deficient intergrain regions.

The structural parameters of the LCMC samples are listed in Table I. The parent $La_{0.7}Ca_{0.3}MnO_{3-\delta}$ compound belongs to the $O'$-type orthorhombic structure[2] with lattice parameters $a_0=5.4568$ Å, $b_0=5.5017$ Å, and $c_0=7.7126$ Å satisfying $c_0/\sqrt{2}<a_0<b_0$. These data correlate well with the results of Ref. 5. The samples with $0.05 \leqslant x \leqslant 0.15$ are rhombohedrally distorted with $a \cong 2c_0$ and $\alpha \cong 91.5°$. The fact that lattice constants are scarcely dependent on doping level seems to support the results of Ref. 9 showing that copper ions in manganites are in both $2^+$ and $3^+$ charge states. Unidentified phases with weak ($<5\%$) peaks at $2\theta \cong 12.4°$ and 24.9° were revealed in LCMC with $x=0.10$ and 0.15, but we believe that these phases have little effect on the transport and magnetoresistance properties of the samples.

Data on the normalized resistivity $\rho/\rho_{max}$ as a function of temperature $T$ are plotted in Fig. 2a for LCMC samples with $x=0$; 0.05; 0.10, and 0.15 (the data for $x=0.075$ and 0.125 are omitted for clarity). In all the samples $\rho$ increases drastically with decreasing $T$ to a maximum at $T=T_p$, after which a metallic behavior appears. The variation of $T_p$ with $x$ is nonmonotonic: its value first falls from 193 K ($x=0$) to 108 K ($x=0.10$) and then gradually grows, reaching 120 K at $x=0.15$; $\rho_{max}$ decreases with increasing $x$ from about 6000 ($x=0$) to 1000 ($x=0.15$) $\Omega \cdot$cm. Although at $T<T_p$ the $\rho(T)$ dependence is metallic ($d\rho/dT>0$), the resistivity at the lowest measured temperature ($T=77$ K) is greater than $\rho$(300 K). The lowest $\rho$(77 K), which is $\sim 150$ $\Omega \cdot$cm for this series of samples, is much larger than $\rho_{Mott} \approx 5-10\,\Omega \cdot$cm estimated from the Mott minimum metallic conductivity.[25]

In the high-temperature region, the variation of the resistivity conforms well to the expression

$$\rho(T) = \rho_0 T \exp(E_a/kT) \tag{1}$$

predicted for small-polaron hopping conductivity.[4,26] The activation energy $E_a$ is weakly dependent on $x$ and is equal to 0.2 and 0.14 eV for the samples with extreme concentrations of Cu, $x=0$ and 0.15, respectively. When going from higher temperatures, the measured resistivity progressively deviates from that predicted by (1). The temperature at which difference between the experimental and fitted data exceeds 5% is denoted as $T_a$. It is the temperature below which not only the electrical but also the magnetoresistive and magnetic properties deviate from those typical of an insulating para-

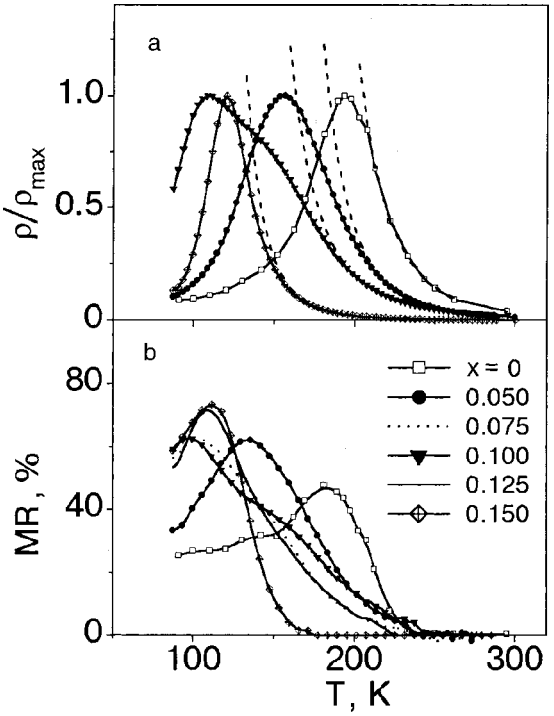


FIG. 2. Normalized resistance versus temperature for polycrystalline $La_{0.7}Ca_{0.3}Mn_{1-x}Cu_xO_{3-\delta}$ samples. The dotted lines denote the resistance fitted according to the adiabatic small-polaron hopping model (a). Temperature dependence of the magnetoresistance in a field $H=1.5$ T (b).

magnet. For all the samples, the effect of magnetic field on the resistance becomes noticeable at $T<T_a$ and reaches a maximum at $T_{MR}$, slightly below $T_p$ (Fig. 2b). The peak values of the magnetoresistance $MR_{\max}$ measured in a field of 1.5 T are about 48% and 73% for LCMC with $x=0$ and 0.15, respectively.

The field dependence of the magnetoresistance at $T=77$ K is presented in Fig. 3. For compositions with higher values of $T_p$ ($x\leqslant 0.05$) the $MR(H)$ curves show a sharp drop at low fields ($<0.2$ T) followed by a more gradual change at

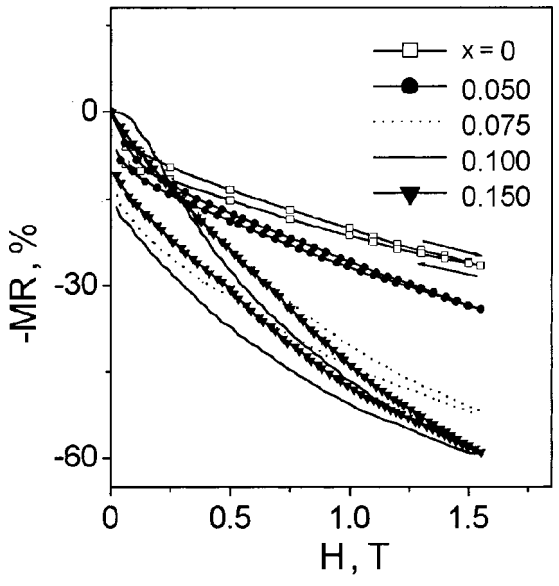


FIG. 3. Magnetoresistance versus field for $La_{0.7}Ca_{0.3}Mn_{1-x}Cu_xO_{3-\delta}$ measured at $T=77$ K (the data for $x=0.125$ are omitted).

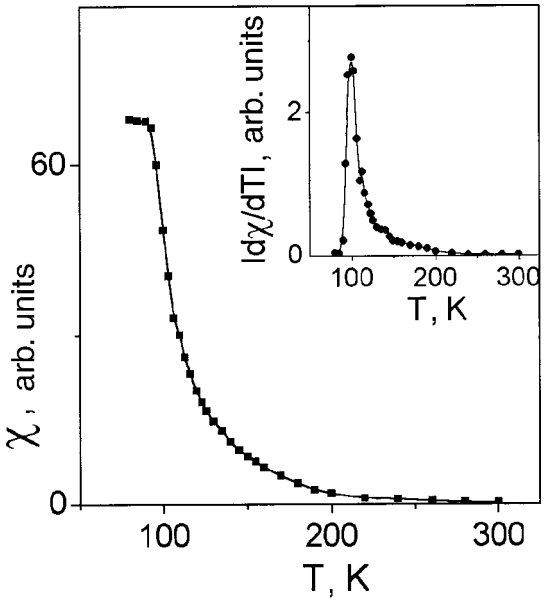


FIG. 4. AC magnetic susceptibility $\chi$ of $La_{0.7}Ca_{0.3}Mn_{0.90}Cu_{0.10}O_{3-\delta}$ and the absolute value of its derivative $|d\chi/dT|$ as functions of temperature.

$H>0.2$ T. In both regions $\rho$ changes almost linearly with $H$. It is now well established that the low-field $MR$ component in manganites originates from a high degree of spin polarization of the conduction electrons, and it is ascribed to intergrain spin-polarized tunneling[27] or spin-dependent scattering of polarized electrons at the grain boundaries.[24]

The variation of $MR$ with $H$ is completely different in the samples with $x>0.05$. All the curves are nonlinear in the whole field range examined, and their hysteretic behavior is pronounced, especially for the composition with $x=0.10$. This effect may be a result of increased magnetic inhomogeneity caused by the introduction of Cu ions in the Mn sublattice, or it may indicate the appearance of other kinds of magnetic ordering.[7,8] To shed further light on the origin of the highly hysteretic behavior of $MR(H)$, we performed AC magnetic susceptibility measurements on LCMC with $x=0.10$. The temperature dependence of both $\chi$ and $|d\chi/dT|$, which are plotted in Fig. 4, seems to show that there is no other transition except for the paramagnetic–ferromagnetic one, but the transition region is extremely broadened.

The concentration dependence of the characteristic temperatures $T_a$, $T_p$, and $T_{MR}$ is displayed in Fig. 5a. It is seen that apart from $T_a$, which tends to decrease gradually with increasing $x$, the rest of the quantities do not change monotonically as functions of $x$. Such unusual behavior seems to be closely connected with the considerable broadening of both the resistive and magnetic transitions observed near $x=0.10$. To give a clear visual demonstration of this relationship, we used the difference between $T_a$ and $T_p$ for a quantitative characterization of the width of the resistive transition and plotted it as a function of copper content in Fig. 5b. A very narrow transition region ($\Delta T=14$ K) is observed at $x=0$. As $x$ grows, $\Delta T$ first increases, exhibits a maximum near $x=0.10$ ($\Delta T_{\max}=81$ K), and then gradually decreases and reaches 45 K at $x=0.15$. Such a strong broadening of the resistive transition near $x=0.10$ suggests the presence of structural or magnetic inhomogeneities, and it can be a rea-

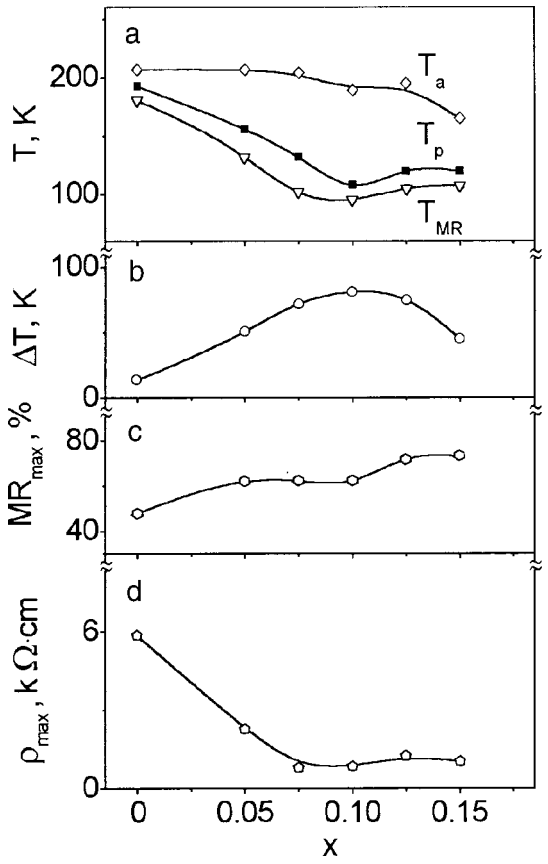


FIG. 5. Concentration dependence of the characteristic temperatures $T_a$, $T_p$, and $T_{MR}$ (a); the temperature width of the resistive transition (b); the maximum value of the magnetoresistance in a field $H=1.5$ T (c); the maximum value of the resistivity $\rho_{\max}$ (d).

son for reduced sensitivity of the electronic transport to magnetic field. As can be seen from Fig. 5c, $MR_{\max}(x)$ exhibits a local minimum in the vicinity of $x=0.10$, although it grows continuously at $x\leqslant 0.075$ and $x>0.10$.

An unusual effect of Cu doping on electronic transport properties was observed earlier in the $La_{0.8}Sr_{0.2}Mn_{1-x}Cu_xO_{3-\delta}$ system.[7,8] The authors carried out a careful examination of compounds with $x=0$, 0.1, 0.2 ... . It was found that substitution of 10% Cu lowers the Curie temperature from 320 to 280 K, and 20% Cu is enough to completely destroy the ferromagnetic state. At low temperatures, the samples with $x=0$ and 0.1 were found to be metallic ferromagnets, while in those with $x\geqslant 0.2$ a semiconducting spin-glass state was revealed. Contrary to $La_{0.8}Sr_{0.2}MnO_{3-\delta}$, in which a sharp change near the Curie temperature was observed on the magnetization versus temperature curve, in $La_{0.8}Sr_{0.2}Mn_{0.9}Cu_{0.1}O_{3-\delta}$ the magnetic transition was quite broadened, and the $\rho$ versus $T$ dependence exhibited two peaks. For the latter sample, the authors attributed the low-temperature resistance peak to enhanced scattering of spin polarons on ''frozen-in'' magnetic disorder, which might exist below $T_C$.

An issue of crucial importance for the analysis of Cu-doped manganites, although it has remained unclear hitherto, is the valence state of the Cu ions. It is known that copper in perovskite compounds may appear in $2^+$ and $3^+$ states.[7–9,11] The authors of Refs. 7–9 analyzed their experimental results at the assumption that the Cu ions are divalent. Nevertheless, Tikhonov *et al.* carried out a careful analysis of the structural properties of the $La_{1-z}Sr_zMn_{1-x}Cu_xO_3$ ($z=0$, 0.1, 0.3; $x=0-0.5$) system and concluded that copper is trivalent in these compounds, but in the low-doping region ($0<x\leqslant 0.1$) a fraction of the Cu ions may also be found in the $2^+$ state. It seems that these results show the way to understand the quite complex behavior of Cu-doped manganites.

Manganese ions play a key role in the determination of both the electrical and magnetic properties of the materials under consideration. The electrical conductivity and ferromagnetism are described in terms of the transfer of electrons between $Mn^{3+}$ ($t_{2g}^3e_g^1$) to $Mn^{4+}$ ($t_{2g}^3e_g^0$) ions; the magnetic interaction is double exchange, which is sensitive to the Mn–O–Mn overlap. The conductivity depends on the electron spin alignment of the hopping electron and is enhanced by application of a magnetic field that reduces spin disorder. The double exchange, which favors itinerant electron behavior, is opposed by strong electron–phonon coupling due in part to a Jahn–Teller splitting of the Mn $e_g$ states, by antiferromagnetic superexchange, and by charge and orbital ordering, all of them favoring insulating behavior. Thus the introduction of copper ions in the Mn sublattice is expected to drastically affect all these competing interactions, and this may cause profound changes in the magnetic and electrical properties. First, Cu substitution for Mn is expected to suppress ferromagnetism because of the absence of the double-exchange interaction between neighboring Mn and Cu ions.[7,11–13] In our case, the general reduction of $T_a$ with growing Cu content seems to support this idea. Nevertheless, the introduction of Cu ions in the Mn sublattice also gives rise to local structure, spin, and charge distortions, especially when the copper is in the $2^+$ state. If Cu is divalent, two different effects might occur as the amount of copper increases. First, there is a local change in the lattice constant caused by the incorporation of the significantly bigger ion, that might lead to enhancement of structural and magnetic inhomogeneity and, as a result, to temperature broadening of the magnetic transition. At the same time, this effect might also be accompanied by a drop in electrical resistivity due to relieving of the local strain in the rest of the sample.[11–13] Second, according to the charge neutrality condition, insertion of divalent Cu ions in the system converts part of the $Mn^{3+}$ into $Mn^{4+}$ which might lead to the appearance of regions with improved conductivity due to the rise in the $Mn^{4+}/Mn^{3+}$ ratio.[7,11]

The effect in which the resistivity decreases upon Cu doping was observed in Refs. 7, 11, and 12 as well as in this study. Figure 5b shows $\rho_{\max}$ for the samples under investigation as a function of copper concentration. It is seen that $\rho_{\max}$ drastically drops with $x$ for $x<0.10$, while it remains almost constant at $0.10\leqslant x\leqslant 0.15$. It is difficult to explain this character of $\rho_{\max}(x)$ by any kind of Cu segregation, but by assuming a mixed valence of Cu ions in the region $0\leqslant x\leqslant 0.10$, this curve well supplements those presented in Fig. 5a–c.

## CONCLUSIONS

Based on the present investigations, we draw the following conclusions.

1) Substitution of Cu for Mn tends to suppress ferromagnetism in the compound $La_{0.7}Ca_{0.3}MnO_{3-\delta}$ due to the absence of the double-exchange interaction between neighboring Mn and Cu ions.

2) Significant temperature broadening of both ferromagnetic and resistive transitions near $x=0.10$ leads to anomalous behavior of $T_p$, $T_{MR}$, and $MR_{\max}$ as a function of copper concentration.

3) The concentration dependence of $\rho_{\max}$, which mainly reflects the properties of intergrain area for each sample with a fixed value of $x$, substantially changes its character in just the same range of $x$ where anomalies of the other electrical and magnetic parameters are observed (i.e., near $x=0.10$).

4) All of the above peculiarities are well explained by assuming that copper is trivalent in the $La_{0.7}Ca_{0.3}Mn_{1-x}Cu_xO_{3-\delta}$ system while in the low-doping region ($0<x\leqslant 0.1$) a fraction of the Cu ions is also in the $2^+$ state.

The authors are grateful to S. V. Cherepov for performing the AC magnetic susceptibility measurements and to D. I. Podyalovskii for the EPR studies. We thank E. V. Shypil and J. S. Moodera for assistance with the DC magnetization measurements. The research described in this publication was made possible in part by Award No. UP1-370 of the CRDF.

*E-mail: atov@imag.kiev.ua

[1] H. Y. Hwang, S.-W. Cheong, P. G. Radaelly, M. Marezio, and B. Batlogg, Phys. Rev. Lett. **75**, 914 (1995).
[2] J. B. Goodenough, J. Appl. Phys. **81**, 5330 (1997).
[3] P. G. Radaelly, G. Iannone, M. Marezio, H. Y. Hwang, S.-W. Cheong, J. D. Jorgensen, and D. N. Argyriou, Phys. Rev. B **56**, 8265 (1997).
[4] M. Rubinstein, D. J. Gillespie, J. E. Snyder, and T. M. Tritt, Phys. Rev. B **56**, 5412 (1997).
[5] J. R. Sun, G. H. Rao, B. G. Shen, and H. K. Wong, Appl. Phys. Lett. **73**, 2998 (1998).
[6] G. Turilli and F. Licci, Phys. Rev. B **54**, 13052 (1996).
[7] L. Haupt, R. von Helmolt, U. Sondermann, K. Bärner, Y. Tang, E. R. Griessinger, E. Ladizinsky, and R. Braunstein, Phys. Lett. A **165**, 473 (1992).
[8] Y. Tang, I. Shaltout, R. Braunstein, R. von Helmolt, L. Haupt, and K. Bärner, Phys. Status Solidi B **182**, 509 (1994).
[9] I. L. Tikhonova, A. Yu. Zuev, and A. N. Petrov, Zh. Fiz. Khim. **72**, 1794 (1998).
[10] I. O. Troyanchuk, D. D. Khalyavin, E. F. Shapovalova, K. Bärner, and H. Szymczak, in *Proceedings of the Eighth European Magnetic Materials and Application Conference* (7–10 June 2000), Kiev, Ukraine.
[11] K. Ghosh, S. B. Ogale, R. Ramesh, R. L. Greene, T. Venkatesan, K. M. Gapchup, R. Bathe, and S. I. Patil, Phys. Rev. B **59**, 533 (1999).
[12] S. A. Sergeenkov, H. Bougrine, M. Ausloos, and R. Cloots, JETP Lett. **69**, 858 (1999).
[13] S. A. Sergeenkov, M. Ausloos, H. Bougrine, A. Rulmont, and R. Cloots, JETP Lett. **70**, 481 (1999).
[14] N. A. Belous, A. N. Pogorilyi, A. I. Tovstolytkin, S. V. Cherepov, A. G. Belous, and O. Z. Yanchevski, Ukr. Fiz. Zh. **45**, 198 (2000).
[15] O. Yanagisava, M. Izumi, K.-H. Huang, W.-Z. Hu, Yi Shen, K. Nakanishi, Y. Takahashi, and H. Nojima, J. Magn. Magn. Mater. **211**, 254 (2000).
[16] G. J. Snyder, R. Hiskes, S. DiCarolis, M. R. Beasley, and T. H. Geballe, Phys. Rev. B **53**, 14434 (1996).
[17] L. E. Hueso, F. Rivadulla, R. D. Sánchez, D. Caeiro, C. Jardon, C. Vázquez-Vázquez, J. Rivas, and M. A. López-Quintela, J. Magn. Magn. Mater. **189**, 321 (1998).
[18] P. Schiffer, A. P. Ramírez, W. Bao, and S.-W. Cheong, Phys. Rev. Lett. **75**, 3336 (1995).
[19] J. M. De Teresa, K. Dorr, K. H. Muller, L. Schultz, and R. I. Chakalova, Phys. Rev. B **58**, 5928 (1998).
[20] B. Dabrowski, K. Rogacki, X. Xiong, P. W. Klamut, R. Dybzinski, J. Shaffer, and J. D. Jorgensen, Phys. Rev. B **58**, 2716 (1998).
[21] M. Rajeswary, R. Shreekala, A. Goyal, S. E. Lofland, S. M. Bhagat, K. Ghosh, R. P. Sharma, R. L. Greene, R. Ramesh, and T. Venkatesan, Appl. Phys. Lett. **73**, 2672 (1998).
[22] C. Rettori, D. Rao, J. Singley, D. Kidwell, S. B. Oseroff, M. T. Causa, J. J. Neumeier, K. J. McClellan, S.-W. Cheong, and S. Schultz, Phys. Rev. B **55**, 3083 (1997).
[23] F. Rivadulla, L. E. Hueso, C. Jardon, C. Vázquez-Vázquez, M. A. López-Quintela, J. Rivas, M. T. Causa, C. A. Ramos, and R. D. Sánchez, J. Magn. Magn. Mater. **196, 197**, 470 (1999).
[24] X. W. Li, A. Gupta, G. Xiao, and G. Q. Gong, Appl. Phys. Lett. **71**, 1124 (1997).
[25] R. Mahendiran, S. K. Tivary, A. K. Raychaudhuri, T. V. Ramakrishnan, R. Mahesh, N. Rangavittal, and C. N. R. Rao, Phys. Rev. B **53**, 3348 (1996).
[26] D. C. Worledge, G. J. Snyder, M. R. Beasley, T. H. Geballe, R. Hiskes, and S. DiCarolis, J. Appl. Phys. **80**, 5158 (1996).
[27] H. Y. Hwang, S.-W. Cheong, N. P. Ong, and B. Batlogg, Phys. Rev. Lett. **77**, 2041 (1996).

## LOW-DIMENSIONAL AND DISORDERED SYSTEMS

# Dynamic dielectric susceptibility tensor of a randomized *f–d* magnet

A. B. Beznosov* and E. S. Orel

*B. Verkin Institute for Low Temperature Physics and Engineering, National Academy of Sciences of Ukraine, pr. Lenina 47, 61103 Kharkov, Ukraine*

(Submitted December 11, 2000; revised January 16, 2001)
Fiz. Nizk. Temp. **27**, 508–518 (May 2001)

The magnetic contribution to the dynamic dielectric susceptibility tensor $\chi^{\alpha\beta}(\omega)=\chi_1^{\alpha\beta}(\omega)+i\chi_2^{\alpha\beta}(\omega)$ of a system of randomized quasilocal optical dipoles of a magnetic conductor is calculated by the method of two-time retarded Green's functions. The spectrum of $\chi^{\alpha\beta}(\omega)$ consists of a coherent component $\chi_{\rm coh}^{\alpha\beta}$ and an incoherent component $\chi_{\rm incoh}^{\alpha\beta}$ which are formed by electronic excitations with zero and arbitrary quasimomentum, respectively. Far from the resonance frequencies (where $\chi$ is represented by only a dispersion part) the off-diagonal components $\chi_2^{\alpha\neq\beta}(\omega)$ are linear to leading order in the effective field $\Delta_M=\zeta/2-\mu_B H_0$ ($\zeta$ is the spin–orbit interaction constant, $\mu_B$ is the Bohr magneton, and $H_0$ is the magnetic field), whereas the magnetic contribution to the diagonal components $\chi_1^{\alpha\alpha}(\omega)$ is quadratic in $\Delta_M$.
 [DOI: 10.1063/1.1374723]

### INTRODUCTION

A heightened interest in the optical properties of magnetically concentrated compounds has been holding steady for the last 20 years, largely in connection with the requirements of devices for the writing, reading, and storage of information in today's computer industry. At the same time, optical methods are some of the main tools used for the direct study of the energy spectrum and the character of the electronic states of condensed matter, which, in particular, determine the transformation of its properties upon changes in temperature. For this reason, the optical behavior of systems that undergo magnetic phase transformations is of interest in condensed-matter physics.

More often than not, the presence of *d* or *f* elements in the chemical formula of a magnetically ordered system serves as an indicator of its atomic structure. The electrons of the magnetically active *d* and *f* shells, owing to the presence of the so-called centrifugal barrier,[1] is quasilocal, i.e., their motion through the crystal is of a tunneling nature (intersite hopping) and the corresponding energy bands are rather narrow. Therefore, in those cases when the characteristic time of an external influence on a system (e.g., the period of an electromagnetic wave interacting with it) is shorter than the intersite hopping time, these electrons, on the one hand, behave as local, while, on the other hand, because of the coherence of the intersite hops, which depends on the degree of translational order in the system, they are sensitive to the long-range order, including the magnetic.[2]

A strong spin–orbit interaction leads to correlated behavior of the spin and orbital moments of *f* and *d* electrons in their motion through the crystal (the corresponding ''*j*-polaron'' concept was formulated in Ref. 2), which is substantially reflected in the dependence of the optical properties of the substance on the degree of magnetic order. This picture contains the prerequisites for understanding the mechanisms of the interaction of light with randomized systems of quasilocal optical dipoles, in which the randomization is of both a temperature-related[2,3] and a structural[4] nature. The structural (including magnetostructural) randomness occurs in disordered alloys, metallic and spin glasses, etc., while one can speak of temperature-related randomization in cases where the characteristic period of the temperature fluctuations of the quasilocal optical dipoles (the fluctuations of the directions of their axes, which are determined by the orientation of the total angular momenta of the rare-earth ions, were considered in Refs. 2 and 3) is longer than the period of the electromagnetic wave. For the systems mentioned in the previous paragraph, both types of randomization are important in the optical range, from the infrared to the vacuum ultraviolet.

An electron moving in a magnetic medium is acted on by the Lorentz force,[5] which leads to the Hall effect at low frequencies and to the Kerr and Faraday magnetooptic effects at optical frequencies.[5–7] The theory of magnetooptic effects in ordered metals has a long history (besides Refs. 5–7, we might mention Refs. 8–11 as some of the published sources characterizing the development of the magnetooptics of systems related to those considered in the present paper), but the same cannot be said of the magnetooptics of randomized systems. At the same time, this is a topical issue, since an appreciable number of modern materials for microelectronics are randomized systems.[12–14]

The goal of this paper is to construct a theory of magnetooptic effects in a system of randomized quasilocal optical dipoles. In contrast to Refs. 5–11, where models of either free or localized electrons were used, here we consider a model of quasilocal electrons. We base this model (as in Refs. 2–4, 15, and 16) on the picture of narrow-band magnetic conductors proposed by Nagaev.[6] Here the macroscopic magnetooptic effect arises as a result of a system-

 

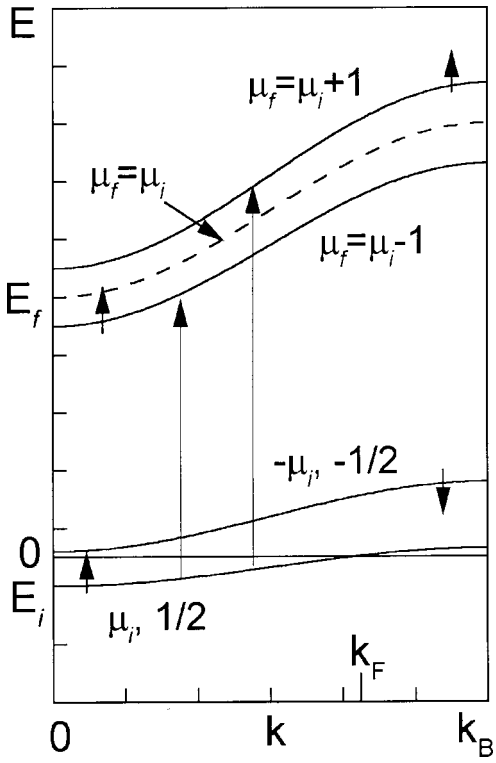


FIG. 1. Schematic form of the electron energy spectrum $E_{f(i)}(\mathbf{k})$ of the initial $i$ and final $f$ states of the investigated magnetooptic electronic transition $i\to f$: $E_f(0)-E_i(0)=E_{fi}\gg W_{f(i)}$, where $W$ is the width of the electron band, $k_F$ and $k_B$ are the Fermi and Brillouin wave vectors, respectively, $\mu$ is the magnetic quantum number, the arrows indicate the projection of the electron spin on the magnetic moment of the system, and the zero of energy is at the Fermi level. Only those zones $f$ to which transitions from the zone $i$ contribute to the off-diagonal susceptibility $\chi^{xy}(\varepsilon)$ are shown.

wide averaging of quasilocal intra-atomic analogs of the Hall effect[1)] for electrons moving in the electric field of a light wave in the effective magnetic field produced by the spin–orbit interaction plus a contribution from the magnetic induction of the substance.

## MODEL OF A *d–f* METAL

The magnetic conductor model considered corresponds in its general features with the schematic illustration of the electron energy spectrum of metallic gadolinium (see Refs. 2 and 3). It contains narrow, partially filled electron bands ($i$), originating from the atomic $d$ orbitals, and free bands ($f$), separated from them by wide energy gaps and deriving from the other atomic states (Fig. 1).[2)] The spin–orbit interaction lifts the degeneracy with respect to the magnetic quantum number $\mu$ in the bands $i$ and $f$, and the strong intra-atomic exchange interaction with localized spins (in rare-earth metals, with the spins of the $4f$ shells) splits the spin subbands so that one of them, belonging to the band $i$ ($|i,\mathbf{k},-\mu,-1/2\rangle$), lies entirely above the Fermi level (this is not a fundamental condition for this approach, but it simplifies the calculation). The degeneracy with respect to the magnetic and spin quantum numbers is also lifted by an external magnetic field.

For simplicity we shall consider only one such subband (i.e., split with respect to both spin and $\mu$) from the lower band $i$ (the subband with indices $\mu_i$,1/2 in Fig. 1) and only three from the upper band $f$ (with indices $\mu_f=\mu_i-1$, $\mu_f=\mu_i$, and $\mu_f=\mu_i+1$ in Fig. 1) with the spin direction along the magnetization (along the $z$ axis, indicated by the symbol $\uparrow$).

## QUASILOCAL OPTICAL DIPOLES

The interaction of light with a quasilocal optical dipole at site $\lambda$ of the crystal lattice is described in the occupation-number representation by the Hamiltonian

$$\mathcal{H}_{\lambda\,\mathrm{int}}=\int d\Xi\Psi_\lambda^+(\mathbf{x},\xi)\mathcal{H}_{\mathrm{int}}\Psi_\lambda(\mathbf{x},\xi), \tag{1}$$

where

$$\Psi_\lambda(\mathbf{x},\xi)=\sum_{\tau,\mu,\sigma}\varphi_{\lambda,\tau,\mu}(\mathbf{x})\chi_{\lambda,\tau,\mu,\sigma}(\xi)c_{\lambda,\tau,\mu,\sigma}$$

is the electron field operator; $\varphi_{\lambda,\tau,\mu}(\mathbf{x})$ is the atomic electronic wave function defined in the local coordinate system at the site with translation *vector* $\lambda$ (see, e.g., Refs. 2–4); $\chi_{\lambda,\tau,\mu,\sigma}(\xi)$ is the spin function, $c^+_{\lambda,\tau,\mu,\sigma}$ and $c_{\lambda,\tau,\mu,\sigma}$ are the Fermi creation and annihilation operators of the state $|\lambda,\tau,\mu,\sigma\rangle$, $\tau=i,f$ is the index of the orbital state (for specificity we shall assume that $i=l$, $f=l+1$, where $l$ is the orbital quantum number); $\mu$ and $\sigma$ are the magnetic and spin quantum numbers, respectively; the integration over $d\Xi$ extends over the spatial variables $\mathbf{x}$ and also includes summation over the spin variable $\xi$;

$$\mathcal{H}_{\mathrm{int}}=-\frac{e}{m_ec}\mathbf{A}\cdot\mathbf{p};\quad \mathbf{A}=A_0\mathrm{e}^{i(\mathbf{Q}\cdot\mathbf{r}-\omega t)}$$

is the vector potential of the field of the electromagnetic wave ($\omega$ is the frequency of the wave, $\tilde\omega=\omega+i\gamma$, $\gamma\to0$ ensures adiabaticity of the turning on of the interaction), $c$ and $\mathbf{Q}$ are the velocity and the wave vector of the light wave, respectively, and $\mathbf{p}$, $e$, and $m_e$ are the momentum operator, charge, and mass of the electron.[3)]

The matrix elements in (1) are conveniently expressed in terms of the local dipole moments of the electronic transition $i\to f$ at the site $\lambda$:

$$\begin{aligned}\langle\lambda,f,\mu',\sigma|\mathcal{H}_{\mathrm{int}}|\lambda,i,\mu,\sigma\rangle&=\langle\lambda,f,\mu',\sigma|-\frac{e}{m_ec}\mathbf{A}\cdot\mathbf{p}|\lambda,i,\mu,\sigma\rangle\\&=-\frac{\omega_{fi}}{\omega}\mathbf{E}_0\cdot\mathbf{D}_{\lambda fi}^{\mu'\mu}\mathrm{e}^{i(\mathbf{Q}\cdot\lambda-\tilde\omega t)},\end{aligned}$$

where $\mathbf{E}_0$ is the electric field amplitude of the light wave, $D_{\lambda fi}^{\alpha\mu'\mu}=\langle\lambda,f,\mu',\sigma|er^\alpha|\lambda,i,\mu,\sigma\rangle$ is the $\alpha$th component of the matrix element of the electric dipole moment vector of the electronic transition $i\to f$ ($r^\alpha$ is the $\alpha$th component of the electron coordinate operator), and $\omega_{fi}$ is the frequency of the transition $i\to f$.

The nature of the magnetooptic phenomena in reality lies in the difference of the spectra of the right and left circular components of the electric polarization induced in the substance. Therefore, from now on it makes sense to consider the circular components of the electric dipole moment operator of the transition $i\to f$:

$$\hat{D}^{\pm}_{\lambda\mu}=\sum_{\sigma}\ (D^{\pm}_{\lambda fi\mu}c^{+}_{\lambda,f,\mu\pm1,\sigma}c_{\lambda,i,\mu,\sigma}$$
$$+D^{\pm}_{\lambda if\mu}c^{+}_{\lambda,i,\mu,\sigma}c_{\lambda,f,\mu\pm1,\sigma}). \quad (2)$$

Here

$$D^{\pm}_{\lambda fi\mu}=\langle\lambda,f,\mu\pm1,\sigma|er^{\pm}|\lambda,i,\mu,\sigma\rangle,$$
$$D^{\pm}_{\lambda,if\mu}=\langle\lambda,i,\mu,\sigma|er^{\pm}|\lambda,f,\mu\mp1,\sigma\rangle,$$
$$r^{\pm}=\frac{x\pm iy}{\sqrt{2}},$$

and we have dropped the indices $i$ and $f$ from the notation for the operator $\hat{D}^{\pm}_{\lambda\mu}$.

In the present model the magnetooptic effects are governed solely by these matrix elements.

The atomic electronic wave functions, which, as we have said, for the sake of specificity and simplicity we shall use as the site basis states in the crystal, obey the relations[17]

$$\langle l+1,\mu\pm1|r^{\pm}/r|l,\mu\rangle=\pm\left[\frac{(l+2\pm\mu)(l+1\pm\mu)}{(2l+3)(2l+1)}\right]^{1/2},$$
$$\langle l-1,\mu\pm1|r^{\pm}/r|l,\mu\rangle=\mp\left[\frac{(l\mp\mu)(l-1\mp\mu)}{(2l+1)(2l-1)}\right]^{1/2}, \quad (3)$$
$$\langle l,\mu|r^{-}/r|l+1,\ \mu+1\rangle\langle l+1,\ \mu+1|r^{+}/r|l,\mu\rangle$$
$$=\frac{(l+2+\mu)(l+1+\mu)}{(2l+3)(2l+1)},$$
$$\langle l,\mu|r^{+}/r|l+1,\ \mu-1\rangle\langle l+1,\mu-1|r^{-}/r|l,\mu\rangle$$
$$=\frac{(l+2-\mu)(l+1-\mu)}{(2l+3)(2l+1)}.$$

It follows directly from (3) that the matrix elements in (2) obey the relations $D^{\mp}_{if}D^{\pm}_{fi}=(D^{\pm}_{fi})^{*}D^{\pm}_{fi}=|D^{\pm}_{fi}|^2$ (the symbol $*$ denotes the complex conjugate) and

$$|D^{+}_{fi\mu}|^2>|D^{-}_{fi\mu}|^2, \quad \mu>0,$$
$$|D^{+}_{fi\mu}|^2<|D^{-}_{fi\mu}|^2, \quad \mu<0,$$
$$|D^{+}_{fi\mu}|^2=|D^{-}_{fi\mu}|^2, \quad \mu=0.$$

In randomized systems one is interested in mean values over the crystal,

$$\langle D^{\pm}_{fi\mu}\rangle=N^{-1}\sum_{\lambda}\ \langle\lambda,f,\mu\pm1,\sigma|er^{\pm}|\lambda,i,\mu,\sigma\rangle$$

and the rms fluctuations

$$d^{\pm}_{fi\mu}=\left[N^{-1}\sum_{\lambda}\ (D^{\pm}_{\lambda fi\mu}-\langle D^{\pm}_{fi\mu}\rangle)^2\right]^{1/2}.$$

For simplicity we shall henceforth neglect the difference between $\langle D^{+}_{fi\mu}\rangle$ and $\langle D^{-}_{fi\mu}\rangle$ and thus between $d^{+}_{fi\mu}$ and $d^{-}_{fi\mu}$ (strictly, this corresponds to the case $\mu=0$ and does not affect the main results of this paper in the case of arbitrary $\mu$). Furthermore, in view of the aforementioned choice of a fixed character of $\mu$ and $\sigma$, we shall drop them from the indices of the final expressions for the dielectric susceptibility. In such a case the notation for the crystal-averaged electric dipole moments and the rms fluctuations are simplified to $D$ and $d$, respectively.

## ROLE OF RANDOMIZATION OF THE SYSTEM

The randomness of the system of quasilocal electric dipoles induced by the electric field of the light wave can have a structural (including magnetostructural) origin (disordered alloys, spin glasses, etc.) or can result from thermal fluctuations of the local characteristics of the system (as we have said, this could be thermal fluctuations of the local quantization axes, which are determined by the directions of the magnetic moments of the $4f$ shells of the rare-earth metal ions[2,3]).

Let us consider for the sake of definiteness a spin glass in a metal with localized magnetic moments of the $4f$ shells. Below the glass temperature the thermal average of the $z$ projection of the spin is nonzero for each site containing $4f$ spins in the system, and in the local coordinate systems all of these averages are equal. The average value of the local magnetic moment over the crystal is zero, while its mean square value is nonzero.[18] It is obvious that the magnetooptic effect arises at each ''magnetic'' site, but the crystal as a whole will not exhibit effects determined by its magnetization.

Thus the spatial randomization of the dipole moment (2) has an essential effect on the optical properties of the system. At the same time, in the electronic Hamiltonian of the crystal written in the tight-binding approximation, the randomization of the local quantization axes of the ''magnetic'' sites will lead only to a certain randomization of the electron intersite hopping integral without substantially changing its value and will thus not materially alter the properties of the metal. Therefore, if the system is randomized but its metallic character is preserved, the random component $\delta\mathcal{H}$ of the total Hamiltonian $\mathcal{H}=\mathcal{H}_0+\delta\mathcal{H}$ can be treated as a small correction to the Hamiltonian $\mathcal{H}_0$ of the translationally invariant system. In application to the problem addressed in this paper this influence of the randomization on the electron energy spectrum can be reduced to the replacement of the real energy of the crystal by a complex quantity,[19,20] which, as one might expect, does not qualitatively affect the spectrum of sufficiently high-energy interband electronic transitions.

The electric dipole moment induced in the crystal by the field of an electromagnetic wave can be evaluated by averaging the corresponding eigenvalues with the density matrix determined by the total Hamiltonian $\tilde{\mathcal{H}}=\mathcal{H}_0+\delta\mathcal{H}+\mathcal{H}'_{\rm int}$. It is clear that the linear response[21–23] of the system calculated for the regular part of the interaction Hamiltonian $\mathcal{H}'_{\rm int}=\Sigma_{\lambda}\mathcal{H}_{\lambda\rm int}$, will be determined mainly by the Hamiltonian $\mathcal{H}_0$.

In analyzing the response of the system to the random part of the perturbation $\mathcal{H}'_{\rm int}$ we argue as follows. As we have said, the breaking of the translational symmetry of the system can be taken into account by replacing the real energies $\varepsilon(\mathbf{k})$ of the Bloch $\mathbf{k}$ states by complex quantities $\varepsilon(\mathbf{k})+i\hbar/\tau(\mathbf{k})$. This means that the $\mathbf{k}$ states are damped with a characteristic time $\tau(\mathbf{k})\to\infty$ as $\delta\mathcal{H}\to0$. In other words, the $\mathbf{k}$-space representation works well (i.e., the indeterminacy of the quasimomentum is small and the nonvertical electronic

transitions under the influence of an external field with a wave vector $\mathbf{Q}=0$ are unimportant) provided that the random site corrections to the energy are not too large: if the frequency $\omega_{fi}$ of the electronic transition is high enough that $\pi/\omega_{fi} \ll \tau(\mathbf{k})$, then the response of the system to an external influence is formed in less time than it takes for appreciable changes to occur in the amplitudes of the Bloch states. At the same time, if the random site corrections $d_\lambda$ to the dipole moment in the interaction Hamiltonian $\mathcal{H}'_{\text{int}}$ are statistically independent (in many cases this is a good approximation), so that all of the **k**-harmonics in the Fourier expansion of $\mathcal{H}'_{\text{int}}$ are equiprobable, we immediately obtain the electronic excitations with any quasimomentum, independently of the value of the variance $d^2$ of the dipole moment.

Thus the influence of the randomization of $\mathcal{H}'_{\text{int}}$ and $\mathcal{H}$ on the optical excitation spectra are distinguishable in both the quantitative and qualitative respects. The main influence on the excitation spectra of a substance comes only from the randomizing of the interaction Hamiltonian, $\mathcal{H}'_{\text{int}}$, as will be discussed below, and we shall use the energies of the perfect crystal as the eigenvalues of the system Hamiltonian $\mathcal{H}$. Here, since the operator $\mathcal{H}'_{\text{int}}$ (like $\mathcal{H}$) must be constructed on regular electronic states, all of the randomization effects will be reflected in the values of $c$-numbers, i.e., by the corresponding coefficients of the matrix elements in expression (2).

## HAMILTONIAN

In view of what we have said, let us consider the following Hamiltonian $\mathcal{H}$ of our system in the occupation number representation:

$$\mathcal{H}=\sum_{\substack{\lambda\\ \tau,\mu,\sigma}} U_{\tau,\mu,\sigma} c^{+}_{\lambda,\tau,\mu,\sigma} c_{\lambda,\tau,\mu,\sigma} + \sum_{\substack{\lambda,\eta\\ \tau,\mu,\sigma}} T_{\tau,\sigma} c^{+}_{\lambda+\eta,\tau,\mu,\sigma} c_{\lambda,\tau,\mu,\sigma}, \tag{4}$$

$$U_{\tau,\mu,\sigma}=E_{\tau,\sigma}-\mu_B H_0(\mu+2\sigma)_\tau+\zeta_\tau\mu\sigma,$$

$$\tau=i,f, \quad \zeta_f=\zeta>0.$$

Here $T_{\tau,\sigma}$ is the hopping integral for hops between nearest-neighbor sites $(\lambda,\lambda+\eta)$; $E_i$ and $E_f$ are the energies of the occupied $(i)$ and unoccupied $(f)$ ''bare'' local states (the zeroth approximation in the hopping integral); $\zeta_\tau$ is the spin–orbit interaction constant; $H_0$ is the external magnetic field; $\mu_B$ is the Bohr magneton.

It is assumed that the parameters of the Hamiltonian satisfy the inequalities $T \ll E_{fi}$, $\zeta \ll E_{fi}$, and $\mu_B H_0 \ll E_{fi}$; $E_{fi}=E_f-E_i$ is the energy of the electronic transition $i \to f$ between the centers of the bands of filled $(i)$ and empty $(f)$ states (Fig. 1).

The main characteristics of the electron energy spectrum of conducting magnets are determined by the interaction potential of the conduction electrons with ions, by the electron intersite hopping integrals, and by the self-interactions in the system of conduction electrons. Of these last, only the diagonal part of the spin–orbit interaction, which is of fundamental importance for magnetooptic phenomena, is included explicitly in Hamiltonian (4). It should be noted that the one-site exchange interaction of the conduction electrons with local magnetic moments and the internal exchange interactions in the medium of conduction electrons give rise to low-frequency collective excitations[16,24] in the system, and this should generally be reflected in the magnetooptic spectra. These subtle effects do not alter the main conclusions of this paper, since we are considering only high-frequency one-electron excitations, so that we need not explicitly include the exchange terms in the Hamiltonian of the system (the diagonal part of the one-site exchange interaction between local and quasilocal electrons is included in $E_{\tau,\sigma}$).

The Fourier transformation

$$c^{+}_{\lambda,\tau,\mu,\sigma}=\frac{1}{\sqrt{N}}\sum_{\mathbf{k}} c^{+}_{\mathbf{k},\tau,\mu,\sigma} e^{i\mathbf{k}\cdot\lambda},$$

$$c_{\lambda,\tau,\mu,\sigma}=\frac{1}{\sqrt{N}}\sum_{\mathbf{k}} c_{\mathbf{k},\tau,\mu,\sigma} e^{-i\mathbf{k}\cdot\lambda}$$

diagonalizes the quadratic form (4), bringing it to the form

$$\mathcal{H}=\sum_{\substack{\mathbf{k}\\ \tau,\mu,\sigma}} E_{\tau,\mu,\sigma}(\mathbf{k}) n_{\mathbf{k},\tau,\mu,\sigma},$$

where

$$n_{\mathbf{k},\tau,\mu,\sigma}=c^{+}_{\mathbf{k},\tau,\mu,\sigma} c_{\mathbf{k},\tau,\mu,\sigma}$$

is the occupation number operator of the states $|\mathbf{k},\tau,\mu,\sigma\rangle$;

$$E_{f,\mu\pm1,\sigma}(\mathbf{k})=E_{f,\sigma}+T_{f,\sigma}(\mathbf{k})+\zeta_{\mu\sigma}-\mu_B H_0(\mu+2\sigma)\pm\Delta_M$$

and

$$E_{i,\mu,\sigma}(\mathbf{k})=E_{i,\sigma}+T_{i,\sigma}(\mathbf{k})+\zeta_i\mu\sigma-\mu_B H_0(\mu+2\sigma)$$

are the energies in the upper and lower band, respectively;

$$T_{\tau,\sigma}(\mathbf{k})=T_{\tau,\sigma}\sum_{\mathbf{h}} e^{i\mathbf{k}\cdot\mathbf{h}}$$

is the kinetic energy of the quasilocal electrons;

$$\Delta_M=\zeta\sigma-\mu_B H_0$$

is the ''effective'' magnetic field in energy units.

## DYNAMIC DIELECTRIC SUSCEPTIBILITY

The electrical polarization of a nonuniform stationary medium (for simplicity we consider a crystal lattice containing $N$ sites, at each of which an electric dipole can be induced by a quantity with a random or determinate dependence on $\lambda$) in the field of an electromagnetic wave with frequency $\omega$ and wave vector $\mathbf{Q}$ is determined by the nonlocal dynamic dielectric susceptibility[18]

$$\chi^{\alpha\beta}(\mathbf{Q},\mathbf{Q}',\tilde{\varepsilon})=\frac{1}{N}\sum_{\lambda,\lambda'}\langle\chi^{\alpha\beta}_{\lambda,\lambda'},(\tilde{\varepsilon})\rangle_c e^{i(\mathbf{Q}\cdot\lambda-\mathbf{Q}'\cdot\lambda')},$$

where $\mathbf{Q}'$ is the wave vector of the polarization of the medium; $\varepsilon$ is the photon energy ($\tilde{\varepsilon}=\hbar\tilde{\omega}$, where $\hbar$ is Planck's constant); the symbol $\langle\ldots\rangle_c$ denotes averaging, over all possible configurations, of the distribution of random values of the magnitudes of the quasilocal optical dipoles in the crystal;

$$\chi^{\alpha\beta}_{\lambda,\lambda'}(\tilde{\varepsilon}) = -\frac{1}{v_a}\langle\langle \hat{D}^{\alpha}_{\lambda}|\hat{D}^{\beta}_{\lambda'}\rangle\rangle_{\tilde{\varepsilon}}$$

is the contribution to the nonlocal dynamic dielectric susceptibility from the electronic transitions $i \to f$, written in the site representation in the Kubo formalism of linear response theory;[6,21–23] $\langle\langle \ldots|\ldots\rangle\rangle_{\tilde{\varepsilon}}$ is the two-time retarded Green's function in the energy representation;[20–22] $\hat{D}^{\alpha}_{\lambda}$ is the dipole moment operator of the transition $i \to f$; $v_a$ is the volume of the crystal per site.

In the geometry under study (in which the magnetic field $\mathbf{H}_0$, the average spin $\langle \mathbf{s} \rangle$ of the quasilocal electrons, and the wave vector $\mathbf{Q}$ of the light wave are parallel to the $z$ axis of the crystal) the only nonzero components of the dynamic dielectric susceptibility tensor in an isotropic medium are $\chi^{xx} = \chi^{yy} = \chi^0 + \chi^{\parallel}$, $\chi^{zz} = \chi^0$, and $\chi^{xy} = -\chi^{yx} = i\chi^{\perp} = -ig$. Here $\chi^0$ is the susceptibility in the absence of magnetization; $\chi^{\parallel}$ is the contribution to the diagonal susceptibility due to the magnetization of the electronic system; $i\chi^{\perp}$ is the corresponding ''magnetic'' contribution to the off-diagonal susceptibility, which differs from $\chi^{xy}$ by a factor of $i$; $g$ is the $z$ component of the gyration vector, which is often used in a phenomenological approach to magnetooptics.[5–7] Often $\chi^{\perp}$ is used in place of $\chi^{xy} = -\chi^{yx}$ (Refs. 25–27), since it has a more familiar physical meaning of its real and imaginary parts, which describe the polarization of the substance and the absorption of electromagnetic waves, respectively. The relation with the dynamic dielectric permittivity $\varepsilon^{\alpha\beta}(\omega)$ has the form $\varepsilon^{\alpha\beta}(\omega) = \delta^{\alpha\beta} + 4\pi\chi^{\alpha\beta}$, where $\delta^{\alpha\beta}$ is the Kronecker delta.

The off-diagonal ''magnetic'' contribution to the dynamic dielectric susceptibility is given by

$$\chi^{\perp}(\mathbf{Q},\mathbf{Q}',\tilde{\varepsilon}) = -\frac{\chi^{+}(\mathbf{Q},\mathbf{Q}',\tilde{\varepsilon}) - \chi^{-}(\mathbf{Q},\mathbf{Q}',\tilde{\varepsilon})}{2}, \tag{5}$$

and the relation to the diagonal ''magnetic'' components is

$$\chi^{0}(\mathbf{Q},\mathbf{Q}',\tilde{\varepsilon}) + \chi^{\parallel}(\mathbf{Q},\mathbf{Q}',\tilde{\varepsilon}) = \frac{\chi^{+}(\mathbf{Q},\mathbf{Q}',\tilde{\varepsilon}) + \chi^{-}(\mathbf{Q},\mathbf{Q}',\tilde{\varepsilon})}{2}, \tag{6}$$

where $\chi^{+}(\mathbf{Q},\mathbf{Q}',\tilde{\varepsilon})$ and $\chi^{-}(\mathbf{Q},\mathbf{Q}',\tilde{\varepsilon})$ are the susceptibilities for right and left circularly polarized fields, respectively.

For a system of quasilocal optical dipoles with a random spatial modulation the circular components of the susceptibility are given by

$$\chi^{\mp}(\mathbf{Q},\mathbf{Q}',\tilde{\varepsilon}) = \frac{1}{N}\sum_{\lambda\lambda'} \langle \chi^{\mp}_{\lambda\lambda'}(\tilde{\varepsilon})\rangle_c e^{i(\mathbf{Q}\lambda - \mathbf{Q}'\lambda')}, \tag{7}$$

where

$$\chi^{\mp}_{\lambda\lambda'}(\tilde{\varepsilon}) = -\frac{1}{2v_a}\sum_{\sigma}\{\langle D^{\mp}_{\lambda i f\mu} D^{\pm}_{\lambda' f i\mu}\rangle_c G^{\pm}_{fi\mu\sigma}(\lambda,\lambda',\tilde{\varepsilon}) + \langle D^{\mp}_{\lambda f i\mu} D^{\pm}_{\lambda' i f\mu}\rangle_c G^{\pm}_{if\mu\sigma}(\lambda,\lambda',\tilde{\varepsilon})\}, G^{\pm}_{fi\mu\sigma}(\lambda,\lambda',\tilde{\varepsilon}) = \langle\langle c^{+}_{\lambda,i,\mu,\sigma} c_{\lambda,f,\mu\pm1,\sigma} | c^{+}_{\lambda',f,\mu\pm1,\sigma}, c_{\lambda',i,\mu,\sigma}\rangle\rangle_{\tilde{\varepsilon}},$$

$$G^{\pm}_{if\mu\sigma}(\lambda,\lambda',\tilde{\varepsilon}) = \langle\langle c^{+}_{\lambda,f,\mu\mp1,\sigma} c_{\lambda,i,\mu,\sigma} | c^{+}_{\lambda',i,\mu,\sigma} c_{\lambda',f,\mu\mp1,\sigma}\rangle\rangle_{\tilde{\varepsilon}}.$$

The result of averaging over configurations can be expressed in terms of an average over the crystal. Neglecting the difference between $\langle D^{\mp}_{\lambda i f\mu} D^{\pm}_{\lambda' f i\mu}\rangle_c$ and $\langle D^{\mp}_{\lambda f i\mu} D^{\pm}_{\lambda' i f\mu}\rangle_c$, dropping the index $\mu$, and restricting discussion to the case of statistically independent sites, we obtain

$$\langle D^{\mp}_{\lambda i f\mu} D^{\pm}_{\lambda' f i\mu}\rangle_c = \langle D^{\mp}_{\lambda f i\mu} D^{\pm}_{\lambda' i f\mu}\rangle_c = D^2 + d^2\delta_{\lambda,\lambda'},$$

$$\delta_{\lambda,\lambda'} = \begin{cases} 1, & \lambda = \lambda' \\ 0, & \lambda \neq \lambda' \end{cases}. \tag{8}$$

Substituting (8) into (7), changing from the coordinate (real-space) representation to the wave-vector ($\mathbf{k}$-space) representation in the fermion operators, and doing the summation over $\lambda$ and $\lambda'$, we obtain two susceptibility components: a coherent component $\chi_{\mathrm{coh}}$, determined by $D^2$, the square of the crystal-averaged value of the quasilocal optical dipoles, and an incoherent component $\chi_{\mathrm{incoh}}$, determined by $d^2$, the crystal-averaged value of the square of their fluctuations:

$$\chi^{\pm}(\mathbf{Q},\mathbf{Q}',\tilde{\varepsilon}) = \chi^{\pm}_{\mathrm{coh}}(\mathbf{Q},\mathbf{Q}',\tilde{\varepsilon}) + \chi^{\pm}_{\mathrm{incoh}}(\mathbf{Q},\mathbf{Q}',\tilde{\varepsilon});$$

$$\chi^{\mp}_{\mathrm{coh}}(\mathbf{Q},\mathbf{Q}',\tilde{\varepsilon}) = -\frac{D^2}{v_a N}\sum_{R}[G^{\pm}_{fi\mu\sigma}(\mathbf{k},\mathbf{k}',\mathbf{k}_1,\mathbf{k}_1',\tilde{\varepsilon}) + G^{\pm}_{if\mu\sigma}(\mathbf{k},\mathbf{k}',\mathbf{k}_1,\mathbf{k}_1',\tilde{\varepsilon})]\delta_{\mathbf{k}',\mathbf{k}+\mathbf{Q}}\delta_{\mathbf{k}',\mathbf{k}_1-\mathbf{Q}'},$$

$$\chi^{\mp}_{\mathrm{incoh}}(\mathbf{Q},\mathbf{Q}',\tilde{\varepsilon}) = -\frac{d^2}{v_a N^2}\sum_{R}[G^{\pm}_{fi\mu\sigma}(\mathbf{k},\mathbf{k}',\mathbf{k}_1,\mathbf{k}_1'\tilde{\varepsilon}) + G^{\pm}_{if\mu\sigma}(\mathbf{k},\mathbf{k}',\mathbf{k}_1,\mathbf{k}_1',\tilde{\varepsilon})]\delta_{\mathbf{k}+\mathbf{k}_1+\mathbf{Q}}\delta_{\mathbf{k}'+\mathbf{k}_1'+\mathbf{Q}'}, \tag{9}$$

$$G^{\pm}_{fi\mu\sigma}(\mathbf{k},\mathbf{k}',\mathbf{k}_1,\mathbf{k}_1',\tilde{\varepsilon}) = \langle\langle c^{+}_{\mathbf{k},i,\mu,\sigma} c_{\mathbf{k}',f,\mu\pm1,\sigma} | c^{+}_{\mathbf{k}_1,f,\mu\pm1,\sigma} c_{\mathbf{k}_1',i,\mu,\sigma}\rangle\rangle_{\tilde{\varepsilon}},$$

$$G^{\pm}_{if\mu\sigma}(\mathbf{k},\mathbf{k}',\mathbf{k}_1,\mathbf{k}_1',\tilde{\varepsilon}) = \langle\langle c^{+}_{\mathbf{k},f,\mu\mp1,\sigma} c_{\mathbf{k}',i,\mu,\sigma} | c^{+}_{\mathbf{k}_1,i,\mu,\sigma} c_{\mathbf{k}_1',f,\mu\mp1,\sigma}\rangle\rangle_{\tilde{\varepsilon}};$$

$$R = \{\mathbf{k},\mathbf{k}',\mathbf{k}_1,\mathbf{k}_1',\sigma\}.$$

## CALCULATIONS

The expression for the susceptibility follows from the solution of the equations of motion for the Green's functions in formulas (9), which have the form

$$\langle\langle A|B\rangle\rangle_{\omega} = \frac{i}{2\pi}\langle[A,B]\rangle + \langle\langle[A,H]|B\rangle\rangle_{\omega},$$

where $[A,B]$ is the commutator of operators $A$ and $B$. A calculation gives

$$G^{\pm}_{fi\mu\sigma}(\mathbf{k},\mathbf{k}',\mathbf{k}_1,\mathbf{k}_1',\tilde{\varepsilon}) = \frac{n_{\mathbf{k},i,+\mu\sigma} - n_{\mathbf{k}',f,\mu\pm1,\sigma}}{\tilde{\varepsilon} - E_{fi,\mu\pm1}(\mathbf{k}',\mathbf{k})}\delta_{\mathbf{k},\mathbf{k}_1'}\delta_{\mathbf{k}',\mathbf{k}_1} = G^{\pm}_{fi\mu\sigma}(\mathbf{k},\mathbf{k}',\tilde{\varepsilon})\,\delta_{\mathbf{k},\mathbf{k}_1'}\delta_{\mathbf{k}',\mathbf{k}_1}, \tag{10}$$

$$G^{\pm}_{if\mu\sigma}(\mathbf{k},\mathbf{k}',\mathbf{k}_1,\mathbf{k}_1',\tilde{\varepsilon}) = \frac{n_{\mathbf{k},f,\mu\mp1,\sigma} - n_{\mathbf{k}',i,\mu,\sigma}}{\tilde{\varepsilon} + E_{fi,\mu\pm1}(\mathbf{k}',\mathbf{k})}\delta_{\mathbf{k},\mathbf{k}_1'}\delta_{\mathbf{k}',\mathbf{k}_1} = G^{\pm}_{if\mu\sigma}(\mathbf{k},\mathbf{k}',\tilde{\varepsilon})\,\delta_{\mathbf{k},\mathbf{k}_1'}\delta_{\mathbf{k}',\mathbf{k}_1}, \tag{11}$$

$$E_{fi,\mu\pm1,\sigma}(\mathbf{k}',\mathbf{k})=E_{f,\mu\pm1,\sigma}(\mathbf{k}')-E_{i,\mu,\sigma}(\mathbf{k}). \tag{12}$$

Substituting (10)–(12) into (9), we obtain

$$\chi^{\mp}_{\rm coh}(\mathbf{Q},\mathbf{Q}',\tilde{\varepsilon})=-\frac{D^2}{v_aN}\times\sum_{\mathbf{k}\sigma}\{G^{\pm}_{fi\mu\sigma}(\mathbf{k},\mathbf{k}+\mathbf{Q},\tilde{\varepsilon})+G^{\pm}_{if\mu\sigma}(\mathbf{k},\mathbf{k}+\mathbf{Q},\tilde{\varepsilon})\}\delta_{\mathbf{Q},\mathbf{Q}'}, \tag{13}$$

$$\chi^{\mp}_{\rm incoh}(\mathbf{Q},\mathbf{Q}',\tilde{\varepsilon})=-\frac{d^2}{v_aN^2}\times\sum_{\mathbf{kk}'\sigma}\{G^{\pm}_{fi\mu\sigma}(\mathbf{k},\mathbf{k}',\tilde{\varepsilon})+G^{\pm}_{if\mu\sigma}(\mathbf{k},\mathbf{k}',\tilde{\varepsilon})\}\delta_{\mathbf{Q},\mathbf{Q}'}. \tag{14}$$

## RESULTS

Using Eqs. (5)–(7), (13), and (14) and taking into account that $\chi_{\rm coh}(\mathbf{Q},\mathbf{Q}';\tilde{\varepsilon})$ and $\chi_{\rm incoh}(\mathbf{Q},\mathbf{Q}';\tilde{\varepsilon})$ are related to the wave vector $\mathbf{Q}$ of the electromagnetic wave and the wave vector $\mathbf{Q}'$ of the polarization of the system as

$$\chi_{\rm coh}(\mathbf{Q},\mathbf{Q}';\tilde{\varepsilon})=\chi_{\rm coh}(\mathbf{Q};\tilde{\varepsilon})\,\delta_{\mathbf{Q},\mathbf{Q}'}$$

and

$$\chi_{\rm incoh}(\mathbf{Q},\mathbf{Q}';\tilde{\varepsilon})=\chi_{\rm incoh}(\tilde{\varepsilon})\,\delta_{\mathbf{Q},\mathbf{Q}'}$$

in the case of a uniform external field ($\mathbf{Q}=0$, i.e., the wavelength of the light is much greater than the characteristic lengths of the spatial modulation of the system of quasilocal optical dipoles) in the limit $\gamma\to0$ we obtain the following expressions for the dynamic dielectric susceptibility $\chi(\varepsilon)=\chi_1(\varepsilon)+i\chi_2(\varepsilon)$:

$$\chi^{xy}_{1\rm coh}(0;\varepsilon)=\frac{\pi D^2}{v_a}[N_{fi}(\varepsilon+\Delta_M)-N_{fi}(\varepsilon-\Delta_M)],$$

$$\chi^{xy}_{2\rm coh}(0;\varepsilon)=\frac{4\varepsilon\Delta_MD^2}{v_aN}\times\sum_{\mathbf{k}}\frac{n_{\mathbf{k},i}E_{fi}(\mathbf{k})}{\{\varepsilon^2-[E_{fi}(\mathbf{k})+\Delta_M]^2\}\{\varepsilon^2-[E_{fi}(\mathbf{k})-\Delta_M]^2\}}, \tag{15}$$

$$\chi^{xy}_{1\rm incoh}(\varepsilon)=\frac{\pi d^2}{v_a}[\tilde{N}_{fi}(\varepsilon+\Delta_M)-\tilde{N}_{fi}(\varepsilon-\Delta_M)],$$

$$\chi^{xy}_{2\rm incoh}(\varepsilon)=\frac{4\varepsilon\Delta_Md^2}{v_aN^2}\times\sum_{\mathbf{kk}'}\frac{n_{\mathbf{k},i}E_{fi}(\mathbf{k},\mathbf{k}')}{\{\varepsilon^2-[E_{fi}(\mathbf{k},\mathbf{k}')+\Delta_M]^2\}\{\varepsilon^2-[E_{fi}(\mathbf{k},\mathbf{k}')-\Delta_M]^2\}}, \tag{16}$$

$$\chi^{0}_{1\rm coh}(0;\varepsilon)+\chi^{\parallel}_{1\rm coh}(0;\varepsilon)=-\frac{2D^2}{v_aN}\times\sum_{\mathbf{k}}\frac{n_{\mathbf{k},i}E_{fi}(\mathbf{k})[\varepsilon^2-E^2_{fi}(\mathbf{k})+\Delta^2_M]}{\{\varepsilon^2-[E_{fi}(\mathbf{k})+\Delta_M]^2\}\{\varepsilon^2-[E_{fi}(\mathbf{k})-\Delta_M]^2\}}, \tag{17}$$

$$\chi^{0}_{2\rm coh}(0;\varepsilon)+\chi^{\parallel}_{2\rm coh}(0;\varepsilon)=\frac{\pi D^2}{v_a}[N_{fi}(\varepsilon+\Delta_M)+N_{fi}(\varepsilon-\Delta_M)],$$

$$\chi^{0}_{1\rm incoh}(\varepsilon)+\chi^{\parallel}_{1\rm incoh}(\varepsilon)=-\frac{2d^2}{v_aN^2}\times\sum_{\mathbf{kk}'}\frac{n_{\mathbf{k},i}E_{fi}(\mathbf{k},\mathbf{k}')[\varepsilon^2-E^2_{fi}(\mathbf{k},\mathbf{k}')+\Delta^2_M]}{\{\varepsilon^2-[E_{fi}(\mathbf{k},\mathbf{k}')+\Delta_M]^2\}\{\varepsilon^2-[E_{fi}(\mathbf{k},\mathbf{k}')-\Delta_M]^2\}}, \tag{18}$$

$$\chi^{0}_{2\rm incoh}(\varepsilon)+\chi^{\parallel}_{2\rm incoh}(\varepsilon)=\frac{\pi d^2}{v_a}[\tilde{N}_{fi}(\varepsilon+\Delta_M)+\tilde{N}_{fi}(\varepsilon-\Delta_M)].$$

In expressions (15)–(18) we have used the notation

$$E_{fi}(\mathbf{k},\mathbf{k}')=E_f-E_i+T_f(\mathbf{k}')-T_i(\mathbf{k})+\zeta\mu/2,$$

$$E_{fi}(\mathbf{k})=E_{fi}(\mathbf{k},\mathbf{k}),$$

$$N_{fi}(\varepsilon)=\frac{1}{2N}\sum_{\mathbf{k}}n_{\mathbf{k},i}\delta[\varepsilon-E_{fi}(\mathbf{k})],$$

$$\tilde{N}_{fi}(\varepsilon)=\frac{1}{2N^2}\sum_{\mathbf{k},\mathbf{k}'}n_{\mathbf{k},i}\delta[\varepsilon-E_{fi}(\mathbf{k}',\mathbf{k})],$$

and we have dropped the indices $\mu$ and $\sigma$. We have taken into account that in the model used, the system described by the ''unperturbed'' Hamiltonian $\mathcal{H}$ is uniformly magnetized, the lower band $i$ is partially filled ($n_{\mathbf{k},i}\equiv n_{\mathbf{k},i,\mu,\sigma}\neq0$, $n_{\mathbf{k},i,-\mu,-\sigma}=0$, $\sigma=1/2$), while the upper band $f$ is completely empty ($n_{\mathbf{k}',f,\mu\pm1,\sigma}=0$).

Expanding expressions (15)–(18) in series far from resonance ($|\varepsilon-E_{fi}|\gg\Delta_M$), we obtain to leading order in $\Delta_M$:

$$\chi^{xy}(0;\varepsilon)=\chi^{xy}_2(0;\varepsilon),$$

$$\chi^{xy}_{2\rm coh}(0;\varepsilon)=\frac{4D^2\varepsilon\Delta_M}{v_aN}\sum_{\mathbf{k}}\frac{n_{i,\mathbf{k}}E_{fi}(\mathbf{k})}{[\varepsilon^2-E^2_{fi}(\mathbf{k})]^2}, \tag{19}$$

$$\chi^{xy}_{2\rm incoh}(0;\varepsilon)=\frac{4d^2\varepsilon\Delta_M}{v_aN^2}\sum_{\mathbf{k},\mathbf{k}'}\frac{n_{i,\mathbf{k}}E_{fi}(\mathbf{k},\mathbf{k}')}{[\varepsilon^2-E^2_{fi}(\mathbf{k},\mathbf{k}')]^2}.$$

$$\chi^{0}(0;\varepsilon)+\chi^{\parallel}(0;\varepsilon)=\chi^{0}_1(0;\varepsilon)+\chi^{\parallel}_1(0;\varepsilon),$$

$$\chi^{0}_{1\rm coh}(0;\varepsilon)+\chi^{\parallel}_{\rm tcoh}(0;\varepsilon)=\frac{2D^2}{v_aN}\sum_{\mathbf{k}}\frac{n_{i,\mathbf{k}}E_{fi}(\mathbf{k})}{E^2_{fi}(\mathbf{k})-\varepsilon^2}\left\{1+\frac{\Delta^2_M[E^2_{fi}(\mathbf{k})+3\varepsilon^2]}{[E^2_{fi}(\mathbf{k})-\varepsilon^2]^2}\right\}, \tag{20}$$

$$\chi^{0}_{1\rm incoh}(0;\varepsilon)+\chi^{\parallel}_{1\rm incoh}(0;\varepsilon)=\frac{2d^2}{v_dN^2}\sum_{\mathbf{kk}'}\frac{n_{i,\mathbf{k}}(\mathbf{k},\mathbf{k}')}{E^2_{fi}(\mathbf{k},\mathbf{k}')-\varepsilon^2}\left\{1+\frac{\Delta^2_M[E^2_{fi}(\mathbf{k},\mathbf{k}')+3\varepsilon^2]}{[E^2_{fi}(\mathbf{k},\mathbf{k}')-\varepsilon^2]^2}\right\}.$$

In the static limit ($\varepsilon=0$), formulas (19) and (20) become

$$\chi^{xy}(0;0)=0;$$

$$\chi^{0}(0;0)+\chi^{\parallel}(0;0)=\chi^{0}_1(0;0)+\chi^{\parallel}_1(0;0),$$

$$\chi^{2}_{\rm coh}(0;0)+\chi^{\parallel}_{\rm coh}(0;0)=\frac{2D^2}{v_aN}\sum_{\mathbf{k}}\frac{n_{i,\mathbf{k}}}{E_{fi}(\mathbf{k})}\left\{1+\frac{\Delta^2_M}{E^2_{fi}(\mathbf{k})}\right\}, \tag{21}$$

$$\chi^{0}_{\rm incoh}(0;0)+\chi^{\parallel}_{\rm incoh}(0;0)=\frac{2d^2}{v_aN^2}\sum_{\mathbf{k},\mathbf{k}'}\frac{n_{i,\mathbf{k}}}{E_{fi}(\mathbf{k},\mathbf{k}')}\left\{1+\frac{\Delta^2_M}{E^2_{fi}(\mathbf{k},\mathbf{k}')}\right\}.$$

From a comparison of expressions (19) and (20) we see that the off-diagonal susceptibility $\chi^{xy}$, unlike the diagonal susceptibility $\chi^0+\chi^{\|}$, does not change sign on passage through the resonance region.

For transitions in a system of localized electrons ($T(\mathbf{k})=0$) the spectra of $\chi_{\rm coh}$ and $\chi_{\rm incoh}$ become similar, and instead of formulas (19) and (21) we have

$$\chi^{xy}(0;\varepsilon)=\frac{4\langle|D_\lambda|^2\rangle\varepsilon\Delta_M ZE_{fi}}{v_a(E_{fi}^2-\varepsilon^2)^2}, \tag{22}$$

$$\chi^0(0;0)+\chi^{\|}(0;0)=\frac{2\langle|D_\lambda|^2\rangle Z}{v_a E_{fi}}\left\{1+\frac{\Delta_M^2}{E_{fi}^2}\right\}, \tag{23}$$

where $\langle|D_\lambda|^2\rangle=D^2+d^2$ is the mean-square modulus of the dipole moment at site λ, and $Z$ is the number of ''magnetooptical'' electrons per atom (in the present case this is the number of electrons on level $i$).

The dependence of the real parts $\chi_{1\rm coh}^{xy}$ and $\chi_{1\rm incoh}^{xy}$ on the photon energy is shown in Fig. 2.

## DISCUSSION

Expressions (15) and (16) give a complete qualitative description of the magnetic contribution to the dynamic dielectric susceptibility of a system of quasilocal optical dipoles. As compared to the situation in perfect crystals, in the present case the spectrum of $\chi^{\alpha\beta}(\omega)$ decomposes into two components:[2,3] coherent $\chi_{\rm coh}^{\alpha\beta}$ and incoherent $\chi_{\rm incoh}^{\alpha\beta}$. The first is formed by direct (or vertical) electronic transitions, i.e., transitions that conserve the quasimomentum of the electron, and the second by indirect (nonvertical) transitions, i.e., transitions with arbitrary changes of the electron quasimomenta. The intensity of the coherent component is proportional to the square of the crystal-averaged value of the electric dipole moment of the optical transition, while the intensity of the incoherent component is proportional to the mean square fluctuation of the electric dipole moment.

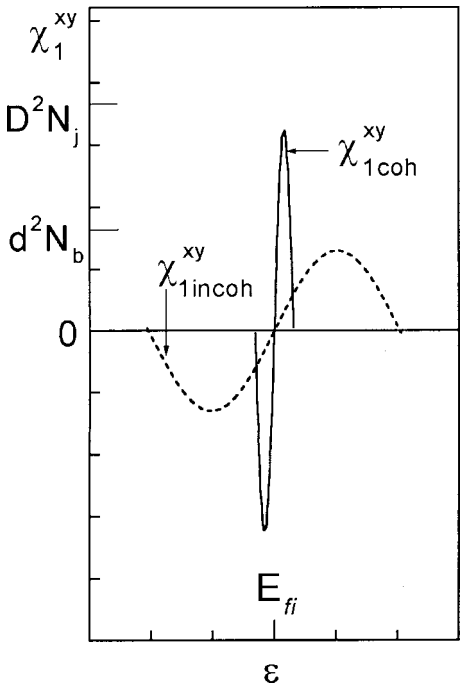


FIG. 2. Schematic form of the calculated spectrum $\chi_1^{xy}(\varepsilon)$ of the real part of the off-diagonal dielectric susceptibility of a randomized $f-d$ magnet: $E_{fi}$ is the energy of the electronic transition $i\to f$, $D=\langle D_\lambda\rangle$ is the average dipole moment of this transition, $d=\langle d_\lambda^2\rangle^{1/2}$ is the spatial fluctuation of the moment $D_\lambda$, the parameters $N_b$ and $N_j$ are proportional to the product of the maximum values of the electronic densities of states in bands $i$ and $f$ and to their interband density of states, respectively; the horizontal scale is in units of $T_i$.

Far from the resonance frequencies $E_{fi,\mu\pm1}$ the dispersion part (polarizability) $\chi_2^{xy}(\omega)$ of the off-diagonal component is linear to leading order in the magnetic field $H_0$ and spin–orbit interaction constant $\zeta$, while the diagonal magnetic contributions $\chi_1^{\|}(\omega)$ are quadratic with respect to the effective field $\Delta_M=\zeta/2-\mu_B H_0$. The structure of formula (22) is analogous to that of the Nagaev formula,[6] and formula (23) gives the magnetic contribution to the static dielectric susceptibility.

The basis functions of the Hamiltonian of our model are the eigenfunctions of the operator for the $z$ projection of the orbital angular momentum, which commutes with the Hamiltonian of the orbital motion of the system of electrons in a magnetic field.[21] This model contains two resonance frequencies $E_{fi,\mu\pm1}$, unlike the model with a Hamiltonian based on the eigenfunctions of the crystalline field (see, e.g., Ref. 6). In the latter case the energy spectrum to a first approximation in $\zeta$ (and $H_0$) contains only one resonance frequency, $E_{fi}$,[28] but far from the resonance region both models give the same results. The choice between the two models (or their modifications) for describing the magnetooptical spectra in the immediate proximity of the resonances is dictated by the value of the ratio of $\Delta_M$ to the corresponding crystal-field parameter of the system under study.

As can be seen from Eqs. (17) and (18), the spectrum of $\chi^0(\varepsilon)+\chi^{\|}(\varepsilon)$ differs from the diagonal dielectric susceptibility of nonmagnetic origin (see, e.g., Ref. 1). The absorption part $\chi_2^0(\varepsilon)+\chi_2^{\|}(\varepsilon)$ contains two peaks equidistant from $E_{fi}$, which, however, have the same shape as the ''nonmagnetic'' absorption peak. The dispersion part $\chi_1^0(\varepsilon)+\chi_1^{\|}(\varepsilon)$ also has two characteristic ''oscillations'' separated from $E_{fi}$, which are analogous to the contributions to the usual ''nonmagnetic'' dynamic dielectric susceptibility.

The magnetooptic effect arises in the interaction of light with each atom individually, even in the absence of an external magnetic field, as a result of the spin–orbit interaction, but in the case when the crystal-averaged magnetic moment is zero, there is no macroscopic effect. For calculating the dielectric susceptibility of the system in the absence of macroscopic magnetization it is necessary to include in the calculation scheme (e.g., in a pseudoalloy model) an equal number of sites with the electronic transitions

$$|\lambda,i,\mu,\sigma\rangle\to|\lambda,f,\mu\pm1,\sigma\rangle$$

and

$$|\lambda,i,-\mu,-\sigma\rangle\to|\lambda,f,-\mu\mp1,-\sigma\rangle.$$

Here the spectra of $\chi^+(\varepsilon)$ and $\chi^-(\varepsilon)$ each contain two resonance frequencies and coincide completely. As a result, $\chi^{xy}(\varepsilon)=0$, while $\chi^{\|}(\varepsilon)\neq0$, so that relation (23) can explain the experimentally observed correction, quadratic in the magnetic moment of the ion, to the static electronic polarizability of iron oxides[29,30] and rare-earth elements.[31]

The authors are grateful to V. V. Eremenko and N. F. Kharchenko for their interest and support, and to A. A. Loginov for a constructive discussion.

This study was supported in part by grants from the International Science Foundation and the Government of Ukraine (ISF#U9L000 and ISF/UA#U9L200), and by the Kamerlingh Onnes Laboratory, Leiden and the Netherlands Organization for Applied Scientific Research.

*E-mail: beznosov@ilt.kharkov.ua

[1)]The analogy between the Hall and Faraday effects[6] due to the polarization (or ''dispersion,'' in distinction to the ''absorption'') component of the ''magnetic'' contribution to the off-diagonal dielectric susceptibility.

[2)]The symbols $i$ and $4f$ used to denote $\sqrt{-1}$ and the magnetically active shell of the rare-earth ions are easily distinguished by context from the indices $i$ and $f$ of the initial and final electronic states.

[3)]In this model $m_e$ is the mass of a free electron, since we are essentially talking about intra-atomic transitions $i \rightarrow f$.

[1] J. M. Ziman, *Principles of the Theory of Solids*, Cambridge University Press, Cambridge (1972); Mir, Moscow (1974).
[2] A. B. Beznosov, V. P. Gnezdilov, and V. V. Eremenko, JETP Lett. **38**, 587 (1983); Fiz. Nizk. Temp. **10**, 954 (1984) [Sov. J. Low Temp. Phys. **10**, 498 (1984)].
[3] A. B. Beznosov, V. V. Eremenko, and V. P. Gnezdilov, J. Magn. Magn. Mater. **43**, 243 (1984); **54–57**, 1251 (1986).
[4] A. B. Beznosov, V. P. Gnezdilov, and V. V. Eremenko, Pis'ma Zh. Tekh. Fiz. **10**, 14906 (1984) [Sov. Tech. Phys. Lett. **10**, 629 (1984)]; Zh. Tekh. Fiz. **55**, 1866 (1985) [Sov. Phys. Tech. Phys. **30**, 1095 (1985)].
[5] L. D. Landau and E. M. Lifshitz, *Electrodynamics of Continuous Media* [Pergamon Press, Oxford (1960); Izd. Fiz.-Mat. Lit., Moscow (1959)].
[6] E. L. Nagaev, *Physics of Magnetic Semiconductors* [Mir, Moscow (1983); Nauka, Moscow (1979)].
[7] A. V. Sokolov, *Optical Properties of Metals* [in Russian], Izd. Fiz.-Mat. Lit., Moscow (1961).
[8] B. R. Cooper, Phys. Rev. A **139**, 1505 (1965).
[9] J. L. Erskine and E. A. Stern, Phys. Rev. B **8**, 1239 (1973).
[10] H. Ebert, Rep. Prog. Phys. **59**, 1665 (1996).
[11] V. N. Antonov, A. N. Yaresko, A. Ya. Perlov, V. V. Nemoshkalenko, P. M. Oppeneer, and H. Eschrig, Fiz. Nizk. Temp. **25**, 527 (1999) [Low Temp. Phys. **25**, 387 (1999)].
[12] N. F. Mott and E. A. Davis, *Electron Processes in Non-Crystalline Materials* [Clarendon Press, Oxford (1979); Mir, Moscow (1982)].
[13] É. L. Nagaev, Usp. Fiz. Nauk **166**, 833 (1996).
[14] V. M. Loktev and Yu. G. Pogorelov, Fiz. Nizk. Temp. **26**, 231 (2000) [Low Temp. Phys. **26**, 171 (2000)].
[15] E. S. Orel and A. B. Beznosov, in *Physical Phenomena in Solids* [in Russian], edited by V. V. Ul'yanov, KhGU, Kharkov (1995), p. 41.
[16] É. S. Orel and A. B. Beznosov, Ukr. Fiz. Zh. **40**, 579 (1995).
[17] A. A. Sokolov, I. M. Ternov, and V. Ch. Zhukovskiĭ, *Quantum Mechanics* [in Russian], Nauka, Moscow (1979).
[18] R. M. White, *The Quantum Theory of Magnetism* [McGraw-Hill, New York (1970); Mir, Moscow (1985)].
[19] H. Jones, Phys. Rev. **134**, 958 (1964).
[20] H. Ehrenreich and L. Schwartz, *The Electronic Structure of Alloys*, Vol. 31 of Solid State Physics [Academic Press, New York (1976); Mir, Moscow (1979)].
[21] A. S. Davydov, *Solid State Theory* [in Russian], Nauka, Moscow (1976).
[22] D. N. Zubarev, *Nonequilibrium Statistical Thermodynamics* [Consultants Bureau, New York (1974); Nauka, Moscow (1971)].
[23] K. Elk and W. Gasser, *Die Methode der Greenschen Funktionen in der Festkorperphysik*, Akademie-Verlag, Berlin (1979).
[24] E. V. Kuz'min, G. A. Petrakovskiĭ, and É. A. Zavadskiĭ, *Physics of Magnetically Ordered Substances* [in Russian], Nauka, Novosibirsk (1976).
[25] P. N. Argyres, Phys. Rev. **97**, 334 (1955).
[26] G. S. Krinchik and V. A. Artem'ev, Zh. Éksp. Teor. Fiz. **53**, 1901 (1967) [Sov. Phys. JETP **26**, 1080 (1968)].
[27] A. V. Malakhovskiĭ, *Selected Topics in the Optics and Magnetooptics of Compounds of Transition Elements* [in Russian], Nauka, Novosibirsk (1992).
[28] S. V. Vonsovskiĭ, *Magnetism*, Vols. 1 and 2 [Wiley, New York (1974); Nauka, Moscow (1971)].
[29] A. B. Beznosov, V. V. Eremenko, and A. I. Galuza, *Abstracts of the International Conference on Magnetism*, San Francisco (1985), 1Pe13.
[30] A. B. Beznosov, A. I. Galuza, and V. V. Eremenko, in *Advances in Magneto-Optics II*, *Proceedings of the 2nd International Symposium on Magneto-Optics*, Sept. 10–13, 1991, Kharkov, Ukraine (edited by V. V. Eremenko and A. B. Beznosov), Fiz. Nizk. Temp. **18**, Suppl. S1, p. 183 (1992) [*sic*].
[31] A. B. Beznosov and A. I. Galuza, *Abstracts of the XIV All-Russia Conference on the Physics of Ferroelectrics* [in Russian], Iv. Gos. Univ., Ivanovo (1995), p. 310.

Translated by Steve Torstveit

# Fermi-liquid cyclotron modes in quasi-two-dimensional conductors

O. V. Kirichenko and V. G. Peschansky*

*B. Verkin Institute for Low Temperature Physics and Engineering, National Academy of Sciences of Ukraine, pr. Lenina 47, 61103 Kharkov, Ukraine*

(Submitted December 11, 2000)
Fiz. Nizk. Temp. **27**, 519–522 (May 2001)

The spectrum of normal vibrational modes propagating along the direction of an external static magnetic field in conductors with a sharply anisotropic dispersion relation of the charge carriers is obtained with allowance for their Fermi-liquid interaction. © *2001 American Institute of Physics.* [DOI: 10.1063/1.1374724]

A Fermi liquid of conduction electrons can support the propagation of weakly damped waves which are absent in a gas of charge carriers. By studying these waves one can make a detailed investigation of correlation effects in the electron subsystem of a conducting medium.[1–4] In metals, however, the experimental observation of Fermi-liquid waves is complicated by the fact that their spectrum lies near the plasma frequency $\omega_p=(4\pi Ne^2/m)^{1/2}$, which is extremely high because of the high charge-carrier density $N$ ($e$ is the charge of the electron, and $m$ is the characteristic effective mass of the conduction electrons).

Recently a large class of organic compounds having a layered structure and exhibiting metallic conduction has been synthesized. For such conductors the plasma frequency is much smaller than for ordinary metals, and the specifics of the quasi-two-dimensional electron energy spectrum gives rise to peculiar Fermi-liquid eigenmodes, which are apparently easy to study experimentally.[5]

Let us consider the propagation of waves along the normal to the layers of an organic conductor in an external magnetic field $\mathbf{H}_0$, with allowance for correlation effects in the electron system. In a layered conductor the energy $\varepsilon$ of the charge carriers depends weakly on the projection of their quasimomentum $\mathbf{p}$ on the normal to the layers ($z$ axis) and can be written in the form

$$\varepsilon(\mathbf{p})=\sum_{n=0}^{\infty}\varepsilon_n(p_x,\,p_y)\cos\frac{anp_z}{\hbar}, \tag{1}$$

where $\hbar$ is Planck's constant and $a$ is the distance between layers. The coefficients multiplying the cosines in expression (1) fall off rapidly with increasing index $n$, so that the maximum value of $\varepsilon_1(p_x,p_y)$ at the Fermi surface ($\varepsilon(\mathbf{p})=\varepsilon_F$) is equal to $\eta\varepsilon_F$, where the quasi-two-dimensionality parameter $\eta$ of the electron spectrum is much less than unity.

The electromagnetic field in the conductor is found from Maxwell's equations

$$\begin{aligned}&\operatorname{curl}\mathbf{H}=\frac{4\pi}{c}\mathbf{j}+\frac{1}{c}\frac{\partial\mathbf{E}}{\partial t},\\ &\operatorname{curl}\mathbf{E}=-\frac{1}{c}\frac{\partial\mathbf{B}}{\partial t},\quad \mathbf{B}=\mathbf{H}+4\pi\mathbf{M},\end{aligned} \tag{2}$$

supplemented by the constitutive relations of the medium.

In order to find the relation between the current density $\mathbf{j}$ and the electric field $\mathbf{E}$, we must solve the kinetic equation for the nonequilibrium correction $-\psi(\partial f_0/\partial\varepsilon)$ to the Fermi distribution function $f_0$ of the charge carriers. The function $\psi$ satisfies an equation which to first order in the weak electric field of a monochromatic wave $\mathbf{E}(\mathbf{r},t)=\mathbf{E}(\mathbf{r})\exp(-i\omega t)$ and in the relaxation-time approximation for the collision integral takes the form

$$-i\omega\psi+\left(\mathbf{v}\cdot\frac{\partial}{\partial\mathbf{r}}+\frac{1}{\tau}+\frac{\partial}{\partial t_H}\right)\Phi=e\mathbf{v}\cdot\mathbf{E}, \tag{3}$$

where $\mathbf{v}$ is the electron velocity, $\tau$ is the relaxation time, $\partial/\partial t_H=e/c(\mathbf{v}\times\mathbf{H})\cdot\partial/\partial\mathbf{p}$, $c$ is the speed of light, and the functions $\Phi$ and $\psi$ are related to each other by the integral relation[6,7]

$$\begin{aligned}\Phi(\mathbf{r},\mathbf{p},\sigma)=\psi(\mathbf{r},\mathbf{p},\sigma)-\sum_{\sigma'}\int\frac{d^3p'}{(2\pi\hbar)^3}\frac{\partial f_0(\varepsilon)}{\partial\varepsilon}\\ \times\psi(\mathbf{r},\mathbf{p}',\sigma')L(\mathbf{p},\sigma;\mathbf{p}',\sigma'),\end{aligned} \tag{4}$$

where

$$L(\mathbf{p},\sigma;\mathbf{p}',\sigma')=L_0(\mathbf{p},\sigma;\mathbf{p}',\sigma')+\hat{\sigma}\hat{\sigma}'L_1(\mathbf{p},\sigma;\mathbf{p}',\sigma') \tag{5}$$

is the Landau–Silin correlation function and $\hat{\sigma}$ is the Pauli matrix.

By solving the kinetic equation (3) jointly with the integral relation (4), we can find the electric current density

$$j=-\int\frac{2d^3p}{(2\pi\hbar)^3}\frac{\partial f_0(\varepsilon)}{\partial\varepsilon}e\mathbf{v}\Phi. \tag{6}$$

We now limit the discussion to the first term in expression (5). Taking the second term into account leads to the appearance of the spin waves predicted by Silin[8] and observed experimentally in Ref. 9. However, in quasi-two-dimensional conductors the oscillations of the spin density are quite hard to observe, since at low temperatures the de Haas–van Alphen effect is manifested more clearly in them, and the amplitude of the oscillations of the magnetization $\mathbf{M}$ due to this effect is much larger than the paramagnetic part of $\mathbf{M}$.

 

We assume that the $z=0$ surface of the conductor is specularly reflective for charge carriers, and for the sake of brevity in the calculations we write their dispersion relation in the form

$$\varepsilon=\frac{p_x^2+p_y^2}{2m}-\eta v_0\frac{\hbar}{a}\cos\frac{ap_z}{\hbar}, \tag{7}$$

where $v_0^2=2\varepsilon_F/m$.

If the external magnetic field $H_0$ is applied along the normal to the layers, then it follows from the equations of motion that

$$\begin{aligned} &v_x=v_\perp\cos\varphi;\quad v_y=-v_\perp\sin\varphi;\quad v_z=\eta v_0\cos\theta;\\ &v_\perp^2=v_0^2+2\eta v_0\frac{\hbar}{ma}\cos\theta. \end{aligned} \tag{8}$$

Here $\theta=p_za/\hbar$, $\varphi=\Omega t_H$, and the cyclotron frequency $\Omega=eH_0/mc$.

In layered conductors the interaction between electrons belonging to different layers is much smaller than the interaction between electrons in the same layer, and the correlation function, like the energy of the quasi-two-dimensional electrons, depends only weakly on $p_z$. It is appropriate to assume that the correlation function is proportional to the product of the electron velocities, $\mathbf{v}\cdot\mathbf{v}'$. Then, in the case of dispersion relation (7), in the leading approximation in the small parameter $\eta$ it can be represented by the formula

$$L_0=\Lambda\cos(\varphi-\varphi'). \tag{9}$$

This makes it possible to simplify the integral equation (5) substantially, as it can now be written in the form

$$\begin{aligned} \Phi(\theta,\varphi)=\psi(\theta,\varphi)+\frac{\tilde\Lambda}{(2\pi)^2}\\ \times\int_{-\pi}^{\pi}d\theta'\int_{-\pi}^{\pi}d\varphi'\,\psi(\theta',\varphi')\cos(\varphi-\varphi'), \end{aligned} \tag{10}$$

where $\tilde\Lambda=m\Lambda/2\pi\hbar^2a$.

The model we have used for the Fermi-liquid interaction suggests that the functions $\psi$ and $\Phi$ be written as the sum of two harmonics:

$$\psi(\theta,\varphi)=\psi^+(\theta)e^{i\varphi}+\psi^-(\theta)e^{-i\varphi}. \tag{11}$$

Using Eq. (10) we easily obtain the relation

$$\psi^\pm=\Phi^\pm-\lambda\overline{\Phi^\pm}. \tag{12}$$

Here

$$\overline{\Phi}=\frac{1}{2\pi}\int_{-\pi}^{\pi}d\theta\Phi(\theta),\quad \lambda=\frac{\tilde\Lambda}{1+\tilde\Lambda}.$$

We continue the electric field in an even manner into the region of negative $z$ and use the Fourier representation

$$\Phi^\pm(z)=\int_{-\infty}^{\infty}\Phi^\pm(k)dk\exp(ikz). \tag{13}$$

Eliminating $\psi$ from the kinetic equations by using formula (12) and then equating the coefficients of $e^{i\varphi}$ and $e^{-i\varphi}$, we easily obtain two algebraic equations,

$$\begin{aligned} &\Phi^\pm(k)(-i\tilde\omega+ikv_z\pm i\Omega)\Phi^\pm(k)\\ &\quad=\frac{ev_\perp}{2}E^\pm(k)-i\omega\lambda\overline{\Phi^\pm(k)}, \end{aligned} \tag{14}$$

relating the functions $\Phi^\pm$ with the circularly polarized Fourier components of the electric field $E^\pm(k)=E_x(k)\pm iE_y(k)$. Here $\tilde\omega=\omega+i/\tau$.

From Eq. (14) we find

$$\Phi^\pm=\frac{ie}{2\tilde\omega}R^\pm E^\pm\left(v_\perp+\lambda\omega\frac{\overline{v_\perp R^\pm}}{\tilde\omega-\omega\lambda\overline{R^\pm}}\right), \tag{15}$$

where

$$R^\pm=\frac{\tilde\omega}{\tilde\omega-kv_z\mp\Omega}.$$

As we see from formulas (6) and (8), the circularly polarized components of the current $j^\pm(k)=j_x(k)\pm ij_y(k)$ satisfy the expression

$$J^\pm(k)=\frac{em}{\pi\hbar^2a}\overline{v_\perp\Phi^\pm(k)}. \tag{16}$$

Substituting this expression into Maxwell's equations in the Fourier representation, we obtain two equations describing two cyclotron waves of different polarization:

$$\begin{aligned} &\left\{k^2c^2-\omega^2+\frac{e^2m\omega}{\hbar^2a\tilde\omega}\left(\overline{v_\perp^2R^\pm}+\frac{\lambda\omega\overline{(v_\perp R^\pm)^2}}{\tilde\omega-\lambda\overline{R^\pm}}\right)\right\}E^\pm(k)\\ &\quad=-2E^\pm(0). \end{aligned} \tag{17}$$

It is easy to evaluate the explicit form of the expressions appearing here:

$$\begin{aligned} &\overline{R^\pm}=\frac{\tilde\omega}{\sqrt{(\tilde\psi\mp\Omega)^2-(\eta kv_0)^2}},\\ &\overline{v_\perp R^\pm}=v_0\overline{R^\pm},\quad \overline{v_\perp^2R^\pm}\approx v_0^2\overline{R^\pm} \end{aligned} \tag{18}$$

and, substituting them into formula (17), we obtain the final equation for the electric field in the conductor in the leading approximation in the small parameter $\eta$:

$$\begin{aligned} &\left\{k^2c^2-\omega^2\left(1+\frac{\omega_p^2}{-\omega\sqrt{(\tilde\omega\mp\Omega)^2-(\eta kv_0)^2}+\omega^2\lambda}\right)\right\}E^\pm\\ &\quad=-2E^\pm(0). \end{aligned} \tag{19}$$

We obtain the eigenmode spectrum from the dispersion relation

$$k^2c^2-\omega^2\left(1+\frac{\omega_p^2}{-\omega\sqrt{(\tilde\omega\mp\Omega)^2-(\eta kv_0)^2}+\omega^2\lambda}\right)=0. \tag{20}$$

If the following condition holds:

$$(\omega\mp\Omega)^2-(\lambda\omega)^2<(\eta k v_0)^2<(\omega\mp\Omega)^2, \quad (21)$$

then at frequencies below the plasma frequency and in the collisionless limit ($\tau=\infty$) there exist real solutions for $k$ which are absent in the gas approximation. They describe cyclotron modes due to correlation effects in the conductor. The dispersion relation of these excitations has the form

$$\omega^{\pm}=\frac{\sqrt{(\eta k v_0)^2-[(\eta k v_0)^2-[(\eta k v_0)^2-\Omega^2](\lambda-\omega_p^2/k^2c^2)^2}\pm\Omega}{1-(\lambda-\omega_p^2/k^2c^2)^2}, \quad \Omega<|\eta k v_0|. \quad (22)$$

The Fermi-liquid cyclotron modes exist for $k>k_{\min}=\omega_p/c\sqrt{\lambda}$, and so $\omega_{\min}=\omega_0/\sqrt{\lambda}\pm\Omega$, where $\omega_0=\omega_p\eta v_0/c$. The presence of two waves is due to the fact that the magnetic field lifts the degeneracy of the spectrum of oscillations of the electromagnetic field.

The dependence of $\omega/\omega_0$ on $k/k_{\min}$ is shown in Fig. 1.

The penetration depth of the Fermi-liquid cyclotron waves into the conductor can be determined by measuring the surface impedance $Z$, which relates the field at the surface of the sample with the value of the total current:

$$Z^{\pm}=-\frac{4\pi i\omega}{c^2}\frac{E^{\pm}(0)}{E^{\pm}(0)}. \quad (23)$$

Using formula (20), we obtain

$$Z^{\pm}=-4\pi i\omega\int_{-\infty}^{\infty}dk \times\left(k^2c^2+\frac{\omega\omega_p^2}{\sqrt{(\tilde{\omega}\mp\Omega)^2-(\eta k v_0)^2}-\omega\lambda}\right)^{-1}. \quad (24)$$

Figure 2 shows the frequency dependence of $\mathrm{Re}\,Z^{\pm}/Z_0$, $Z_0=8\eta v_0/c^2$.

It is not hard to see that for an arbitrary quasi-two-dimensional dispersion relation of the charge carriers the spectrum of eigenmodes in a magnetic field will have approximately the same form as we have obtained for the case in which the dependence of the energy of the electrons on their quasimomentum is described by relation (7). If the dispersion relation of the charge carriers is substantially anisotropic in the plane of the layers, then two Fermi-liquid modes exist even in the absence of magnetic field. In this case an external magnetic field will only shift the window of transparency of the conductor for electromagnetic waves; this makes it easy to detect the Fermi-liquid modes and thus to study correlation effects in an electron Fermi liquid.

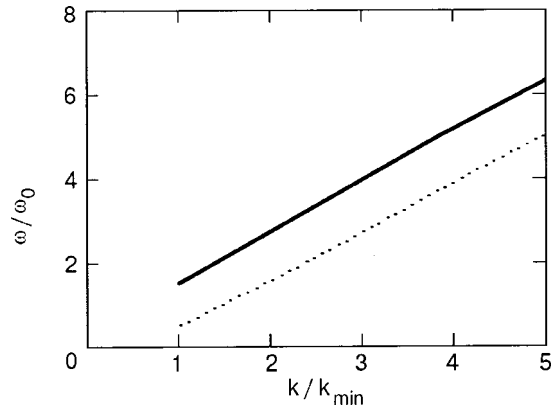


FIG. 1. Dispersion relation for a collective mode with electric field $E^+$ (solid line) and a collective mode with electric field $E^-$ (dotted line); $\lambda=0.5$.

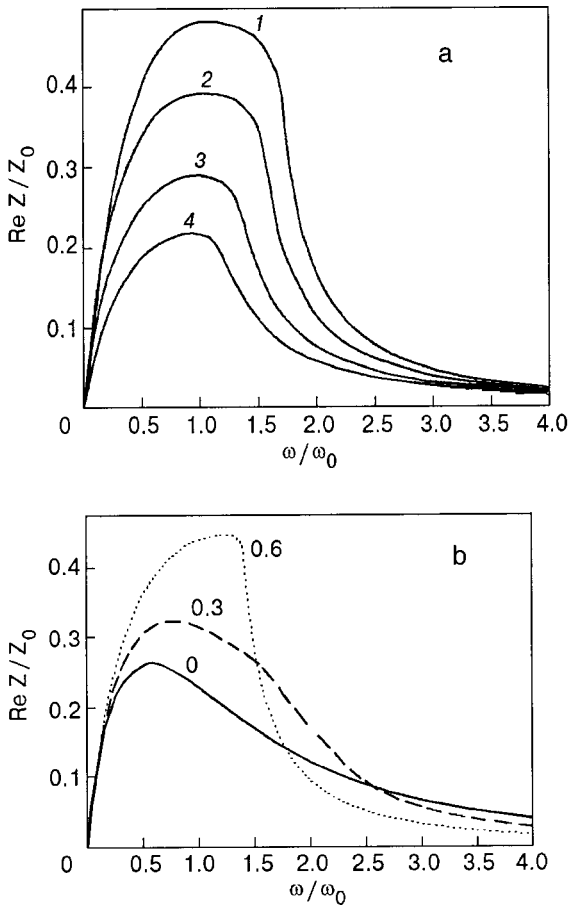


FIG. 2. Frequency dependence of the ratio $\mathrm{Re}\,Z/Z_0$. The excitation of collective modes with electric field $E^+$ (curves *1* and *2*) and electric field $E^-$ (curves *3* and *4*) for different values of the magnetic field: $\Omega/\omega_0=0.25$ (curves *1* and *4*), $\Omega/\omega_0=0.1$ (curve *2* and *3*), $\lambda=0.5$ (a); the excitation of modes with electric field $E^+$ for different values of the Fermi-liquid interaction parameter $\lambda$, $\Omega/\omega_0=0.1$ (b).

*E-mail: vpeschansky@ilt.kharkov.ua

[1] V. P. Silin, Usp. Fiz. Nauk, **94**, 185 (1967) [Sov. Phys. Usp. **10**, 139 (1968)].
[2] D. Pines and P. Nozières, *Theory of Quantum Liquids* [Benjamin, New York (1966); Mir, Moscow (1967)].
[3] A. S. Kondrat'ev and A. E. Kuchma, *Electron Liquid of Normal Metals* [in Russian], Izd. LGU, Leningrad (1980).
[4] D. G. Lominadze, *Cyclotron Waves in Plasma* [in Russian], Metsniereba, Tbilisi (1975).
[5] V. M. Gokhfeld and V. G. Peschansky, Fiz. Nizk. Temp. **25**, 43 (1999) [Low Temp. Phys. **25**, 32 (1999)].
[6] L. D. Landau, Zh. Éksp. Teor. Fiz. **30**, 1058 (1956) [Sov. Phys. JETP **3**, 920 (1956)].
[7] V. P. Silin, Zh. Éksp. Teor. Fiz. **33**, 495 (1957) [Sov. Phys. JETP **6**, 387 (1958)].
[8] V. P. Silin, Zh. Éksp. Teor. Fiz. **35**, 1243 (1958) [Sov. Phys. JETP **8**, 870 (1959)].
[9] S. Schultz and G. Dunifer, Phys. Rev. Lett. **18**, 283 (1967).

Translated by Steve Torstveit

# Piezoelectric mechanism of orientation of a bilayer Wigner crystal in a GaAs matrix

D. V. Fil*

*Institute of Single Crystals, National Academy of Sciences of Ukraine, pr. Lenina 60, 61001 Kharkov, Ukraine*

(Submitted December 21, 2000)
Fiz. Nizk. Temp. **27**, 523–531 (May 2001)

A mechanism for orientation of bilayer classical Wigner crystals in a piezoelectric medium is considered. For the GaAs system the piezoelectric correction to the electrostatic interaction between electrons is calculated. It is shown that taking into account the correction due to the piezoelectric effect leads to a dependence of the total energy of the electron crystal on its orientation with respect to the crystallographic axes of the surrounding matrix. A generalization of Ewald's method is obtained for calculating the anisotropic interaction between electrons in a Wigner crystal. The method is used to calculate the energy of bilayer Wigner crystals in electron layers parallel to the crystallographic planes (001), (0−11), and (111) as a function of their orientation and the distance between layers, and the energetically most favorable orientation for all types of electron lattices in a bilayer system is found. It is shown that phase transitions between structures with different lattice symmetry in a Wigner crystal can be accompanied by a change of its orientation. © *2001 American Institute of Physics.*
[DOI: 10.1063/1.1374725]

## 1. INTRODUCTION

It is known that a system of electrons in the presence of a neutralizing positive background at sufficiently low temperatures and densities goes into a Wigner crystal state. In particular, this situation takes place in two-dimensional electron layers in AlGaAs–GaAs heterojunctions. The formation of a Wigner crystal phase occurs under the condition that the average distance between electrons is much greater than the effective Bohr radius (in the absence of an external magnetic field) or the cyclotron radius (in high magnetic fields). The latter situation corresponds to a filling factor $\nu \ll 1$. In quantum Hall systems the formation of modulated electron structures can occur in other regimes as well. For example, skyrmion lattices can arise in the quantum ferromagnet regime ($\nu \approx 1,1/3$).[1] In low magnetic fields ($\nu \approx N+1/2$, where $N$ is an integer and $N \geqslant 4$) the formation of stripe structures can occur at the top, partially filled Landau level. The formation of such structures was predicted theoretically[2] and confirmed experimentally[3] by observation of the resulting strong anisotropy of the conductivity.

An interesting question is that of the orientation of the nonuniform electron structures relative to the crystallographic axes of the surrounding matrix. In the two-dimensional electron layers realized in AlGaAs heterostructures, an important influence on the orientation of the electron lattice can be exerted by the piezoelectric interaction between the electron and elastic subsystems. This possibility was first pointed out in relation to Wigner crystals in Refs. 4 and 5. A piezoelectric mechanism for the orientation of the stripe structure was considered in Ref. 6. In particular, in that paper an effect was detected wherein a reorientation of the stripes in bilayer systems arises in the case when the period of the structure is greater than the distance between layers. In Ref. 6 the electron subsystem was described using a charge-density-wave model. The purpose of the present paper is to examine the piezoelectric mechanism of orientation of nonuniform electronic structures in bilayer systems in another limiting case, corresponding not to a charge density wave but to a classical Wigner crystal. As in Ref. 6, we use a model which takes into account the anisotropy of the elastic constants of the crystalline matrix. We develop an approach whereby the energy of a system with an anisotropic interaction between electrons can be calculated exactly; this approach is a generalization of Ewald's method for calculating Coulomb sums. As a particular case we obtain results pertaining to a monolayer system. This topic was discussed previously in Ref. 5, where consideration was limited to the model situation of an isotropic crystal. Such a model does not answer the question of the specific orientation that will be realized in the GaAs system, the elastic properties of which are described by three elastic constants rather than two. Furthermore, the method of rapidly convergent lattice sums was not used in Ref. 5. For the case of bilayer systems, as far as we know, the question of a piezoelectric mechanism of orientation of a Wigner crystal has not been considered before.

The lattice symmetry of a classical Wigner crystal is determined by the minimum of its Coulomb energy. In a monolayer system the minimum is achieved for a hexagonal lattice.[7] In a bilayer system with the same electron density in the two layers, five types of electron lattice can form. The structure, dynamical properties, and melting criterion of such systems have been studied in detail in Refs. 8–10. Quantum bilayer Wigner crystals in an external magnetic field were treated in Refs. 11 and 12. The possibility of formation of bilayer Wigner crystals in superfluid helium films was examined in Refs. 13 and 14.

In a classical bilayer Wigner crystal the transition between different crystalline phases is regulated by the parameters $\eta = d\sqrt{n}$, where $d$ is the distance between layers and $n$

 

is the electron density in the layer. The case $\eta=0$ corresponds to a monolayer system with a doubled density, and the case $\eta=\infty$ to a system of two noninteracting layers. In both cases the minimum energy corresponds to hexagonal lattices, with a period differing by a factor of $\sqrt{2}$. Therefore, for finite $\eta$ there must be transition phases: rectangular, square, and rhombic.

The piezoelectric interaction, generally speaking, can lead to a shift of the boundaries between phases. In GaAs the piezoelectric interaction is rather weak, and so the indicated effect will be small. Nevertheless, since the Coulomb interaction in a system with cubic lattice symmetry is isotropic, the piezoelectric correction to the interaction between electrons can be important for determining the orientation of the electron crystal.

## 2. ENERGY OF THE PIEZOELECTRIC INTERACTION BETWEEN ELECTRONS IN A WIGNER CRYSTAL

Consider an infinite piezoelectric medium. The electrostatic potential $\varphi$ of an electron placed at the origin of the coordinate system is given by the following system of equations:

$$\begin{aligned} &\operatorname{div}\mathbf{D}=4\pi e\,\delta(0),\\ &\partial\sigma_{ik}/\partial x_k=0, \end{aligned} \tag{1}$$

where

$$D_i=-\varepsilon_{ik}\frac{\partial\varphi}{\partial x_k}-4\pi\beta_{i,kl}u_{kl} \tag{2}$$

is the electric displacement vector, and

$$\sigma_{ik}=\lambda_{iklm}u_{lm}-\beta_{l,ik}\frac{\partial\varphi}{\partial x_l} \tag{3}$$

is the stress tensor. Here $\varepsilon_{ik}$ is the dielectric tensor, $\lambda_{iklm}$ is the tensor of elastic constants, $\beta_{l,ik}$ is the tensor of piezoelectric moduli, and $u_{ik}$ is the strain tensor. After a transformation to the Fourier components, the system of equations (1) reduces to an algebraic system, and one can easily write the solution for the electrostatic potential. Let us write it out explicitly for a cubic system, the properties of which are determined by three elastic constants $c_{11}$, $c_{12}$, and $c_{44}$, one piezoelectric modulus $e_{14}$, and the dielectric constant $\varepsilon$:

$$\varphi_{\mathbf{q}}=\frac{4\pi e}{\varepsilon q^2}-\frac{(4\pi)^2 e}{\varepsilon q^2}\chi\frac{P(q_x,q_y,q_z)}{q^8 s_1^2(\mathbf{q})s_2^2(\mathbf{q})s_3^2(\mathbf{q})\rho^3}+O(\chi^2), \tag{4}$$

where $\chi=e_{14}^2/\varepsilon c_{11}$ is a small parameter in which the expansion is done, $s_i(\mathbf{q})$ is the velocity of sound with polarization $i$ in the direction $\mathbf{q}$, and $\rho$ is the density of the medium. The function $P$ is a homogeneous 8th-degree polynomial of the form

$$\begin{aligned} P(q_x,q_y,q_z)=q^2\Bigg(a_1q_x^2q_y^2q_z^2+a_2\sum_{l\neq k}q_l^4q_k^2\Bigg)\\ +a_3\sum_{l\neq k}q_l^Aq_k^A, \end{aligned} \tag{5}$$

where $l,k=x,y,z$, and

$$\begin{aligned} &a_1=c_{11}(2c_{12}^2-2c_{11}c_{12}+c_{44}^2-2c_{11}c_{44}),\\ &a_2=c_{11}^2c_{44},\\ &a_3=\frac{1}{2}c_{11}(c_{11}+c_{12})(c_{11}-c_{12}-2c_{44}). \end{aligned} \tag{6}$$

The $x,y,z$ axes are directed along the fourfold axes of the crystalline matrix. As we see from formula (4), the electrostatic potential contains a correction $\delta\varphi_{\mathbf{q}}$, the presence of which is due to the piezoelectric interaction. In an isotropic crystal, in which the sound velocity is independent of the direction and the coefficient $a_3$ in (5) is zero, the correction linear in $\chi$ can be represented as an expansion in a finite number of spherical harmonics:

$$\delta\varphi_{\mathbf{q}}=-\frac{(4\pi)^2 e}{\varepsilon q^2}\chi\sum_n\sum_{m=-n}^{n}A_{nm}Y_{nm}(\Theta_{\mathbf{q}},\psi_{\mathbf{q}}), \tag{7}$$

where $n$ is even and $n\leqslant 6$. In Eq. (7) $\psi_{\mathbf{q}}$ and $\Theta_{\mathbf{q}}$ are the polar and azimuthal angles, respectively. The coefficients $A_{nm}$ are expressed in terms of the longitudinal and transverse sound velocities. Expansion (7) in the case of an anisotropic crystal will also contain higher harmonics allowed by the symmetry of the system. The coefficients $A_{nm}$ for the anisotropic case can be found numerically. A calculation of these coefficients for the GaAs system ($c_{11}=12.3\times10^{11}$ dyn/cm$^2$, $c_{12}=5.7\times10^{11}$ dyn/cm$^2$, $c_{44}=6.0\times10^{11}$ dyn/cm$^2$) shows that the main contribution to the sum in (7) is given by the same harmonics ($n\leqslant 6$) as in the isotropic system (the coefficients of the higher harmonics are at least an order of magnitude smaller). It should be noted that, because the relations between the expansion coefficients are determined by three rather than two elastic constants, the problem cannot be reduced to isotropic even by limiting consideration to the lowest harmonics.

Using expansion (7), one can easily find the correction to the electrostatic interaction between electrons in a piezoelectric medium. After doing the inverse Fourier transformation we find

$$\delta V(\mathbf{r})=-\frac{e^2\chi}{\varepsilon r}G(\Theta_{\mathbf{r}},\psi_{\mathbf{r}}), \tag{8}$$

where

$$\begin{aligned} G(\Theta_{\mathbf{r}},\psi_{\mathbf{r}})=4\pi\sum_{nm}A_{nm}(-1)^{n/2}\\ \times\frac{n!}{2^n[(n/2)!]^2}Y_{nm}(\Theta_{\mathbf{r}},\psi_{\mathbf{r}}). \end{aligned} \tag{9}$$

The form of the function $G$ calculated for the GaAs crystal is shown in Fig. 1 (the coordinate axes are chosen along the fourfold axes). As we see from Eq. (8), the interaction between electrons contains a contribution corresponding to attraction, the strength of which depends on the direction of $\mathbf{r}$ and decays as $1/r$. Since this decay is as slow as that of the Coulomb interaction, the convergence of the lattice sums will be slow. Therefore, for correct calculation of the piezoelectric correction to the energy of a Wigner crystal one must use a method of rapidly convergent sums, modified to take into account the anisotropy of the interaction.

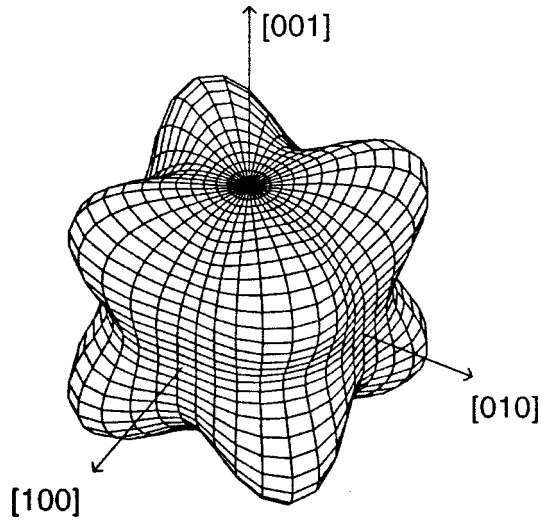


FIG. 1. Anisotropy of the piezoelectric interaction between electrons in the GaAs crystal.

Consider a bilayer electron system placed in an infinite piezoelectric medium and oriented normal to some crystalline direction. In this case it is convenient to make a change of variable in Eq. (9) to the new angles $\Theta$ and $\psi$, measured from the normal to the surface of the electron layer and from an axis lying in the plane of the layer, respectively (the overall structure of expression (9) is preserved — only the values of the expansion coefficients are changed). If the structure of the electron crystal is assumed fixed, then its orientation is determined by the contribution of the terms in (9) which depend on the angle $\psi_{\mathbf{r}}$ in the chosen reference frame. The latter correspond to harmonics with $m \neq 0$. For calculating the lattice sums we rewrite the dependence of the $\psi_{\mathbf{r}}$-dependent part of the interaction between electrons in the form

$$V_{\mathrm{an}}(r,\Theta_{\mathbf{r}},\psi_{\mathbf{r}}) = -\frac{e^2\chi}{\varepsilon r}\sum_{l\geqslant 0}\sum_{|m|>0} B_{lm}\cos^l\Theta_{\mathbf{r}}\sin^{|m|}\Theta_{\mathbf{r}}\mathrm{e}^{im\psi_{\mathbf{r}}}. \tag{10}$$

Using the explicit form of the spherical harmonics, we can express the coefficients $B_{lm}$ in terms of the coefficients $A_{nm}$. Since the index $n$ in Eqs. (7) and (9) takes on only even values, the coefficients $B_{lm}$ are nonzero only for $l$ and $m$ having the same parity. If we keep a finite number of spherical harmonics in expansion (9), then the sum in (10) will also contain a finite number of terms. We note that to preserve the point symmetry with respect to the angle $\psi$ when a finite number of harmonics is taken into account, the transformation to the indicated coordinate system should be done in Eq. (4) and then the values of the expansion coefficients in (7) should be found numerically.

Taking Eq. (10) into account, we write the anisotropic contribution to the energy of the electron crystal in the form

$$E_{\mathrm{an}} = E_{\mathrm{an}}^{\mathrm{in}} + E_{\mathrm{an}}^{\mathrm{out}} + E_{\mathrm{an}}^{BG}, \tag{11}$$

where

$$E_{\mathrm{an}}^{\mathrm{in}} = -\frac{e^2\chi}{\varepsilon}\sum_{|m|>0} B_{0m}\sum_{\mathbf{R}\neq\mathbf{R}'}\frac{1}{|\mathbf{R}-\mathbf{R}'|}\mathrm{e}^{im\psi_{\mathbf{R}'-\mathbf{R}}} \tag{12}$$

corresponds to the contribution of the interaction within the layers,

$$E_{\mathrm{an}}^{\mathrm{out}} = -\frac{e^2\chi}{\varepsilon}\sum_{l\geqslant 0}\sum_{|m|>0} B_{lm} \times \sum_{\mathbf{R},\mathbf{R}'}\frac{d^l|\mathbf{R}-\mathbf{R}'-\mathbf{c}|^{|m|}}{[|\mathbf{R}-\mathbf{R}'-\mathbf{c}|^2+d^2]^{(|m|+l+1)/2}}\mathrm{e}^{im\psi_{\mathbf{R}'+\mathbf{c}-\mathbf{R}}} \tag{13}$$

describes the contribution of the interlayer interaction, and $E_{\mathrm{an}}^{BG}$ gives the correction to the interaction with the positive neutralizing background. The vectors $\mathbf{R}$ and $\mathbf{R}'$ in Eqs. (12) and (13) are lattice vectors, and the vector $\mathbf{c}$ specifies the displacement of the upper sublattice relative to the lower. The lattice sums in (12) and (13) can be reduced to a rapidly convergent form with the use of a modified version of Ewald's method (see Appendix). Employing this method gives

$$E_{\mathrm{an}} = -\frac{Ne^2\chi}{\varepsilon}\sqrt{n}(S_{\mathrm{in}}+S_{\mathrm{out}}), \tag{14}$$

where $N$ is the total number of particles in the layer, and

$$S_{\mathrm{in}} = \sum_m B_{0m}\left\{\sum_{\mathbf{R}\neq 0}\mathrm{e}^{im\psi_{\mathbf{R}}}\Phi(m,\pi nR^2) + i^{|m|}\sum_{\mathbf{G}\neq 0}\mathrm{e}^{im\psi_{\mathbf{G}}}\Phi\left(m,\frac{G^2}{4\pi n}\right)\right\}, \tag{15}$$

$$S_{\mathrm{out}} = \sum_{lm} B_{lm}\left\{\sum_{\mathbf{R}}\frac{d^l|\mathbf{R}+\mathbf{c}|^{|m|}}{[|\mathbf{R}+\mathbf{c}|^2+d^2]^{(|m|+l)/2}} \times \mathrm{e}^{im\psi_{\mathbf{R}+\mathbf{c}}}\Phi(l+|m|,\pi n[|\mathbf{R}+\mathbf{c}|^2+d^2]) + i^{|m|}\sum_{\mathbf{G}\neq 0}\mathrm{e}^{-i\mathbf{G}\cdot\mathbf{c}+im\psi_{\mathbf{G}}}\Psi\left(l,m,\frac{G^2}{4\pi n},\pi nd^2\right)\right\}, \tag{16}$$

where $\mathbf{G}$ are reciprocal lattice vectors. In Eqs. (15) and (16) we have introduced the functions

$$\Phi(m,x) = \sqrt{\pi/x}\frac{\Gamma[(|m|+1)/2,x]}{\Gamma[(|m|+1)/2]}, \tag{17}$$

$$\Psi(l,m,x,y) = \frac{1}{2}\sqrt{\pi/x}\frac{1}{\Gamma[(l+|m|+1)/2]} \times \sum_{s=0}^{N(l,m)} C_{N(l,m)+s}^{2s}(xy)^{(|m|+l-2s)/4} \times [\mathrm{e}^{-2\sqrt{xy}}F(s,\sqrt{x}-\sqrt{y}) + (-1)^{(l+|m|-2s)/2}\mathrm{e}^{2\sqrt{xy}}F(s,\sqrt{x}+\sqrt{y})]. \tag{18}$$

In Eq. (18) the $C_i^j$ are binomial coefficients, $N(l,m) = \max[(|m|-l)/2,(l-|m|-2)/2]$, and

$$F(s,z) = \Gamma(s+1/2) - \mathrm{sgn}(z)\,\gamma(s+1/2,z^2). \tag{19}$$

In Eqs. (17)–(19) $\Gamma(x)$ is the gamma function, and $\Gamma(k,x)$ and $\gamma(k,x)$ are incomplete gamma functions. We note that for $l,m$ equal to zero (these terms have not been taken into

TABLE I. Structure parameters of bilayer Wigner crystals.

| Type of lattice | Primitive vectors of the direct lattice | | Primitive vectors of the reciprocal lattice | | Displacement vector of the sublattices in adjacent layers | Variable parameter | Electron density |
|---|---|---|---|---|---|---|---|
| | $\mathbf{R}_1$ | $\mathbf{R}_2$ | $\mathbf{G}_1$ | $\mathbf{G}_2$ | $\mathbf{c}$ | | |
| Simple hexagonal | $(a, 0)$ | $(0, \sqrt{3}a)$ | $(2\pi/a, 0)$ | $(0, 2\pi/a\sqrt{3})$ | $a/2\ (1, \sqrt{3})$ | – | $1/a^2\sqrt{3}$ |
| Rectangular | $(a, 0)$ | $(0, a\delta)$ | $(2\pi/a, 0)$ | $(0, 2\pi/a\delta)$ | $a/2\ (1, \delta)$ | $1<\delta<\sqrt{3}$ | $1/a^2\delta$ |
| Square | $(a, 0)$ | $(0, a)$ | $(2\pi/a, 0)$ | $(0, 2\pi/a)$ | $a/2\ (1, 1)$ | – | $1/a^2$ |
| Rhombic | $(a, 0)$ | $a(\cos\alpha, \sin\alpha)$ | $\frac{2\pi}{a}(1, -\cot\alpha)$ | $\left(0, \frac{2\pi}{a\sin\alpha}\right)$ | $\frac{a}{2}(1+\cos\alpha, \sin\alpha)$ | $\frac{\pi}{3}<\alpha<\frac{\pi}{2}$ | $\frac{1}{a^2\sin\alpha}$ |
| Double hexagonal | $(a, 0)$ | $(a/2, a\sqrt{3}/2)$ | $\frac{2\pi}{a}(1, -1/\sqrt{3})$ | $(0, 4\pi/a\sqrt{3})$ | $a/2(1, 1/\sqrt{3})$ | – | $2/a^2\sqrt{3}$ |

account, since they give a direction-independent contribution to the Coulomb interaction) the sums (15) and (16) reduce to the known expressions for the isotropic case.[7,8]

## 3. ORIENTATION OF A BILAYER WIGNER CRYSTAL IN A GaAs MATRIX

Let us use the results of the previous Section to determine the orientation of bilayer Wigner crystals lying in the planes (001), $(0-11)$, and (111) in the GaAs matrix. In describing the piezoelectric interaction with allowance for anisotropy of the elastic constants, we keep in expansion (7) only the harmonics with $n \leqslant 18$ and $|m| \leqslant 12$. We note that in the cases considered below, harmonics with $n > 6$ only influence the orientation of hexagonal structures in layers parallel to the (001) plane and that of square structures in layers parallel to the (111) plane. In these cases the symmetry of the system leads to the vanishing of the contribution of the lower harmonics to the energy of the Wigner crystal.

The structure of a Wigner crystal in a bilayer system is specified by the primitive lattice vectors $\mathbf{R}_1$ and $\mathbf{R}_2$ and the vector $\mathbf{c}$ of the relative displacement of the sublattices in adjacent layers. The values of these vectors for the five types of lattice considered are listed in Table I. The values of $\eta$ for which the change of lattice symmetry occurs were obtained in Ref. 8. Since we will have need of the functions $\delta(\eta)$ (for a rectangular lattice) and $\alpha(\eta)$ (for a rhombic lattice), we have repeated the calculations of Ref. 8. According to the results of these calculations, the transition between the rectangular and square phases occurs at $\eta \approx 0.263$, that between the square and rhombic phases at $\eta \approx 0.621$, and that between the rhombic and double hexagonal at $\eta \approx 0.732$. The first two are second-order transitions, and the last is first-order. These results reproduce those of Ref. 8. (We will not analyze the transition between the simple hexagonal and rectangular phases, which, according to Ref. 8, occurs at $\eta = 0.006$, since at this transition the orientation of the electron crystal changes only slightly.)

The anisotropic contribution to the energy of a bilayer electron crystal as a function of its orientation in the (001), $(0-11)$, and (111) planes is shown in Figs. 2, 3, and 4 for various values of the parameter $\eta$ (the energy is given as the energy per electron in units of $e^2\chi\sqrt{n}/2\varepsilon$).

For a two-dimensional Wigner crystal lying in the (001) plane, the anisotropic contribution to the energy of the

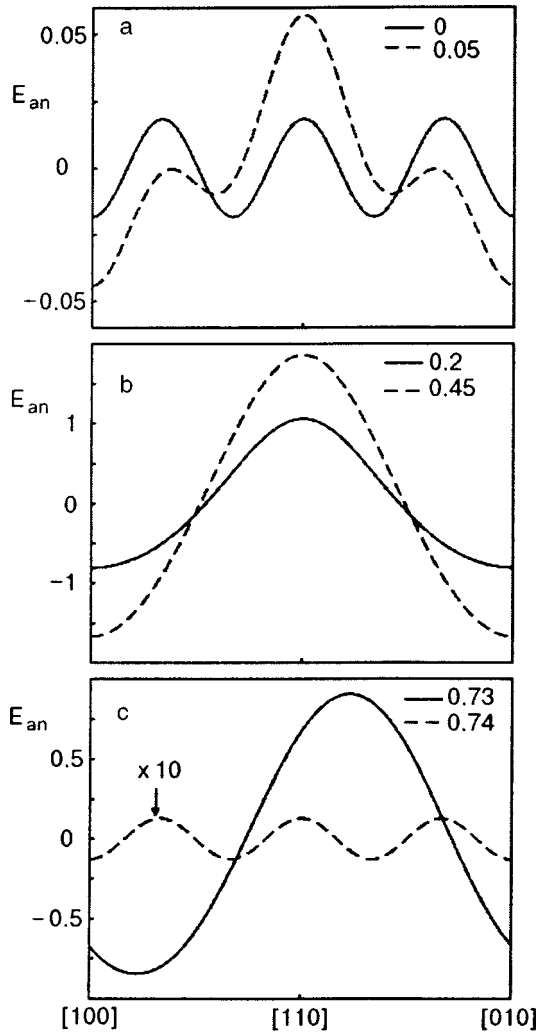


FIG. 2. Dependence of the anisotropic part of the piezoelectric contribution to the energy of a bilayer Wigner crystal in the (001) plane on the direction of $\mathbf{R}_1$; the energy is given as the energy per electron in units of $e^2\chi\sqrt{n}/2\varepsilon$ for various values of the parameter $\eta$: the simple hexagonal lattice and the rectangular lattice at small $\eta$ (a); the rectangular lattice at large $\eta$ and the square lattice (b); the rhombic and double hexagonal lattices near the point of the first-order transition (c).

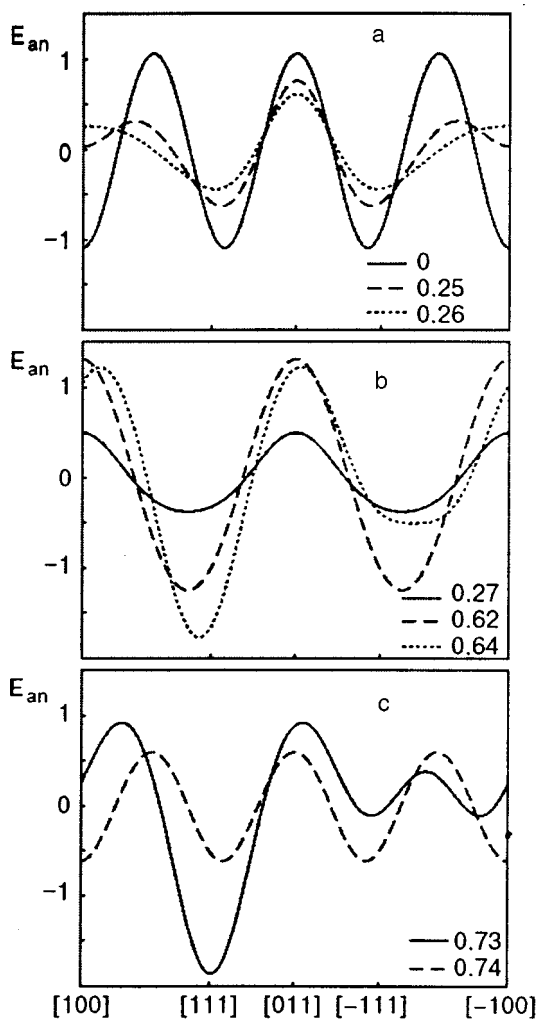


FIG. 3. Dependence of the anisotropic part of the energy of a Wigner crystal in the plane (0–11) on the direction of $\mathbf{R}_1$ for different $\eta$: the simple hexagonal and rectangular lattices (a); the square lattice and the rhombic lattice near the point of the second-order transition (b), the rhombic and double hexagonal lattices near the first-order transition (c).

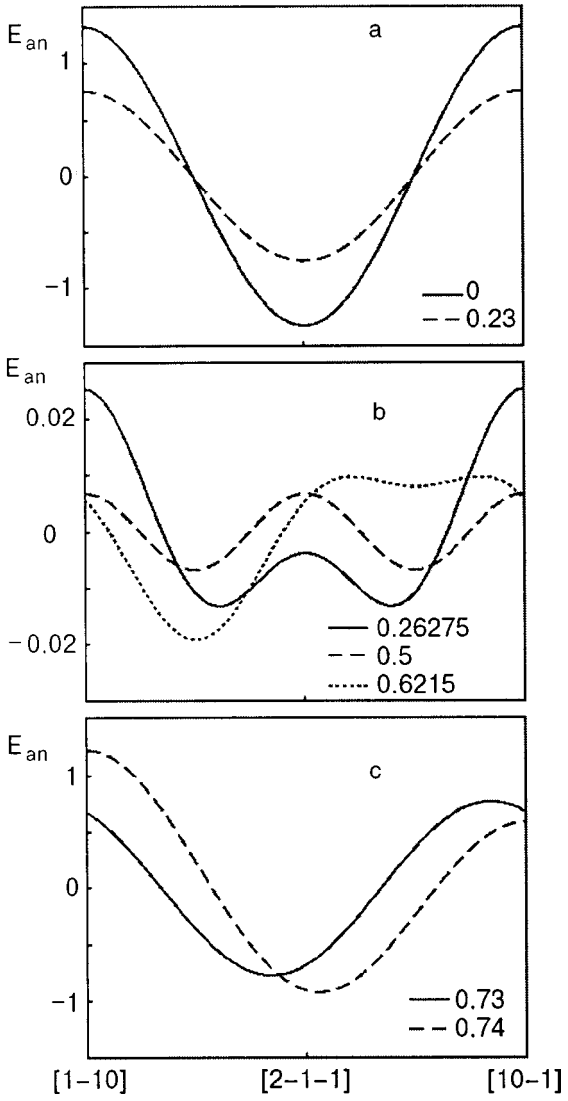


FIG. 4. Dependence of the anisotropic part of the energy of a Wigner crystal in the (111) plane on the direction of $\mathbf{R}_1$ for different $\eta$: the simple hexagonal and rectangular lattices (a); the rectangular and rhombic lattices near the second-order transitions, and the square lattice (b); the rhombic and double hexagonal lattices (c).

simple hexagonal structure does not exceed $2\times10^{-2}$ (in the indicated units). A minimum of the energy is reached at an angle between $\mathbf{R}_1$ and the [100] axis which is a multiple of 30°. The absolute minimum of the energy of the rectangular phase occurs when one of the primitive lattice vectors is directed along the [100] axis. At small $\eta$ there are also local minima corresponding to angles $\beta\approx\pm30°$ between $\mathbf{R}_1$ and one of the fourfold axes. With increasing $\eta$ the local minima vanish, and the anisotropy energy increases substantially. A minimum of the energy of the square phase corresponds to an orientation of the primitive lattice vectors along the fourfold axes. The vector **c** here is oriented along one of the twofold axes. This orientation of the vector **c** is preserved in the rhombic phase as well (the vectors $\mathbf{R}_1$ and $\mathbf{R}_2$ rotate smoothly on changes in $\eta$). The transition to the hexagonal phase as the parameter $\eta$ is increased further is accompanied by a jumplike change in the orientation of the vectors $\mathbf{R}_1$ and **c** and a sharp decrease in the anisotropy energy.

In the case of two-dimensional electron layers parallel to the $(0-11)$ plane, the calculation gives the following results. A minimum of the energy of the hexagonal structures is reached when one of the primitive lattice vectors is oriented along the [100] axis. When the distance between layers is increased and the rectangular structure is formed, there arise two equilibrium orientations, one of which corresponds to a local minimum ($\mathbf{R}_1$ directed along the [100] axis) and the other to a global minimum ($\mathbf{R}_1$ directed at an angle $\beta\approx60°$ to the [100] or [−100] axis). Near the points of transition to the square phase the local minimum vanishes, and a rapid reorientation of the electron lattice occurs. The energy of the square phase is minimum when one of the lattice vectors is directed at an angle $\beta=45°$ to the [100] axis, i.e., to the vector **c**, which is parallel to the [100] or the [011] axis. After the transition to the rhombic phase the direction of the vector **c** parallel to the [011] axis corresponds to the global minimum, while the direction parallel to the [100] axis corresponds to a local minimum. As $\eta$ is increased, the local minimum splits into two, corresponding to a direction of the vector **c** at an angle $\pm\beta$ ($\beta<30°$) to this axis. At the transition to the double hexagonal phase all three minima become equal (the orientation of $\mathbf{R}_1$ changes abruptly at this transition).

In a bilayer structure lying parallel to the (111) plane the minimum of the energy of the simple hexagonal and rectangular phases correspond to a direction of $\mathbf{R}_1$ at an angle $\beta = 30°$ to one of the twofold axes lying in the (111) plane. As the point of transition to the square phase is approached, the anisotropic contribution decreases sharply. A sharp reorientation occurs near the transition point. For the square phase a minimum of the energy is reached when the vector $\mathbf{R}_1$ is directed at an angle $\beta = \pm 15°$ to one of the twofold axes. At the transition to the rhombic phase the anisotropy again increases. The energy of the rhombic phase is minimum in the case when the vector **c** is oriented along one of the twofold axes. At the transition to the double hexagonal phase the orientation of the vector **c** changes abruptly — it deviates somewhat from the twofold axis. We note that in the double hexagonal phase the energetically most favorable orientation of the lattice vectors differs from the case of the simple hexagonal phase. The latter is due to the absence of a center of inversion in the double hexagonal structure.

The results show that the orientation of a bilayer Wigner crystal in a piezoelectric matrix is determined by the plane in which the electron layer is located, the type of electron lattice, and the value of the parameter $\eta$. Interestingly, the abrupt (jumplike) character of the reorientation is observed not only at the transition from the rhombic to the double hexagonal phase (this is the expected effect, since it accompanies a first-order transition). A very rapid reorientation also takes place at the second-order transition from the rectangular to the square phase.

The value of the anisotropy energy is determined by the parameter $\chi$, which in GaAs is of the order of $2\times10^{-4}$. The typical difference between the Coulomb energy in the different phases is of the order of $10^{-2}e^2\sqrt{n}/\varepsilon$ per electron,[7,8] i.e., according to the results reported, the piezoelectric interaction in the system under study is approximately two orders of magnitude smaller; hence, it has a weak influence on the phase diagram and only determines the orientation of the electron crystal. Nevertheless, in other systems in which the value of the piezoelectric modulus is larger, one can expect a radical rearrangement of the phase diagram. Analogous effects for a monolayer system were discussed in Ref. 4. The approach considered in the present paper makes it possible to investigate this possibility in detail for the case of bilayer electron crystals.

## APPENDIX

Let us transform to the rapidly convergent form of the expression

$$S_{\pm m}=\sum_{\mathbf{R}\neq 0}\frac{e^{\pm im\psi_{\mathbf{R}}}}{R}, \tag{A1}$$

where $m>0$. We introduce the function

$$T_{\pm m}(\mathbf{r},\mathbf{q})=e^{-i\mathbf{qr}}\sum_{\mathbf{R}}\frac{e^{i\mathbf{q}\cdot(\mathbf{R}+\mathbf{r})\pm im\psi_{\mathbf{r}+\mathbf{R}}}}{|\mathbf{r}+\mathbf{R}|}-\frac{e^{\pm im\psi_{\mathbf{r}}}}{r} \tag{A2}$$

such that

$$S_{\pm m}=\lim_{\mathbf{r}\to 0,\mathbf{q}\to 0}T_{\pm m}(\mathbf{r},\mathbf{q}). \tag{A3}$$

We use the identity

$$\frac{\gamma[(m+1)/2,x]+\Gamma[(m+1)/2,x]}{\Gamma[(m+1)/2]}\equiv 1. \tag{A4}$$

With allowance for (A4) the quantity $T_{\pm m}$ can be written in the form a sum

$$T_{\pm m}(\mathbf{r},\mathbf{q})=T_{\pm m,1}(\mathbf{r},\mathbf{q})+T_{\pm m,2}(\mathbf{r},\mathbf{q}), \tag{A5}$$

where

$$T_{\pm m,1}(\mathbf{r},\mathbf{q})=\sum_{\mathbf{R}\neq 0}\frac{e^{i\mathbf{q}\cdot\mathbf{R}\pm im\psi_{\mathbf{r}+\mathbf{R}}}}{|\mathbf{r}+\mathbf{R}|}\times\frac{\Gamma[(m+1)/2,\pi n|\mathbf{r}+\mathbf{R}|^2]}{\Gamma[(m+1)/2]}-\frac{e^{\pm im\psi_{\mathbf{r}}}}{r}\frac{\gamma[(m+1)/2,\pi nr^2]}{\Gamma[(m+1)/2]}, \tag{A6}$$

$$T_{\pm m,2}(\mathbf{r},\mathbf{q})=e^{-i\mathbf{q}\cdot\mathbf{r}}\sum_{\mathbf{R}}\frac{e^{i\mathbf{q}\cdot(\mathbf{r}+\mathbf{R})\pm im\psi_{\mathbf{r}+\mathbf{R}}}}{|\mathbf{r}+\mathbf{R}|}\times\frac{\gamma[(m+1)/2,\pi n|\mathbf{r}+\mathbf{R}|^2]}{\Gamma[(m+1)/2]}. \tag{A7}$$

We note that the last term in (A6) vanishes in the limit $\mathbf{r}\to 0$.

For the transformation $T_{\pm m,2}$ we substitute the definition of the function $\gamma(\alpha,x)$ into (A7):

$$T_{\pm m,2}(\mathbf{r},\mathbf{q})=\frac{2}{\Gamma[(m+1)/2]}e^{-i\mathbf{qr}}\int_0^{\sqrt{\pi n}}d\xi\xi^m\sum_{\mathbf{R}}|\mathbf{r}+\mathbf{R}|^m\times\exp[i\mathbf{q}\cdot(\mathbf{r}+\mathbf{R})\pm im\psi_{\mathbf{r}+\mathbf{R}}-\xi^2|\mathbf{r}+\mathbf{R}|^2]. \tag{A8}$$

Expanding (A8) in a Fourier series in the reciprocal lattice vectors, we get

$$T_{\pm m,2}(\mathbf{r},\mathbf{q})=\frac{2n}{\Gamma[(m+1)/2]}\times\sum_{\mathbf{G}}e^{-i(\mathbf{q}+\mathbf{G})\cdot\mathbf{r}}\int_0^{\sqrt{\pi n}}d\xi\xi^m\int d^2\rho\rho^m\times\exp[i\rho\cdot(\mathbf{q}+\mathbf{G})\pm im\psi_\rho-\xi^2\rho^2]. \tag{A9}$$

Evaluating the integral over $\boldsymbol{\rho}$, we find

$$T_{\pm m,2}(\mathbf{r},\mathbf{q})=i^m\frac{2\pi n}{\Gamma[(m+1)/2]}\sum_{\mathbf{G}}e^{-i(\mathbf{q}+\mathbf{G})\cdot\mathbf{r}\pm im\psi_{\mathbf{q}+\mathbf{G}}}\times\left(\frac{|\mathbf{q}+\mathbf{G}|}{2}\right)^m\int_0^{\sqrt{\pi n}}d\xi\frac{1}{\xi^{m+2}}\times\exp\left(-\frac{|\mathbf{q}+\mathbf{G}|^2}{4\xi^2}\right). \tag{A10}$$

Making the change of variables $\xi=|\mathbf{q}+\mathbf{G}|/2t$, we arrive at the form

$$T_{\pm m,2}(\mathbf{r},\mathbf{q})=i^m\frac{2\pi n}{\Gamma[(m+1)/2]}\sum_{\mathbf{G}}e^{-i(\mathbf{q}+\mathbf{G})\cdot\mathbf{r}\pm im\psi_{\mathbf{q}+\mathbf{G}}}\times\frac{1}{|\mathbf{q}+\mathbf{G}|}\Gamma\left(\frac{m+1}{2},\frac{|\mathbf{q}+\mathbf{G}|^2}{4\pi n}\right). \tag{A11}$$

Substituting formulas (A1), (A3), (A7), and (A11) into Eq. (12) and introducing the function (17), we arrive at Eq. (15). The term with $\mathbf{G}=0$ in (A11) drops out, since it cancels with the intralayer interaction with the positive neutralizing background that appears in $E_{\rm an}^{BG}$.

An analogous transformation may be done for the sum

$$S_{l,\pm m}=\sum_{\mathbf{R}}\frac{d^l|\mathbf{R}+\mathbf{c}|^m e^{\pm im\psi_{\mathbf{R}+\mathbf{c}}}}{(|\mathbf{R}+\mathbf{c}|^2+d^2)^{(l+m+1)/2}}. \tag{A12}$$

Here we also use the identity (A4), with $m$ replaced by $m+l$. We get

$$S_{l,\pm m}=T_{l,\pm m,1}(0,0)+\lim_{\mathbf{r}\to 0,\mathbf{q}\to 0}T_{l,\pm m,2}(\mathbf{r},\mathbf{q}), \tag{A13}$$

where

$$T_{l,\pm m,1}(0,0)=\sum_{\mathbf{R}}\frac{d^l|\mathbf{R}+\mathbf{c}|^m e^{\pm im\psi_{\mathbf{R}+\mathbf{c}}}}{(|\mathbf{R}+\mathbf{c}|^2+d^2)^{(l+m+1)/2}} \times\frac{\Gamma[(l+m+1)/2,\pi n(|\mathbf{R}+\mathbf{c}|^2+d^2)]}{\Gamma[(l+m+1)/2]}. \tag{A14}$$

The quantity $T_{l,\pm m,2}(\mathbf{r},\mathbf{q})$, after we change to summation over $\mathbf{G}$ and do the integration over $\boldsymbol{\rho}$, reduces to the form

$$T_{l,\pm m,2}(\mathbf{r},\mathbf{q})=i^m\frac{2\pi n}{\Gamma[(l+m+1)/2]} \times\sum_{\mathbf{G}}\exp[-i\mathbf{G}\cdot\mathbf{c}-i(\mathbf{q}+\mathbf{G})\cdot\mathbf{r}\pm im\psi_{\mathbf{q}+\mathbf{G}}]d^l \times\left(\frac{|\mathbf{q}+\mathbf{G}|}{2}\right)^m\int_0^{\sqrt{\pi n}}d\xi\,\xi^{l-m-2} \times\exp\left(-\xi^2d^2-\frac{|\mathbf{q}+\mathbf{G}|^2}{4\xi^2}\right). \tag{A15}$$

Evaluation of the integral in (A15) gives

$$T_{l,\pm m,2}(\mathbf{r},\mathbf{q})=i^m\frac{\pi n}{\Gamma[(l+m+1)/2]} \times\sum_{\mathbf{G}}e^{-i\mathbf{G}\cdot\mathbf{c}-i(\mathbf{q}+\mathbf{G})\cdot\mathbf{r}\pm im\psi_{\mathbf{q}+\mathbf{G}}} \times\frac{1}{|\mathbf{q}+\mathbf{G}|}\sum_{s=0}^{N(l,m)}C_{N(l,m)+s}^{2s} \times\left(\frac{|\mathbf{q}+\mathbf{G}|d}{2}\right)^{(m+l-2s)/2}\left\{e^{-|\mathbf{q}+\mathbf{G}|d}\left[\Gamma\left(s+\frac{1}{2}\right)-\mathrm{sgn}(f_-)\,\gamma\left(s+\frac{1}{2},f_-^2\right)\right]+(-1)^{(l+m-2s)/2}e^{|\mathbf{q}+\mathbf{G}|d}\Gamma\left(s+\frac{1}{2},f_+^2\right)\right\}, \tag{A16}$$

where

$$f_\pm=\frac{|\mathbf{q}+\mathbf{G}|}{2\sqrt{\pi n}}\pm\sqrt{\pi n}\,d, \tag{A17}$$

$$N(l,m)=\max\left(\frac{m-l}{2},\frac{l-m-2}{2}\right). \tag{A18}$$

In deriving (A16) we took into account that in the problem considered, the parameters $l$ and $m$ have the same parity. The term with $\mathbf{G}=0$ in (A16) is compensated by the interaction with the positive background of the adjacent layer. Using (A13), (A14), and (A16), we can write the contribution of the interlayer interaction in the form (16).

*E-mail: fil@isc.kharkov.com

[1] L. Brey, H. A. Fertig, R. Cote, and A. H. McDonald, Phys. Rev. Lett. **75**, 2562 (1995).
[2] A. A. Koulakov, M. M. Fogler, and B. I. Shklovskii, Phys. Rev. Lett. **76**, 499 (1996); M. M. Fogler, A. A. Koulakov, and B. I. Shklovskii, Phys. Rev. B **54**, 1853 (1996).
[3] M. P. Lilly, K. B. Cooper, J. P. Eisenstein, L. N. Pfeiffer, and K. W. West, Phys. Rev. Lett. **82**, 394 (1999); R. R. Du, D. C. Tsui, H. L. Stormer, L. N. Pfeiffer, and K. W. West, Solid State Commun. **109**, 389 (1999).
[4] É. I. Rashba and E. Ya. Sherman, Fiz. Tekh. Poluprovodn. **21**, 1957 (1987) [Sov. Phys. Semicond. **21**, 1185 (1987)].
[5] E. Ya. Sherman, Phys. Rev. B **52**, 1512 (1995).
[6] D. V. Fil, Fiz. Nizk. Temp. **26**, 792 (2000) [Low Temp. Phys. **26**, 581 (2000)].
[7] L. Bonsall and A. A. Maradudin, Phys. Rev. B **15**, 1959 (1977).
[8] G. Goldoni and F. M. Peeters, Phys. Rev. B **53**, 4591 (1996).
[9] I. V. Schweigert, V. A. Schweigert, and F. M. Peeters, Phys. Rev. Lett. **82**, 5293 (1999).
[10] I. V. Schweigert, V. A. Schweigert, and F. M. Peeters, Phys. Rev. B **60**, 14665 (1999).
[11] L. Zheng and H. A. Fertig, Phys. Rev. B **52**, 12282 (1995).
[12] S. Narasimhan and T. L. Ho, Phys. Rev. B **52**, 12291 (1995).
[13] Yu. M. Vil'k and Yu. P. Monarkha, Fiz. Nizk. Temp. **10**, 886 (1984) [Sov. J. Low Temp. Phys. **10**, 469 (1984)].
[14] Yu. M. Vil'k and Yu. P. Monarkha, Fiz. Nizk. Temp. **11**, 971 (1985) [Sov. J. Low Temp. Phys. **11**, 535 (1985)].

Translated by Steve Torstveit

## PHYSICAL PROPERTIES OF CRYOCRYSTALS

# X-ray studies of phase transitions in solid oxygen

A. I. Prokhvatilov,[a] N. N. Galtsov, and A. V. Raenko

*B. Verkin Institute for Low Temperature Physics and Engineering, National Academy of Sciences of Ukraine, pr. Lenina 47, 61103 Kharkov, Ukraine*

(Submitted December 28, 2000)
Fiz. Nizk. Temp. **27**, 532–538 (May 2001)

X-ray studies of the phase composition, lattice parameters, and molar volumes are carried out at the phase transitions in solid oxygen. In the region of the low-temperature transition a two-phase state is observed in a region having a width of 2 K on cooling of the samples and less than 0.8 K on heating. The width of the temperature hysteresis and the jump in volume at the transition are determined. The mean value of the volume jump is $\sim 0.5 \pm 0.2\%$. The structural characteristics found are convincing evidence that the low-temperature magnetic transformation in solid oxygen, like the high-temperature orientational transition, is a first-order transition. It is shown that at relatively high rates of passage through the $\beta - \gamma$ transition, owing to the significant jump in volume and the high stress level, it is possible to supercool the $\gamma$ phase down to helium temperature and to superheat the intermediate $\beta$ phase almost to the melting temperature. © *2001 American Institute of Physics.* [DOI: 10.1063/1.1374726]

### INTRODUCTION

Two phase transitions at the equilibrium vapor pressure occur in solid oxygen below the melting temperature: a high-temperature phase transition $\gamma \rightarrow \beta$ at $T = 43.80$ K, and a transition $\beta \rightarrow \alpha$ at $T = 23.88$ K.[1,2] The first of these transitions is accompanied by an increase in the degree of orientational order of the molecules and a lowering of the symmetry from the partially ordered cubic structure $Pm3n$ to the rhombohedral structure $R\bar{3}m$ with a collinear arrangement of molecules parallel to the threefold axis of the lattice. Here the volume change of the lattice reaches 5.4%. The $\beta - \alpha$ transition occurs without a change of the orientational structure, but an ordering of the magnetic moments of the molecules in the crystal occurs and an antiferromagnetic quasi-two-dimensional monoclinic phase of symmetry $C2/m$ is formed.[1,3–5]

Until recently the order of the $\alpha - \beta$ phase transition had not been conclusively determined. Like the magnetic transformations in classical magnets such as $KMnF_4$, this transition can be classified as second-order. Evidence for this is provided by the experimental data showing almost no volume jump at the transition,[1] the temperature behavior of the magnon frequency,[6] the presence of the λ anomaly in the specific heat, and the absence of hysteresis effects in the low-temperature transition region.[7] However, there is also some serious evidence contradicting this view and favoring a first-order classification. According to estimates,[8–11] this transition is accompanied by a change in density of up to 0.5%, characteristic anomalies of the anisotropy of the magnetic susceptibility,[12] hysteresis effects in neutron scattering[13] and in the specific heat,[14–16] a small latent heat of transition,[17–19] and, as has been revealed by x-ray[20] and spectroscopic[21] measurements, the existence of a two-phase region. The authors of some theoretical papers[22–24] are also inclined toward the opinion that the $\alpha - \beta$ phase transformation in oxygen is a first-order transition.

The contradictory results listed above and the absence of detailed structural diffraction data for solid oxygen, particularly in the region of the low-temperature phase transition, was our main motivation for making a detailed study of the features of the behavior of the structural characteristics of solid oxygen and how they are affected by the thermal prehistory of the samples and the rate of change of the temperature in the single-phase regions and at the high-temperature transition. We also studied the possibility of supercooling of the high-temperature cubic phase and superheating of the intermediate rhombohedral phase at the high-temperature transition, which is accompanied by a significant jump in volume. The results of these studies were reported briefly in the materials of an international conference.[25] In the present paper they are set forth in more detail, with a discussion of all the currently available information about the questions touched on in this paper, and some additional facts are reported.

### EXPERIMENTAL PROCEDURE

Studies were done by an x-ray method (using the $K_\alpha$ radiation of the Fe anode) on polycrystalline samples of better than 99.99% pure $O_2$. A DRON-3M diffractometer was used, with personal-computer-based automated modes of operation and collection of the diffraction data. The samples were obtained by condensation from the gas phase on a flat copper substrate in the vacuum-tight chamber of a special cryostat[26] mounted on the goniometric unit of the diffractometer. The condensation temperature was 30 K. The polycrystalline samples obtained (grain size $\sim 10^{-4}$ mm) were annealed without any visible change of the substructure as the temperature was raised to 40–42 K with a hold of 20–30

 

min. After the annealing, the temperature of the samples was decreased to 25 K and, with a step of 0.1–0.2 K, was passed through the $\beta-\alpha$ transition to the temperature at which the phase transformation was completed ($T\sim 22$ K); diffractograms were recorded at each point, and then the same procedure was followed with the temperature points hit in reverse order. The time between the recording of the diffractograms at adjacent temperature points was 20–25 min, and it took 2–3 hours to pass through the phase transition in one direction. The cooling of the $\gamma$ phase and heating of the $\beta$ phase in the region of the high-temperature transition were done at the highest rate possible in our experiments, 10 deg/min. The temperature was stabilized to within $\pm 0.05$ K during the recording of the diffractograms at the different points. The error of measurement of the lattice parameters was not over $\pm 0.02\%$.

## RESULTS AND DISCUSSION

This study confirms the previous observation[20] of a two-phase state of solid oxygen in the region of the low-temperature phase transformation. Figure 1 shows x-ray diffractograms which clearly illustrate the presence of the $\alpha$ and $\beta$ phases in the region $T_{\alpha-\beta}$. We see that as the temperature is lowered at $T<T_{\alpha-\beta}=23.88$ K, the reflections from the intermediate $\beta$ phase remain along with the newly appearing reflections from the $\alpha$ phase. At the successively lower temperature steps there occurs a redistribution of the intensities, with the reflections from the $\alpha$ phase, which is stable at these temperatures, becoming stronger and the diffractions from the supercooled $\beta$ phase becoming weaker and then vanishing completely. Subsequently increasing the temperature of the samples to above $T_{\alpha-\beta}$ reveals a superheating of a certain part of the $\alpha$ phase, but in a notably narrower temperature interval than for the supercooling of the intermediate $\beta$ phase (see Fig. 1b). A 2-hour hold at a fixed temperature in the region of the two-phase state did not have any effect, and so the observed two-phase state is relatively stable. According to the data of Ref. 21, 11-hour holds in the two-phase region at 23.5 K result in a change of the phase composition of the samples by only 3%. The constancy of the phase composition over relatively long periods of time also serves as indirect evidence of the absence of appreciable temperature gradients in the samples, which if present might have been responsible for the existence of two phases in the sample in the phase transition region. Temperature gradients have largely been eliminated in our experiments by the technique used to prepare the samples and by the design features of the experimental cell and cryostat. Condensation of the substance from the gas phase can produce fine-grained snowlike samples up to 0.1 mm thick. The samples are formed on a flat substrate, a massive copper block surrounded by helium and nitrogen heat shields.

According to the data obtained in the present study, the supercooling of the $\beta$ phase on average can reach 1–2 K, while the superheating of the $\alpha$ phase reaches 0.4–0.8 K. Here it must be kept in mind that in the present case, when we talk of the superheating or supercooling of a phase we are not referring to the hysteresis of the phase transition temperature but to regions of coexistence of two phases. In this connection it should be mentioned that in previous studies of

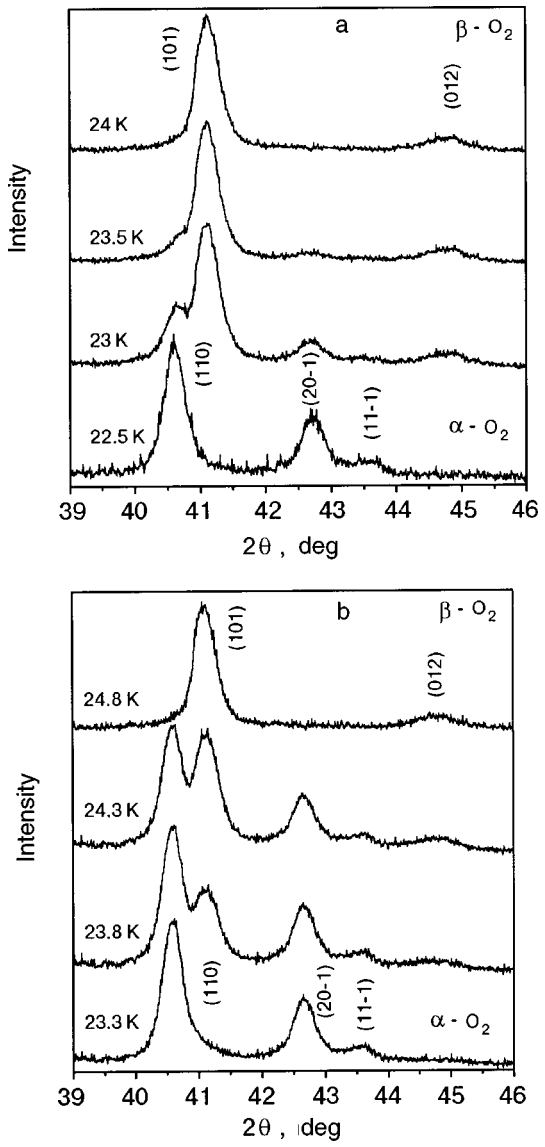


FIG. 1. Initial part of the x-ray diffractograms of polycrystalline oxygen, obtained as the temperature was lowered from the existence region of the $\beta$ phase to that of the $\alpha$ phase (a) and as the temperature was raised from the existence region of the $\alpha$ phase to that of the $\beta$ phase (b). The diffractograms for different temperatures are shifted relative to one another along the intensity axis by a constant amount.

solid oxygen[20] the two-phase region was indicated as 23.5–24.5 K. In addition, the authors of Ref. 20 were unable to establish hysteresis of the phase transition temperature at a limit of 0.3 K (the temperature step used). In the present study, with one-third as large a temperature step (0.1 K), we were also unable to detect a shift of the temperature of the start of the phase transformation $T_{\alpha-\beta}=23.88$ K on heating, but in practically all of the experiments on cooling the phase transformation usually started 0.2–0.3 K below $T_{\alpha-\beta}$. Curiously, analogous behavior of the characteristics of the orientational $\alpha-\beta$ phase transformation, down to even their absolute values, has been observed in solid nitrogen[27] during passage through $T_{\alpha-\beta}$ on heating and cooling. The large spread in values of the hysteresis and two-phase regions for oxygen indicated above reflect the real situation and are apparently determined by the high sensitivity of the low-temperature $\alpha-\beta$ transition to a number of factors preceding

the measurements — slight differences in the conditions during condensation and annealing of surface samples, in the rates of cooling the samples from the $\gamma$ phase, in the rates of change of the temperature from one step to another, etc. We therefore were unable to achieve better reproducibility of the values of the temperature hysteresis and two-phase coexistence region than is indicated above. These factors must also be taken into account in a comparison of the results of different studies, although in that case there is an important additional factor — the purity of the samples.

In connection with the problems of the temperature hysteresis and two-phase state of solid oxygen discussed above, it is of interest to examine our results against the background of published data obtained by other methods. The most detailed study of these questions has been done by the method of FTIR spectroscopy, which was used to investigate the behavior of the vibrational frequencies and the fundamental absorption bands of isolated CO impurity molecules and of the oxygen host matrix at the $\alpha-\beta$ transition.[21] The impurity concentration in the samples was quite low: $CO/O_2=4\times10^{-8}$. Those experiments established the presence of hysteresis of the transition temperature at a limit of 0.15 K and in, approximately the same interval, a coexistence region of the $\alpha$ and $\beta$ phases of oxygen. It was noted that the temperatures of the phase transition on cooling and heating are equal to 23.85 K and 24 K, respectively. The reproducibility of these values for a series of samples was not worse than 0.1 K. In spectroscopic studies of the pure matrix on the same samples, it was established that the phase transition occurs on heating in the region 23.85–23.9 K and on cooling in the region 23.80–23.75 K. Consequently, in comparison with our data, considerably smaller values of the temperature hysteresis and two-phase coexistence region were obtained in Ref. 21. On the other hand, in previous x-ray,[20] neutron diffraction,[13] and calorimetric[14,15] studies the values obtained for the temperature hysteresis and two-phase regions at $T_{\alpha-\beta}$ are close to those given in the present paper. The discrepancy in the characteristics of the low-temperature transition in different papers may be due to the quantity and type of impurities, to structural defects, and to different levels of stress in the samples. In this connection we mention the special studies in Ref. 21 of the influence of CO impurity molecules on the phase transitions in oxygen. It was found that the presence of CO molecules in an amount $(3-4)\times10^{-7}$ causes appreciable (up to 0.6 K) widening of the two-phase region, and the transition occurs in the interval 23.9–23.3 K. Such a strong impurity effect was attributed, with justification, to the features of the $O_2$–CO phase diagram and to the possible presence of a triple eutectoid point in the given binary system below $T_{\alpha-\beta}$.

The simultaneous presence of reflections of $\alpha$- and $\beta$-$O_2$ made it possible to determine with relatively good accuracy ($\pm0.1\%$) the difference of the phase volumes in the temperature interval of phase coexistence and at the point of the phase transformation without recourse to the methods of high-accuracy precision measurements of the lattice parameters. Figure 2 shows our results on the molecular volumes of the intermediate and low-temperature phases of solid oxygen on cooling and heating near $T_{\alpha-\beta}$. Also shown are some previously obtained data[1] on the temperature dependence of the molar volume of oxygen in the region of the low-temperature transition. According to the data of the present study, the low-temperature magnetostructural transformation in oxygen is accompanied by a volume jump of $\sim0.1\pm0.04$ cm$^3$/mole. This value of $\Delta V$ is in satisfactory agreement with earlier estimates[10,19] of the volume jump at the $\alpha-\beta$ transition, based on studies of the specific heat and compressibility (0.117 cm$^3$/mole), the structure parameters (0.12 cm$^3$/mole),[8] and the magnetic susceptibility under pressure (0.135 cm$^3$/mole$\pm10\%$)[28] and on an analysis of a large set of data in Ref. 11 ($0.13\pm0.11$ cm$^3$/mole). However, our value differs considerably from the estimates based on previous x-ray studies [0.49 cm$^3$/mole (Ref. 9) and $<0.05$ cm$^3$/mole (Ref. 1)].

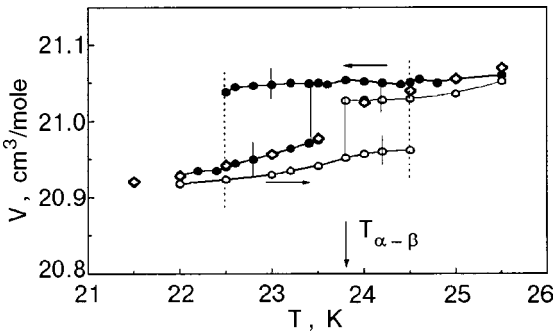


FIG. 2. Temperature dependence of the molar volume of solid oxygen in the region of the low-temperature $\alpha-\beta$ phase transition on cooling (●) and heating (○); ◇ — data of Ref. 1.

In numerous calorimetric measurements[7,11,15–19,29–34] attempts have been made to estimate or determine the heat of the $\alpha-\beta$ transition. The values of the heat of transition obtained in the different studies fluctuates over wide limits. The majority of the values found lie in the interval from 17.5 cal/mole (Ref. 29) to 24 cal/mole (Ref. 18). At the same time, according to the data of Ref. 34 the heat of transition is extremely small, not over 2.4 cal/mole, whereas, according to the results of Refs. 7 and 33, the specific heat of oxygen has a $\lambda$-type anomaly in the $\alpha-\beta$ transition region and the transition is not accompanied by heat loss. Using the average heat of transition according to the data of Ref. 2 (21.49 cal/mole) and the value of the change of the phase transition temperature with applied pressure, $dP/dT=333$ bar/K,[10,35] we have estimated the value of the volume jump with the Clausius–Clapeyron formula: $\Delta V=0.114$ cm$^3$/mole, which (with allowance for the possible errors in the calculation) agrees satisfactorily with the data of direct measurements given above.

Thus in this paper we have obtained convincing direct structural evidence (volume jump, hysteresis effects, two-phase coexistence region) in support of the previously stated opinion[14,20,21] that the low-temperature phase transition in solid oxygen is a first-order structural transformation. The character of this transition and its structural characteristics are determined by the features of the intermolecular interaction and the appreciable magnetostriction effect. The latter gives rise to interphase elastic stresses that change the order of the transition and promote ''wedging'' of the phases upon passage through the phase transition point, and the value of the temperature hysteresis and the width of the existence

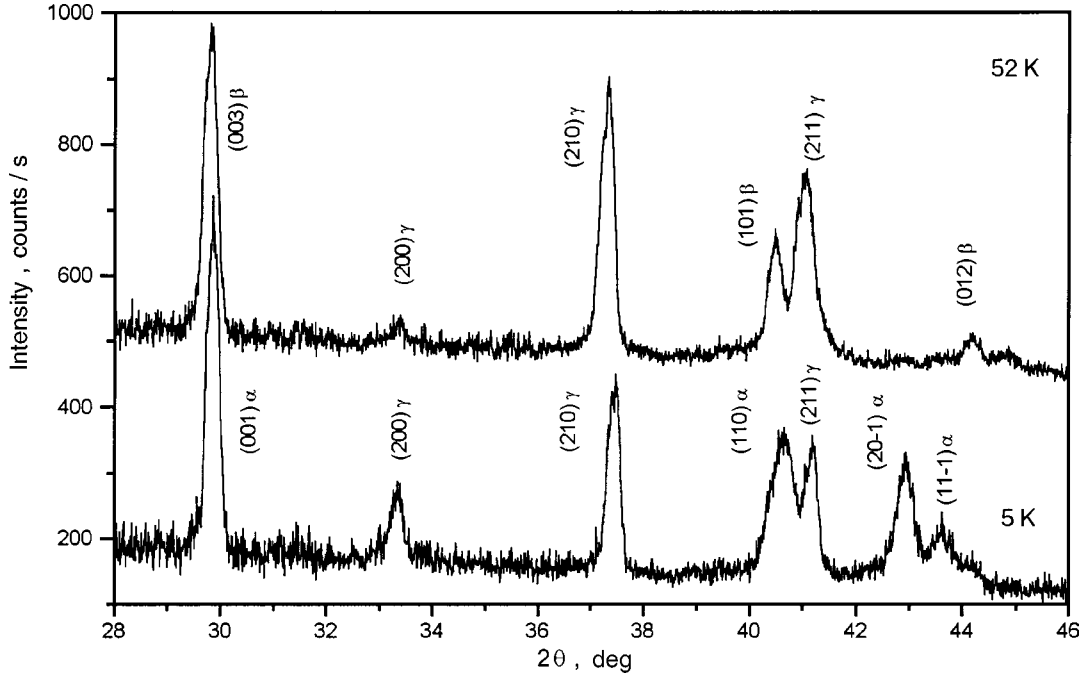


FIG. 3. X-ray diffractograms illustrating the supercooling of the $\gamma$ phase to helium temperature and the superheating of the $\beta$ phase to pre-melting temperatures. The diffractograms obtained at different temperatures are shifted relative to each other along the intensity axis by a constant amount (300 counts/s).

region of the two-phase state depend on the level of stresses and relaxation processes.

Careful and detailed studies in the region of $T_{\alpha-\beta}$ are needed not only for establishing the order of the transition and determining its structural characteristics but also in connection with another question that requires an experimental check. According to some theoretical papers,[36–38] the transition from the low-temperature two-sublattice phase with a quasi-two-dimensional antiferromagnetic ordering of the molecular spins to the intermediate three-sublattice phase with short-range magnetic order should come about through an intermediate phase with helicoidal ordering of the magnetic moments. Therefore, another task of the present structural studies was to observe the intermediate phase predicted by the theory. However, in spite of a careful temperature scanning through the region of the $\alpha-\beta$ phase transition, no intermediate magnetic phase was observed.

The high-temperature orientational phase transition $\beta-\gamma$ in oxygen is a first-order transition, but with a substantially (almost an order of magnitude) larger volume change (1.19 $cm^3$/mole)[1] than at the low-temperature transition. Consequently, appreciable interphase elastic strains should arise in the samples at the phase transition. Here, however, it should be taken into account that this transition occurs at rather high temperatures, where the relaxation processes are substantially less sluggish. Because of this, the hysteresis effects at the transition can be smoothed out considerably, especially at low rates of temperature scanning. We have done studies of the possibility of obtaining metastable states on passage through the region of the high-temperature transition at a high scanning rate. As a result, we have found that at the highest rates of cooling under our experimental conditions ($>10$ deg/min) the high-temperature $\gamma$ phase can be supercooled all the way down to helium temperature. A typical x-ray diffractogram for these samples is shown in Fig. 3. In addition to the monoclinic $\alpha$ phase, which is stable in this temperature region, an appreciable content of cubic crystals of the $\gamma$ phase was observed in the samples. On the reverse temperature path through the inverse transition the amount of the supercooled phase decreased with time only for $T>25$ K, in the existence region of the $\beta$ phase. One-hour holds at these temperatures led to the complete transition of the $\gamma$ phase to the equilibrium $\beta$ phase. On rapid heating of the samples through the $\beta-\gamma$ transition at approximately the same rates as for the cooling, an appreciable fraction of the crystals of the intermediate $\beta$ phase were usually preserved all the way up to pre-melting temperatures (see Fig. 3). One-hour holds at 52 K did not lead to the complete vanishing of the reflections from the $\beta$-$O_2$ crystals.

There is another curious fact in connection with the passage through the high-temperature transition and the existence region of the intermediate phase. Even at a relatively slow rate of cooling (2–3 deg/min) from the existence region of the $\gamma$ phase to helium temperatures, in a number of cases reflections attributable to the so-called $\alpha'$ phase[39,40] were observed in addition to those from the equilibrium $\alpha$ and $\beta$ phases. This new phase was preserved without visible changes on subsequent heating all the way up to the transition to $\gamma$-$O_2$. Consequently, the formation of the $\alpha'$ phase in solid oxygen is due not only to the presence of molecular impurities in the samples[40] but apparently also to the presence of relatively large interphase stresses arising in the samples after the phase transition, which is accompanied by an appreciable jump in volume. It should be noted, however, that at the cooling rates indicated above, we did not achieve any noticeable supercooling of the high-temperature phase.

We conclude with the following remarks. Despite the recent direct experimental evidence in favor of a first-order

transition, the question of the heat of transition is still not conclusively resolved. Accounting for the significant discrepancies in the results of different investigators will require additional high-precision calorimetric measurements in the $T_{\alpha-\beta}$ region; that should provide a conclusive answer to this question.

The fact that the high-temperature $\gamma$ phase can be supercooled to helium temperatures lends interest to the study of its magnetic and thermodynamic properties as well. At faster rates of cooling than the highest achieved in this study it is entirely possible that the $\gamma$ phase will be frozen in throughout the entire volume of the sample. The structure and dynamics of the lattice in such a phase should differ from the equilibrium ones at high temperatures. The oxygen molecules in the two sublattices (the spherically disordered and plane-disordered sublattices of the equilibrium $\gamma$ phase) are frozen into *n*-fold degenerate orientational states, in which case a state of the orientational glass type will most likely form. For describing the orientational structure formed in this case, the most suitable model, it seems to us, is that of the static disordering of the molecules in the $\gamma$-$O_2$ lattice, which was proposed earlier[41] on the basis of an analysis of the neutron diffraction studies. It should be noted that supercooled $\gamma$-$O_2$ provides a unique opportunity to study the properties of an orientational glass in a pure cryocrystal, undiluted by a spherically symmetric impurity. Orientational glasses are ordinarily formed in supercooled phases of binary solutions of molecular cryocrystals, one of whose components is an inert element.[42] Such systems contain significant displacement strain fields due to the difference of the molecular parameters of the components. In the case under discussion it is not necessary to take this circumstance into account in the data analysis because there are no concentrated local displacements in supercooled $\gamma$-$O_2$ crystals. One can get an idea of the transformation of the orientational subsystem of $\gamma$-$O_2$ upon its supercooling from the behavior of the high-pressure phase $\delta$-$N_2$, which is isomorphic to it. Isobaric cooling of this phase leads to a transition $\delta \rightarrow \varepsilon$, accompanied by localization of the molecular orientations and a lowering of the symmetry from $Pm3n$ to $R\bar{3}c$ (Refs. 43 and 44). The number of molecules is conserved at the transition, and the rhombohedral distortion of the initial cubic cell is small. Since the symmetry group $R\bar{3}c$ is a subgroup of $Pm3n$, it is not ruled out that the phase transformation $\delta \rightarrow \varepsilon$ can be second-order. Indeed, according to Raman studies,[45] the phase transition to the $\varepsilon$ phase is preceded by a still weaker transformation in the orientational subsystem which can be characterized as a second-order transition.

In studying supercooled $\gamma$-$O_2$ one can also expect some new features in the magnetic properties. As was shown in Ref. 46, the high-temperature $\gamma$ phase of oxygen is a quasi-one-dimensional magnet with a strong interaction of the molecular spins in chains of plane-disordered molecules. The cooling of such a structure to helium temperatures can lead not only to quantitative but possibly also to qualitative changes in the magnetic subsystem. In particular, the likelihood of formation of an ordered magnetic structure of the one-dimensional magnet type is not ruled out.

The authors are grateful to Yu. A. Freiman for a discussion of the results of this study and for helpful advice.

[a)]E-mail: prokhvatilov@ilt.kharkov.ua

[1] I. N. Krupskiĭ, A. I. Prokhvatilov, Yu. A. Freĭman, and A. I. Erenburg, Fiz. Nizk. Temp. **5**, 271 (1979) [Sov. J. Low Temp. Phys. **5**, 130 (1979)].
[2] V. G. Manzhelii, A. I. Prokhvatilov, V. G. Gavrilko, and A. P. Isakina, *Structure and Thermodynamic Properties of Cryocrystals (Handbook)*, Begell House Inc., New York (1998).
[3] R. A. Alikhanov, Zh. Éksp. Teor. Fiz. **45**, 813 (1967) [*sic*].
[4] M. F. Collins, Proc. Phys. Soc. **89**, 415 (1966).
[5] R. A. Alikhanov, JETP Lett. **5**, 349 (1967).
[6] T. G. Blocker, M. A. Kinch, and F. G. West, Phys. Rev. Lett. **22**, 853 (1969).
[7] C. H. Fagerstroem and A. C. Hollis-Hallet, J. Low Temp. Phys. **1**, 3 (1969).
[8] C. S. Barrett and L. Meyer, Phys. Rev. **160**, 694 (1967).
[9] C. S. Barrett, L. Meyer, and J. Wasserman, J. Chem. Phys. **47**, 592 (1967).
[10] R. Stevenson, J. Chem. Phys. **27**, 673 (1957).
[11] H. M. Roder, J. Phys. Chem. Ref. Data **7**(3), 949 (1978).
[12] C. Uyeda, K. Sugiyama, and M. Date, J. Phys. Soc. Jpn. **54**, 1107 (1985).
[13] P. W. Stephens and C. F. Majkrzak, Phys. Rev. B **33**, 1 (1986).
[14] L. Lipinski, A. Szmyrka-Grzebyk, and H. Manuszkiewicz, Cryogenics **36**, 921 (1996).
[15] A. Szmyrka-Grzebyk, L. Lipinski, and H. Manuszkiewicz, J. Low Temp. Phys. **111**, 399 (1998).
[16] H. J. Hoge, Rev. Natl. Bur. Std. **44**, 321 (1950).
[17] M. P. Orlova, *Temperature, Its Measurement and Control in Science and Industry* **3**, Part 1, 179 (1962).
[18] J. Ancsin, in *Temperature Measurement 1975*, edited by B. F. Filling and T. J. Quinn, IOP Conference Series No. 26, Institute of Physics, Bristol (1975).
[19] W. F. Giauque and H. L. Jonston, J. Am. Chem. Soc. **51**, 2300 (1929).
[20] A. S. Baryl'nik and A. I. Prokhvatilov, Fiz. Nizk. Temp. **20**, 912 (1994) [Low Temp. Phys. **20**, 716 (1994)].
[21] M. Minenko, M. Vetter, A. Brodyanski, and H. J. Jodl, Fiz. Nizk. Temp. **26**, 947 (2000) [Low Temp. Phys. **26**, 699 (2000)].
[22] R. LeSar and R. D. Etters, Phys. Rev. B **37**, 5364 (1988).
[23] Yu. V. Gaididei and V. M. Loktev, Fiz. Nizk. Temp. **7**, 1305 (1981) [Sov. J. Low Temp. Phys. **7**, 634 (1981)]; B. Kuchta T. Luty, and R. J. Meier, J. Phys. C: Solid State Phys. **20**, 585 (1987).
[24] A. J. R. de Silva and L. M. Falikov, Phys. Rev. B **52**, 2325 (1995).
[25] N. N. Galtsov, A. I. Prokhvatilov, Yu. A. Freiman, and S. M. Tret'yak, in *Abstracts of the Third International Conference on Cryocrystals and Quantum Crystals*, Szklarska Poreda, Poland, July 28–August 4, 2000.
[26] A. I. Prokhvatilov, I. N. Krupskiĭ, L. D. Yantsevich, and A. S. Baryl'nik, Prib. Tekh. Éksp. **3**, 261 (1981).
[27] I. N. Krupskii, A. I. Prokhvatilov, and A. I. Érenburg, Fiz. Nizk. Temp. **1**, 359 (1975) [Sov. J. Low Temp. Phys. **1**, 178 (1975)].
[28] J. M. Dundon, Phys. Lett. A **61**, 58 (1977).
[29] A. Eucken, Verh. Dtsch. Phys. Ges. **18**(1), 4 (1916).
[30] K. Clusius, Z. Phys. Chem. B **3**, 41 (1929).
[31] K. Clusius and A. Franck, Z. Phys. Chem. B **42**, 395 (1939).
[32] A. S. Borovik-Romanov, Zh. Éksp. Teor. Fiz. **21**, 1304 (1951).
[33] A. S. Borovik-Romanov, M. P. Orlova, and P. G. Strelkov, Dokl. Akad. Nauk SSSR **99**, 699 (1954).
[34] W. R. G. Kemp and C. P. Peckup, *Temperature, Its Measurement and Control in Science and Industry* **4**, Pt. 1 (*Proceedings of the Fifth Symposium on Temperature, Washington, D.C., June 21–24, 1971*), Instrument Society of America, Pittsburgh, Pa. (1972).
[35] J. W. Stewart, J. Phys. Chem. Solids **12**, 122 (1959).
[36] V. A. Slyusarev, Yu. A. Freĭman, and R. P. Yankelevich, Fiz. Nizk. Temp. **7**, 536 (1981) [Sov. J. Low Temp. Phys. **7**, 265 (1981)].
[37] R. D. Etters, A. A. Helmi, and K. Kobashi, Phys. Rev. B **28**, 2166 (1983).
[38] R. Rastelli and A. Tassi, J. Phys. C **19**, L423 (1986).
[39] E. M. Horl, Acta Crystallogr. B **25**, 2515 (1969).
[40] I. N. Krupskii, A. I. Prokhvatilov, Yu. A. Freiman, and A. I. Erenburg, ''Structure, low-energy elementary excitation spectrum and thermodynamic properties of solid oxygen,'' Preprint ITP-79-4E, Kiev (1979).
[41] D. E. Cox, E. J. Samuelsen, and K. H. Beckurts, Phys. Rev. B **7**, 3102 (1973).
[42] U. T. Höchly, K. Knorr, and A. Loidl, Adv. Phys. **39**, 405 (1990).
[43] R. L. Mills, B. Olinger, and O. T. Cromer, J. Chem. Phys. **84**, 2837 (1986).

[44] V. G. Manzhelii and Yu. A. Freiman (Eds.), *Physics of Cryocrystals*, AIP Press, New York (1996).
[45] M. J. M. Scheerboom and J. A. Schouten, Phys. Rev. Lett. **71**, 2252 (1993).
[46] A. P. Brodyanskiĭ and Yu. A. Freĭman, Fiz. Nizk. Temp. **11**, 1292 (1985) [Sov. J. Low Temp. Phys. **11**, 714 (1985)].

Translated by Steve Torstveit

## LATTICE DYNAMICS

# Low-temperature orientational ordering and possible domain structures in $C_{60}$ fullerite

V. M. Loktev*

*Bogolyubov Institute for Theoretical Physics of the National Academy of Sciences of Ukraine, 14b, Metrologichna Str., Kiev 143, 03143 Ukraine; Centro de Física do Porto, Universidade do Porto, Rua do Campo Alegre 687, 4169-007 Porto, Portugal*

Y. G. Pogorelov

*Centro de Física do Porto, Universidade do Porto, Rua do Campo Alegre 687, 4169-007 Porto, Portugal*

J. N. Khalack

*Bogolyubov Institute for Theoretical Physics of the National Academy of Sciences of Ukraine, 14b, Metrologichna Str., Kiev 143, 03143 Ukraine*

(Submitted December 22, 2000; revised February 12, 2001)
Fiz. Nizk. Temp. **27**, 539–546 (May 2001)

Based on a simple model for the ordering of hexagons on a square planar lattice, an attempt is made to consider the possible structure of $C_{60}$ fullerite in its low-temperature phase. It is shown that hexagons representing fullerenes oriented along the $C_3$ axes of the sc lattice can be ordered into an ideal structure with four nonequivalent molecules in the unit cell. Then the energy degeneracy for the rotation of each hexagon by $\pi/3$ around its $C_3$ axis leaves the translational and orientational order in this structure but leads to a random distribution of $\pi/3$ rotations and hence to an ''averaged'' unit cell with two molecules. However, the most relevant structural defects are not these intrinsic ''misorientations'' but some walls between domains with different sequences of the above-mentioned two (nonideal) sublattices. Numerical estimates are made for the anisotropic intermolecular potential, showing that the anisotropy is noticeably smaller for molecules in walls than in domains.  [DOI: 10.1063/1.1374727]

### 1. INTRODUCTION

Study of the equilibrium thermodynamic properties of $C_{60}$ fullerite remains an active topic in low-temperature physics (see recent reviews[1,2]). In particular, recent experiments on its heat conduction[3] and linear thermal expansion[4] have revealed anomalies peculiar to this unique object. This relates to the following properties observed in experiments:

i) Rather short ($\sim$ 50 intermolecular spacings) mean free path for acoustic phonons, evidencing the presence of a rather high amount (up to 10%) of structural or impurity scatterers, despite the only less than $10^{-2}$ wt. % impurities present in the initial material.

ii) The negative (and really huge, up to $10^2$) value of the Grüneisen coefficient in solid $C_{60}$ at $T \sim 10$ K.

In particular, to explain the low-temperature behavior of the heat conduction in nominally pure $C_{60}$ fullerite, processes of scattering of the phonon heat carriers by some defects of an orientational nature were invoked in Ref. 3. Namely, it was supposed that upon cooling of the crystal some single, ''orientationally disordered'' $C_{60}$ molecules remain quenched in it. In that case their relative number should reach several percent, or in other words, so many molecules become ''orientational impurities'' that one of them can be found among nearest neighbors of each ''regular'' molecule. This was justified by estimates showing that if the anisotropic part of the intermolecular interaction (AIMI) contains two minima with a relatively small ($\sim 10^2$ K) energy difference but separated by a rather high ($\approx 3 \times 10^3$ K) energy barrier, a considerable number of molecules can remain frozen in the metastable state at $T \sim 10^2$ K and a reasonable cooling rate. However, estimates based on a single-particle treatment considering the relaxation of each molecule independent of the others, in a fixed (static) environment, can hardly be consistent. All the molecules are equivalent in the crystal, equally and self-consistently participating in the formation of the crystalline (molecular or mean) field at each of them, and therefore the barriers should also depend on the relaxing molecules themselves. Consequently, energy estimates for several particular orientations of a single molecule[5] can hardly give a proper value of the shortest time of escape from its metastable state.[1)]

At least, it should be noted that a great number of misoriented molecules can transform the crystal into an ''orientational solution'' or even into a glass (if this will be accompanied by unlimited extension of the relaxation times spectrum). The idea of an orientational glass and the resulting competition between the isotropic and anisotropic parts of the intermolecular potential was proposed in Ref. 6 to explain the anomalously large negative thermal expansion of solid $C_{60}$ discovered by Aleksandrovskii *et al.*[4] However, at present no numerical estimates are available for this mecha-

 

nism that could confirm the observed expansion.

The above-mentioned problems with justification of the proposed physics of anomalous thermal behavior of solid $C_{60}$ suggest that one seek some alternatives, more compatible with the translational invariance of a crystal. In this communication, one such mechanism is proposed, related to the possible existence of several orientational domains in the sc phase of solid $C_{60}$, separated by well-defined domain walls. The latter could play the role of effective scatterers for phonon heat carriers. Besides, the higher symmetry of the local crystalline field on the $C_{60}$ molecules within the walls can restore the conditions for their almost free rotation, which is necessary (see Ref. 4 and references therein) to account for the negative thermal expansion.

## 2. MODEL

It is well known (see, for example, the reviews[7,8]) that below the point of orientational melting $T_m^{(\mathrm{high})} \approx 260\,\mathrm{K}$ the fcc lattice of $C_{60}$ fullerite is divided into four sc sublattices with one of the $C_3$ axes of the molecule oriented along one of the cube diagonals (which also are crystalline $C_3$axes). It is of interest to note that the corresponding $Pa3$ structure, characteristic for the simplest molecular cryocrystals, where (even small) quadrupole–quadrupole interactions dominate,[9] allows one to assume the presence of an induced quadrupole moment on $C_{60}$ in pure fullerite, despite its complete absence for the free $C_{60}$ molecule.[2)] Also, it can be expected that no ''transverse'' ordering with respect to each of these axes takes place until the low-temperature transition at $T_m^{(\mathrm{low})} \approx 90\,\mathrm{K}$. But since the molecules $C_{60}$ are truncated icosahedra having fivefold axes among their symmetry elements, they cannot be completely ordered into an sc lattice because of the impossibility of simultaneous optimization of the local (crystal-field) and intermolecular potentials. Therefore certain kinds of defects are inevitable at low temperatures, either point (individual) or extended (collective).

The first type of defects is usually related to some local disturbance of the structural or compositional order, while the second (dislocations, domain walls, twin boundaries, etc.) can exist even with a fully uniform background. Local disorder in fullerite could be due to, for example, isotopically substituted $C_{60}$ molecules, of $C_n$ fullerenes with $n \neq 60$, or impurities like $H_2$. But the samples of $C_{60}$ fullerite with the above-mentioned anomalies of the low-temperature properties were especially prepared and purified, so that there were no physical reasons for any appreciable content of foreign local defects.

Then a more plausible source of low-temperature anomalies can be sought in extended (topological) defects, and in view of the possibility for several energetically equivalent domain structures to exist under reduced cubic symmetry, these defects can be associated with the walls between such domains.

Of course, even a simple cubic lattice made of so complex and symmetrical a molecule as $C_{60}$ presents great technical difficulties for straightforward calculation of the total (and still unknown) intermolecular potential, defined by high-order multipole moments with great number of components (for a general review, see Ref. 12), and of related low-energy (nonlinear) excitations in the crystal. Hence, not claiming to give quantitative predictions for real fullerite, we limit ourselves below to consideration of a strongly simplified model including the relevant features of fullerite: reduction of the crystalline point symmetry by its incompatibility with the molecular symmetry, a double-well potential of AIMI, and the related possibility of domains and domain walls.

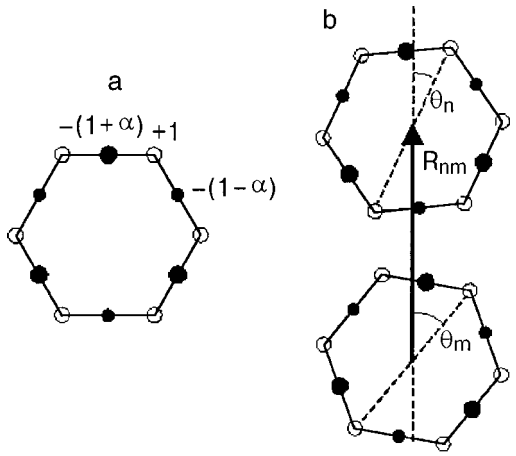


FIG. 1. Charge distribution adopted for the model hexagonal molecule (a) and possible orientations of two molecules with centers positioned at **n** and **m** (b).

Let us consider a system of flat hexagonal molecules (simulating $C_{60}$ molecules seen along the $C_3$ axis)[3)] located in sites of a rigid square planar (sp) lattice, modeling the $3D$ fcc lattice. To evaluate the angular part of the pair interaction between electrically neutral hexagons, we suppose two kinds[4)] negative charges, $-(1 \pm \alpha)$, located at the centers of the hexagonal sides, and unit positive charges at their vertices (see Fig. 1a). Such a distribution of negative charges recalls single covalent bonds at the borders between pentagons and hexagons and the double bonds between two hexagonal rings in a truncated icosahedral molecule. Here the charge and geometric asymmetry parameter $\alpha$, reducing the $C_6$ symmetry of a hexagon down to $C_3$, reflects one of the most important features of real $C_{60}$ fullerene: the 120° alternation of such rings around each of its hexagons.

The total Coulomb energy of a pair of hexagons (Fig. 1b) reads:

$$V_{\mathbf{nm}}(\theta_{\mathbf{n}}, \theta_{\mathbf{m}}) = \sum_{\mu,\sigma} V_{\mathbf{nm}}^{(\mu\sigma)}(\theta_{\mathbf{n}}, \theta_{\mathbf{m}}), \tag{1}$$

where the indices $\mu$, $\sigma$ take the values $v$, $b$, or $B$, related to vertices and to bonds with smaller and greater negative charges, respectively, and the particular terms are:

$$V_{\mathbf{nm}}^{(vv)}(\theta_{\mathbf{n}}, \theta_{\mathbf{m}}) = \sum_{j,k=0}^{5} \left\{ \left[ R_{\mathbf{nm}} + \cos\left( \theta_{\mathbf{n}} + \frac{\pi j}{3} \right) - \cos\left( \theta_{\mathbf{m}} + \frac{\pi k}{3} \right) \right]^2 + \left[ \sin\left( \theta_{\mathbf{n}} + \frac{\pi j}{3} \right) - \sin\left( \theta_{\mathbf{m}} + \frac{\pi k}{3} \right) \right]^2 \right\}^{-1/2}, \tag{2}$$

$$V_{\mathbf{nm}}^{(vb)}(\theta_{\mathbf{n}},\theta_{\mathbf{m}}) = -(1-\alpha)\sum_{j=0}^{5}\sum_{k=0}^{2}\left\{\left[R_{\mathbf{nm}}+\cos\left(\theta_{\mathbf{n}}+\frac{\pi j}{3}\right)\right.\right.$$
$$\left.-\frac{\sqrt{3}}{2}\cos\left(\theta_{\mathbf{m}}+\pi\frac{4k+1}{6}\right)\right]^2+\left[\sin\left(\theta_{\mathbf{n}}+\frac{\pi j}{3}\right)$$
$$\left.\left.-\frac{\sqrt{3}}{2}\sin\left(\theta_{\mathbf{m}}+\pi\frac{4k+1}{6}\right)\right]^2\right\}^{-1/2}$$
$$=V_{\mathbf{mn}}^{(bv)}(\theta_{\mathbf{m}},\theta_{\mathbf{n}})=\frac{1-\alpha}{1+\alpha}V_{\mathbf{nm}}^{(vB)}(\theta_{\mathbf{n}},-\theta_{\mathbf{m}})$$
$$=\frac{1-\alpha}{1+\alpha}V_{\mathbf{mn}}^{(Bv)}(\theta_{\mathbf{m}},-\theta_{\mathbf{n}}), \qquad (3)$$

$$V_{\mathbf{nm}}^{(bb)}(\theta_{\mathbf{n}},\theta_{\mathbf{m}})=(1-\alpha)^2\sum_{j,k=0}^{2}\left\{R_{\mathbf{nm}}+\frac{\sqrt{3}}{2}\right.$$
$$\times\left[\cos\left(\theta_{\mathbf{n}}+\pi\frac{4j+1}{6}\right)\right.$$
$$\left.-\cos\left(\theta_{\mathbf{m}}+\pi\frac{4k+1}{6}\right)\right]^2+\frac{3}{4}\left[\sin\left(\theta_{\mathbf{n}}\right.\right.$$
$$\left.\left.+\pi\frac{4j+1}{6}\right)-\sin\left(\theta_{\mathbf{m}}+\pi\frac{4k+1}{6}\right)\right]^2\Bigg\}^{-1/2}$$
$$=\frac{1-\alpha}{1+\alpha}V_{\mathbf{nm}}^{(bB)}(\theta_{\mathbf{n}},\theta_{\mathbf{m}})$$
$$=\frac{1-\alpha}{1+\alpha}V_{\mathbf{nm}}^{(Bb)}(-\theta_{\mathbf{n}},-\theta_{\mathbf{m}})$$
$$=\left(\frac{1-\alpha}{1+\alpha}\right)^2V_{\mathbf{nm}}^{(BB)}(-\theta_{\mathbf{n}},-\theta_{\mathbf{m}}), \qquad (4)$$

$R_{\mathbf{nm}}=|\mathbf{n}-\mathbf{m}|$ is the distance between the centers of the hexagons at the sites $\mathbf{n}$ and $\mathbf{m}$ of the sp lattice; $\theta_{\mathbf{n}}$, $\theta_{\mathbf{m}}$ are the relative orientation angles; the distance from center to vertex is unity. It can be noticed that, due to the $C_3$ symmetry of charges in a hexagon, the clockwise and counterclockwise rotations are not equivalent in the AIMI.

Despite the simplified geometry of the sp lattice of hexagons and the neglect of quantum effects (charge delocalization, covalency, etc.), one can expect this rather rough model to give the correct qualitative behavior of the AIMI and its dependence on the charge distribution within the molecule and a reasonable estimate of the contributions from different mutual configurations of molecules.

### 3. PAIR INTERACTIONS AND ORDERING TYPES

The numerical results for the AIMI, Eq. (1), are shown in Fig. 2 for some typical mutual configurations and several values of the asymmetry parameter $\alpha$. First of all, it is seen that, for $\alpha\neq 0$, the AIMI for two hexagons possesses a distinct 120° periodicity and two-hump profiles. This reflects correctly the AIMI for two $C_{60}$ molecules, where a double-well potential describes the so-called pentagon and hexagon configurations[14] (see also Figs. 7–10 of Ref. 13, in which analogous curves calculated to clarify what form of AIMI can best fit the orientational mean-field energy of $C_{60}$ fullerite at room temperatures). It is also seen that with decreasing

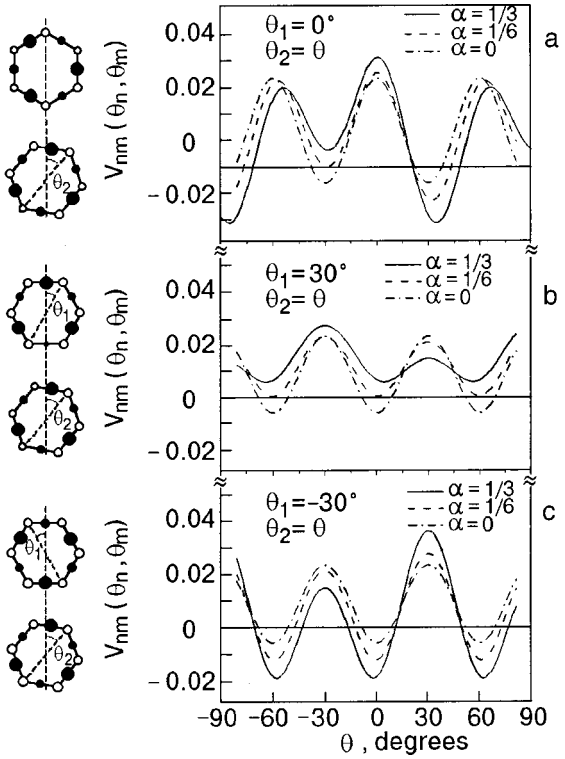


FIG. 2. AIMI of the most characteristic (shown at left) mutual configurations of hexagons at a fixed orientation of one of them. The axes and rotation angles correspond to Fig. 1b. The intermolecular distance $R_{12}$ was chosen as 3 (in units of the hexagon side).

asymmetry of the negative charge distribution, the AIMI becomes smoother, though some minima (see Fig. 2a and 2b) become deeper, so that in the limit $\alpha\rightarrow 0$ all the minimum energies are equal and negative.

It follows from Fig. 2 that for all asymmetry values except $\alpha=0$, the most stable configuration is that in which a vertex of one molecule points to a greater negative charge of a neighboring molecule (Fig. 2a and 2c) while the maximum repulsion corresponds to parallel neighboring sides with such negative charges. In the case $\alpha=0$, at least, the 60° periodicity corresponding to the $C_6$ axis is restored, nevertheless leaving the same most stable configuration (vertices against sides).

Knowledge of the pair interaction and the most stable configurations for two hexagons enables one to order them in a sp lattice. Then the AIMI requires that one of the long axes of each hexagon be oriented along a crystalline axis and its nearest neighbors be rotated by $\pi/6$. This readily divides the sp lattice into two inter-twinned ones, with long hexagon axes aligned with $x$ (''horizontal,'' H) and $y$ (''vertical,'' V), respectively. But taking into account that a molecule has two non-equivalent positions with respect to negative charges for each alignment, the ideal order of such hexagons in the sp lattice corresponds to ''parquets'' (one of them is shown in Fig. 3) with four molecules in the unit cell: two horizontal, denoted 1 and 3, and two vertical, 2 and 4. Then each of the two above-mentioned sublattices contains only even or odd positions. Here the long-range order holds not only for translations and orientations but also for the charge pattern. It should be also noted that, because of incompatible point groups for asymmetric hexagons and the sp lattice, it is im-

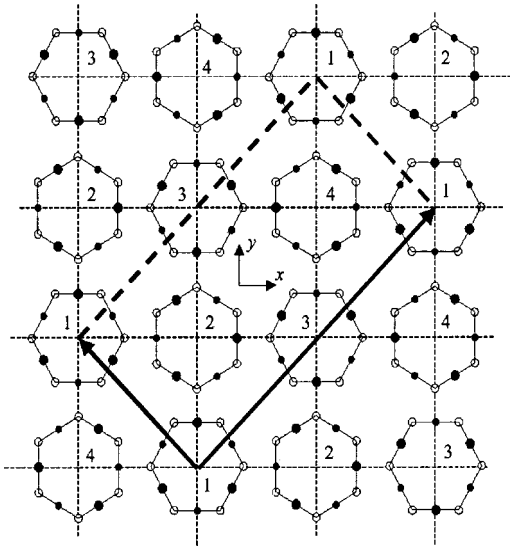


FIG. 3. An example of ordering of hexagons into the sp lattice with four molecules in the unit cell and its translation vectors. Equivalent structures can be obtained by all permutations preserving opposite parities between nearest neighbors.

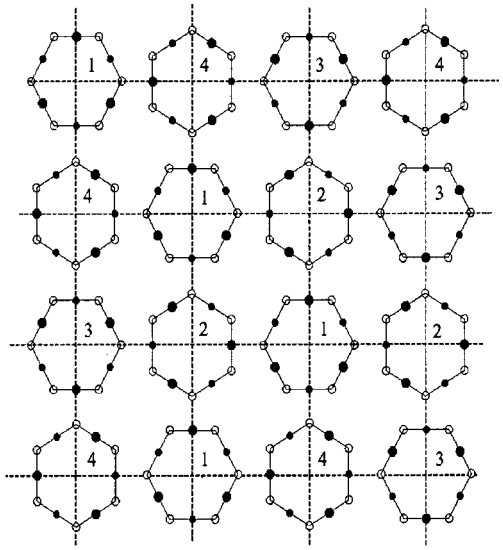


FIG. 4. Fragment of sp lattice structure obtained by random substitutions $1\leftrightarrow 3$ and $2\leftrightarrow 4$ introduced into the ideal 4-sublattice structure in Fig. 3.

possible to arrange all nearest neighbors of each hexagonal molecule in positions with maximum negative AIMI. Though some of its neighbors occur at the metastable minima of the AIMI, nevertheless the total energy balance proves to be negative and stable.

This kind of order is peculiar by its frustration, or the energy degeneracy with respect to the substitutions $1\leftrightarrow 3$ and $2\leftrightarrow 4$. These transformations are just generated by a $C_6$ rotation, which is not an element of the symmetry group of a molecule with the asymmetric charge distribution (see Fig. 1 a). This, in turn, implies that the sp lattice of hexagons, preserving the above-described translational and orientational order,[5)] can be created in a thermodynamic way with a specific disorder left within even and odd sites. This transforms the ideally ordered 4-sublattice substructure into a nonideal 2-sublattice structure like the simulated fragment shown in Fig. 4. In such a crystal the $C_6$ rotation intrinsically enters the point symmetry group of a molecule.

Evidently, 4- or 2-sublattice structures admit the existence of several equivalent arrangements with permutated sublattices separated by certain extended defects: domain walls or antiphase boundaries. These defects might effectively contribute to the low-temperature thermal properties of the system. Below we consider an example of such a defect in a 2-sublattice structure.

#### 4. DOMAIN WALL STRUCTURE

The above-indicated structure of 2-sublattice ordering of hexagons in the sp lattice provides equal conditions for all of them, and the above-mentioned disorder does not result in any characteristic isolated defects. This is also seen from Fig. 2, which shows the rather high barriers between the stable and metastable minima. Hence, each hexagon, either in the 4- or 2-sublattice structure, stays near an AIMI minimum that defines its libration spectrum.

However, this does not at all prevent defects in such a crystal. In particular, in the course of thermodynamic growth, there can appear, as usual, some vacancies and dislocations (which will not be discussed here) and also a specific kind of defects, the antiphase boundaries, characteristic for any multi-sublattice orientational (vector or tensor) structure. They emerge between regions identical in their coordination but different in the attribution of molecular orientations to sublattices.

Actually, the transition from rotation to libration of molecules is a first-order transition, realized through the formation of nuclei (domains) of orientational order with a definite attribution of sublattices to molecular orientations. Expansion of such domains (see Fig. 5) leads them to contact each other, forming a continuous ordered structure. There are two possible modes of such a ''meeting.'' At the contacts …HVHV→←HVHV… or …VHVH→←VHVH… the two structures match perfectly, producing a single coherent domain. But the contacts …VHVH→←HVHV… or …HVHV→←VHVH… produce a mismatch, so that the closest molecules to the boundary should be orientationally adjusted to provide a continuous transition from one domain to another. Evidently, far from the boundary such domains are indistinguishable, and the boundary itself is just a consequence of the initial conditions of the growth. Moreover, no visible thermodynamic mechanisms for domain structure formation (like those known, for instance, in 2-sublattice antiferromagnets)[15,16] can be indicated in this system of orientationally ordered hexagons.

To describe consistently the 2-sublattice structure, let us redefine the orientation angle $\theta_{\mathbf{n},i}$ for an ''averaged'' molecule (possessing $C_6$ symmetry) at the $i$th site in $n$th unit cell as the smallest positive angle between one of its vertices and the $y$ axis (see Fig. 1b). Then for each unit cell we can naturally define the two angles,

$$\varphi_{\mathbf{n}}=\theta_{\mathbf{n},2}-\theta_{\mathbf{n},1}, \quad \psi_{\mathbf{n}}=\theta_{\mathbf{n},2}+\theta_{\mathbf{n},1}, \tag{5}$$

which play the role of order parameters. For the two fragments of ordered structures shown in Fig. 5 the corresponding values are uniform in space: $\varphi_{\mathbf{n}}=\varphi_{\mathrm{I}}=\pi/6$, $\psi_{\mathbf{n}}=\psi_{\mathrm{I}}=\pi/6$ in domain I, and $\varphi_{\mathbf{n}}=\varphi_{\mathrm{II}}=-\pi/6$, $\psi_{\mathbf{n}}=\psi_{\mathrm{II}}=\pi/6$ in

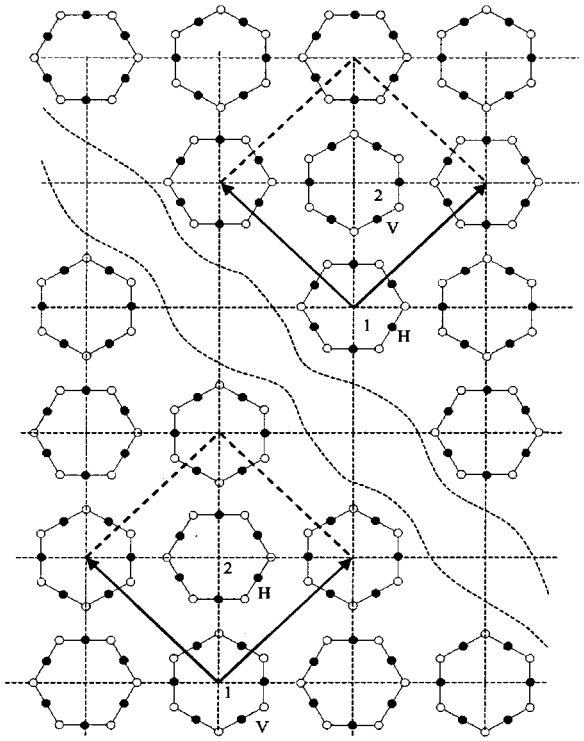


FIG. 5. A schematic of the growth and approaching of two domains with orientationally ordered subsystems of hexagons. In domain I (upper right) vertically oriented molecules $(V, \theta=0)$ are located in the sites of the 1st sublattice and horizontally oriented molecules $(H, \theta=\pi/6)$ in the 2nd sublattice, and vice versa in domain II (lower left).

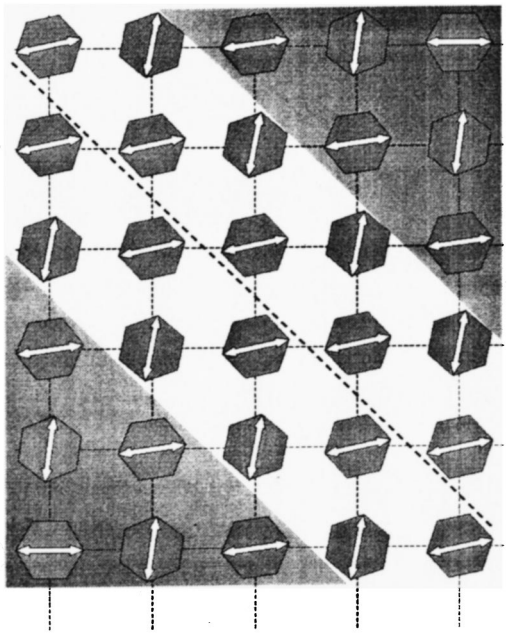

FIG. 6. Domain wall (clear region) between two domains (dark regions, I and II of Fig. 5). For convenience, the directors show the molecules' orientations tilted with respect to the related asymptotes. The dashed line corresponds to the order parameter $\varphi=0$.

domain II. Thus the two domains are distinguished by inversion of the parameter $\varphi$, like 180° domains in a 2-sublattice antiferromagnet.

One can build a boundary between these two domains, located at the origin and characterized by the unit normal vector $\mathbf{d}$, so that $\varphi_{\mathbf{n}}$ changes when $\mathbf{n}$ crosses the domain wall, reaching asymptotic values $\varphi_{\mathbf{n}}\to\varphi_{\mathrm{I}}$ at $\xi=\mathbf{n}\cdot\mathbf{d}\to-\infty$, $\varphi_{\mathbf{n}}\to\varphi_{\mathrm{II}}$ at $\xi\to\infty$, and providing a minimum of the energy functional:

$$E[\varphi_{\mathbf{n}},\psi_{\mathbf{n}}]=\sum_{\mathbf{n}} V_{\mathbf{n}}(\varphi_{\mathbf{n}},\psi_{\mathbf{n}}),$$

$$V_{\mathbf{n}}(\varphi_{\mathbf{n}},\psi_{\mathbf{n}})=\sum_{\rho} V_{\mathbf{n},\mathbf{n}+\rho}(\theta_{\mathbf{n}},\theta_{\mathbf{n}+\rho}). \tag{6}$$

Using the above numerical simulation to estimate the AIMI, we conclude that the function $V_{\mathbf{n}}(\varphi_{\mathbf{n}},\psi_{\mathbf{n}})$ is well approximated by the sum of symmetric and antisymmetric parts: $V_{\mathbf{n}}^{(s)}(\psi_{\mathbf{n}})+V_{\mathbf{n}}^{(as)}(\varphi_{\mathbf{n}})$. Then the antisymmetric part proves to be the softest mode, so that the energy functional, Eq. (6), in the continuum approximation $\varphi_{\mathbf{n}}\to\varphi(\xi)$ can be written as

$$E\left[\varphi,\frac{\partial\varphi}{\partial\xi}\right]=\int_{-\infty}^{\infty}\left[\frac{1}{2}a^2 v_1\left(\frac{\partial\varphi}{\partial\xi}\right)^2+\frac{1}{36}v_2\cos 6\varphi\right]d\xi. \tag{7}$$

In this approximation the inhomogeneous reorientations of hexagons across the domain boundary can be described by the sine-Gordon equation:

$$\frac{\partial^2\varphi}{\partial\xi^2}+\frac{1}{3}d_{DW}^{-2}\sin 6\varphi=0, \tag{8}$$

where the domain wall width $d_{DW}=a\sqrt{v_1/v_2}$ is of the order of lattice constant $a$. This is related to the fact that, unlike the common situation in magnets where, as a rule, $v_1$ (the exchange or stiffness constant) is much greater than $v_2$ (the relativistic anisotropy), in the present system both constants have the same origin in intermolecular interactions and hence the same order of magnitude. Although, strictly speaking, Eq. (8) in this situation is only valid far enough from the domain boundary, the orientations of the discrete hexagons (obtained from a certain infinite discrete set of equations) will follow the ''kink'' solution $\varphi(\xi)=(1/3)\arcsin\tanh(\xi/2d_{DW})$ with sufficient accuracy. The factor 1/3 here and in Eq. (8) provides the correct asymptotic behavior for $\varphi(\xi):\varphi(\pm\infty)=\pm\pi/6$. This also expresses the analogy of the $\pi/3$ rotation between the domains under study with the $\pi$ rotation between 180° domains in ferro- and antiferromagnets.

Figure 6 presents an example of a relatively narrow domain wall in the sp lattice of hexagons. A perceptible rotation of the molecules with respect to their orientations in the domains occurs within the stripe of ~2–3 lattice parameters $(d_{DW}\sim a)$, and hence the misorientations are localized only in the domain wall. Notice that the 4-sublattice structure admits a richer systematics of domains (up to 4) and domain boundaries between them.

To examine how the dynamics of misoriented molecules differs from that of molecules in the domain, we estimated the antisymmetric part of the AIMI, $V_{DW}^{(as)}(\varphi_{DW})$, for the closest unit cell to the center of the domain wall. The corresponding potential relief shown in Fig. 7 is noticeably smoother, and its minima, having the same $\pi/3$ periodicity, are much flatter than those for $V_{\mathbf{n}}^{(as)}(\varphi_{\mathbf{n}})$. Therefore the ''orientational defect,'' or molecules in the domain wall, should display a softer libration spectrum, with increasing density to lower energies. Besides, a specific low-energy excitation

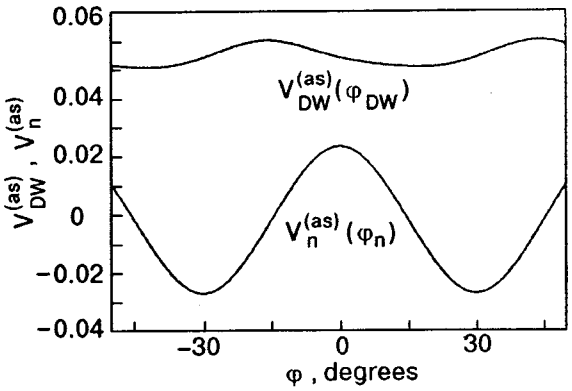


FIG. 7. Potential reliefs of the antisymmetric parts of the AIMI in a domain and at the center of a domain wall.

mode can appear, corresponding to oscillations of the antisymmetric order parameter $\varphi_{DW}$ which propagate along the wall (a ''bending'' mode of orientational, not translational, origin).

The above-mentioned characteristics of a domain wall can be important for the low-temperature behavior of the crystal. First of all, the collective defects should be stronger scatterers for thermal phonons than any point defects, especially if the phonon wavelength ($\lambda_T \sim \hbar v_s/(k_B T)$, where the sound velocity $v_s \sim 3\times 10^5$ cm/s; Ref. 3) becomes comparable with $d_{DW}$. Besides, a weaker AIMI in the domain walls can permit the molecules there to remain almost free rotators down to a much lower temperature than the temperature of orientational freezing for the rest of the crystal.

## 5. CONCLUSION

The above discussion shows how peculiar the dynamics of low-energy excitations can be in such a simple model system as that of hexagons on a square lattice. In particular, for asymmetrical hexagons (possessing a $C_3$ axis) this lattice turns out to be frustrated, which does not exclude the possibility of its glassy behavior. But even the frustrated lattice can be divided into two sublattices, leading to domain structure and domain walls. The latter, being of orientational origin, are able to effectively scatter the excitations of other origins, in particular, the phonons. However, the detailed analysis of such scattering goes beyond the scope of this work.

It seems that the above results could also be relevant for fullerite. First of all, this relates to the possibility that the $C_6$ rotation around the fixed orientation of each $C_{60}$ molecule in the sc phase could effectively become an element of the point symmetry group of the averaged crystal. Although the energy degeneracy conditioned by the corresponding random ''transverse'' fullerene orientations also admits the existence of an orientational glass state of fullerite, the crystal as a whole remains uniform, and no reasons can be found for any distinct point defects, including misorientations. However, extended topological defects such as orientational domain walls (which should not disrupt the initial attribution of $C_{60}$ molecules to cube diagonals), can exist even in a homogeneous system and provide an effective channel for the dissipation of low-energy quasiparticles. At the same time, it must also be noted that domains obtained in fact concern the fullerite with doubled lattice (or 8-sublattice fcc crystal structure observed experimentally[17,18]).

Certainly, a more detailed theoretical study of these issues demands more realistic models of the fullerene and fullerite structures.

One of us (V.M.L.) gratefully appreciates the suggestions from A. N. Aleksandrovskii, V. G. Manzhelii, and L. P. Mezhov-Deglin for calling his attention to the original experimental results concerning thermal anomalies in fullerites. He also expresses his gratitude to J. Lopes dos Santos and Centro do Física do Porto (Portugal) for kind hospitality permitting this work to be done. It was supported in part by NATO grant CP/UN/19/C/2000/PO, Program OUTREACH (V.M.L.) and Portuguese project PRAXIS XXI 2/2.1/FIS/302/94 (Yu.G.P.). Last, we would like to thank Dr. A. V. Nikolaev for reading the manuscript and kindly informing us of Refs. 11 and 13 where some of the above-mentioned questions (in particular, concerning AIMI) are discussed.

*E-mail: vloktev@bitp.kiev.ua

[1)]The collective character of crystalline modes should be also taken into account. A well-known example is vibrational or magnetic spectra resulting from single-particle levels with an excitation gap of the order of the interparticle interaction, which is considerably softened (down to Goldstone gapless behavior) after collectivization. Orientational modes are not an exception in this sense.

[2)]Evidently, a number of thermal rotational excitations of the $C_{60}$ molecules are present at $T > T_m^{(high)}$, all of them associated with certain multipole distortions. The lowest energies ($\sim 10^2$ cm$^{-1}$; Ref. 10) relate to intramolecular quadrupole vibrations, indistinguishable from rotations. The self-consistent admixture of these excitations into the molecular ground state in the crystal field reduces (below $T_m^{(high)}$) the almost spherical symmetry down to axial, contributing to the total energy gain. One can therefore suppose that below $T_m^{(high)}$ the definite orientation of fullerenes along a $C_3$ axis is fixed and long-ranged, corresponding to a common ordering of quadrupoles. Otherwise, the sc lattice cannot be realized. By the way, the quadrupole moment of the $C_{60}$ molecule in polymer phases of $AC_{60}$ (A=K, Rb, Cs) has been considered previously.[11]

[3)]Since the same threefold rotational symmetry holds for fullerene molecules projected on cube faces.

[4)]Such sort of modeling was earlier used by number of authors (see, for example, Ref. 13 and references therein) to improve the form of intermolecular potential.

[5)]Strictly speaking, the $C_6$-rotated molecule can change its distances to nearest neighbors, but we ignore this practically small effect in view of the average translational invariance of the lattice. At the same time, the AIMI analysis shows that the orientational order is not perturbed even under $C_6$ rotations.

[1] O. Gunnarsson, Rev. Mod. Phys. **69**, 575 (1997).
[2] H. Kuzmany, B. Burger, and J. Kürty, in *Optical and Electronic Properties of Fullerenes and Fullerene-Based Materials*, edited by J. Shinar, Z. V. Vardeny, and Z. H. Kaffafi, Marsel Dekker, New York (2000).
[3] V. B. Efimov, L. P. Mezhov-Deglin, and R. K. Nikolaev, JETP Lett. **65**, 687 (1997).
[4] A. N. Aleksandrovskii, V. B. Esel'son, V. G. Manzhelii, A. V. Soldatov, B. Sundquist, and B. G. Udovichenko, Fiz. Nizk. Temp. **23**, 1256 (1997) [Low Temp. Phys. **23**, 943 (1997)]; **26**, 100 (2000); **26**, 75 (2000).
[5] R. C. Yu, N. Tea, M. B. Salamon, D. Lorents, and R. Malhotra, Phys. Rev. Lett. **23**, 2050 (1992).
[6] V. M. Loktev, Fiz. Nizk. Temp. **25**, 1099 (1999) [Low Temp. Phys. **25**, 823 (1999)].
[7] V. M. Loktev, Fiz. Nizk. Temp. **18**, 217 (1992) [Sov. J. Low Temp. Phys. **18**, 149 (1992)].

[8] A. P. Ramírez, Condens. Matter News **3**, 6 (1994).
[9] B. I. Verkin and A. F. Prikhot'ko (Eds.), *Cryocrystals*, Naukova Dumka, Kiev (1983).
[10] P. J. Horoysky and M. L. W. Thewalt, Phys. Rev. B **48**, 11446 (1993).
[11] K. H. Michel and A. V. Nikolaev, Phys. Rev. Lett. **85**, 3197 (2000).
[12] R. M. Lynden-Bell and K. H. Michel, Rev. Mod. Phys. **66**, 721 (1994).
[13] P. Launois, S. Ravy, and R. Moret, Phys. Rev. B **55**, 2651 (1997).
[14] M. David, R. Ibberson, T. Dennis, and K. Prassides, Europhys. Lett. **18**, 219 (1992).
[15] V. G. Bar'yakhtar, A. N. Bogdanov, and D. A. Yablonskii, Usp. Fiz. Nauk **156**, 47 (1988).
[16] E. V. Gomonaj and V. M. Loktev, Fiz. Nizk. Temp. **25**, 699 (1999) [Low Temp. Phys. **25**, 520 (1999)]; cond-mat/0010258 (2000).
[17] G. Van Tendeloo, S. Amelinckx, M. A. Verheijen, P. H. M. van Loosdrecht, and G. Meijer, Phys. Rev. Lett. **69**, 1065 (1992).
[18] E. J. J. Groenen, O. G. Poluektov, M. Matsushita, J. Schmidt, J. H. van der Waals, and G. Mejer, Chem. Phys. Lett. **197**, 314 (1992).

This article was published in English in the original Russian journal. Reproduced here with stylistic changes by AIP.

## LOW-TEMPERATURE PHYSICS OF PLASTICITY AND STRENGTH

# Low-temperature $\alpha$ peak of the internal friction in niobium and its relation to the relaxation of kinks in dislocations

V. D. Natsik, P. P. Pal'-Val',* L. N. Pal'-Val', and Yu. A. Semerenko

*B. Verkin Institute for Low Temperature Physics and Engineering, National Academy of Sciences of Ukraine, pr. Lenina 47, 61103 Kharkov, Ukraine*
(Submitted November 3, 2000)
Fiz. Nizk. Temp. **27**, 547–557 (May 2001)

The influence of impurities on the parameters of the $\alpha$ peak of the internal friction in single-crystal and polycrystalline niobium is investigated; the internal friction is recorded in the temperature range 200–250 K at a vibrational frequency of $\approx 80$ kHz. It is found that increasing the purity of the samples leads to an increase of the peak location temperature and to an increase of its width and amplitude. The structural sensitivity of this peak was observed previously in a study of the influence on this peak of a preliminary plastic deformation, thermocycling, and low-temperature recovery. A statistical description of the whole set of experimental data is proposed, which takes into account the dependence of the activation energy and attempt period on the impurity concentration and on the characteristic value and statistical scatter of the internal stresses. A new algorithm is developed for analyzing the experimental data to obtain empirical estimates for the values of the activation energy, its variance, the attempt period, and relaxation strength for the different structural states of the samples. It is shown that the $\alpha$ peak is a consequence of the resonant interaction of elastic vibrations with the thermally activated nucleation of kink pairs on dislocation segments lying in the valleys of the Peierls potential relief. Empirical estimates are obtained for the values of the main parameters characterizing this process. It is found that the properties of the $\alpha$ peak in niobium are in qualitative agreement with Engelke's theory of the nucleation and relaxation of dislocation kinks. © *2001 American Institute of Physics.* [DOI: 10.1063/1.1374728]

### 1. INTRODUCTION

In studying the temperature dependence of the internal friction in niobium samples of different purity and structural perfection at moderately low temperatures, different investigators have repeatedly detected acoustic absorption peaks having properties typical for the $\alpha$ peaks in bcc metals. The peak location temperature $T_p$ varies from 90 to 200 K as the vibrational frequency is varied over a wide range, from infrasonic frequencies of the order of $10^{-3}$ Hz to ultrasonic frequencies of the order of $10^5$ Hz.[1–13]

As a rule, a preliminary plastic deformation of the samples or the action of thermoelastic stresses during thermocycling lead to an increase of the height and width of the absorption peaks and to a shift of $T_p$ to higher temperatures. A subsequent long low-temperature annealing brings about a reverse change of these parameters of the absorption peak. These features of the behavior of the shape and parameters of this absorption peak indicate that it is sensitive to the details of the defect structure of the samples—in particular, to the statistical ensemble of dislocations and the random internal stress fields produced by them, which are introduced in the crystalline samples during plastic deformation. It should be noted that such a relaxation resonance has also been observed in a study of the internal friction of high-purity iron: at vibrational frequencies of the order of $10^5$ Hz an acoustic relaxation peak is observed at temperatures of the order of 50 K.[14]

In Refs. 13 and 14 it was shown that to a first approximation the aforementioned internal friction peak corresponds to a certain thermally activated relaxation process with a relaxation time depending exponentially on the temperature $T$:

$$\tau(T) = \tau_0 \exp\left(\frac{U_0}{kT}\right), \tag{1}$$

where $U_0$ is the activation energy, $\tau_0$ is the attempt period, and $k$ is Boltzmann's constant. For the $\alpha$ peak in niobium the following estimates have been obtained:[13] $U_0 \approx 0.15$ eV, $\tau_0 \approx 1 \times 10^{-10}$ s.

In Refs. 13 and 14 it was shown that the influence of plastic deformation on the shape and parameters of the $\alpha$ peaks of mechanical relaxation can be explained by the statistical character of the parameters of the elementary relaxators responsible for the given peak together with the assumption that the plastic deformation affects the variance of the activation energies and the volume density of relaxators. The main features of the influence of plastic deformation correspond to the assumption that the attempt period $\tau_0$ is unchanged and that a statistical distribution of the activation energy $U$ arises which is described by a probability density of the quasi-Gaussian type with variance $D^2$:

 

$$P(U)=\frac{1}{\sqrt{2\pi}D}\left(\frac{U}{U_0}\right)\exp\left[-\frac{(U-U_0)^2}{2D^2}\right],$$
$$D\ll U_0. \tag{2}$$

In Refs. 13 and 14 it was also established that the correct microscopic interpretation of the relaxation process is possible only with the use of experimental data obtained under identical conditions by identical methods of measurement of the internal friction on samples with a controlled defect structure. Various authors have proposed several possible microscopic mechanisms for the relaxation processes responsible for the peak. The most probable of them are thermally activated nucleation of kink pairs on rectilinear dislocation segments lying in the valleys of the Peierls relief of the first order, and also thermally activated diffusion of single kinks along dislocation lines through Peierls barriers of the second order. However, neither hypothesis has been confirmed by the whole set of experimental data obtained in the systematic study of samples of the same kind. It can be said that it is not completely certain at present that all of the acoustic relaxation resonances described in the literature[1–13] for niobium in the given temperature and frequency ranges correspond to the same relaxation process. Therefore an unambiguous microscopic interpretation of the given relaxation process will require additional experimental studies. In particular, it would be good to study how the $\alpha$ peak is affected not only by plastic deformation but also by another factor that can substantially alter the structure of the samples: the introduction of impurities in them.

Our goals for this paper were as follows:

—to study experimentally the influence of variations of the structural state of the samples (changes of the impurity content, going from single crystals to polycrystalline samples, the effects of thermoelastic stress) on the parameters of the relaxation resonance in niobium at moderately low temperatures, 150–300 K;

—to systematize the accumulated set of experimental data;

—to develop further the theory of the relaxation resonance in the presence of a statistical distribution of activation energies of the process with allowance for the possible structural sensitivity of the attempt period;

—to discuss the possible microscopic mechanisms responsible for the observed relaxation resonance.

## 2. EXPERIMENTAL PROCEDURE

The samples were rectangular parallelepipeds with dimensions of $3\times3\times21$ mm. They were cut out from single-crystal and polycrystalline niobium of different purities by an electrospark method, then ground on abrasive powders until the desired shape and geometric parameters were obtained, and finally subjected to a chemical polishing to remove the mechanically damaged surface layers. The crystallographic orientation of the longitudinal axis of the single-crystal samples was determined from the Laue pattern to an accuracy of $\pm1°$.

The polycrystalline samples had a coarse-grained structure of the ''bamboo'' type, i.e., the dimensions of the transverse cross section of the samples ($3\times3$ mm) were smaller than the grain size (5–12 mm). The initial dislocation density in the samples was $\sim10^5-10^6$ cm$^{-2}$. A spectral analysis showed that the main substitutional impurity atoms were Mo, Ta, and Zr. The amount of interstitial impurities N, O, and H was reduced to a minimum by a long high-temperature anneal, first in flowing oxygen at a pressure of $\sim10^{-3}$ Pa and then in an ultrahigh vacuum of $\sim10^{-8}$ Pa.[15] As an integral measure of the purity of the samples we used the reduced resistance ratio $RRR=R_{300}/R_0$; it is well known that for metallic solid solutions the values of the parameter $RRR$ are inversely proportional to the impurity concentration. The $RRR$ was determined by measuring the temperature dependence of the resistance of the samples in the interval 2–300 K and then extrapolating the experimental data to 0 K and zero external magnetic field, an applied field having been used to bring the samples to the normal state at temperatures below the superconducting transition temperature $T_c\approx9.3$ K.[16] The main characteristics of the samples are listed in Table I.

TABLE I. Basic characteristics of the samples.

| Sample | Orientation | *RRR* |
|---|---|---|
| Nb-37 | Single crystal ⟨100⟩ | 37 |
| Nb-290 | Coarse-grained polycrystal | 290 |
| Nb-660 | Coarse-grained polycrystal | 660 |
| Nb-970 | Coarse-grained polycrystal | 970 |
| Nb-10 000 | Single crystal ⟨100⟩ | 10 000 |

Acoustical measurements were done by the double composite vibrator method.[17,18] Resonance methods are suited for the study of rather subtle dislocation effects because they are capable of measuring the decrement $\delta$ of the vibrations to rather good accuracy. Longitudinal standing waves with a frequency $f$ of the order of 70–90 kHz were excited in the samples at a constant amplitude of the ultrasonic strain $\varepsilon_0\sim10^{-7}$, which corresponded to the amplitude-independent region. The values of the vibrational frequencies for samples with different structures are presented in Table II. The temperature dependence of the decrement $\delta(T)$ of the vibrations was measured in the temperature interval $150\,\mathrm{K}<T<300\,\mathrm{K}$. The measurements were done both on heating and on cooling. The rate of cooling and heating of the samples during the measurement of the temperature dependence of the damping decrement $\delta$ was $\sim1$ K/min.

We note that experience in making acoustic measurements in the cooling–heating mode has led to the conclusion that thermocycling provides an important means of altering the structural state of a sample.[13–16]

## 3. RESULTS OF THE MEASUREMENTS

Figure 1 shows the temperature dependence of the decrement $\delta(T)$ for polycrystalline samples with different impurity concentrations: the results of the measurements during the first cooling from room temperature to 150 K (Fig. 1a), and the data obtained on the same samples during a subsequent heating from 150 to 300 K (Fig. 1b). Figure 2 shows the temperature spectrum of the absorption $\delta(T)$ for single-crystal samples with different impurity concentrations during the first heating from 150 to 300 K after a preliminary cool-

TABLE II. Dependence of the parameters of the absorption peak on the structural state of the samples.

| Sample | Measurement cycle | $f$, kHz | $10^4\,\delta_{bg}$ | $T_h$, K | $T_p$, K | $T_h^{(-)}$, K | $T_h^{(+)}$, K | $K_{\exp}$ | $10^{10}\tau_0$, s | $d$ | $10^3 C_r \Delta_0$ |
|---|---|---|---|---|---|---|---|---|---|---|---|
| Nb-970 | 1st cooling | 83 | 1.4 | 79 | 234 | 204 | 260 | 1.61 | 11.0 | 0 | 1.8 |
| Nb-660 | | 87 | 1.4 | 78 | 221 | 192 | 242 | 1.56 | 6.7 | 0 | 1.2 |
| Nb-290 | | 79 | 1.4 | 55 | 198 | 180 | 222 | 1.48 | 3.0 | 0 | 0.35 |
| Nb-970 | 1st heating | 83 | 0.9 | – | 275 | 221 | – | – | 11.0 | 1.7 | 5.69 |
| Nb-660 | | 87 | 0.9 | – | 255 | 205 | – | – | 6.7 | 2.0 | 3.38 |
| Nb-290 | | 79 | 0.9 | – | 251 | 204 | – | – | 3.0 | 2.2 | 3.48 |
| Nb-10 000 | 1st heating | 73 | 1.9 | – | 265 | 215 | – | – | 16.0 | 1.2 | 5.50 |
| Nb-37 | | 83 | 1.9 | 86 | 226 | 191 | 243 | 1.39 | 0.8 | 2.3 | 0.74 |

ing to 6 K. In the all cases the temperature dependence of the decrement $\delta(T)$ exhibited pronounced peaks of the internal friction against a low background. Their location on the temperature axis and their characteristic width depend substantially on the structural state of the samples, which was varied both by varying the impurity concentration and by thermocycling. Increasing the impurity concentration, both for the polycrystalline and for the single-crystal samples, leads to a substantial shift of the peak location $T_p$ to lower temperatures (see Fig. 3a) and to a lowering of the peak amplitude (Fig. 3b). The shift of $T_p$ to higher temperatures and the broadening of the peak under the influence of thermoelastic stresses during thermocycling are in agreement with the trends described previously.[13,14]

An important characteristic of the peaks is their width. As a quantitative characteristic of the absorption peaks in the physics of internal friction, one very often encounters the parameter

$$T_h = T_h^{(+)} - T_h^{(-)}, \tag{3}$$

where $T_h^{(+)}$, $T_h^{(-)}$ are the temperatures at which $\delta(T_h^{(+)}) = \delta(T_h^{(-)}) = (1/2)\,\delta_{\max}$ (here $\delta$ denotes the values of the decrement with the background subtracted off). The values of the background absorption, the temperature $T_p$, and the width $T_h$ of the peak under discussion for various types of structural states of the sample are given in Table II.

In analyzing the experimental data one often has to deal with acoustic relaxation peaks observed under conditions of

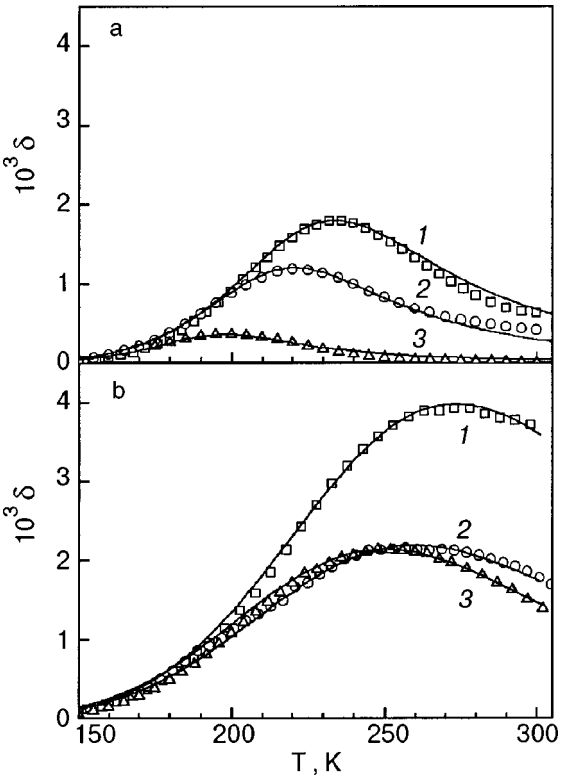


FIG. 1. Internal friction peaks in coarse-grained polycrystalline niobium of different purity: $RRR = 970$ (*1*), 660 (*2*), 290 (*3*). The temperature dependences of the decrement $\delta(T)$ were obtained during the first cooling of the samples from room temperature to 150 K (a) and during a subsequent heating from 150 to 300 K (b). A constant background $\delta_{bg} = 1.4\times10^{-4}$ has been subtracted from the experimental data. The solid lines show the theoretical curves calculated according to formula (6) for the values of the parameters given in Table II.

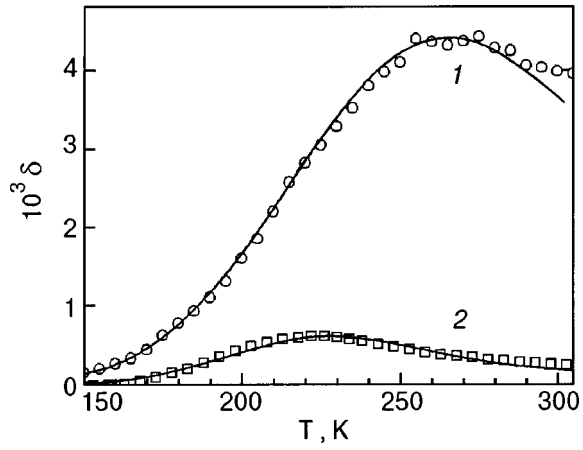


FIG. 2. Internal friction peaks in single-crystal ⟨100⟩ niobium of different purity: $RRR = 10\,000$ (*1*), 37 (*2*). The curves were obtained during the first heating from 150 to 300 K. A constant background $\delta_{bg} = 1.9\times10^{-4}$ has been subtracted from the experimental data. The solid lines show the theoretical curves calculated according to formula (6) for the values of the parameters given in Table II.

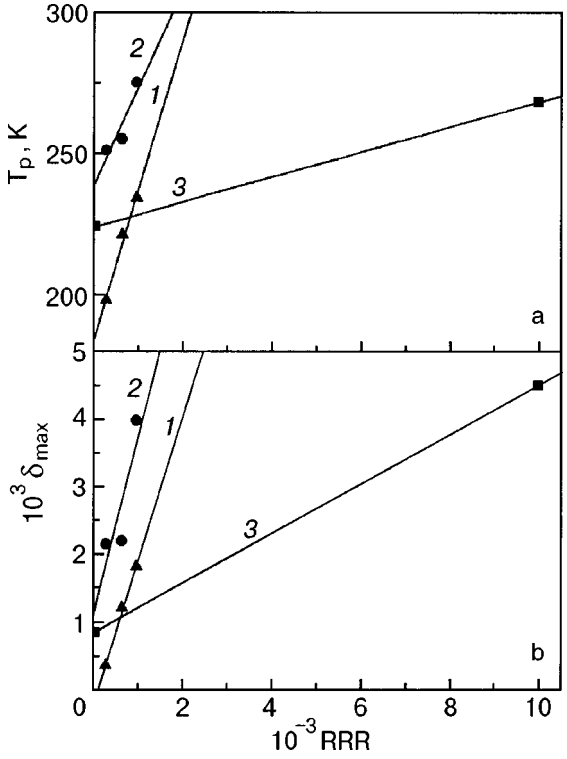


FIG. 3. Temperature location $T_p$ (a) and amplitude $\delta_{\max}$ (b) of the acoustic absorption peaks versus the parameter *RRR* characterizing the purity of the samples: *1*—polycrystalline samples, first cooling from 300 to 150 K; *2*—polycrystalline samples, heating from 150 to 300 K after the first cooling; *3*—single crystals, heating from 150 to 300 K after the first cooling.

rather large background absorption, and the use of the parameter $T_h$ requires a correct subtraction of the background. Moreover, if the background depends even slightly on temperature over the width of the peak, then the correct procedure for subtracting the background becomes difficult. In our opinion, a more convenient characteristics of the width of the peak, with less dependence on the background absorption, are the parameters $T_k^{(-)}$, $T_k^{(+)}$, and $T_k = T_k^{(+)} - T_k^{(-)}$, where $T_k^{(\mp)}$ are the inflection points on the $\delta(T)$ curves, at which $\partial^2\delta(T)/\partial T^2 = 0$. The values of the temperatures $T_k^{(\mp)}$ for the peak under discussion are also given in Table II.

## 4. ANALYSIS OF THE EXPERIMENTAL RESULTS

In Ref. 13 it was shown that the relaxation process under discussion results from the interaction of the elastic vibrations of the sample with a system of a single type of relaxators of a dislocation nature, which in the perfect crystal have the same activation energy $U_0$ and the same attempt period $\tau_0$. In the absence of statistical scatter of the values of these parameters, the temperature dependence of the decrement of the vibrations will exhibit a Debye peak

$$\delta(T,\omega) = 2C_r\Delta_0 \frac{\omega\tau}{1+\omega^2\tau^2}, \tag{4}$$

where $\tau(T)$ is the relaxation time (1), $C_r$ and $\Delta_0$ are the dimensionless concentration and the ''power'' of the elementary relaxators, respectively, and $\omega = 2\pi f$ is the angular frequency of the vibrations. The temperature $T_p^{(0)}$ and width $T_h^{(0)}$ for this peak are given by the relations

$$T_p^{(0)} = \frac{U_0}{k\ln\Omega}, \quad T_h^{(0)} = \frac{2T_p^{(0)}}{\ln\Omega} = \frac{2U_0}{k(\ln\Omega)^2}, \quad \Omega = \frac{1}{\omega\tau_0}. \tag{5}$$

The introduction of additional dislocations in the crystal, changes of the internal stress under external loading or thermocycling, changes in the impurity concentration in the crystal, and other factors of a similar nature can have a very substantial effect on all of the above-mentioned parameters of the relaxation process and can lead to changes in the peak temperature $T_p$, in the peak height $\delta_{\max} = C_r\Delta_0$, and in the parameters $T_h$ and $T_k$ characterizing the width of the peak.

### 4.1. Influence of thermocycling and the impurity concentration on the parameters of the relaxation process

The analysis in Refs. 13 and 14 showed that the shift of the temperature $T_p$ of the acoustic relaxation peak to higher temperatures and the broadening of the peak due to thermocycling can be interpreted as being due to the influence of the thermoelastic stresses on the statistical distribution of activation energies of the elementary relaxators. If the statistical distribution for $U$ is described by the function (2) and the statistical scatter for $\tau_0$ is neglected, then Eq. (4) should be replaced by the more complicated expression

$$\overline{\delta} = C_r\Delta_0 F_1(\theta,\Omega,d), F_1 = \frac{2\Omega\theta^2}{\sqrt{\pi}d\ln\Omega} \times \int_1^\infty dx \frac{\ln x}{x^2+\Omega^2} \exp\left[-\left(\frac{\theta\ln x - \ln\Omega}{d}\right)^2\right]; \tag{6}$$

$$\theta = \frac{T}{T_p^{(0)}}, \quad d = \frac{\sqrt{2}D}{kT_p^{(0)}} = \frac{\sqrt{2}D}{U_0}\ln\Omega. \tag{7}$$

The function $F_1$ can be calculated by numerical integration methods, which for different values of the dispersion parameter $d$ give a series of peaks of varying shape and temperature location.[13] At small values of $d$ the function $F_1(\theta,\Omega,d)$ has a maximum with respect to temperature at $\theta \approx 1$ and practically coincides with the Debye peak, while increasing the value of $d$ leads to a broadening of the peak and a shift of the peak to higher temperatures. As a result of a numerical analysis for the peak temperature $T_p$ and peak width $T_h$ in the case $d \leqslant 2$ we obtain the simple analytical approximations

$$T_p = T_p^{(0)}\left[1 + 2\left(\frac{d}{\ln\Omega}\right)^2\right], \quad T_h = T_h^{(0)}(1+d); \quad T_h^{(0)} = \frac{2T_p^{(0)}}{\ln\Omega}. \tag{8}$$

Using this formula and the experimental data obtained for the first cooling on polycrystalline samples with different impurity concentrations (Table II), one can see that the influence of impurities on the relaxation process under discussion does not reduce simply to a change in the variance of the activation energies (i.e., in the dispersion parameter $d$). From Eq. (8) in the case of two structural states differing by the values of this parameter ($d_1$ and $d_2$), we obtain

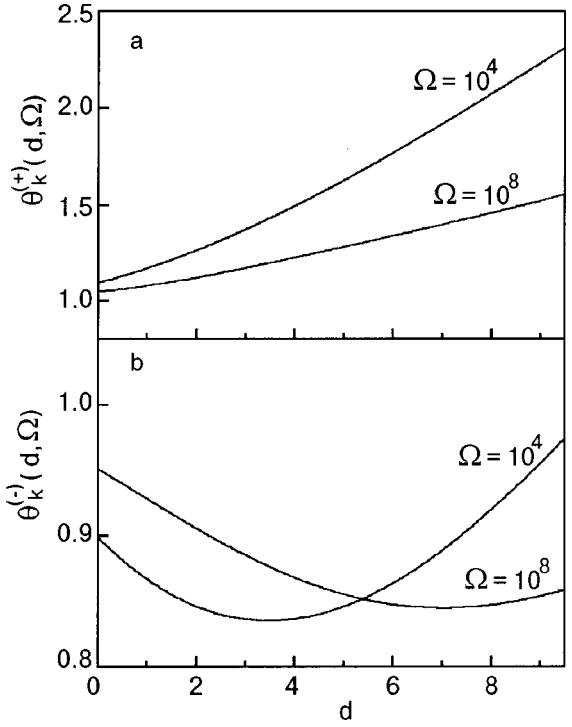


FIG. 4. Dependence of the temperatures of the inflection points $\theta_k^{(\mp)}$ for the high-temperature (a) and low-temperature (b) wings of the function $F_1(\theta,\Omega,d)$ on the parameters $\Omega$ and $d$; the data were obtained by numerical methods.

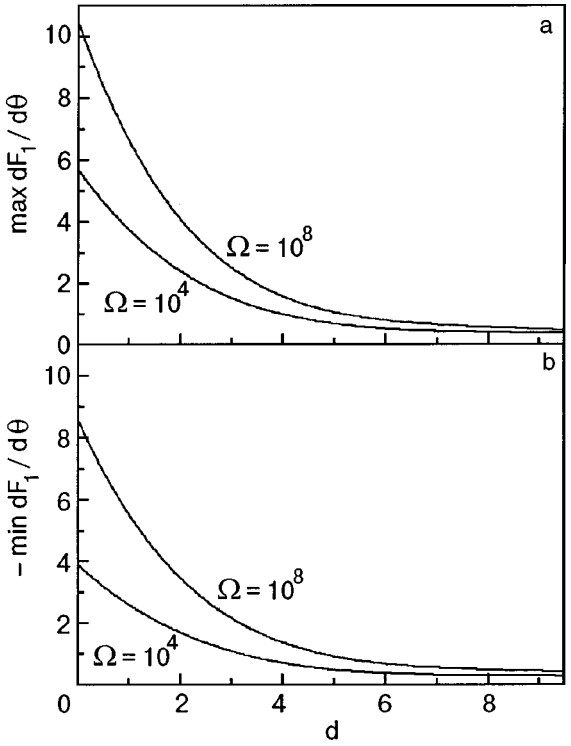


FIG. 5. Dependence of the values of the extrema of the function $\partial F_1(\theta,\Omega,d)/\partial\theta$ on the values of the parameters $\Omega$ and $d$; the data were obtained by numerical methods.

$$\frac{T_p^{(1)}-T_p^{(0)}}{T_p^{(2)}-T_p^{(0)}}=\left[\frac{T_h^{(1)}-T_h^{(0)}}{T_h^{(2)}-T_h^{(0)}}\right]^2. \tag{9}$$

For polycrystalline samples with a high concentration of impurities (Nb-60), one has, according to Ref. 13, $U_0 \approx 0.15$ eV and $\tau_0 \approx 1\times 10^{-10}$ s, and therefore at a vibrational frequency $f \approx 80$ kHz we have $T_p^{(0)} \approx 176$ K and $T_h^{(0)} \approx 35$ K. If we assume that the impurity does not affect the value of $\tau_0$, then these values should be the same for samples with other impurity concentrations (Nb-970 and Nb-290). Then during the first cooling for Nb-970 one has the differences $T_p^{(1)}-T_p^{(0)} \approx 58$ K and $T_h^{(1)}-T_h^{(0)} \approx 44$ K, while for Nb-290 samples the corresponding differences are $T_p^{(2)}-T_p^{(0)} \approx 22$ K and $T_h^{(2)}-T_h^{(0)} \approx 20$ K. It is easy to see that the ratio of these differences deviates very strongly from formula (9). Thus the shift of the peak temperature and the change of the peak width caused by the change in impurity concentration cannot be interpreted as being a consequence of additional statistical scatter of the activation energy of the relaxators.

The above conclusion compels us to seek the cause of the observed impurity effect in an influence of the impurity concentration on the parameter $\tau_0$. Such an influence is inherent to a number of mechanisms of dislocation relaxation,[19–25] and it is therefore quite natural to make that conjecture. However, it is difficult to check this experimentally because of the need to take into account the impurity effect against the background of an appreciable statistical scatter in the values of $U$.

### 4.2. New method of obtaining empirical estimates for the attempt period $\tau_0$ in crystals with different defect structures

A numerical analysis of expression (6) for $\overline{\delta}(\theta,\Omega,d)$ showed that there exists a possibility of obtaining empirical estimates for the parameter $\Omega=(\omega\tau_0)^{-1}$ at arbitrary values of $d$. These estimates are based on the recording of the characteristic temperatures $T_k^{(\mp)}$ introduced at the end of Sec. 3, which correspond to the inflection points on the temperature dependence of the decrement of vibrations.

The dimensionless temperatures $\theta_k^{(\mp)}$ are maxima and minima of the derivative $\partial F_1(\theta,\Omega,d)/\partial\theta$, and in the presence of scatter in the activation energies their values depend on the dispersion parameter $d$. The use of numerical methods allows one to determine both the values of the temperatures $\theta_k^{(\mp)}$ and the values of the extrema of the derivative $[\partial F_1(\theta,\Omega,d)/\partial\theta]_{\theta=\theta_k^{(\mp)}}$ at different values of the parameters $\Omega$ and $d$ (Figs. 4 and 5). As we see from these figures, those characteristics of the peak have a very substantial dependence on the dispersion parameter $d$. At the same time, as a result of a numerical analysis we have established an interesting property of the function $F_1(\theta,\Omega,d)$ which we have been unable to obtain analytically: the ratio of the extrema

$$K=\left|\frac{\max \partial F_1(\theta,\Omega,d)/\partial\theta}{\min \partial F_1(\theta,\Omega,d)/\partial\theta}\right|, \tag{10}$$

which is formally a function of two parameters, has an extremely strong dependence on the frequency parameter $\Omega$ but is practically independent of the dispersion parameter $d$ (Fig. 6). In experiments, as a rule, the inequality $\Omega=(\omega\tau_0)^{-1} \gg 1$ holds, which corresponds to the inequality $\ln\Omega \geqslant 2$. For such values of the frequency parameter the graph of the func-

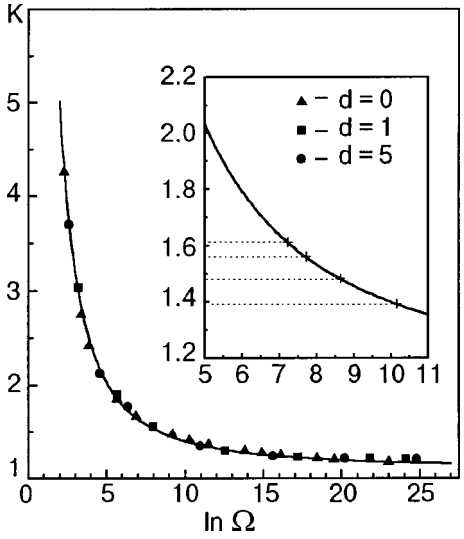


FIG. 6. Dependence of the dimensionless parameter $K(\Omega)$ characterizing the shape of the acoustic relaxation peak (6) on the inverse dimensionless frequency $\Omega$ (results of a numerical analysis); the solid line shows the analytical approximation (11). The inset shows a fragment of this graph, corresponding to the interval of the actual values of $\ln \Omega$ for the conditions of our experiment (see Table II); the dotted lines denote $K$ values obtained in the analysis of the experimental data.

tion $K=K(\Omega)$ obtained by numerical methods admits the following simple analytical approximation to an accuracy of the order of 2%:

$$K(\Omega)=1.1+\frac{14}{0.4+(\ln\Omega)^{5/3}}. \tag{11}$$

Thus by recording the peak on the $\delta_{\exp}(T)$ curve and performing a numerical differentiation, we acquire the capability of finding the values of $K(\Omega)$ for the different structural states. By comparing these values with the plot in Fig. 6 or with formula (11), we can easily estimate the empirical value of $\tau_0$.

We note that in the general case the attempt period $\tau_0$ can be a comparatively weak (power-law) function of temperature and can, together with the activation energy $U_0$, exhibit some statistical scatter. The method of determining $\tau_0$ proposed in this Section neglects these circumstances, since their influence on the parameters of the low-temperature peaks of the internal friction can be treated as being relatively weak against the background of effects governed by the argument of the exponential function in the expression (1) for the relaxation time.[13]

#### 4.3. Quantitative comparison of the experimental data with the theoretical dependences

In our experiments the data needed to carry out the procedure described above were obtained for the absorption peaks in polycrystalline samples during the first cooling and in the single-crystal sample Nb-37 during the first heating; the corresponding values of $K_{\exp}$ are given in Table II. In the other cases the large shift of the top of the peak and the broadening of the peak on the high-temperature side did not allow us to estimate the position of the inflection point on the high-temperature slope of the peak.

Having values for the vibrational frequency $\omega=2\pi f$ and $K_{\exp}$ for each of the samples (see Table II), we can easily use the graph in Fig. 6 or formula (11) to obtain empirical estimates of $\tau_0$ (Table II). Using these estimates and a test value of $U_0$, we can with the aid of numerical methods choose values of $d$ and $C_r\Delta_0$ for the corresponding samples and experimental conditions (cooling, heating) and compare the experimental dependence of $\delta_{\exp}(T)-\delta_{bg}$ with the temperature dependence of the function $\overline{\delta}=C_r\Delta_0F_1(\theta,\Omega,d)$. The result of such a comparison is shown in Fig. 1a. It turned out that the peaks recorded during the first cooling of the polycrystalline samples correspond to a single value of the activation energy, $U_0=0.15$ eV, with zero dispersion parameter, and the attempt period $\tau_0$ systematically decreases with increasing impurity concentration.

Turning to an analysis of the absorption peaks recorded during the first heating of the polycrystalline samples and the single crystal Nb-10000, in the absence of experimental data on $K(\Omega)$ one can treat $\tau_0$ together with $d$ and $C_r\Delta_0$ as adjustable parameters and, by varying them, try to fit the function $\overline{\delta}=C_r\Delta_0F_1(\theta,\Omega,d)$ to the experimental points $\delta_{\exp}(T)-\delta_{bg}$. Here it is natural to start with the values of $\tau_0$ obtained from analysis of the peaks recorded during the first cooling for the corresponding impurity concentrations. The results for the case of the polycrystalline samples are shown in Fig. 1b, and the empirical values of $\tau_0$, $d$, and $C_r\Delta_0$ for these peaks are given in Table II. It turns out that the idea that the value of $\tau_0$ remains the same on going from cooling to heating is confirmed by the results of a computer analysis, but an extremely large statistical scatter appears in the values of the activation energy ($d\approx 2$).

An analogous fitting procedure can also be done in an analysis of the absorption peak recorded during the first heating of the single crystal Nb-10000 (see Fig. 2 and Table II).

#### 4.4. Dislocation mechanism for the relaxation resonance

Of all the acoustic relaxation mechanisms described in the literature, our experimental data corresponds best to a mechanism of thermally activated nucleation of pairs of kinks on dislocation lines lying in the valleys of the Peierls relief.[20–25] Relaxation due to kink pairs was originally proposed by Seeger for interpreting the low-temperature peaks of the internal friction observed by Bordoni in a study of fcc metals.[20,26] Later this mechanism was successfully applied to an analysis of the $\alpha$ peaks in bcc metals as well.[24,27] For this mechanism the role of the activation energy is played by $U_0=2W_k$, the energy required for the formation of two kinks of opposite sign, and with energies $W_k$, on a dislocation line. The energy characteristics of kinks on dislocations lying in the preferred slip planes in typical bcc metals, of which niobium is one, have been studied in detail both in different physical experiments and by the numerical methods of molecular dynamics. These studies have yielded the characteristic estimates $U_0=2W_k\sim 0.1-0.2$ eV. The value found in the present study, $U_0=0.15$ eV, falls in this interval and thus provides the first serious justification for invoking the mechanism of nucleation of kink pairs for interpreting the internal friction peak investigated in this paper.

Previously, in an analysis of this peak we called atten-

tion to two more features that are evidence of its connection with dislocation processes:[13]

—the high sensitivity of the temperature location and height of the peak to external influences (thermoelastic stresses, preliminary plastic deformation, etc.);

—the anomalously large values of the attempt period, $\tau_0 \sim 10^{-9}-10^{-10}$ s, in comparison with the period of atomic vibrations.

The present study of the influence of impurities on the parameters of the $\alpha$ peak in niobium has provided additional arguments in support of the view that this peak is due to thermally activated processes of kink pair nucleation. It is known that impurities can influence this process in two ways. First, the elastic fields existing around impurity atoms should, generally speaking, give rise to certain statistical deviations of the activation energy from its value $U_0 = 2W_k$ in the absence of impurities. This effect has a substantial influence on the kinetics of the motion of dislocations through Peierls barriers only if the impurity concentration is sufficiently high and the impurity atoms are sufficiently ''powerful'' force centers deforming the crystal lattice. In a study of the plastic flow of concentrated alloys based on a number of bcc metals[28–32] and tin,[33] such an influence of impurities was manifested as an impurity softening effect. However, it is not necessary to invoke this effect for interpreting the results of our experiments on the influence of impurities on the $\alpha$ peak of acoustic relaxation, since the impurity concentration does not affect the empirical values of the parameter $d$ (see the first three rows in Table II).

Impurity atoms also act as pinning centers for dislocation lines, dividing them into segments of finite length $L_i(c)$, which depends substantially on the impurity concentration $c$: the characteristic length of the segments decreases with increasing concentration. The pinning points of the segments limit the trip lengths of the kinks that arise on the dislocation lines and can thereby have a strong influence on the kinetics of the movement of dislocations between neighboring valleys of the Peierls relief. The kinetic theory of the nucleation and relaxation of kink pairs on dislocation segments of finite length was developed by Engelke in a series of papers.[22,23] Unfortunately, these papers do not contain simple analytical expressions giving the explicit dependence of the relaxation time $\tau(T, L_i)$ and the temperature location $T_p(L_i)$ and height $\delta_{\max}(L_i)$ of the corresponding internal friction peak on the mean length $L_i$ of the segments (the dependences are given only in the form of graphs). The main qualitative results of those papers reduce to two conclusions:

—the attempt period $\tau_0$ in the expressions for the relaxation time depends substantially on the length $L_i$ of the segment; it increases with increasing $L_i$ and has a typical value much larger than the periods of the atomic vibrations;

—the internal friction peak increases and shifts to higher temperatures as $L_i$ increases.

It follows from general arguments that the average characteristic length of a dislocation segment in a solid solution is related to the impurity concentration as $L_i \cong ac^{-\nu}$, where $a$ is the lattice parameter and $1 < \nu < 2$ is a numerical parameter. It can therefore be stated that the Engelke theory[22,23] provides a qualitative explanation for all of the main features (reflected in Table II) of the concentration dependence of the parameters of the $\alpha$ peak in niobium. In particular, the method we have proposed here and in Refs. 13 and 14 for obtaining empirical estimates for the parameters $\tau_0$, $U_0$, $d$, and $C_r\Delta_0$, which determine the relaxation time and the ''strength'' of the relaxation process responsible for the peak, has allowed us to establish that the activation energy is insensitive to changes in the impurity concentration of the niobium samples at relatively low impurity concentrations and that the parameters $\tau_0$ and $\delta_{\max} = C_r\Delta_0$ depend strongly on the impurity concentration (Table II, Fig. 3b), in qualitative agreement with the predictions of the theory.[22,23]

Thus the estimates obtained for the values of the activation energy $U_0 \approx 0.15$ eV and the characteristic values of the attempt period $\tau_0 \sim 10^{-9}-10^{-10}$ s, the previously established sensitivity of $d$ and $C_r\Delta_0$ to the thermoelastic stresses, and the dependence of $\tau_0$ and $C_r\Delta_0$ on the impurity concentration ovserved in the present study allow us to conclude with a high degree of certainty that the $\alpha$ peak of acoustic relaxation in niobium is due to a resonant interaction of the acoustic vibrations with the process of thermally activated nucleation of kink pairs on dislocation segments lying in the valleys of the Peierls relief.

## 5. CONCLUSION

In this paper we have continued our detailed experimental study and theoretical analysis of the $\alpha$ peak of the internal friction in niobium, an endeavor which was begun in Ref. 13. At the $\sim$80 kHz elastic vibrational frequencies realized in our experiments, this peak was observed at moderately low temperatures, 200–250 K. This peak is characterized by a high structural sensitivity: we have previously detected a substantial shift in the position of the peak on the temperature axis and a change in its height and width under thermoelastic stresses and also as a result of a preliminary plastic deformation and low-temperature recovery.[13] In this study analogous effects were recorded with changing impurity concentrations in the samples.

The theoretical interpretation of the properties of the peak are based on the assumption that it is due to a thermally activated relaxation process of a dislocation nature, with a statistical description of this process. The proposed theory takes into account the dependence of the activation parameters (activation energy and attempt period) on the impurity concentration and on the characteristic value and statistical scatter of the internal stresses, which are taken into account by the choice of a special statistical distribution function for the activation energy. The proposed method and algorithm for numerical analysis of the experimental data make it possible to obtain empirical estimates of the values of the activation energy, its variance, the attempt period, and the strength of the relaxation for different structural states of the samples.

A statistical analysis of the entire set of experimental data obtained in the study of the $\alpha$ peak in niobium has led to the conclusion that this peak is a consequence of the resonant interaction of elastic vibrations with the process of thermally activated nucleation of kink pairs on the dislocation segments lying in the valleys of the Peierls relief. We have obtained empirical estimates of the parameters characterizing this process. Qualitative agreement is found between the ex-

perimentally determined properties of the $\alpha$ peak in niobium and Engelke's proposed kinetic theory of the nucleation and relaxation of dislocation kinks.[22,23]

The authors thank S. N. Smirnov for helpful discussions and advice concerning the problems touched upon in this paper.

*E-mail: palval@ilt.kharkov.ua

[1] L. J. Bruner, Phys. Rev. **118**, 399 (1960).
[2] R. H. Chambers and J. Schultz, Acta Metall. **8**, 585 (1960).
[3] R. H. Chambers and J. Schultz, Phys. Rev. Lett. **6**, 273 (1961).
[4] P. G. Bordoni, M. Nuovo, and L. Verdini, Phys. Rev. **123**, 1204 (1961).
[5] J. Schultz and R. H. Chambers, Bull. Am. Phys. Soc. **9**, 214 (1964).
[6] E. J. Kramer and C. L. Bauer, Phys. Rev. **163**, 407 (1967).
[7] F. M. Mazzolai and M. Nuovo, Solid State Commun. **7**, 103 (1969).
[8] R. Chambers, in *Physical Acoustics*, Vol. II, Part A, edited by W. P. Mason [Academic Press, New York (1965); Mir, Moscow (1969)].
[9] R. Klam, H. Schultz, and H.-E. Schaefer, Acta Metall. **27**, 205 (1979).
[10] N. Kuramochi, H. Mizubayashi, and S. Okuda, Scr. Metall. **14**, 1047 (1980).
[11] V. V. Zoninashvili, I. A. Naskidashvili, U. Messerschmidt, V. A. Melik-Shakhnazarov, N. M. Yastrebov, and L. M. Kolesnikova, Phys. Status Solidi A **75**, K205 (1983).
[12] N. Kuramochi, H. Mizubayashi, and S. Okuda, Phys. Status Solidi A **104**, 453 (1987).
[13] V. D. Natsik, P. P. Pal-Val, L. N. Pal-Val, and Yu. A. Semerenko, Fiz. Nizk. Temp. **25**, 748 (1999) [Low Temp. Phys. **25**, 558 (1999)].
[14] V. D. Natsik, P. P. Pal-Val, L. N. Pal-Val, and Yu. A. Semerenko, Fiz. Nizk. Temp. **26**, 711 (2000) [Low Temp. Phys. **26**, 522 (2000)].
[15] B. Fellmuth, H. Maas, and D. Elefant, Metrologia **21**, 169 (1985).
[16] P. P. Pal'-Val', V. D. Natsik, and L. N. Pal'-Val', Fiz. Nizk. Temp. **21**, 647 (1995) [Low Temp. Phys. **21**, 505 (1995)].
[17] P. P. Pal'-Val' and H.-J. Kaufmann, Fiz. Nizk. Temp. **9**, 325 (1983) [Sov. J. Low Temp. Phys. **9**, 163 (1983)].
[18] V. D. Natsik, P. P. Pal'-Val', and S. N. Smirnov, Akust. Zh. **44**, 640 (1998) [Acoustical Phys. (Moscow) **44**, 553 (1998)].
[19] A. V. Granato and K. Lücke, J. Appl. Phys. **27**, 583 (1956).
[20] A. Seeger, Philos. Mag. **1**, 651 (1956).
[21] A. D. Brailsford, Phys. Rev. **122**, 778 (1961).
[22] H. Engelke, Phys. Status Solidi **36**, 231 (1969).
[23] H. Engelke, Phys. Status Solidi **36**, 245 (1969).
[24] A. Seeger and C. Wüthrich, Nuovo Cimento **33**, 38 (1976).
[25] F. Louchet, L. P. Kubin, and D. Vesely, Philos. Mag. **39**, 433 (1979).
[26] D. Niblett, in *Physical Acoustics*, Vol. III, Part A, edited by W. P. Mason [Academic Press, New York (1966); Mir, Moscow (1969), p. 99].
[27] A. Seeger and P. Schiller, in *Physical Acoustics*, Vol. III, Part A, edited by W. P. Mason [Academic Press, New York (1966); Mir, Moscow (1969), p. 428].
[28] A. Urakami and M. E. Fine, in *Proceedings of the First International Conference on the Mechanical Behavior of Materials*, Kyoto, Japan (1971).
[29] B. V. Petukhov, Fiz. Tverd. Tela (Leningrad) **13**, 1445 (1971) [Sov. Phys. Solid State **13**, 1204 (1971)].
[30] A. Sato and M. Meshii, Acta Metall. **21**, 753 (1973).
[31] L. P. Kubin, F. Louchet, J. P. Peyrade, P. Groh, and P. Cottu, Acta Metall. **27**, 343 (1979).
[32] H. Suzuki, in *Dislocations in Solids*, Vol. 4: *Dislocations in Metallurgy*, North-Holland, Amsterdam (1979), p. 191.
[33] V. P. Soldatov, V. D. Natsik, A. N. Diulin, and G. I. Kirichenko, Fiz. Nizk. Temp. **26**, 214 (2000) [Low Temp. Phys. **26**, 160 (2000)].

Translated by Steve Torstveit

## SHORT NOTES

# Thermal conductivity of fullerite $C_{60}$ crystals at low temperatures

V. B. Efimov, L. P. Mezhov-Deglin,[a] R. K. Nikolaev, and N. S. Sidorov

*Institute of Solid State Physics, Russian Academy of Sciences, 142432 Chernogolovka, Moscow District, Russia*

(Submitted November 21, 2000)
Fiz. Nizk. Temp. **27**, 558–560 (May 2001)

The thermal conductivity $\kappa$ of extended crystals of fullerite $C_{60}$ with transverse dimensions $L$ of the order of a few millimeters is measured at low temperatures (down to 0.6 K). It is found that in the range from 7 to 0.6 K the temperature dependence of the thermal conductivity of the better of the samples is close to cubic, $\kappa(T)\sim T^3$, and the effective phonon mean free path estimated from the measured thermal conductivity and the published value of the specific heat of fullerite [J. R. Olson *et al.*, Science **259**, 1145 (1993)] has a value ($l_p \approx 0.6$ $\mu$m) that is practically independent of temperature and much less than $L$, i.e., the phonon mean free path is limited by strong scattering on defects in the bulk of the sample. © *2001 American Institute of Physics.* [DOI: 10.1063/1.1374729]

The results of measurements of the thermal conductivity of fullerite $C_{60}$ crystals below room temperature have been discussed previously in Ref. 2 (measurements in the range from ~290 to 30 K) and 3 (working interval 240–8 K). It was found that the thermal conductivity of the crystal in the fcc phase below 300 K is practically independent of temperature and increases abruptly near 260 K in the region of the phase transition of fullerite to the simple cubic (sc) phase. On further decrease of the temperature the thermal conductivity of the crystal in the sc phase increases, passes through a rather flat maximum at $T \approx 20$–15 K, and then decreases in proportion to the change in specific heat of the samples.

In this paper we present the results of measurements of the thermal conductivity of fullerite $C_{60}$ crystals at lower temperatures (in the interval 7–0.6 K). As in our previous study,[3] the fullerite crystals were grown from the gas phase in vacuum. A preliminary triple distillation of the initial 99.99% pure $C_{60}$ powder in high vacuum made it possible to remove traces of the solvents and to decrease the $C_{70}$ impurity content in the grown crystals. The thermal conductivity measurements were made by the standard method of a steady heat flux in a refrigerator containing liquid $^3$He. The initial samples were in the shape of polyhedra up to 10 mm long, with a transverse cross-sectional area of several square millimeters. The lower end of the sample was glued to a copper cold finger connected to a vessel containing $^3$He. A resistance heater was glued to the upper end of the sample. The temperature distribution along the sample with the heater turned on was measured by two carbon resistance thermometers calibrated according to the vapor pressure of liquid helium. Preliminary results of these studies were presented in a talk at the 32nd All-Russia Conference on Low Temperature Physics (LT-32).[4]

The results of the thermal conductivity measurements of the better of the samples, which was 6 mm long and had a transverse cross-sectional area of 6 mm$^2$, are given in Fig. 1 (▲). For illustration the temperature dependence of the thermal conductivity $\kappa(T)$ of one of the crystals investigated in Ref. 3 is also shown. The straight lines correspond to dependences $\kappa(T)\sim T^2$ and $T^3$. We see that in the temperature interval 7–0.6 K the experimental data are better described by a dependence of the type $\kappa(T)\sim T^3$. By extrapolating the results of these measurements to the higher-temperature region, it is easy to see that the thermal conductivity of this sample at $T \geqslant 10$ K is an order of magnitude higher than that of the samples studied previously. This may be due to both an improvement in the degree of perfection and to a lowering of the concentration of impurity fullerene $C_{70}$ in the initial sample, and also to purely technical causes — perfecting of the technique for mounting the sample in the apparatus and, as a consequence, lowering of the concentration of defects arising in the sample, which is fixed on the cold finger, during thermocycling. Unfortunately, the region of measure-

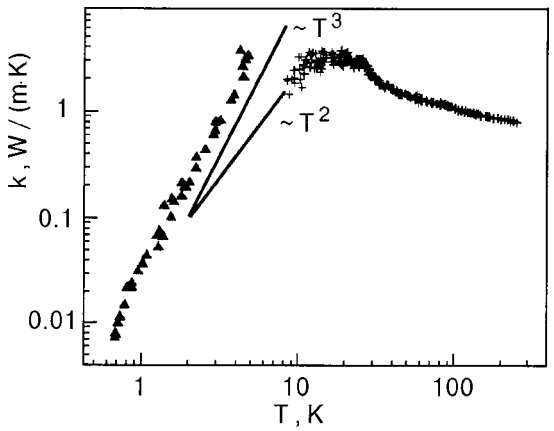


FIG. 1. Thermal conductivity of fullerite crystals: ▲ — data of the present study; + — measurements of Ref. 3. The solid lines correspond to the dependences $\kappa(T)\sim T^2$ and $T^3$.

 

ment of the thermal conductivity in the $^3$He refrigerator is limited to temperatures $T \leqslant 7$ K, and to replace the thermometers and move the fullerite sample to the flow-through cryostat used previously would be very difficult, since fullerite is rather brittle at room temperatures and the indicated procedures are usually accompanied by strong deformation or cracking of the sample.

It was observed in Refs. 2 and 3 that the behavior of the thermal conductivity of fullerite crystals below room temperature can be described in the framework of the standard phonon model of heat transfer in nonconducting crystals. Therefore, by employing the simple gas-kinetic formula

$$\kappa(T) = \frac{1}{3} C(T) v_p^l(T),$$

one can use the results of thermal conductivity measurements to assess the behavior of the effective phonon mean free path $l_p$ in a sample. Here $C(T)$ is the specific heat of the sample, and $v$ is the mean velocity of sound. It is seen in Fig. 1 that in the interval 7–0.6 K the dependence $\kappa(T)$ is close to cubic. From the experimental data reported in Ref. 1, for example, the temperature dependence of the specific heat of fullerite $C_{60}$ in this temperature interval is also close to cubic, $C(T) \sim T^3$. However, the samples studied in Ref. 1 were fine-grained and of much lower purity. Therefore, at our request, A. V. Pal'nichenko at the Institute of Solid State Physics of the Russian Academy of Sciences made measurements of the specific heat of $C_{60}$ crystals in the temperature interval 30–4 K, using samples from the same batch as in Ref. 3. Pal'nichenko's results are practically the same as those in Ref. 1.

Using, for the sake of definiteness, the data of Ref. 1 (the Debye temperature of the crystal in the sc phase was $\Theta \sim 80$ K, so that the mean sound velocity was $v \sim 10^5$ cm), it is easily estimated that in the temperature range $T = 7$–0.6 K the effective mean free path of the phonons in the sample of Fig. 1 reaches $\sim 0.6$ $\mu$m and is practically independent of temperature. Consequently, the maximum values of the phonon mean free paths, even in the better of our samples, is three orders of magnitude smaller than the characteristic dimensions of the sample, $l_p \ll L \sim 1$ mm, and the main role is played by scattering of thermal phonons on defects in the bulk of the sample.

In Refs. 2 and 3 it was pointed out that the maximum phonon mean free path in the sc phase of the fullerite $C_{60}$ crystal can be limited by scattering on frozen-in orientational defects. Near the point of the fcc–sc phase transition at $T \leqslant 260$ K the equilibrium concentration of orientational defects, which arise because of thermal disturbances of the mutual orientation of the fullerene molecules located in neighboring sites of the sc crystal lattice, is close to $x_R \sim 0.5$. As the temperature is lowered, the time $\tau_R$ required for establishing orientational equilibrium in the crystal increases exponentially. Judging from the observed[2] increase in the thermal conductivity of the sample with annealing time at a constant temperature $T = 85$ K, the time $\tau_R$ reaches $\sim 300$ min, so that below 80 K at any reasonable rate of cooling of the sample (of the order of $10^{-2}$ deg/min or faster) the concentration of frozen-in orientational defects in the sample, $x_{FR} \approx x_R(85\text{K})$, is of the order of a few percent, i.e., one can speak of the formation of an orientational glass state in the bulk of the crystal.

It should be noted that the question of the mechanisms of relaxation of the thermal perturbations in the orientational glass and, accordingly, of the behavioral features of the thermal conductivity of fullerite crystals at low temperatures requires a separate theoretical study. In comparing the predictions of the theory with the experimental $\kappa(T)$ curve it must be taken into account that under real conditions the phonon mean free path can be limited by scattering not only on orientational defects but also on nonequilibrium defects such as vacancies, dislocations, and grain boundaries, which can arise in a rigidly clamped crystal (glued to the cold finger) under the influence of the mechanical stresses that arise upon cooling below the fcc–sc phase transition (this transition is accompanied by an $\sim 1\%$ jump in the molar volume). That the defects arising under mechanical stresses have a strong influence on the thermal conductivity of fullerite can be inferred, for example, from the results[5] of measurements of the thermal conductivity of samples prepared by pressing (compacting) of fine-grained powder of pure $C_{60}$ at pressures $P \leqslant 3$ kbar. Below 100 K the thermal conductivity of the samples compacted from the powder was one or two orders of magnitude lower than that of the crystals in Fig. 1. Moreover, their thermal conductivity is practically independent of temperature in the interval 90–15 K and decreases slowly for $T < 15$ K, i.e., the temperature dependence of the thermal conductivity of the compacted samples was close to the well known behavior of the thermal conductivity of amorphous materials or glasses below room temperature (see, e.g., the monograph by Berman[6]). Therefore, it would be extremely interesting to study the relative sizes of the contributions to the thermal resistance of fullerite from the scattering of phonons on defects arising under the influence of mechanical stresses and from scattering on orientational defects. The authors are grateful to Yu. A. Osip'yan for support of this research and to A. V. Pal'nicheko for providing the results of specific heat measurements on $C_{60}$ crystals prior to their publication, and also to A. V. Lokhov and M. K. Makova for assistance in making the measurements. This study was supported in part by the project ''Deformation-2'' of the GNTP of the Ministry of Industry, Science, and Technology of the Russian Federation, ''Topical Problems in Condensed-Matter Physics,'' subtopic ''Fullerenes and Atomic Clusters.''

[a)]E-mail: mezhov@issp.ac.ru

[1] J. R. Olson, K. A. Tropp, and R. O. Pohl, Science **259**, 1145 (1993).
[2] R. C. Yu, N. Tea, M. B. Salamon *et al.*, Phys. Rev. Lett. **68**, 2050 (1992).
[3] V. B. Efimov, L. P. Mezhov-Deglin, and R. K. Nikolaev, JETP Lett. **65**, 687 (1997).
[4] V. B. Efimov, L. P. Mezhov-Deglin, R. K. Nikolaev, and N. S. Sidorov, *Abstracts of the 32nd All-Russia Conference on Low Temperature Physics (LT-32)* [in Russian], Kazan, October 3–6, 2000, p. 123.
[5] V. B. Efimov, L. P. Mezhov-Deglin, and R. K. Nikolaev, Mol. Mater. **11**, 17 (1998).
[6] R. Berman, *Thermal Conduction in Solids* [Clarendon Press, Oxford (1976); Mir, Moscow (1979)].

Translated by Steve Torstveit

## LETTER TO THE EDITOR

# On the nonmonotonic dependence of the critical temperature of the superconducting transition on the carrier density in fullerite $C_{60}$

V. M. Loktev*

*N. N. Bogolyubov Institute of Theoretical Physics, National Academy of Sciences of Ukraine, ul. Tetrologicheskaya 14-b, 03143 Kiev, Ukraine*
(Submitted January 30, 2001)
Fiz. Nizk. Temp. **27**, 561–564 (May 2001)

A simple qualitative explanation for the bell-shaped form of the functions $T_c(n_f)$ in solid $C_{60}$ is proposed ($T_c$ is the critical temperature of the superconducting transition, and $n_f$ is the number of carriers (fermions)—electrons or holes—per molecule). This explanation is based on the many-fold degeneracy of the initial fullerene molecular states from which the conduction and valence bands are formed and the interaction of the carriers with Jahn–Teller intramolecular vibrations. © *2001 American Institute of Physics.* [DOI: 10.1063/1.1374736]

**1.** A recent experimental paper by Schön, Kloc, and Battlogg[1] reported the observation of rather unexpected behavior of the critical temperature $T_c$ of the superconducting transition in solid fullerite, specifically: the value of $T_c$ of fullerite with a hole ($p$) type of conductivity was found to be 52 K, significantly higher (see reviews[2,3]) than in $A_3C_{60}$ fullerides (A is an alkali or alkaline-earth metal) having an electronic ($n$) type of conductivity. Apparently the value of $T_c$ achieved in Ref. 1 is the highest known to date for materials not of the high-$T_c$ superconductor (HTSC) family. Moreover, the same samples of fullerite but with $n$-type conductivity manifested superconducting properties below a different $T_c \approx 11$ K,[1)] which is lower by almost a factor of 5.

The change of the sign of the carriers in Ref. 1 was achieved by a novel transistor technique[1] that permits the injection of charges of a given sign, thereby regulating the type of conductivity depending on the direction of the electric field applied to the sample. Here the density $n_f$ of ''injected'' fermions was determined by the value of the applied electric field. The possibility of varying $n_f$ led to a result that is, at first glance, even stranger: the carrier-density dependence $T_c(n_f)$ in pure (i.e., undoped) fullerite exhibited the bell-shaped form that is typical for many HTSCs, both for $n_f = n_e$ and for $n_f = n_h$. However, the difference from HTSCs is that in the latter, as a rule, $n_f \approx 0.1-0.2$ (see, e.g., the review[5]), whereas in solid $C_{60}$ the maximum of $T_c(n_e)$ occurs at $n_e \approx 3$ amd that of $T_c(n_h)$ at $n_h \approx 3.5-4$ carriers per cell (or, equivalently, per fullerene molecule).

In analyzing their truly remarkable measurements, the authors of Ref. 1, working from the numerical results of Refs. 6 and 7, tried to find possible causes of this surprising and different behavior of conducting $C_{60}$ crystals with opposite signs of the carriers. Here the main factor, according to Ref. 1, is the occupation of the respective (degenerate) bands—the conduction band in the fullerides or $n$-fullerite and the valence band in $p$-fullerite. Nevertheless, their interpretation left out certain essential facts which we call attention to in this paper.

**2.** It is known (see Refs. 1–3) that the conduction band of fullerite is formed from the threefold degenerate $t_{1u}$ states of the $C_{60}$ molecule, while the valence band is formed from the fivefold degenerate state $h_u$. In a cubic crystalline field they behave differently:[8] the triplet state remains unchanged (if one ignores the shift of the term), i.e., degenerate, while the $h_u$ state decomposes into a doublet $e_u \equiv \{\varepsilon_u, \theta_u\}$ and a triplet $t_{2u}$ (interestingly, the first of these is also unsplit by the trigonal component of the crystalline field, which is capable of causing a weak distortion of the spherical shape of fullerene to a uniaxial ellipsoid). This splitting in each molecule may be appreciable, since it is due to the Coulomb field of the molecules surrounding it, which on average have a charge of the same sign. In essence the situation is similar to the splitting of the (also fivefold degenerate) $3d$ state of the transition metal ions in the electric field of the ligands. In fullerite, however, the role of the ligands is played by the same ionized molecules, whose charge (in contrast to the charge of the ligands) is not constant but is determined by the electric field applied to the sample. In fields of different direction and strength the charge can vary from 0 (in the absence of field) to $-3$ (complete filling of the $t_{1u}$ states) or $+10$ (completely emptying of the $h_u$ shell). Several cases of the occupation by holes of the ground states (with allowance for Hund's rule) of ionized fullerene are shown in Fig. 1, in which, by analogy with transition metals, it is assumed that the lower of the split states in the crystal is the triplet.[2)]

The gradual filling of the hole states corresponds to a certain direction of the external electric field, which might be called the ''acceptor'' direction. In the oppositely directed, ''donor'' field, the electrons occupy the conduction band. Both types of occupation take place, as we have said, without the use of any sort of dopants.

**3.** It should be mentioned that the analogy with the $3d$ states is in general not complete. First, the $d$ electrons ordinarily remain localized (in any case, for an integer valence), and the corresponding substances are magnetic nonmetals. Their transition to the metallic state is accompanied by the

 

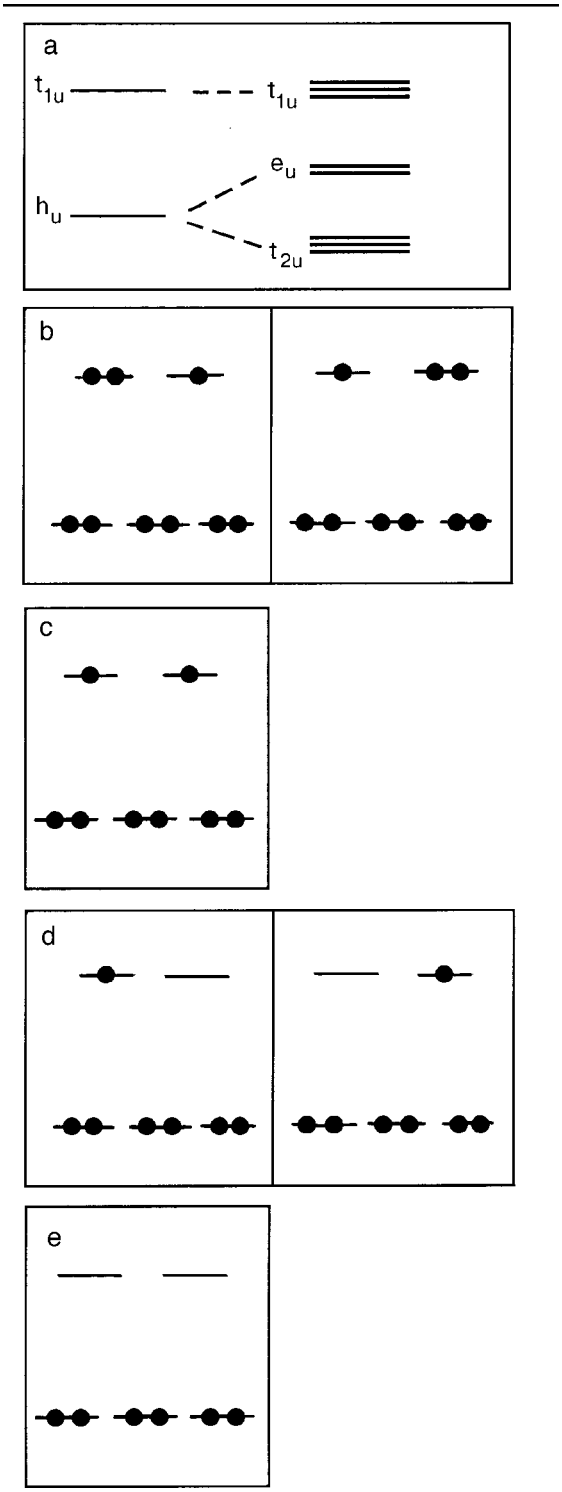


FIG. 1. Qualitative picture of the splitting of the molecular term $h_u$ in the cubic crystalline field of fullerite (a) and several states of fullerene corresponding to its different valences: b—one hole in the $e_u$ state (orbital doublet, configuration $h_u^9$); c—two holes (singlet, $h_u^8$); d—three holes (doublet, $h_u^7$); e—four holes (singlet, $h_u^6$).

addition of excess charges into the initial insulating state in order to ''avoid'' the strong intra-atomic repulsion, which is taken into account in the Hubbard model, for example. Fullerene is not a point object, and several excess valence electrons (holes) in its shells (in the presence of the 60 ''landing sites'') can occupy $\pi$ states on different C atoms, avoiding direct contact with one another. Therefore, the Hubbard correlation in $C_{60}$, while possibly not small, does not prevent the metallization of the fullerite for any $n_f$, provided that the corresponding bands are not completely filled.

As shown in Fig. 1, the valence band will be formed from the states of the $e_u$ doublet as long as $n_h \leqslant 4$. Here (under otherwise equal conditions) it should be somewhat narrower than the triplet state, and this in itself promotes the enhancement of possible superconductivity in view of the increase of the corresponding density of holes states.[9] This is not the most important factor, however. More importantly, the singly (and positively) charged state (see Fig. 1b) is an orbital doublet, subject to Jahn–Teller (JT) distortion. And doublet states (such as, e.g., $3d^9$ in $Cu^{2+}$), as is well known,[8] are the most strongly interacting with the symmetry-lowering deformations of fullerene. For the hole states these JT ions are $C_{60}^+$ and $C_{60}^{3+}$, for which the dynamic JT effect begins to appear; it is described by the Hamiltonian[10]

$$H_{JT}=\sum_{\mathbf{n},\sigma}\sum_{\lambda_1,\lambda_2}\chi_{\mathbf{n}}^{\lambda_1\lambda_2}a_{\mathbf{n}\lambda_1\sigma}^{+}a_{\mathbf{n}\lambda_2\sigma}u_{\mathbf{n}}^{\lambda_1\lambda_2} \tag{1}$$

and pertains to each molecule. In Eq. (1) $\chi_{\mathbf{n}}{}^{\lambda_1\lambda_2}$ is the matrix element that mixes the different components $\lambda_1 \neq \lambda_2$ $(=\varepsilon_u, \theta_u)$ of the $e_u$ doublet; $u_{\mathbf{n}}^{\lambda_1\lambda_2}$ is the coordinate of the normal JT oscillations (in principle there may be several of these oscillations[2,10,11]); $a_{\mathbf{n}\lambda\sigma}^{+}$ is the creation operator for a hole in state $\lambda$ with spin $\sigma$ on molecule $\mathbf{n}$. The use of (1) as the coupling operator of the carriers with the JT phonons is justified in that the width of the electron bands in fullerite is not very large, so that the constant $\chi_{\mathbf{n}}^{\varepsilon_u\theta_u}$ can be considered small.

It should be mentioned that while the width and structure of the conduction band of fullerite have been calculated and are sufficiently well known (see Refs. 12–15), there is as yet no such information available about its valence band, if one is asking about the presence of doublet–triplet splitting of the initial $h_u$ multiplet. However, at a qualitative level it can be stated that with increasing hole density $n_h$, which is controlled by the chemical potential, the $C_{60}$ molecule can be self-consistently charged, transitioning from one valence state to another. While the operator (1) corresponds to the intramolecular processes, the hopping operator corresponds to an intermolecular one, and the strongest distortion of the shape of the molecule (and, hence, the maximum value of the constant $\chi_{\mathbf{n}}^{\varepsilon_u\theta_u}$) should be expected when it transitions from the JT (orbitally degenerate) to the non-JT state. This conclusion has in essence been confirmed experimentally.[1]

Indeed, in the samples with *n*-type conductivity the sequence from one- to five-electron occupation occurs via the following chain of molecular valence states: triplet–triplet–singlet–triplet–triplet, while in the *p*-type samples (see Fig. 1) the sequence is doublet–singlet–doublet–singlet (if one has only the $e_u$ doublet in mind). In other words, in the first case the strongest superconducting properties should be exhibited by the samples with densities near $n_e \approx 3$, for which the dynamic JT effect is operative, and in the second case practically any densities will do: both $n_h \approx 1-2$, when the largest growth of $T_c(n_h)$ occurs (and is observed), and $n_h \approx 3-4$, when it reaches a maximum and begins to fall off on

account of the filling of the band. Interestingly, in neither case does $T_c(n_f)$ follow the dependence of the density of states of the quasiparticle bands, so the latter must not be mainly responsible for the behavior of $T_c(n_f)$. A calculation of the actual value of the critical temperature for different $n_f$ can be done using the theory developed in Ref. 10, which takes into account the different mechanisms that increase $T_c$ in fullerite.

**4.** Of course, the arguments presented above cannot be regarded as a theory of superconductivity in fullerite $C_{60}$ with a *p*-type subsystem of carriers. One can only say that a study of the electronic states of this crystal should be based on a molecular approach, as, for example, in the theory of small-radius excitons, since such states in molecular crystals are to a large degree formed from states of the individual (noninteracting) molecules. In addition, one must use pseudospin tensor operators (see Refs. 16 and 17) in order to take into account to the fullest extent the many-electron character of the terms, the possibility of orbital ordering, and the interaction of the carriers with JT oscillations. We propose to develop such an approach in a separate paper. From this standpoint it would be of interest to investigate experimentally the *p*-type fullerite in higher acceptor fields in order to confirm (or refute) the conjecture of the splitting of the $h_u$ term and the existence of a valence band formed from the deeper, triplet states (for $n_h>4$).

This study was supported by grant NATO CP/UN/19/C/2000/PO and was done at the Physics Center of the University of Porto (Portugal), the attention and hospitality of whose coordinator, J. Lopes dos Santos, is gratefully acknowledged.

*E-mail: vloktev@bitp.kiev.ua

[1)] Interestingly, those same authors have used this technique to achieve metallization and to observe the superconducting state in many molecular crystals of the aromatic series, which are classic objects in the physics of Frenkel excitons (Ref. 4).

[2)] Although the ''ligand'' molecules in fullerite are positively charged and it would seem that the splitting should have the opposite sign, the electronic functions of fullerene are many-particle and odd, and their matrix elements have not yet been calculated. Besides, the adopted arrangement of the terms more likely corresponds to the observed picture (see below).

[1] J. H. Schön, Ch. Kloc, and B. Battlogg, Nature (London) **408**, 549 (2000).
[2] V. M. Loktev, Fiz. Nizk. Temp. **18**, 217 (1992) [Low Temp. Phys. **18**, 149 (1992)].
[3] O. Gunnarsson, Rev. Mod. Phys. **69**, 575 (1997).
[4] J. H. Schön, Ch. Kloc, and B. Battlogg, Nature (London) **406**, 704 (2000).
[5] V. M. Loktev, Fiz. Nizk. Temp. **22**, 3 (1996) [Low. Temp. Phys. **22**, 1 (1996)].
[6] I. I. Mazin, S. N. Rashkeev, V. P. Antropov, O. Jersen, A. I. Lichtenstein, and O. K. Andersen, Phys. Rev. B **45**, 5114 (1992).
[7] R. C. Haddon, T. Siegrist, R. M. Fleming, P. M. Bridenbaugh, and R. A. Laudise, J. Mater. Chem. **5**, 1719 (1995).
[8] A. Abragam and B. Bleaney, *Electron Paramagnetic Resonance of Transition Ions*, Clarendon Press, Oxford (1970).
[9] S. Erwin, in *Buckminsterfullerenes*, edited by W. E. Billups and M. A. Ciufolini, VCH, New York (1992), p. 217.
[10] V. M. Loktev and É. A. Pashitskiĭ, JETP Lett. **55**, 478 (1992); Zh. Éksp. Teor. Fiz. **103**, 594 (1993) [JETP **76**, 297 (1993)].
[11] M. Schlüter, M. Lannoo, M. Needels, and A. Baraff, Preprint ATT Bell Labs, New York (1992).
[12] M. L. Stanton and M. D. Newton, J. Chys. Chem. **92**, 2141 (1989).
[13] Y. Huang, D. F. R. Gilson, and I. S. Butler, J. Phys. Chem. **95**, 5723 (1991).
[14] J. H. Weaver, J. L. Martins, T. Komeda, Y. Chen, T. R. Ohno, G. H. Kroll, and N. Troullier, Phys. Rev. Lett. **66**, 1741 (1991).
[15] S. Saito and A. Oshiyama, Phys. Rev. Lett. **66**, 2637 (1991).
[16] V. M. Loktev and Yu. G. Pogorelov, Fiz. Nizk. Temp. **26**, 271 (2000) [Low Temp. Phys. **26**, 171 (2000)].
[17] Y. Tokura and N. Nagaosa, Science **288**, 462 (2000).

Translated by Steve Torstveit

## NEWS ITEMS

# 32nd Conference on Low Temperature Physics (Kazan, Russia, October 3–6, 2000)

V. G. Peschanskiĭ and É. Ya. Rudavskiĭ

*B. Verkin Institute for Low Temperature Physics and Engineering, National Academy of Sciences of Ukraine, pr. Lenina 47, 61103 Kharkov, Ukraine*

D. A. Tayurskiĭ

*V. I. Ul'yanov Kazan State University, Kazan, Russia*
(Submitted December 20, 2000)
Fiz. Nizk. Temp. **27**, 565–573 (May 2001)

[DOI: 10.1063/1.1374737]

The 32nd Conference on Low Temperature Physics was held on October 3–6, 2000 in Kazan, Russia under the auspices of the Scientific Council on Low Temperature Physics of the Russian Academy of Sciences, the Ministry of Science of the Russian Federation, the V. I. Ul'yanov Kazan State University, and the Physicotechnical Institute of the Kazan Research Center of the Russian Academy of Sciences. The conference was supported by the Russian Foundation for Basic Research, the NIOKR Foundation of the Tatarstan Academy of Sciences, and the Research–Education Center REC-007 of Kazan University.

For many years Kazan has been a world center of physical science, so it is not surprising that four of the 14 reports scheduled for the plenary sessions by the conference Organizing Committee, chaired by A. F. Andreev, the Vice-President of the Russian Academy of Sciences, were the work of Kazan physicists.

The participants in the conference included more than 200 scientists from Russia and the Commonwealth of Independent States as well as a number of well-known physicists from Great Britain, the USA, Slovakia, the Czech Republic, Poland, Finland, and Japan.

In addition to the 14 plenary reports, 85 reports were read at the four sectional sessions, and 180 were presented at poster sessions.

The best-represented sections were ''Superconductivity'' (102 reports) and ''Low Temperature Solid State Physics'' (92 reports). Electronic phenomena at low temperatures were discussed in the section ''Nanostructures and Low-Dimensional Systems,'' and the results of theoretical and experimental research on the physical properties of liquid helium and cryocrystals at the section ''Quantum Liquids and Crystals.''

In the section ''Low Temperature Solid State Physics'' attention was devoted mainly to the problems of low-temperature magnetism.

The plenary report by M. S. Tagirov, ''Dielectric Van Vleck paramagnets in high magnetic fields and at low temperatures'' was devoted to the results of theoretical and experimental research by Kazan physicists in collaboration with the High Field Magnet Laboratory of the Max Planck Institute, Grenoble, France and the University of Kanazawa, Japan. In magnetic fields that are high enough that the energy of an ion in the external field is comparable to the splitting of the Stark structure, the states of the electronic and nuclear subsystems of a dielectric Van Vleck paramagnet at low temperatures are strongly intermixed, and one can speak of a coupled electronic–nuclear subsystem. In that case the magnetic properties of the Van Vleck ions acquire a number of new features. As an example, data were presented on the influence of high magnetic fields on the properties of the dielectric Van Vleck paramagnets thulium ethylsulfate $Tm(C_2H_5SO_4)_2 \cdot 9H_2O$(TmES) and thulium double fluoride $LiTmF_4$.

Research on cooperative quantum phenomena and the peculiarities of the formation of the ground state in quasi-one-dimensional magnets of the $CuGeO_3$ and $NaV_2O_5$ type was the subject of a plenary report by A. I. Smirnov (P. L. Kapitsa Institute of Physical Problems, Russian Academy of Sciences, Moscow) entitled, ''Magnetic defects in quasi-one-dimensional magnets with a gapped excitation spectrum.'' In $CuGeO_3$ the copper ions form chains with a strong antiferromagnetic exchange interaction. At the spin–Peierls transition the period of the chains doubles, a singlet ground state forms, and a gap opens up in the spectrum of magnetic excitations. The substitution of impurity ions for the copper or germanium leads to a decrease of the phase transition temperature, i.e., to the formation of long-range antiferromagnetic order. The magnetic excitations in sodium divanadate behave in an analogous way.

The phase transition in $NaV_2O_5$, which is caused by a redistribution of the charge between vanadium positions, was observed by A. N. Vasil'ev and M. M. Markina (Physics Department, Moscow State University, Russia) together with J. Müller and M. Lang (Institute of Solid State Chemical Physics, Dresden, Germany) and M. Isobe and Y. Ueda (Tokyo University, Japan). Below the critical temperature of $NaV_2O_5$ there are three inequivalent vanadium positions with valences 4, 4.5, and 5. Besides the charge ordering, a structural transformation with a lowering of the symmetry occurs, and a gap opens up in the spectrum of magnetic excitations. In the majority of experiments these processes

 

occur at the same temperature. However, the thermal expansion data obtained by those authors implies that the phase transition takes place in two stages, since the curve of the temperature dependence of the coefficient of thermal expansion exhibits two sharp peaks at $T_1 = 33.5$ K and $T_2 = 33.8$ K. The redistribution of charge begins at $T_2$, and the gap opens up in the spectrum of magnetic excitations only at $T_1$.

Degenerate antiferromagnetic semiconductors can undergo phase separation into a highly conductive ferromagnetic phase, in which all of the conduction electrons are concentrated, and an insulating antiferromagnetic phase [É. L. Nagaev, JETP Lett. (1972)]. Here there is a tendency toward intermixing of the phases. This problem has again become topical, since similar phenomena have also been observed in high-$T_c$ superconducting (HTSC) materials and manganites. Substantial progress in the study of this problem has now been made by M. Yu. Kagan (P. L. Kapitsa Institute of Physical Problems, Russian Academy of Sciences, Moscow), K. I. Kugel' (Institute of Theoretical and Applied Electrodynamics, Russian Academy of Sciences, Moscow), and D. I. Khomskiĭ (Groningen University, Netherlands), and their research results were presented in the plenary report of M. Yu. Kagan entitled, ''Phase separation in systems with charge ordering.'' Extremely interesting original results for this problem were also contained in the sectional reports by É. L. Nagaev, ''Magnetoelectronic phase separation: geometry and geometric phase transitions,'' and by N. A. Babushkina, A. N. Taldenkov, L. M. Belova, and E. A. Chistotina (Kurchatov Institute Russian Research Center, Moscow), É. Yu. Gorbenko, A. R. Kaul', K. I. Kugel' (Institute of Theoretical and Applied Electrodynamics, Moscow), and D. I. Khomskiĭ (Groningen University, Netherlands), ''Partial isotopic substitution and phase separation in La–Pr manganites,'' and also in the report by I. F. Voloshin, A. V. Kalinov, S. E. Savel'ev, and L. M. Fisher (All-Russia Electrotechnical Institute, Moscow) and N. A. Babushkina, L. M. Belova, E. I. Khomskiĭ, and K. I. Kugel', ''Phase separation in La–Pr manganites and its evolution in a magnetic field.''

The interaction between ferromagnetic layers across a nonferromagnetic spacer in Fe/Cr superlattices was investigated in the temperature range 2–400 K by the ferromagnetic resonance (FMR) method at frequencies of 9.5–37 GHz for longitudinal and transverse excitation of the resonance in a study reported by A. B. Drovosekov, O. V. Zhitnikova, N. M. Kreĭnes, D. I. Kholin, and S. O. Demokritov (P. L. Kapitsa Institute of Physical Problems, Russian Academy of Sciences, Moscow). Besides the acoustic branch, those authors detected a series of additional modes, which apparently correspond to excitation of standing spin waves with wave vectors orthogonal to the film plane. A comparison of the experimental data with the FMR spectrum calculated in the biquadratic exchange model yielded the values of the exchange constants.

A report by M. V. Eremin, S. I. Nikitin, N. I. Silkin, S. Yu. Prosvirin, and R. V. Yusupov (Kazan State University) identified all of the observed optical absorption lines of the pair $Cr^{2+}$–$Cr^{3-}$ in $KZnF_3$. The parameters of the exchange interaction in the ground state and excited state were determined. The details of the transition region were described; the double exchange is superexchange.

V. I. Ivanshin, M. V. Eremin, R. M. Eremina (Kazan State University) and H-A. Krug von Nidda and A. Loid (Augsburg, Germany) presented the results of an EPR study on $La_{1-x}Sr_xMnO_3$ single crystals. The direction of the Dzyaloshinskiĭ–Moriya vector was determined from the angle dependence of the EPR linewidth in the paraphase. At values of $x$ in the interval 0.03–0.1 additional EPR lines were observed, which were attributed to self-trapped states (polarons) of the $Mn^{3+}$–$O^{1-}$ type. The acoustoelectronic effect and the absorption of a surface acoustic wave (SAW) in monolithic layered structures of the piezodielectric $LiNbO_3$ and thin films of the lanthanum manganite $La_{0.67}Ca_{0.33}MnO_3$ were studied by Yu. V. Ilisavskiĭ, A. V. Gol'tsev, K. V. D'yakonov, V. V. Popov, and É. Z. Yakhkind (A. F. Ioffe Physicotechnical Institute, Russian Academy of Sciences, St. Petersburg) and V. P. D'yakonov, A. Klimov, S. Levandovskiĭ, and G. Shimchak (Institute of Physics, Warsaw, Poland). They detected an anomalous longitudinal acoustoelectronic effect, which was even with respect to the wave vector of the acoustic wave. The observed frequency and temperature dependences of the SAW absorption are evidence of a Hutson–White mechanism of sound damping and of the importance of the role of spin disorder in the transport properties of compounds possessing colossal magnetoresistance.

The physics of quantum liquids and crystals was represented at the conference by 5 plenary and 20 sectional reports of experimental and theoretical studies of the superfluid phases of $^3$He and $^4$He and their solutions, solid helium and other cryocrystals, helium films, various complexes in condensed phases of helium, low-dimensional electronic systems over liquid helium, and other problems.

The review presented by J. Parpia (Cornell University, Ithaca, USA) was devoted to an analysis of the various experimental studies of the properties of superfluid $^3$He filling aerogel — a substance with an anomalously high porosity. Such a system affords a unique opportunity to study the influence of disordering on the properties of a superfluid liquid with triplet pairing. Experiments with a torsion generator showed that the presence of aerogel leads to a lowering of the superfluid transition temperature, to a decrease in the density of the superfluid component, and to suppression of superfluidity. The report also analyzed the phase diagram in a magnetic field, the influence of $^4$He impurities on the properties of $^3$He in aerogel, the role of anisotropy, and other factors. It was noted that the influence of the aerogel has a closer resemblance to the influence of impurities than to the influence of a bounded geometry on the properties of a superfluid liquid.

The density of the superfluid component of $^3$He filling the aerogel was also determined in acoustic experiments, which were discussed in the report by A. Golov (University of Manchester, England). Unlike a rigid porous medium, in aerogel the normal component of the superfluid liquid moves together with its walls, and in this case rapid and slow longitudinal modes and a mode of the fourth-sound type were detected. Experiments to observe the transverse sound mode in aerogel containing a superfluid liquid are now being prepared at Manchester.

The plenary report by J. Pickett (University of Lancaster, England) was devoted to an account of recent experiments

with superfluid $^3$He to investigate quantum turbulence in the *B* phase. In the experiment various vibrating wire resonators were used, one of which operated in a supercritical regime. At high velocities the vibrating wire destroys Cooper pairs, and that may lead to the creation of a large number of disordered quantum vortices. We note that this technique is promising as a sensitive instrument for studying the dynamics of vortices at ultralow temperatures.

Among the other papers on superfluid $^3$He we might mention the theoretical paper by A. N. Tarasov (Kharkov Physicotechnical Institute National Research Center, Ukraine) on superfluid Fermi liquid with triplet pairing in a magnetic field and the experimental paper from Kosice, Slovakia, in which by A. Feger, É. Gazho, M. Kupka, L. Lokner, M. Medeova, R. Shcheĭbel, and P. Skiba (Shafarik University and Institute of Experimental Physics, Slovak Academy of Sciences) continued their research on the dynamics of a uniformly precessing magnetic domain in $^3$He-*B*, devoting their main attention to the study of nonlinear effects.

A study of superfluid $^4$He was the subject of a joint paper by theorists I. N. Adamenko, A. V. Zhukov, and K. E. Nemchenko of the Kharkov National University, Ukraine and the experimentalist A. F. White of the University of Exeter, England. The authors called attention to the fact that because of the unusual dispersion of phonons in superfluid $^4$He and the strong angle dependence of the phonon–phonon interaction, the phonons in HeII are divided into two subsystems — low-energy and high-energy. This leads to peculiar kinetics of phonon beams in HeII. A theoretical analysis made it possible to account for a number of the observed effects and to formulate conditions for observation of new features.

Several papers were devoted to the properties of $^3$He–$^4$He liquid solutions. The report by V. K. Chagovets, É. Ya. Rudavskiĭ, G. A. Sheshin, and T. V. Kal'ko (Institute for Low Temperature Physics and Engineering, National Academy of Sciences of Ukraine, Kharkov) discussed experiments on the kinetics of phase separation of superfluid $^3$He–$^4$He solutions uner applied pressures. It was found that in this case the attainable limiting supersaturation is almost an order of magnitude lower than the values predicted by the theory of homogeneous nucleation. Taking the quantum vortices into account as possible centers of nucleation brings the results closer to the experiment but does not give completely quantitative agreement. P. P. Bezverkhiĭ, V. G. Martynets, E. V. Matizen (Institute of Inorganic Chemistry, Siberian Branch of the Russian Academy of Sciences, Novosibirsk) reported measurements of the thermal conductivity and thermodiffusion ratio near the liquid–vapor critical point of the $^3$He–$^4$He solutions and described an analysis of these data from the standpoint of the fluctuation theory of phase transitions and critical phenomena. A. R. Minullin and D. A. Tayurskiĭ (Kazan State University) called attention to the fact that by varying the concentration in $^3$He–$^4$He liquid solutions, one can rather easily change the density of the number of states, and that should give rise to oscillations on the concentration dependence of the magnetic susceptibility of the solutions in a bounded geometry.

The problem of the magnetic coupling between liquid $^3$He and a dielectric Van Vleck paramagnet was the subject of a plenary report by D. A. Tayurskiĭ (Kazan State University). In it a new method was proposed for polarizing liquid $^3$He by the transfer of a highly polarized state of the magnetic moments of the the solid to the nuclear spins of liquid $^3$He by means of a magnetic coupling. The role of a thin solid-state film of $^3$He at the interface between liquid $^3$He and a solid during the transfer of magnetization was discussed, and research results on the properties of liquid $^3$He in contact with several specific dielectric Van Vleck paramagnets — thulium double fluoride and its diamagnetic analog — were analyzed.

One of the traditional topics in the physics of helium is the study of thin films of $^4$He, $^3$He, and their solutions. New effects observed in a $^3$He monolayer were reported at the plenary session by J. Saunders (Royal Holloway, University of London, England). A two-dimensional system of strongly correlated fermions formed in a $^3$He layer adsorbed on a substrate consisting of two layers of deuterated water placed on a graphoil surface. Specific heat and magnetization measurements in the temperature range 1–80 mK made it possible to determine the dependence of the effective mass of the fermionic excitations on the coverage and to observe its divergence at coating thicknesses greater than 5 nm. This effect was interpreted as a Mott–Hubbard transition from a two-dimensional Fermi liquid to a magnetically ordered system, analogous to a metal–insulator transition. J. Nyeki of the same laboratory reported another series of experiments investigating two-dimensional $^3$He adsorbed on the surface of superfluid film of $^4$He. In those experiments a stepwise growth of the specific heat with increasing coverage was observed; this is due to the onset of surface excited states.

The topical problem of Bose–Einstein condensation was considered in the report by D. B. Baranov and V. S. Yarunin (Joint Institute for Nuclear Research, Dubna, Russia). The authors investigated the influence of the gravitational field on the critical temperature for Bose–Einstein condensation and calculated the shift of the condensation temperature of a gas located in a magnetic trap as a result of the gravitational field. It was predicted that by cyclically moving the trap from Earth to space and back to Earth, three Bose condensation could be observed.

The reports of research on quantum crystals presented at the conference involved a diversity of experimental studies in this area. The plenary report by A. Ya. Parshin (Institute of Physical Problems, Russian Academy of Sciences, Moscow) was devoted to the study of the morphology and growth kinetics of $^3$He crystals below 1 mK. In experiments done at the Technical University in Helsinki, Finland, the technique of optical interferometry was used to obtain a three-dimensional image of a crystal growing from the superfluid phase. The growth coefficients were determined for different faces of the crystal, and the period of the faceting, the anisotropy of the growth, and the effect of defects and dissipation were investigated.

In three reports presented by A. N. Gan'shin, V. N. Grigor'ev, V. A. Maĭdanov, A. A. Penzev, É. Ya. Rudavskiĭ, and A. S. Rybalko (Institute for Low Temperature Physics and Engineering, National Academy of Sciences of Ukraine, Kharkov), new results were presented from an experimental

study of two-phase crystals of $^3$He formed as a result of the phase separation of these solid solutions. In particular, those authors studied the dynamics of the growth and dissolution of solid inclusions of $^3$He in a $^4$He matrix, the kinetics of melting and recrystallization of these inclusions, and also the dynamics of liquid drops of $^3$He in a $^4$He crystal. With the aid of precision pressure measurements, the left branch of the line of phase separation of solid solutions of $^3$He in $^4$He was also constructed and the influence of the crystal structure was elucidated. The features of the spin–lattice relaxation in crumbled solid solutions of $^3$He–$^4$He were studied by N. P. Mikhin, V. A. Maĭdanov, and V. A. Polev (Institute for Low Temperature Physics and Engineering, National Academy of Sciences of Ukraine, Kharkov), and they discussed possible mechanisms of magnetic relaxation in a finely dispersed $^3$He phase.

The report by O. A. Korolyuk, B. Ya. Gorodilov, and A. I. Krivchikov (Institute for Low Temperature Physics and Engineering, National Academy of Sciences of Ukraine, Kharkov) was devoted to a study of the effect of thermal shocks on the thermal conductivity of parahydrogen–orthodeuterium solid solutions. Attention was focused on elucidating the mechanisms of phonon scattering on structural defects of the crystal. An interesting effect was discussed in the theoretical paper by V. A. Lykakh and E. S. Syrkin (Institute for Low Temperature Physics and Engineering, National Academy of Sciences of Ukraine, Kharkov). The presence of localized carriers (electrons and holes) in molecular cryocrystals can lead to a reorientation of the axes of the nearest-neighbor molecules along the electric field and to the formation of rotational polarons.

The behavior of extraneous particles in quantum crystals and liquids was studied in other papers as well. S. G. Kafanov, A. Ya. Parshin, I. A. Todoshchenko (Institute of Physical Problems, Russian Academy of Sciences, Moscow) investigated the structure and dynamics of triplet metastable helium molecules in liquid $^4$He and $^3$He. An analysis of the absorption spectrum confirmed the conclusion that there is a microscopic bubble surrounding the molecule in liquid helium. The kinetics of the decomposition of triplet molecules via their mutual recombination was also considered in detail. It was noted that the results are in good agreement with the theory of molecular-diffusion-limited recombination under conditions of a strong van der Waals interaction.

Electrons localized over the surface of liquid helium are another type of extraneous particle. The theory of the electron mobility in this sort of two-dimensional system was developed in a paper by I. N. Adamenko, A. V. Zhukov, and K. É. Nemchenko (Kharkov National University) in which the interactions of all type of quasiparticles were taken into account; this led to an improvement of the agreement between theory and experiment. The reports by Yu. Z. Kovdri, V. A. Nikolaenko, S. P. Gladchenko (Institute for Low Temperature Physics and Engineering, National Academy of Sciences of Ukraine, Kharkov) discussed the experimental study of even lower-dimensional systems — quasi-one-dimensional and one-dimensional electron systems over liquid helium, which were realized with the use of glass optical gratings. Measurement of the carrier mobility in such a system showed that below 1 K it is practically independent of temperature; this may be due to localization of the electrons in a random potential. Data on the resistance and magnetoresistance of a one-dimensional electron system were also presented.

An exotic system — a water condensate in superfluid helium — was obtained by A. M. Kokotin and L. P. Mezhov–Deglin (Institute of Solid State Physics, Chernogolovka, Russia). Those authors introduced gaseous $^4$He containing impurity water vapor into a cell filled with HeII. As a result, porous water complexes (icebergs) permeated with HeII formed, having a characteristic size of the order of a few millimeters. A water gel was observed in which the disperse phase consists of water clusters surrounded by a layer of solidified helium and the dispersion medium is superfluid $^4$He.

Recent years have seen a growing interest in the study of physical phenomena in carbon nanotubes, work which was begun back in 1991. At the present time this problem is attracting the attention of physicist in almost all world science centers.

The Director of the Low Temperature Laboratory of the Technical University in Helsinki, Mikko Paalanen, in his report ''Multiwalled carbon nanotubes as building blocks in nanoelectronics'' at the plenary session, illuminated the prospects for the use of carbon nanotubes in electronics, and the technology of their fabrication was discussed in the reports by S. V. Anonenko, S. N. Mal'tsev, and A. A. Timofeev (Moscow Engineering Physics University) and their collaborators A. I. Romanenko, A. V. Okotrub, O. B. Anikeeva, L. G. Bulusheva, and N. F. Yudinov (Novosibirsk Institute of Inorganic Chemistry, Siberian Branch of the Russian Academy of Sciences) and Cheng Dong and Yongming Ni (Institute of Physics, Chinese Academy of Sciences, Beijing, China).

The plenary report by V. T. Dolgopolov (Institute of Solid State Physics, Chernogolovka) entitled ''Manifestation of a canted antiferromagnetic phase in the transport properties of quantum double wells'' gave a review of the theoretical and experimental papers on the study of the spectrum and transport properties of charge carriers of a two-layer system in a parabolic well with a narrow tunneling barrier at the center. In a quantizing magnetic field in the presence of the asymmetric distribution of the electron density in this system with two subbands and a gap between subbands, a deep minimum of the activation energy is observed in a tilted magnetic field. The activation energy at the minimum is nevertheless finite, attesting to a new insulator–insulator transition. The results are interpreted as predicting the existence of a canted antiferromagnetic phase.

The report by B. P. Vodop'yanov (Kazan Physicotechnical Institute, Russian Academy of Sciences) and L. R. Tagirov (Kazan State University) presented the results of theoretical studies of the conductivity and magnetoresistance of nanosize point contacts. In the quasiclassical approximation the conductance of the nanocontact was calculated for an arbitrary ratio of its radius to the mean free path in the contacting metal. For ferromagnetic metals such as Fe, Co, and Ni, the calculated value of the magnetoresistance can reach several hundred percent; this can explain the recent experiments of Garcia *et al.* on point nanocontacts.

In the section ''Nanostructures and Low-Dimensional Systems,'' due attention was also paid to the study of physical phenomena in heterostructures.

At the A. F. Ioffe Physicotechnical Institute (St. Petersburg, Russia), Shubnikov–de Haas oscillations were observed in a spatially separate electron–hole channel at a *p*-GaInAsSb/*p*-InAs heterointerface in static magnetic fields up to 16 T (V. A. Berezovets, M. P. Mikhaĭlov, K. D. Moiseev, R. V. Parfen'ev, V. I Nizhankovskiĭ) and an interpretation was proposed for the results of magnetoresistance and Hall-effect measurements made by those authors at the International Laboratory of High Magnetic Fields and Low Temperatures at Wroclaw, Poland.

The paper by Yu. M. Gal'perin, I. L. Drichko, A. M. D'yakonov, A. V. Patsekin, and I. Yu. Smirnov (A. F. Ioffe Physicotechnical Institute, St. Petersburg) and A. I. Toropov (Novosibirsk Institute of Semiconductor Physics, Russian Academy of Sciences) presents the results of measurements of the sound absorption coefficient and the propagation velocity of a surface acoustic wave in GaAs/AlGaAs heterstructures in the quantum Hall effect regime. The possibility of determining the localization length of the electrons from acoustic measurements was discussed.

The conductivity of a two-dimensional electron gas at an $In_{0.53}Ga_{0.47}$/InP heterointerface in the case of occupation of one subband or two subbands of the size quantization was studied at the A. F. Ioffe Physicotechnical Institute, St. Petersburg by D. D. Bykanov, S. V. Novikov, T. A. Polyanskaya, and I. G. Savel'ev. The electron concentration in the sample was varied with the aid of frozen-in photoconductivity. The concentration dependence of the diffusion lengths for phase disruption and the spin–orbit scattering of electrons was determined at helium temperature.

Anomalous behavior of the Hall coefficient in *p*-Ge/$Ge_{1-x}Si_x$ heterostructures in low magnetic fields was reported by A. T. Lonchakov, Yu. G. Arapov, V. N. Neverov, and G. I. Kharus (Institute of Metal Physics, Urals Branch of the Russian Academy of Sciences, Ekaterinburg) and O. A. Kuznetsova (Nizhniĭ Novgorod State University, Russia).

The quantum Hall effect in *p*-GaAs/AlGaAs heterostructures was investigated under uniaxial compression by E. V. Bogdanov, N. Ya. Minina, and A. M. Savin (Physics Department, M. V. Lomonosov Moscow State University) jointly with V. Kraak (Humboldt University, Berlin, Germany) and O. P. Hansen (Niels Bohr Institute, Copenhagen University, Denmark).

Photoluminescence, frozen-in photoconductivity, and hopping conductivity were investigated in InAs/GaAs structures with quantum dots grown on vicinal faces (R. A. Lunin, V. A. Kul'bachinskiĭ, V. G. Kytin, A. V. Golikov, A. V. Demin, V. A. Rogozin, B. N. Zvonkov, and S. M. Nekorkin — Physics Department, M. V. Lomonosov Moscow State University). Near 3.2 K the temperature dependence of the resistance undergoes a transition from the Mott law to the Shklovskiĭ–Éfros law.

The results of a study of tunneling through an AlAs/GaAs heterostructure with a thin (2.5 nm) AlAs barrier and spacers were presented by Yu. N. Khanin, E. E. Vdovin, and Yu. V. Dubrovskiĭ (Institute of Problems of Microelectronics Technology, Russian Academy of Sciences, Chernogolovka) and D. K. Maude and J-C. Portal (High Field Magnet Laboratory, Grenoble). A high magnetic field applied parallel to the tunnel current caused the conductivity peak to split, as a result of the appearance of a gap in the tunneling density of states.

V. A. Demikhovskiĭ reported the extremely unexpected finding that the de Haas–van Alphen effect can be observed in ultrahigh magnetic fields of the order of 3000 T (V. Ya. Demkhovskiĭ, A. A. Petrov, and D. V. Khomitskiĭ — Nizhniĭ Novgorod State University). Such values of pulsed magnetic fields have already been obtained at the All-Russia Scientific-Research Institute of Experimental Physics, Sarov, Russia, and in this connection those authors investigated the quantum states of Bloch electrons in fcc crystals. The character of the spectrum of these states depends substantially on the number of magnetic flux quanta per unit cell, and the existence of several series of oscillations of the magnetic susceptibility is a possibility.

A. A. Nikolaeva reported the observation of an anomalous maximum of the resistance of submicron whiskers of bismuth 100–300 nm thick when they were strained by 2.5% under tension (A. A. Nikolaeva, D. V. Gitsu, P. P. Bodyul, F. M. Burchakov — Institute of Applied Physics, Kishinev, Moldova).

The dependence of the Casimir force of attraction of metallic films at low temperatures on the thickness of the film, the state of its surface, the plasma frequency, the electron relaxation frequency, and the Fermi velocity was investigated by S. A. Dubrava and V. A. Yampol'skiĭ (Institute of Radio Electronics, National Academy of Sciences of Ukraine, Kharkov). The Casimir attraction of bulk metals is practically independent of their physical characteristics, but the interaction of thin films, which are transparent to electromagnetic oscillations at the characteristic interaction frequencies, is extremely sensitive to their properties. Measurement of the Casimir force under these conditions can become a new method for studying the physical properties of metallic films.

This was perhaps the first time that the physical properties of quasicrystals had been reported at a cryogenic conference. A. A. Teplov presented the results of studies of the specific heat, electrical resistance, and magnetic susceptibility of the alloy $Al_{70}Pd_{21}Tc_9$ at the Kurchatov Institute Russian Research Center (M. N. Mikheeva, G. K. Panova, A. A. Teplov, M. N. Klopkin, N. A. Chernoplekov, and A. A. Shikov), and some Ekaterinburg physicists reported the results of a study of the electrical and magnetic properties of the quasicrystalline alloys $Al_{63}Cu_{25}Fe_{12}$ (A. F. Prekul, N. Yu. Kuz'min, N. I. Shchegolikhina, and S. Z. Nazarova) and $Al_{70.2}Pd_{21.3}Mn_{8.5}$ (A. A. Rempel', A. V. Korolev, and A. I. Gusev).

V. S. Egorov, F. V. Lykov, and O. A. Repina (Kurchatov Institute Russian Research Center, Moscow) investigated the diamagnetic Condon domains in beryllium. The instability of the homogeneous state of nonmagnetic metals, which was observed in bismuth by D. Shoenberg in the 1960s, is possible only at extremely low temperatures. Recently Condon domains were observed in tin by V. S. Egorov in collaboration with G. Solt, C. Baines, D. Herlach, and U. Zimmermann (Villigen PSI, Switzerland). Upon the formation of

Condon domains the excitation of nonlinear waves of arbitrarily small amplitude becomes possible (O. Galbova — University in Skopje, Macedonia; V. G. Peschansky — Institute for Low Temperature Physics and Engineering, National Academy of Sciences of Ukraine, Kharkov; D. I. Stepanenko — Kharkov National University).

In the report by R. N. Gurzhi (Institute for Low Temperature Physics and Engineering, National Academy of Sciences of Ukraine, Kharkov) entitled ''Spectroscopy of electron–electron interaction in two-dimensional degenerate conductors,'' a novel method of studying the interaction of quasiparticles in two-dimensional degenerate conducting systems was proposed, based on the magnetic-field separation of groups of quasiparticles scattered at different angles with the use of narrow 2D electron beams.

The magnetoresistance of antiferromagnetic chromium under magnetic breakdown conditions was calculated by N. Kh. Useinov (Kazan Pedagogical University) with allowance for the spin degrees of freedom of the conduction electrons.

V. B. Efimov, L. P. Mezhov-Deglin, and N. S. Sidorov (Institute of Solid State Physics, Chernogolovka) measured the thermal conductivity of fullerite at temperatures below 10 K. The dissipative phonon relaxation length remained practically unchanged all the way down to $T=0.5$ K and in different samples had a value in the range 70–100 nm. Those authors attributed this weakness of the temperature dependence to the scattering of phonons on frozen-in orientational defects.

Some topical problems of superconductivity were addressed in plenary reports ''Josephson $\pi$ contacts and their application for creating superconducting qubits,'' by V. V. Ryazanov (Institute of Solid State Physics, Russian Academy of Sciences, Chernogolovka), ''EPR studies of the spin dynamics in cuprate superconductors,'' by B. I. Kochelaev (Kazan State University), and ''Interaction of ferromagnetism and superconductivity in superconductor/ferromagnet layered thin-film systems'' by I. A. Garifullin (Kazan Physicotechnical Institute, Russian Academy of Sciences), and also in 21 reports read at the sectional sessions. Interesting results of research into diverse aspects of superconductivity were also reported in the poster session.

In cuprate superconductors the EPR signal from copper is not detected: either it is absent altogether or it is extremely weakened. The causes for this unusual behavior of the EPR were discussed in the plenary report by B. I. Kochelaev.

Regular networks of Josephson junctions have become a subject of heightened interest in connection with the features of the vortex dynamics in such structures and their possibilities for use as coherent millimeter radiation sources and elements of logic devices. V. V. Ryazanov reported the results of experimental and theoretical studies of the features of the Josephson behavior of superconductor–ferromagnet–superconductor sandwiches (*SFS* junctions) and superconducting two-dimensional networks based on them. It was found that thin-film $Nb–Cu_{1-z}Ni_z–Nb$ sandwiches, at a certain nickel concentration (close to 50%) in the Cu/Ni layer and a certain thickness $d_F$ of the ferromagnetic layer, undergo a transition to the Josephson $\pi$ state on cooling below $T_{tr}$. These *SFS* sandwiches have a reentrant oscillatory temperature dependence of the critical current that goes to zero for $T=T_{tr}$. The transition to the $\pi$ state is also manifested in a half-period shift of the magnetic-field dependence of the transport critical current of a triangular network of *SFS* contacts. This shift is due to the onset of spontaneous currents in the network even at zero external field; this state is degenerate with respect to the two possible directions of the spontaneous currents, and in ordinary Josephson networks it is observed only when a ''frustrating'' magnetic field, equal to a half-integer number of magnetic flux quanta per cell, is applied.

''Internally frustrated'' (or self-frustrated) superconducting chains with $\pi$ contacts can be used to implement a superconducting qubit — the basic element of a hypothetical ''quantum computer,'' which would perform computations based on quantum algorithms. Originally proposed schemes utilizing superconducting ''phase'' qubits were based on magnetically frustrated superconducting chains in which it is necessary to apply one-half magnetic flux quantum in order to create the degenerate two-level coherent quantum system necessary for implementation a qubit. Such a qubit is not isolated from the surroundings (it interacts with them) and, according to estimates, has a shorter coherence time in comparison with a qubit utilizing a $\pi$ contact for creation of the degenerate two-level quantum system. Another possible application of $\pi$ contacts relates to the development of a superconducting digital ''complementary'' electronics, in which the $\pi$ contact is used as an inverter of the superconducting phase.

S. M. Ishikaev and É. V. Matizen (Institute of Inorganic Chemistry, Siberian Branch of the Russian Academy of Sciences, Novosibirsk) used a SQUID magnetometer to study the field dependence of the magnetic moment of square ($100\times100$) Josephson networks with $Nb–NbO_x–Pb$ tunnel junctions with small damping. A regular dependence of the magnetic moment on the field was found, having features at integer and half-integer numbers of magnetic flux quanta, and at a temperature below 5.8 K, jumps were observed on the magnetization curves due to the entry and exit of avalanches of tens and hundreds of fluxons. It was shown that the probability distribution of these processes is in agreement with the theory of self-organized criticality.

T. N. Baturina, Z. D. Kvon, A. E. Plotnikov, and M. N. Kostrikin (Institute of Semiconductor Physics, Siberian Branch of the Russian Academy of Sciences, Novosibirsk) investigated experimentally the properties of a mesoscopic multiply connected *SNS* system based on a superconducting film of platinum silicide 6 nm thick with structurally ideal *SN* interfaces.

The plenary report by I. A. Garifullin gave a review of the results of experimental and theory research on the mutual influence of ferromagnetism and superconductivity in artificially created layered ferromagnet/superconductor ($F/S$) heterostructures. In such systems the temperature $T_c$ of the transition to the superconducting state is an oscillatory function of the ferromagnetic layer thickness $d$. However, the cause of this behavior of $T_c$ can be different for different $F/S$ systems. That author gave an example of unusual behavior of $T_c(d)$. With increasing $d$ in three-layer Fe/V/Fe films, $T_c$ decreases rapidly until the superconductivity vanishes completely, and then at $d=0.95$ nm the superconductivity reap-

pears and $T_c$ increases with $d$, reaching a value of 2 K at saturation. This behavior of the superconductivity may be due to the interference of the wave functions of Cooper pairs reflected by the surface of the film and the $F/S$ interfaces. A comparison of L. R. Tagirov's theory with the experimental data on the suppression of superconductivity by ferromagnetism for the systems Pb/Fe and V/Fe shows that the passage of Cooper pairs through an $F/S$ interface is strongly limited. The ferromagnetic resonance data also indicate that a modulation of the ferromagnetic order occurs under the influence of superconductivity, and, hence, the saturation magnetization of the Fe layers decreases.

The problem of coexistence of superconductivity and ferromagnetism was the subject of a report by Yu. A. Izyumov (Institute of Metal Physics, Urals Branch of the Russian Academy of Sciences, Ekaterinburg), Yu. N. Proshin (Kazan State University), and M. G. Khusainov (Chistopol Branch of Kazan State Technical University). New $0\pi$ and $\pi\pi$ Larkin–Ovchinnikov–Fulde–Ferrel (LOFF) states, having a higher critical temperature of the transition to the superconducting state than the previously known 00 and $\pi 0$ LOFF states, were predicted in $F/S$ superlattices. On this basis they developed an original theory of the proximity effect, taking into account the competition between the one-dimensional and three-dimensional realizations of LOFF states. Quantitative agreement was obtained with the known phase diagrams in $F/S$ systems ($F$: Fe, Gd, Co; $S$: Nb, V, Pb). It was shown that superconductivity in $F/S$ multilayers is a consequence of the pairing of electrons by the BCS mechanism in the $S$ layers together with the pairing by the LOFF mechanism in the $F$ layers.

V. N. Zavaritskiĭ (Institute of Physical Problems, Russian Academy of Sciences, Moscow) investigated the influence of a pulsed magnetic field on the interlayer resistance of BSCCO-2212 single crystals having a critical temperature $T_c = 93$ K. The longitudinal magnetoresistance of the samples in the normal state turned out to be negative, while for $T < T_c$ its field dependence has a maximum.

I. A. Fomin (Institute of Physical Problems, Russian Academy of Sciences, Moscow) studied the broadening of the jump in specific heat of a superconductor near the critical temperature $T_c$ when large-scale and small-scale inhomogeneities are taken into account. For determining the temperature dependence of the specific heat it is sufficient to know the correlation function of the random component of the temperature and the density of states for the linear part of the Ginzburg–Landau equation with this random component.

In the reports by the representatives of the P. N. Lebedev Physics Institute, Russian Academy of Sciences, Moscow, ''Čerenkov resonance interaction of Swihart waves with Josephson vortices'' (V. P. Silin and A. V. Studenov) and ''Čerenkov scaling of Josephson vortices by resonantly trapped waves'' (A. S. Malishevskiĭ, V. P. Silin, and S. A. Uryupin), the approximation of weakly nonlocal Josephson electrodynamics in the Auby–Volkov model was used to describe the induced motion of vortices carrying several magnetic flux quanta and to investigate the Čerenkov interaction of vortices with Swihart waves.

Experiments were done on the suppression of the magnetic moment of textured samples of YBCO by an alternating magnetic field. At sufficiently large amplitudes of the alternating field, which was able to ''transilluminate'' the entire sample, the dc currents vanish — a collapse of the static moment of the sample sets in (I. V. Voloshin, A. V. Kalinov, S. E. Savel'ev, L. M. Fisher — All-Russia Electrical Engineering Institute, Moscow; V. A. Yampolskii — Institute of Radio Electronics, National Academy of Sciences of Ukraine, Kharkov; F. Perez Rodriguez — Institute of Physics, Autonomous University, Puebla, Mexico; M. A. R. Leblanc — University of Ottawa, Canada).

The influence of the structural relaxation on the superconductivity of amorphous thin films of beryllium containing a few atomic percent hydrogen was studied by V. M. Kuzmenko and B. G. Lazarev (Kharkov Physicotechnical Institute National Research Center).

The mechanisms of hysteresis of the magnetic properties of superconducting single crystals of $Bi_2Sr_2CaCu_2O_x$ were studied by Yu. V. Vashakidze, Yu. N. Talanov, and T. S. Shaposhnikova (Kazan Physicotechnical Institute, Russian Academy of Sciences).

The influence of cerium doping on the transport properties of $Nd_2Ce_xCuO_{4+y}$ was discussed by M. I. Ponomarev, A. N. Ignatenkov, N. G. Shelushin, T. B. Charikova, L. D. Sabirzyanova, and G. I. Kharus (Institute of Metal Physics, Urals Branch of the Russian Academy of Sciences, Ekaterinburg).

As a complement the poster session for the section ''Superconductivity'' a seminar was held, devoted to a discussion of the recent interesting theoretical paper by A. A. Abrikosov (Department of Materials Science, Argonne National Laboratory, Argonne, USA) entitled, ''Theory of the high-temperature superconductivity of cuprates, based on experimental results,'' which was presented at the seminar by Ya. G. Ponomarev (Physics Department, Moscow State University).

On October 6, 2000 an open session of the Scientific Council of the Russian Academy of Sciences on the topic ''Low Temperature Physics'' was held, under the chairmanship of Vice-President A. F. Andreev of the Russian Academy of Sciences, to summarize the work of the 32nd Conference. The next, 33rd Conference on Low Temperature Physics is planned for the year 2002.

Translated by Steve Torstveit